EXPERIMENTAL STUDY AND MODELING OF ABRASIVE FLOW FINISHING PROCESS FOR NANOFINISHING OF MACRO TO MICRO FEATURES

A thesis submitted in
partial fulfillment of the requirements
for the degree of

DOCTOR OF PHILOSOPHY

By

Sachin Singh

(126103031)

Department of Mechanical Engineering

Indian Institute of Technology Guwahati

January - 2018

DEPARTMENT OF MECHANICAL ENGINEERING

INDIAN INSTITUTE OF TECHNOLOGY GUWAHATI

GUWAHATI-781039, ASSAM

INDIA

CERTIFICATE

It is certified that the work contained in the thesis entitled **"Experimental Study and Modeling of Abrasive Flow Finishing Process for NanoFinishing of Macro to Micro Features"** submitted by **Mr. Sachin Singh** for the award of the degree of Doctor of Philosophy has been carried out under my supervision in the Department of Mechanical Engineering, Indian Institute of Technology Guwahati. This work has not been submitted elsewhere for the award of any other degree.

Dr. Mamilla Ravi Sankar
Department of Mechanical Engineering
Indian Institute of Technology Guwahati
Guwahati – 781039, India

17th January, 2018

ACKNOWLEDGEMENTS

I would like to express my heartfelt gratitude towards all those who have immensely helped me during this long arduous journey and eventually assisted me to emerge as an experienced researcher and a mature individual.

First and foremost, I must express my deepest sense of appreciation and respect for my thesis supervisor, Dr. M. Ravi Sankar for providing me the opportunity to work under his supervision. I will always remember and be grateful to his persistent guidance, untiring effort, patience and friendliness in the moments of difficulties. The technical and personal lessons that I learned from him are the foundation pillars for the rest of my life.

I would like to thank my doctoral committee members, Prof. P. S. Robi, Dr. Pankaj Biswas and Dr. Subhash Thota for carefully reading the reports at various stages of evaluation and providing many useful comments, which have helped in the development of this thesis. I am thankful to Prof. U. S. Dixit and Dr. A. Reddy for helping me in their field of expertise. My sincere gratefulness to past and present departmental heads Prof. A K Dass and Prof. S. K. Dwivedy for their kind permission for enrollment, registration and several important supports at IIT Guwahati. I am also grateful to all the faculty members of Mechanical Engineering Department for giving me a comfortable and friendly environment for pursuing my research.

I am very fortunate to receive guidance from Prof. V. K. Jain (retired IIT Kanpur). I am thankful and will always be indebted to him. With his expertise and in-depth knowledge in my field of research, he had given various suggestions which brought my thesis work in a good shape.

The most important support for this work came from my parents, Mr. Sunil Kumar Singh and Mrs. Santosh Singh for encouraging me to go still further at every points of life. I will always remember the support and love provided by my sisters Miss. Rakhi Singh and Miss. Yashvika Singh who in spite of being younger to me played a role of elder sisters. In the time of need they took the family responsibilities on their shoulders so that I may not get distracted during my PhD.

Next, I would like to express my sense of gratitude to Mr. N K Das, assistant workshop superintendent and all the staffs of the workshop specially Mr. Mrinal Sarma, Mr. Dilip Chetri, Mr. Dhaneswar Khaklary, Mr. Chandan Banikya and Mr. Ali, for extending their help

in fabrication of the different experimental setups for this work. I sincerely acknowledge the assistance received from Mr. Pranjol Paul, Mr. Saiffuddin Ahmed, Mr. Jiten Basumatary and Mr. Nip Borah in various experimental proceedings. I also wise to express my gratitude to the Central Instrument Facility, IIT Guwahati to providing technical support.

Friends form an important part of this long and enduring journey, and without their constant support and encouragement, the completion of this thesis perhaps would have been an impossible task. I am very fortunate that I found many good friends who became like brothers. Mr. Abhishek Singh, Mr. Ambesh Kumar Jha, Mr. Arpan Kumar Mondal, Mr. Rasmi Ranjan Behera, Mr. Kishor Kumar Gajrani, Mr. Mahesh Patel, Mr. Mukul Parmananda, Mr. Purnendu Kumar Mandal and Mr. Rahul Kesarwani, are few of the many close friends. I am also thankful to co-authors in my work Mr. A. S. Arjun Raj and Mr. Deepu kumar for their contribution.

Lastly, I would also like to acknowledge the contribution of office staff, for helping me with various academic as well as non-academic issues. I consider myself privileged and fortunate to work in the Indian Institute of Technology Guwahati.

Above all, I am thankful to the Almighty.

17th January, 2018 Sachin Singh

ABSTRACT

Finishing is the final operation performed in most of the manufacturing processes. Finishing operations costs as much as 15 % of the total manufacturing cost in a production cycle. In the finishing process, the main criterion is to achieve (minimal) better surface roughness. Surface roughness plays a vital role in deciding the overall functionality of the component during its life span. Smaller the component size more is the effect of surface roughness in determining its functioning. Traditional abrasive finishing processes are used to finish simple components geometries. However, advancement in technology necessitates the use of components made of difficult to finish materials having complex external and internal surface features. Due to the process limitations, traditional finishing processes cannot be used for finishing such components. To overcome the limitations of traditional finishing processes in meeting the modern manufacturing industries demands, several advanced finishing processes are developed by researchers.

Abrasive flow finishing (AFF) process is an advanced finishing process used for finishing of macro and micro features. In the literature several researchers developed various AFF setups, but flexibility of using same setup for finishing of macro featured and micro featured components is limited. Not much attention is paid on finishing surgical stainless steel cylindrical tubes with the help of AFF process. Limited literature is available on finishing of micro features (microholes and microslots) by AFF process. Detailed study in the field of modeling AFF process during finishing of macro features is unavailable. Also, no such modeling for AFF process is done in the field of micro features.

In the current thesis a flexible AFF setup (can be used for finishing macro as well as micro features of workpieces) is designed and fabricated. Economic AFF medium is developed in-house to replace the commercially used expensive AFF medium. Various medium compositions are made for finishing of macro and micro features. Detailed rheological study (static and dynamic) of the developed medium is carried out with the help of parallel plate rheometer.

Current work includes detailed experimental study of the AFF process during finishing of surgical stainless steel (SS 316L) workpieces with macro to micro features. Tubes with an internal diameter of 12.70 mm, microslots with width 440 ± 10 µm and microholes having radius 425 ± 15 µm are finished with the help of developed AFF setup and medium. Surface topography of the initial and finished workpiece surface is studied with the help of non-

contact type profilometer and scanning electron microscope. The best surface roughness obtained is 48 nm, 192 nm and 130 nm during finishing of tubes, microslots and microholes respectively.

Finite element model of the viscoelastic medium during finishing of tubes, microslots and microholes are developed to evaluate the finishing stresses developed during the medium flow. The major development of the analysis is the incorporation of experimentally measured rheological properties of the medium as input. The predicted values of finishing stresses by these models are more accurate compared to the existing models. Surface roughness simulation models are also proposed in this work to predict the surface roughness achieved on the workpiece surface during the AFF process. Developed simulation models are computationally less expensive. Incorporation of the real initial surface roughness profile and abrasive with multiple cutting edges are the major novel points of the simulation model. With a maximum error of 13 %, 7 % and 8 % there is a good agreement between the simulated and experimentally obtained values of percentage change in surface roughness during finishing of tubes, microslots and microholes.

TABLE OF CONTENTS

LIST OF FIGURES

LIST OF TABLES

NOMENCLATURES

A_s (mm^2)	Cross sectional area of the workpiece
C (%)	Wt. % of the abrasive particles in the medium
D (s^{-1})	Rate of deformation tensor
D_{apj} (mm)	Diameter of j^{th} abrasive particle
D_{idj} (mm)	Indentation diameter of j^{th} abrasive particle
d_{hm}(mm)	Diameter of the holes in the medium cylinder flange
d_{im} (mm)	Internal diameter of the medium cylinder
d_{major} (mm)	Major diameter of bolt
d_{minor} (mm)	Minor diameter of bolt
d_{ocr} (mm)	Outer diameter of the connecting rod at the hydraulic cylinder rod end
d_{om} (mm)	Outer diameter of the medium cylinder
d_{pm} (mm)	Pitch circle diameter of the holes in the medium cylinder flange
E_s (GPa)	Young's modulus of AISI 1040 steel
F (N)	Maximum force on the flange of the hydraulic cylinder
F_n, F_s (N)	Normal and tangential forces
F_{Rj} (N)	Average radial force acting on j^{th} abrasive particle
f (N. m^{-3})	Internal forces per unit volume
H_s (mm)	Height of the supporting plate
I	Identity tensor
$I.D._{sr}$ (mm)	Internal diameter of the supporting rod
I_{sr} (mm^4)	Moment of inertia of the supporting rod
L (mm)	Total length of medium that goes through workpiece in one stroke length
L_m (mm)	Medium cylinder length
L_{ms} (mm)	Length of the microslot
L_s (mm)	Length of AFF stroke
L_{sp} (mm)	Length of the supporting plate
L_{sr} (mm)	Length of supporting rod
l_p (mm)	Total length of the piston
M_j (mm)	Maximum positive difference between the Z coordinates of j^{th} abrasive particle cutting edge and the corresponding Z coordinates of the roughness peak at with same Y coordinate
m_{mh}	Number of microhole per workpiece
m_{ms}	Number of microslot per workpiece
N_{bolts}	Total number of bolts

N_{tmaxj}	Maximum numbers of cutting edges of the j^{th} abrasive particle that can take part in the cutting action of roughness peak
n_r	Number of rings
$O.D._{sr}$ (mm)	Outer diameter of the supporting rod
P(MPa)	Internal pressure acting on medium cylinder wall
P_{acting} (N)	Tensile load acting on each supporting rod
$P_{bapplied}$ (N)	Maximum load that can be carried by N_{bolts}
P_{cl} (N)	Maximum crippling load carried by the supporting rod
$P_{crushing}$ (MPa)	Crushing stress generated due to the tensile load on each supporting rod
P_{safe} (MPa)	Safe crippling load
p (MPa)	Hydrostatic pressure
$R_{A,}$ R_B (mm)	Range for the radius of normally distributed abrasive particles
R_a (µm)	Experimental value of surface roughness
R_{as} (µm)	Simulated value of surface roughness
R_{cj} (µm)	Critical surface roughness of the workpiece
R_m (mm)	Radius of medium cylinder
R_{mean} (mm)	Mean radius of the abrasive particle
R_{mh} (mm)	Radius of microhole
R_{pj} (mm)	Radius of the j^{th} abrasive particle
R_t (mm)	Radius of the cylindrical tube
T (Pa)	Total extra stress tensor
t_{ap} (mm)	Axial thickness of the piston ring
t_{hp} (mm)	Piston head thickness
t_{fm} (mm)	Thickness of the medium cylinder flange
t_j (mm)	Maximum indentation depth of j^{th} abrasive particle
t_m (mm)	Wall thickness of medium cylinder
t_{rp} (mm)	Radial thickness of the piston ring
$\hat{U}$ (m. s^{-1})	Velocity vector
V_n , V_s (m. s^{-1})	Normal and tangential velocities
V_m (mm^3)	Volume of medium cylinder
W (mm)	Width of the fractioned medium volume
W_{ms} (mm)	Width of the microslot
X_0 (j), Y_0 (j), Z_0 (j)	Center coordinates of the j^{th} abrasive particle
y_{ir}	Y coordinate of the i^{th} roughness peak
y_{kaj}	Y coordinate of the k^{th} cutting edge of j^{th} abrasive particle

z_{ir}	Z coordinate of the i^{th} roughness peak
z_{kaj}	Z coordinate of the k^{th} cutting edge of j^{th} abrasive particle
z_m (mm)	Maximum height of the roughness peak at a particular AFF stroke
$\% \Delta R_a$	Percentage change in experimental value surface roughness
$\% \Delta R_{as}$	Percentage change in simulated value surface roughness
α	Material constant
λ (s)	Relaxation time
τ (Pa)	Extra stress tensor
ρ_a (kg. mm^{-3})	Density of the abrasive particles
ρ_c (kg. mm^{-3})	Density of the carrier medium
ρ_m (kg. mm^{-3})	Density of the medium
σ_d (mm)	Standard deviation of the radius of normally distributed abrasive particles
σ_{dm} (MPa)	Design stress for medium cylinder material
σ_{dp} (MPa)	Design stress for piston material
σ_p (Pa)	Purely viscoelastic component of extra stress tensor
σ_s (Pa)	Purely viscous component of extra stress tensor
$\overset{\nabla}{\sigma}_p$	Upper-convected derivative of viscoelastic extra stress tensor
σ_{yp} (MPa)	Yield strength of piston material
σ_R (MPa)	Average radial stress generated in the medium
σ_{tbolt} (MPa)	Maximum tensile stress acting on each bolt
σ_{ys} (MPa)	Yield strength of AISI 1040 steel
η_1(Pa. s)	Viscosity factor for the viscoelastic component of the extra stress tensor
η_2 (Pa. s)	Viscosity factor for purely viscous component of the extra stress tensor

List of Abbreviations

AFF	Abrasive flow finishing
SS	Stainless steel
FE	Finite element
CFD	Computation fluid dynamics
2-D	Two dimensional
3-D	Three dimensional
BHN	Brinell hardness number
EDµM	Electrical discharge micro machining
CCRD	Central composite rotatable design

APPENDIX A

Table Values of various constants used during surface roughness simulation

Hardness of the workpiece material	209 BHN
Radius of cylindrical tubes (mm)	6.35
Width of the microslot (mm)	0.450
Radius of microholes (mm)	0.425
Radius of medium cylinder (mm)	30
Stroke length (mm)	68
Mesh size range of the abrasive particle used during simulation (μm)	170 - 190
Density of abrasive particles (kg/m^3)	3220

APPENDIX B

Table *Simulated value of surface roughness at various combinations of abrasive flow finishing parameters obtained after finishing of tubes.*

S. No.	Exp. No.	Factors			Simulated surface roughness		
		P	N	W	Initial R_{as} (µm)	Final R_{as} (µm)	% ΔR_{as}
1	4	5.00	550	45.00	0.630	0.037	94.127
2	15	4.50	500	50.00	0.670	0.037	94.478
3	9	3.70	500	50.00	0.580	0.188	67.586
4	13	4.50	500	41.60	0.540	0.077	85.741
5	20	4.50	500	50.00	0.540	0.044	91.926
6	8	5.00	550	55.00	0.650	0.031	95.231
7	6	5.00	450	55.00	0.600	0.040	93.333
8	19	4.50	500	50.00	0.570	0.036	93.684
9	18	4.50	500	50.00	0.520	0.040	92.308
10	11	4.50	416	50.00	0.570	0.076	86.667
11	5	4.00	450	55.00	0.570	0.066	88.421
12	7	4.00	550	55.00	0.580	0.045	92.241
13	12	4.50	584	50.00	0.620	0.038	93.871
14	14	4.50	500	58.40	0.600	0.038	93.667
15	16	4.50	500	50.00	0.540	0.041	92.407
16	10	5.30	500	50.00	0.650	0.035	94.615
17	17	4.50	500	50.00	0.640	0.032	95.000
18	1	4.00	450	45.00	0.550	0.133	75.818
19	2	5.00	450	45.00	0.580	0.068	88.276
20	3	4.00	550	45.00	0.540	0.081	85.000

Table *Analysis of variance for simulated percentage change in surface roughness obtained after finishing of tubes.*

Source	$\% \Delta R_{as}$		
	F-Value	**p-value Prob> F**	**% Contribution**
Model	20.41	< 0.0001*	
A-P	105.43	< 0.0001*	54.79
B-N	30.88	0.0002*	16.05
C-W	27.81	0.0004*	14.45
AB	0.60	0.4577	0.31
AC	2.43	0.1499	1.26
BC	0.53	0.4818	0.28
A^2	14.47	0.0035*	7.52
B^2	2.52	0.1432	1.31
C^2	0.62	0.4500	0.32
Lack of Fit	1.11	0.253	

Table *Simulated value of surface roughness at various combinations of abrasive flow finishing process input parameters obtained after finishing of microslots.*

S. No.	Exp. No.	Factors			Simulated surface roughness		
		P	N	W	Initial R_{as} (µm)	Final R_{as} (µm)	% ΔR_{as}
1	11	4.50	17	45.00	3.56	0.46	87.08
2	9	3.70	25	45.00	3.60	0.54	85.00
3	14	4.50	25	53.40	3.51	0.15	95.73
4	13	4.50	25	36.60	3.49	0.54	84.53
5	18	4.50	25	45.00	3.49	0.29	91.69
6	8	5.00	30	50.00	3.44	0.13	96.22
7	17	4.50	25	45.00	3.49	0.32	90.83
8	6	5.00	20	50.00	3.59	0.25	93.04
9	10	5.30	25	45.00	3.51	0.19	94.59
10	15	4.50	25	45.00	3.40	0.29	91.47
11	16	4.50	25	45.00	3.43	0.25	92.71
12	7	4.00	30	50.00	3.42	0.23	93.27
13	5	4.00	20	50.00	3.49	0.52	85.10
14	4	5.00	30	40.00	3.50	0.25	92.86
15	2	5.00	20	40.00	3.55	0.36	89.86
16	3	4.00	30	40.00	3.43	0.58	83.09
17	20	4.50	25	45.00	3.40	0.28	91.76
18	12	4.50	33	45.00	3.57	0.21	94.12
19	1	4.00	20	40.00	3.58	0.65	81.84
20	19	4.50	25	45.00	3.57	0.32	91.04

Table *Analysis of variance for simulated percentage change in surface roughness obtained after finishing of microslots.*

Source	$\% \Delta R_{as}$		
	F-Value	**p-value Prob> F**	**% Contribution**
Model	23.13	< 0.0001*	
A-P	86.99	< 0.0001*	40.71
B-N	33.46	0.0002*	15.66
C-W	67.11	< 0.0001*	31.40
AB	0.74	0.4099	0.35
AC	3.19	0.1044	1.49
BC	4.00	0.0734	1.87
A^2	6.46	0.0292*	3.02
B^2	3.42	0.0941*	1.60
C^2	5.28	0.0445*	2.47
Lack of Fit	3.07	0.1220	

*Significant terms

Table *Simulated value of surface roughness at various combinations of abrasive flow finishing process input parameters obtained after finishing of microholes.*

S. No.	Exp. No.	Factors			Simulated Surface roughness		
		P	N	W	Initial R_{as} (µm)	Final R_{as} (µm)	% ΔR_{as}
1	14	4.00	8.00	53.40	1.45	0.09	93.79
2	10	4.90	8.00	45.00	1.54	0.11	92.86
3	8	4.50	10.00	50.00	1.41	0.06	95.74
4	9	3.20	8.00	45.00	1.45	0.23	84.14
5	4	4.50	10.00	40.00	1.28	0.11	91.41
6	12	4.00	11.50	45.00	1.33	0.10	92.48
7	11	4.00	4.50	45.00	1.48	0.21	85.81
8	6	4.50	6.00	50.00	1.34	0.12	91.04
9	3	3.50	10.00	40.00	1.34	0.25	81.34
10	18	4.00	8.00	45.00	1.34	0.11	91.79
11	16	4.00	8.00	45.00	1.53	0.16	89.54
12	2	4.50	6.00	40.00	1.26	0.16	87.30
13	15	4.00	8.00	45.00	1.39	0.14	89.93
14	20	4.00	8.00	45.00	1.40	0.14	90.00
15	7	3.50	10.00	50.00	1.42	0.13	90.85
16	5	3.50	6.00	50.00	1.47	0.19	87.07
17	17	4.00	8.00	45.00	1.44	0.16	88.89
18	1	3.50	6.00	40.00	1.43	0.26	81.82
19	13	4.00	8.00	36.60	1.55	0.22	85.81
20	19	4.00	8.00	45.00	1.30	0.11	91.54

Table *Analysis of variance for simulated percentage change in surface roughness obtained after finishing of microholes.*

Source	$\% \Delta R_{as}$		
	F-Value	**p-value Prob> F**	**% Contribution**
Model	26.83	< 0.0001*	10.99
A-P	101.70	< 0.0001*	41.66
B-N	34.67	0.0002*	14.20
C-W	83.37	< 0.0001*	34.15
AB	2.58	0.1395	1.06
AC	4.63	0.0569	1.90
BC	2.07	0.1812	0.85
A^2	8.16	0.0170*	3.34
B^2	5.01	0.0491*	2.05
C^2	1.24	0.2923	0.51
Lack of Fit	0.70	0.6487	

*Significant terms

Chapter 1

INTRODUCTION AND LITERATURE REVIEW

1.1 Introduction

Finishing is the final operation performed in most of the manufacturing processes. Finishing operations costs as much as 15 % of the total manufacturing cost in a production cycle [1]. In

the finishing process, main criteria is to achieve (minimal) better surface roughness. Surface roughness plays a vital role in deciding the overall functionality of the component during its life span. Smaller the component size more is the effect of surface roughness in determining its functioning. Components with fine surface roughness possess the following advantages:-

- Wear resistant,
- Improved fatigue life,
- Less prone to vibration,
- Corrosion resistant,
- Aesthetic appearance and other.

Traditional abrasive finishing processes are used to finish components with simple geometries. However, advancement in technology necessitates the use of components made of difficult to finish materials having complex external and internal surface features. Due to the process limitations, traditional finishing processes cannot be used for finishing such components. Even if traditional finishing processes are employed, those are uneconomical. In such cases for a surface finish less than one micron, the manufacturing cost escalates very sharply because of expensive equipment requirement and need of trained workers for achieving such fine surface roughness. To overcome the limitations of traditional finishing processes in meeting the modern manufacturing industries demands, several advanced finishing processes are developed by researchers. Abrasive flow finishing (AFF), magnetic abrasive finishing (MAF), magnetic float polishing (MFP) magnetorheological finishing (MRF) and magnetorheological abrasive flow finishing (MRAFF) are some of the advanced finishing processes developed over last few decades.

1.2 Traditional abrasive finishing processes

Owing to simplicity and ease of operation, traditional finishing processes are widely used for finishing of macro components with simple geometric features (flat, cylindrical, etc.). In such processes, a small amount of material is removed by a number of abrasive particles of indefinite shape and size. The abrasive particles can be in bonded (grinding, honing) and unbounded (lapping) form, depending on the suitable traditional finishing process that is employed.

1.2.1 Grinding

Grinding is an abrasive finishing process which uses the multi-point cutting tool composed of abrasive particles. The tool can be in the form of the wheel, stick or any other shape. Surface

roughness obtained by grinding process lies between 0.1 µm to 0.75 µm [2]. However, some of the disadvantages of grinding process are frequent truing and dressing of grinding wheel. Also, heat produced during the grinding process is about 1500 ºC that leads to the development of thermal stresses, thermal cracking and micro-structural changes on the workpiece surface.

1.2.2 Honing

Honing is one of the finishing processes in which both rotary and reciprocating motion is imparted to the tool (hone). It produces a precise workpiece surface finish by abrasive action of abrasive particles on hone. Honing process can achieve surface roughness in the range of 0.02 to 0.32 µm [2]. Due to the process characteristics, it is helpful in limited applications. The process faces difficulties in improving the straightness of the hole, also glazing and loading of honing sticks occurs.

1.2.3 Lapping

Lapping process uses loose abrasive particles for finishing of workpiece. Smoothing of the workpiece surface is achieved by abrasion of abrasive particles, with the help of lap. Particular attention is paid to the selection of the lap, as too hard a lap can cause excessive and rapid wear of abrasive particles, while a soft lap causes the abrasive particles embedded deeply in the lap material. In both the cases, it harms the proper finishing of the workpiece surface. Lapping operation can achieve surface roughness in the range of 0.01 µm to 0.63 µm [2].

1.3 Advanced abrasive finishing processes

Recent advancement in technology is mainly possible due to the revolutionized and automated manufacturing industry. Modern industries such as the automobile, aerospace, medical, missiles, and defense require advanced materials with superior properties compared to commonly used material in terms of strength, hardness and temperature resistance. Also, the modern product requires finishing of complex inaccessible features, with tight tolerances and good surface integrity. Most of the traditional finishing processes employ pre-defined movement of the tool with respect to the workpiece. This is the biggest limitation of the traditional abrasive finishing processes. Also, in modern manufacturing industries, size of components and their geometric features is scaled down from macro to milli, micro and nano level. Finishing of such small components further adds to the limitations of the traditional abrasive finishing processes.

To meet the demands of the modern manufacturing industries several advanced abrasive finishing processes are developed. The advantage of such processes lays in the fact that during their operation there is no pre-defined movement of the tool with respect to workpiece. These processes employ loosely bonded abrasive particles for shearing of the surface roughness peaks which are mixed in an easily deformable carrier (medium). Such processes are capable of finishing soft to hard materials. Also, the workpieces with simple to complex and free form geometries can be easily finished by advanced abrasive finishing processes. Advanced finishing processes are mainly divided into two categories viz. magnetic field assisted advanced finishing (MFAAF) processes and non-magnetic field assisted advanced abrasive finishing (N-MFAAF) processes. MFAAF processes use the magnet (permanent, electromagnet) for the generation of the magnetic field which acts as finishing forces. On the other hand, N-MFAAF processes don't require the magnetic field to assist in the generation of finishing forces.

1.3.1 Magnetic field assisted advanced abrasive finishing processes

Advanced abrasive finishing process such as Magnetic abrasive finishing (MAF), Magnetic float polishing (MFP), Magnetorheological finishing process (MRF) and Magnetorheological abrasive flow finishing (MRAFF) falls in the category of MFAAF processes.

1.3.1.1 Magnetic abrasive finishing process

Magnetic abrasive finishing (MAF) process is developed to finish tubes and flat workpieces made up of hard to machine material.

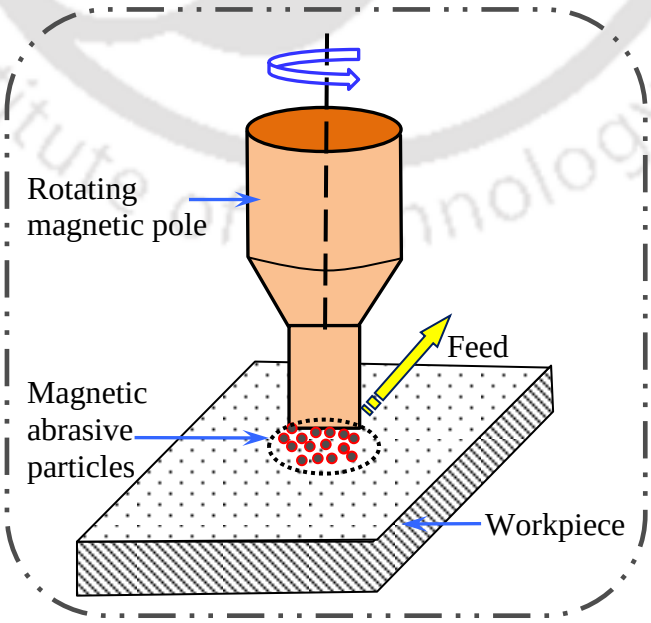

Fig. 1.1 *Schematic diagram of magnetic abrasive finishing process.*

This process employs the use of ferromagnetic particles (carbon iron particles, CIP's) mixed with fine abrasive particles (SiC, Al_2O_3, CBN or diamond) called as ferromagnetic abrasive particles (FAP or magnetic abrasive particles-MAPs). Fig. 1.1 shows the plane MAF process in which finishing action is carriedout by applying the magnetic field across the gap between workpiece and electromagnet. When the magnetic field is applied across the gap, MAPs forms a flexible magnetic abrasive brush (FMAB). This is due to the dipole-dipole attraction between the magnetic poles of MAPs along the magnetic lines of force. The abrasive particles get entangled in between the FMAB chains. This makes FMAB to behave as a multi-point cutting tool during shearing of the surface roughness peaks from the workpiece surface. MAF process is capable of achieving a surface finish of 7.6 nm on stainless steel [3, 4].

1.3.1.2 Magnetic float polishing process

Finishing of components with spherical geometry (e.g. bearing roller, ceramic balls) is carriedout by the magnetic float polishing (MFP) process.

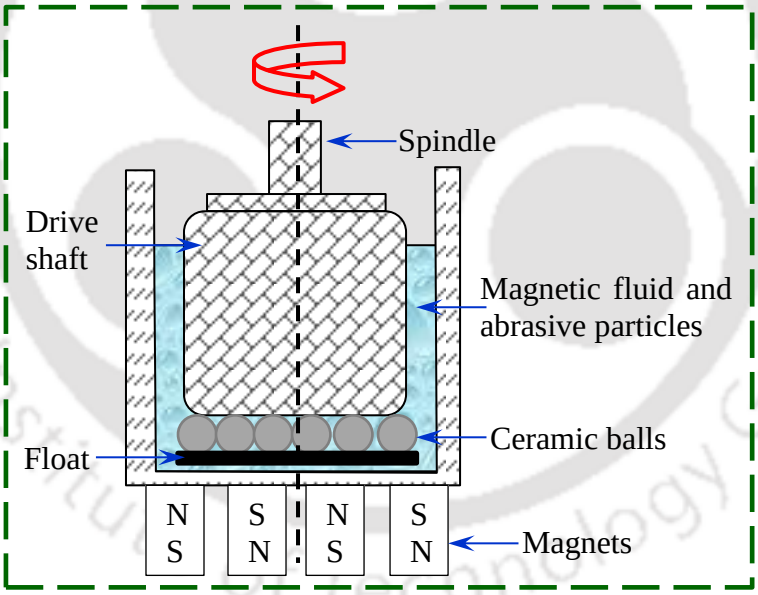

Fig. 1.2 *Schematic diagram of magnetic float polishing process.*

As shown in Fig. 1.2, MFP process setup consists of finishing chamber filled with magnetic fluid that contains abrasive particles, float and ceramic balls. At the bottom of the chamber, a set of strong electromagnets is arranged with alternate north and south poles. The basic principle of the MFP process is based on the ferro-hydrodynamic behaviour of the magnetic fluid under the influence of magnetic field. During the MFP process, magnetic fluid moves in the downward region of the chamber with strong magnetic field. Thus, an

upward buoyant force acts on abrasive particles, float and the ceramic balls that are non-magnetic in nature. The driven shaft then pushes the ceramic balls downwards till the desired level of force is reached. Due to the relative motion between ceramic balls and abrasive particles under the influence of levitation force, finishing on the ceramic balls is achieved. The best surface roughness obtained with MFP on the ceramic balls is 4 nm [5].

1.3.1.3 Magnetorheological finishing process

To overcome the difficulties in finishing high precision lenses made up of brittle materials such as glass which tends to crack during finishing, magnetorheological finishing (MRF) process is developed (Fig. 1.3).

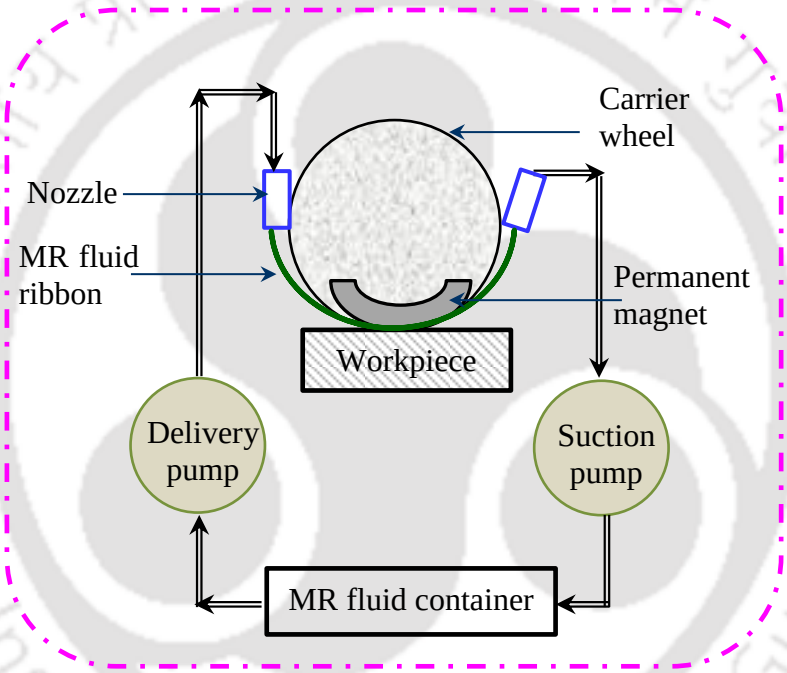

Fig. 1.3 *Schematic diagram of magnetorheological finishing process.*

MRF process relies on the use of a smart fluid known as "Magnetorheological (MR) polishing fluid". The fluid comprises of micron sized magnetizable particles (carbonyl iron particles-CIPs), nonmagnetic abrasive particles (NMAPs) dispersed in a non-magnetic carrier medium such as silicon oil, water, and mineral oil. Under the action of magnetic field, CIPs get magnetized and move closer to the carrier wheel with the high magnetic field. On the other hand, abrasive particles come in contact with the workpiece surface (lens) but remain intact with the carrier medium and CIPs. The normal magnetic force which is transferred by the CIPs to abrasive particles is responsible for abrasive particle penetration into workpiece surface. Material removal in the form of micro/nano chips takes place due to the relative

motion between the abrasive particle and workpiece surface. This process is capable of achieving the surface roughness in the ranges of 10-100 nm in optical lenses [6].

1.3.1.4 Magnetorheological abrasive flow finishing process

Magnetorheological abrasive flow finishing (MRAFF) (Fig.1.4) process is a hybrid technology. It is a combination of AFM (described in the later section) and MRF process. MRAFF process is developed to overcome the shape limitation problem of all the above described processes. It is similar to AFM process except the abrasive medium are entirely different. MRAFF uses a magnetically stiffened slug of MR fluid which is extruded back and forth through the passage formed by workpiece and fixture. When the magnetic field is applied to MR fluid, the CIPs form a columnar structure with abrasives embedded in between the chain and they shear roughness peak from the workpiece surface. The amount of extrusion pressure and bonding strength provided by magnetic field induced structure of MR fluid determines the amount of material which is sheared from the workpiece surface. The process is capable of achieving a surface roughness of 30 nm on stainless steel workpiece [7].

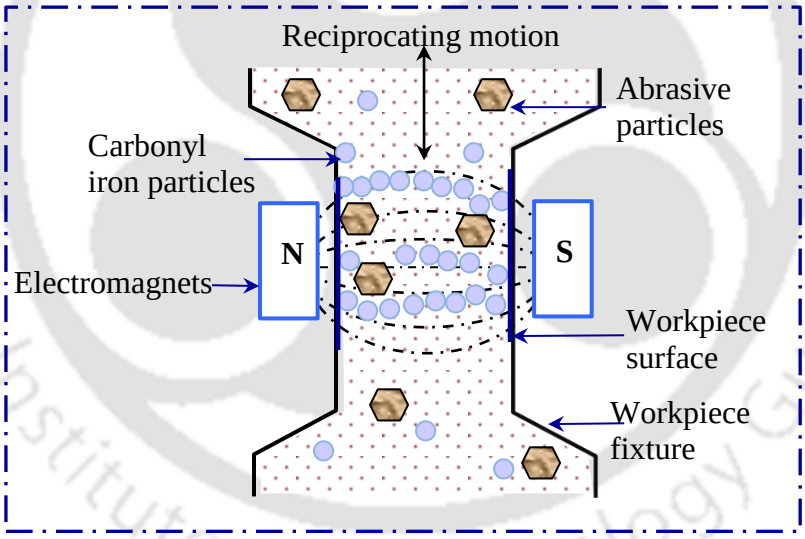

Fig. 1.4 *Schematic diagram of magnetorheological abrasive flow finishing process.*

1.3.2 Non-magnetic field assisted advanced abrasive finishing processes

N-MFAAF processes are the ones that don't involve magnetic field to assist during the finishing process. Finishing forces in such operations can be chemical and mechanical in nature.

1.3.2.1 Chemical mechanical polishing process

Semiconductor industry faces the problem of non-desirable micro/nano scratches on the surface of devices. Also, thin wafers suffer from the problem of planarization. To address

such issues researchers developed chemical mechanical polishing (CMP) process (Fig. 1.5). CMP process involves the combination of chemical and mechanical action. Initially, a chemical reaction takes place between the silica slurry and workpiece material. Later, products of the chemical reaction are removed by mechanical (abrasion) action. The wafer containing abrasive particles (e.g. silica sols) is pressed down by force and rotated against the polishing pad for the removal of reaction products as well as shearing of leftover roughness peaks. CMP is capable of achieving the surface roughness of around 1.16 Å on titanium dioxide thin film [8].

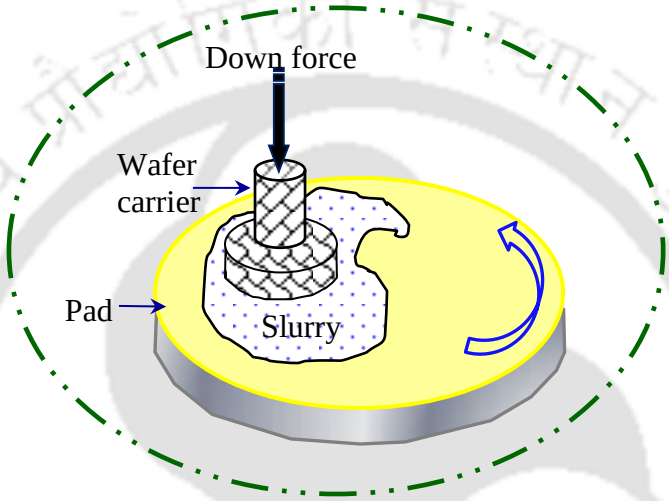

Fig. 1.5 *Schematic diagram of chemical mechanical polishing process.*

1.3.2.2 Abrasive flow finishing process

Abrasive flow finishing (AFF) is an advanced finishing operation that is performed to achieve high surface quality on internal and external difficult to finish surface features. AFF was developed by the extrude hone corporation, USA in 1960's to find a more effective method of deburring hydraulic control blocks, which were deburred by hand at that time. Since deburring is a machining process so it is called as "Abrasive flow machining" (AFM) process. By 1968, the process was successfully developed by Extrude Hone Corporation. Later on, AFM is being used in a vast number of fields for nano-finishing, thus it is referred presently as "Abrasive flow finishing" (AFF) process. AFF is gaining importance because of its ability to give predictable, repeatable and consistent results [1].

1.3.2.2.1 Working principle

Principal components of the AFF setup are upper-lower medium cylinders with pistons, hydraulic drive with hydraulic cylinders, workpiece fixture and supporting frame (Fig. 1.6). The workpiece to be finished is held securely by the fixture and placed in space between the

upper and lower medium cylinders. The primary function of the medium cylinder is to possess the abrasive medium and reciprocate it uniformly across the workpiece surface. AFF process is analogues to the grinding process. Except that in AFF process grinding wheel is replaced by the flexible medium. During the extrusion process, medium becomes a self-forming semisolid that covers the workpiece shape and helps in finishing.

At the start of AFF experiment, usually lower medium cylinder is filled with medium while the upper medium cylinder is empty or nearly empty. Under the action of an external force hydraulically or mechanically the medium is extruded across restricted passage through or past workpiece surface to be finished. After lower medium cylinder discharges whole medium to upper medium cylinder, upper medium cylinder's piston begins to push the medium back to lower medium cylinder. This completes one AFF cycle, back and forth motion of the medium across workpiece continues till the desired surface roughness on workpiece surface is achieved. The advantage of AFF process lays in the fact that it can easily finish workpieces with complex geometries by proper designing of tooling. Thus, the medium can be guided to the selected portion of workpiece that is to be finished.

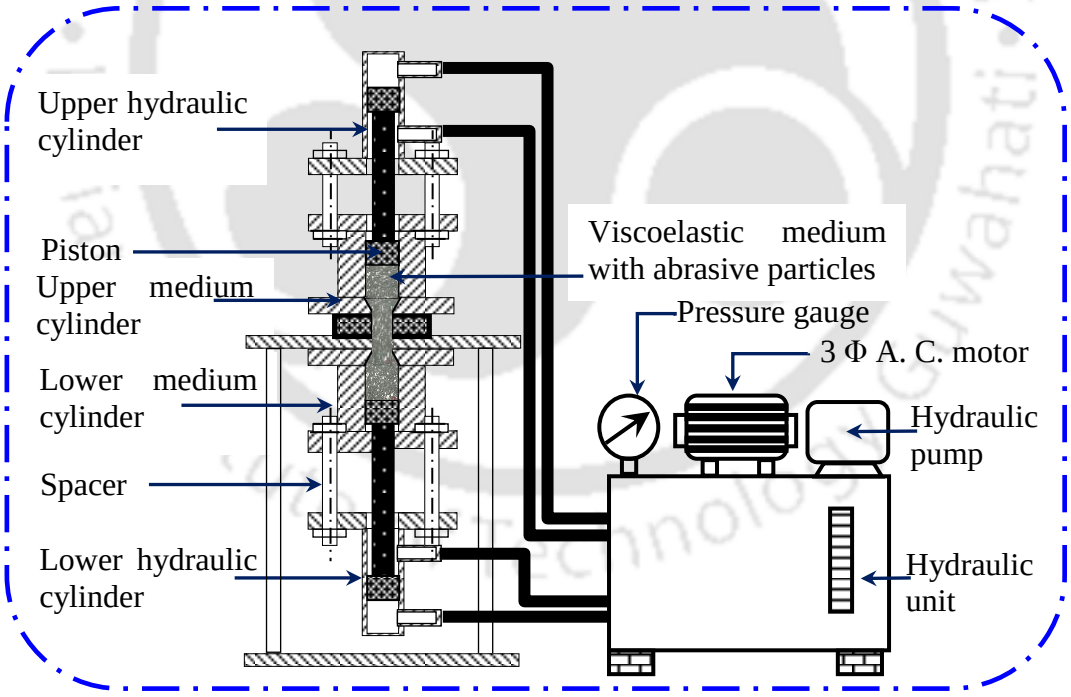

Fig. 1.6 *Schematic diagram of abrasive flow finishing process.*

1.3.2.2.2 Important elements of the abrasive flow finishing process

AFF process mainly comprises of the following four elements, experimental setup, tooling, medium and workpiece as explained in the following subsections:-

i. AFF process setup

AFF process setup is designed according to requirements of the workpiece to be finished. Main elements of the AFF process setup are medium cylinders, hydraulic cylinders, fixture and power supply (hydraulic, mechanical). These components are arranged in vertical or horizontal configuration based on the job requirement and comfort of manufacture.

ii. Tooling

As shown in Fig. 1.7 (a), tooling is used to hold the workpiece tightly in position without leakage of the abrasive medium through it during the AFF process. Tooling is designed keeping in view geometry of the workpiece that to be finished. It directs the flow of the medium across areas of workpieces that to be finished while restricts in the areas that doesn't require finishing.

iii. Medium

AFF medium plays a vital role in the finishing of workpiece. Medium mainly consists of the base polymer, additives (plasticizers, softeners) and abrasive particles. A good AFF medium possesses properties such as mechanically stable, chemically non-reactive, self-deformable, good fluidity and better abrading ability. Here, each abrasive particle acts as a miniature cutting tool. The material from the workpiece surface is removed by mechanical abrasion in form of small chips that are invisible by naked eyes. Medium act as a 'self-deformable stone' and it takes the shape of workpiece when it is extruded through the confined pathway. Due to self-deformability of the medium, it is able to finish 3-D complex shaped components which are not possible otherwise. It is the rheological property of the medium along with other AFF input parameters (extrusion pressure, number of AFF cycles) decides the achievable surface roughness on the workpiece.

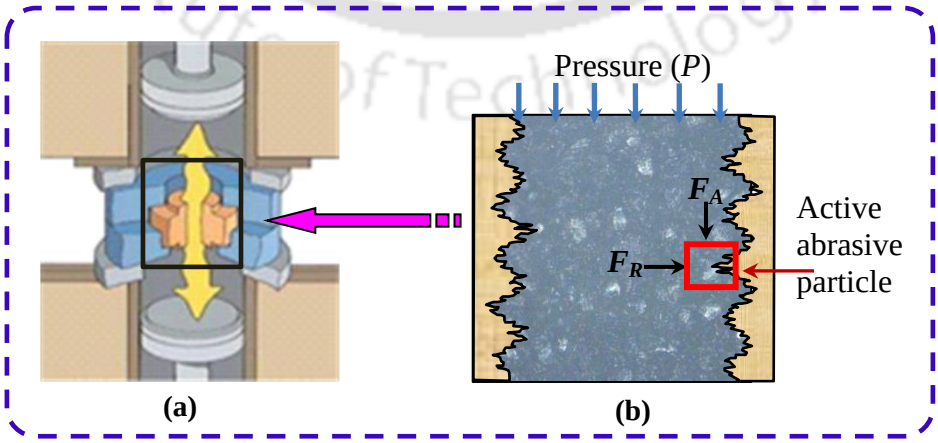

Fig. 1.7 *Schematic diagram showing* ***(a)*** *tooling* ***(b)*** *various finishing forces acting on the medium during its extrusion through the workpiece passageway.*

The base polymer chosen as AFF medium possesses dominating elastic and partial viscous properties. When extrusion pressure (P) is applied on the medium, the elastic component results in the generation of radial force (F_R) while viscous component generates axial force (F_A). The base polymer with other rheological additives acts as a flexible binder to hold abrasive particles and transmit forces developed on the medium to the active abrasive particles. F_R is responsible for indentation of abrasive particles into the workpiece surface while F_A pushes the indented abrasive particle in the axial direction to remove the material by microploughing or microcutting action (Fig. 1.7(b)).

iv. Workpiece

The importance of AFF process lays in its capability to finish components with simple to intricated geometries made up of soft aluminium to tough carbides, ceramics, etc. Components with macro features such as common rail pipes, extrusion dies are finished by the AFF process. Currently, the emphasis is on using AFF process for finishing of micro features in components such as micro holes in turbine blades, diesel injector nozzles, and stents.

1.3.2.3 Recent advances in abrasive flow finishing process

Various researchers modified the basic AFF process in various hybrid processes. Their main aim is to improve the efficiency of AFF process in terms of material removal rate (MRR) and final surface roughness.

i. Electrochemically assisted abrasive flow machining process

Electrochemically assisted abrasive flow machining (ECAFM) process is the combination of abrasive flow machining process and electrochemical machining. ECAFM process replaces the polymer medium of the AFM process by polymeric electrolytes (polypropylene glycol and polyethylene glycol) mixed with abrasive particles. During the ECAFM process, the polymeric electrolyte is forced to flow between workpieces which act as electrodes. Dabrowski et al. [9, 10] proved MRR in ECAFM process is more compared to the AFM process. This is mainly due to double advantageous of ECAFM process in which surface roughness improvement is taking place due to the microcutting and dissolution of the anode workpiece.

ii. Centrifugal force assisted abrasive flow machining process

In centrifugal force assisted abrasive flow machining (CFAAFM) process, a centrifugal force generating (CFG) rod is introduced in the tooling. The centrifugal force that is

generated by the CFG rod adds up with the AFF finishing forces (F_R, F_A) and together enhances the efficiency [11, 12]. Experiments proved that changing shape and velocity of the CFG rod influences the CFAAFM process output responses.

iii. Rotational abrasive flow finishing process

To enhance the performance of the AFF process, Sankar et al. [13, 14] modified to rotational abrasive flow finishing (R-AFF) process. In R-AFF process, the tooling is externally rotated and the medium reciprocates inside it. So, abrasive particle travels in the helical path during R-AFF process as compared to its straight path during the AFF process. This increases the length of their finishing path. During R-AFF process as the rotational speed of the workpiece increases, abrasive particle hit workpiece surface with high velocity. Secondly, an extra component of force (tangential force) adds to the finishing forces (F_R, F_A) generated during AFF process. Thus, surface improvement in case of R-AFF process increases as compared to AFF process.

iv. Drill bit guided abrasive flow finishing process

In drill bit guided abrasive flow finishing (DBG-AFF) process, a freely rotatable drill bit is placed with the help of a special fixture plates in the workpiece finishing zone [15]. Drill bit not only provides random motion to abrasive particles in the medium but also causes the frequent reshuffling of medium. Presence of drill bit increases pressure on the abrasive particles due to increase in restriction on the medium in finishing zone and enhances the productivity of the DBG-AFF process.

v. Ultrasonic assisted abrasive flow machining process

In ultrasonic assisted abrasive flow machining (UAAFM) process, the workpiece is provided a mechanical vibration orthogonally to the medium flow direction. UAAFM consists of a piezo actuator that generates the frequency in the range of 5-200 kHz and a specially designed fixture. The performance of UAAFM process is improved due to the increased relative speed of the abrasive particles with which they hit the workpiece surface. Also, the magnitude of the finishing forces acting on abrasive particle increases due to the ultrasonic vibration of workpiece [16, 17].

1.4 Literature review

Various researchers developed AFF setup, tooling, and medium for finishing the components with macro features. A considerable amount of work in the field of experimental study modeling of the AFF process during macro features finishing is reported in the literature. Few

researchers also reported experimental studies related to finishing of components with micro features by AFF process. The following sub-section describes the work done in various fields of the AFF process.

1.4.1 Design and development of abrasive flow finishing process setups

Based on the macro components geometry to be finished various types of AFF setups are designed. Recently, due to the increased demand of the finely finished components with micro features in various fields (i.e., aerospace, medical), limited research is carriedout on finishing of components with micro features.

i. Designed and development of AFF process setup for finishing of macro featured components

The invention of AFF setup is an improvement over the commonly used finishing methods and apparatus used for finishing components. The main purpose is to achieve an effective means of removing burrs from the interior and exterior surfaces as well as, to improve the surface roughness of components with inaccessible cavities. AFF process can also generate radiusing on the sharp edges of the component which can't be achieved by traditional finishing process. As shown in Fig. 1.8(a), McCarty [18] invented AFF setup in which the workpiece is held in between two medium cylinders. Through the workpiece passage, the medium is extruded from one cylinder to another via reciprocating motion of the pistons. An improved AFF setup is invented by Minear and Nokovich [19]. They emphasized to provide a very rugged support for the extruding chamber on both sides of the workpiece and to incorporate firm clamping of the workpiece between the medium cylinders (Fig. 1.8(b)). Rhoades [20] invented AFF setup for finishing of volute casings of centrifugal pumps. He also designed a restrictive fixture in order to achieve uniform surface finish throughout the casing surface. Rhoades [21] invented reversible unidirectional AFF setup for finishing workpieces with complex geometries (e.g. cylinder heads having multiple intakes and/or exhaust valve per cylinder) (Fig. 1.8(c)). There is a pair of extrusion chamber and the workpiece is attached to one the chamber. Medium is extruded through the workpiece and is allowed to fall in the other chamber. In this setup, one extrusion chamber remains ideal at a time which possesses excessive equipment cost. So, Rhoades [22] further invented a new unidirectional AFF setup in which finishing is achieved by using only one extrusion chamber (Fig. 1.8(d)). The medium after extrusion from the chamber is allowed to collect in the same chamber with the help of gravity by using a collector at the top of chamber. For finishing of workpiece surfaces with large complex edges (injection mold

cavities, gear wheels, turbine blades) Rhoades [23] invented orbital AFF setup which does not involve direct extrusion of abrasive medium through the workpiece is called as orbital AFF. A closed chamber is formed by placing a displacer member adjacent to the workpiece. Relative motion is then created between displacer member and the workpiece to achieve the required finishing action on the workpiece.

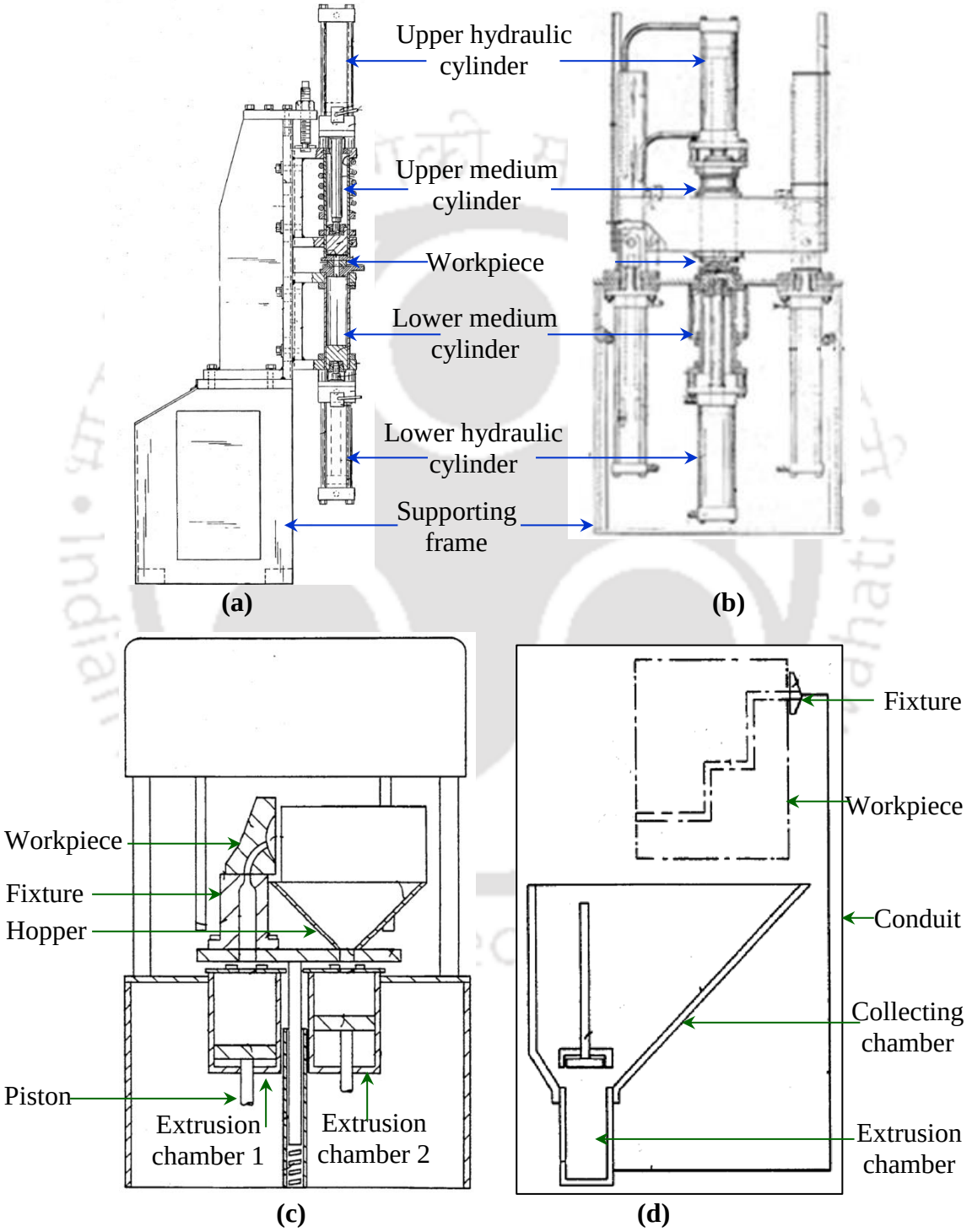

Fig. 1.8 *Central sectional view of AFF setup invented by* ***(a)*** *McCarty [18]* ***(b)*** *Minear et al. [19]* ***(c)*** *Rhoades [21]* ***(d)*** *Rhoades [22].*

Wu [24] developed an AFF process setup for finishing the silicon wafers. Researchers showed the advantages that AFF process possesses compared to CMP process for finishing silicon wafers. The developed AFF setup not only achieves good surface roughness, but also helps in planarization of the silicon wafers. Williams [25] developed an acoustic emission based mechanism for online monitoring AFF process. He developed a co-relation between the acoustic signals developed by workpieces undergoing finishing, medium flow rates and the amount of material removed from the workpiece surface. Liu et al [26] developed AFF process setup for finishing the complex internal surface of the common rail pipe used in common rail direct fuel injection system.

ii. Development of AFF process setup for finishing of micro featured components

Perry [27] developed AFF process setup and tooling for removing material from holes of sizes 20 mil to 1 mil in diameter (1 mil = 0.001 inch). Rhoades et al. [28] developed AFF setup for finishing orifices where the flow rate is of great importance such as fuel injector nozzle tips and turbine blade holes. The main objective of this invention is to attain a specific flow rate of orifice rather than the particular surface roughness. Medium used for finishing these small holes with AFF process can vary from high viscosity to low viscosity. Walch et al. [29] developed an AFF setup that can be used for a range of medium viscosities (1 centipoise to 1,000,000 centipoise) during finishing of orifices. Walch [30] developed an AFF setup with the control mechanism to maintain a constant flow rate and also provided a cooling system for maintaining the constant temperature of the medium. For polishing of micro-bores ranging from sizes 260-500 μm commonly found in various products such as biomedical filters, ink-jet printer nozzles, fuel injection nozzles, high pressure orifices, Yin et al. [31] designed and developed abrasive flow polishing machine. Li et al [32] developed AFF setup especially for finishing microhole found in injector nozzle. To check the reliability of the developed setup, static structural finite element (FE) analysis of various parts is carriedout.

1.4.2 Experimental study of abrasive flow finishing process

Experimental study on the AFF process is divided into two sections i.e., finishing of macro and micro featured components:

i. Experimental study of the AFF process during finishing macro featured components

To determine the factors that affect the MRR and surface roughness during AFF process, Loveless et al. [33] performed AFF experiments on flat workpieces. Authors showed that

AFF output responses not only depends on the various AFF process input parameters (extrusion pressure, abrasive particle size, medium viscosity) but also depend on the prior machining operation as well as initial surface roughness. Jain and Adsul [34] used aluminium and brass to show the role of workpiece hardness along with other AFF input parameters on output responses. Later, Gov et al. [35] carriedout the finishing of flat workpieces made up of hardened tool steel (AISI D2) of varying hardness and concluded that harder materials achieve finer surface roughness than softer ones. Kenda et al. [36] finished AISI D2 and showed that AFF process not only successfully finishes workpieces but also induces compressive residual stress on the workpiece surface. Not only hard metals but brittle materials such as ceramic are also successfully finished by the AFF process using diamond abrasive particle [37]. Gorana et al. [38] carriedout experimental determination of the finishing forces generated during AFF process with the help of dynamometer. Parametric study of AFF process during finishing of cylindrical workpieces is performed by various researchers. Cylindrical workpieces of different material such as cast iron [39], aluminium alloy 6063 [40] and inconel 600 [41] are successfully finished by AFF process. Williams et al. [42] did the experimental study on AFF of stereolithography components. Authors concluded that MRR during the finishing process is greatly affected by abrasive particle size and extrusion pressure. Later, Williams et al. [43] finished the laminated tooling prepared by the rapid tooling method with the help of AFF process. AFF process not only finishes homogenous material workpiece but also successfully finishes heterogeneous material workpieces. This is proved by Sankar et al. [44] and Sushil et al. [45] by finishing metal matrix composite (MMCs) by AFF process. AFF process proved its potential by finishing the components with complex features. Kim et al. [46] carriedout AFF experiments for finishing of spring collets. Authors showed that AFF successfully removed the burrs on the spring collets and SiC abrasive particles proved superior to Al_2O_3 abrasive particles during the experiments. Sarkar and Jain [47] reported finishing of freeform surfaces (Knee joint) using AFF process. Authors concluded that medium temperature is one of the key parameters in determining the final surface roughness on the workpiece. Wu and Gao [48] designed a simple AFF fixture for finishing the large bearing rings raceways (outer diameters of 200 mm and above). Blades of the blisk found in aero-engines are also finished by AFF process. Fu et al. [49] not only successfully finished the blades but also proposed improved fixture to attain uniform surface roughness after AFF process.

ii. Experimental study of the AFF process during finishing micro featured components

Tzeng at al. [50] finished microhole while Lin et al. [51] finished microslit machined on workpieces by using electrical discharge machining (EDM) process. Authors concluded that AFF process successfully removed the recast layer from the workpiece surfaces. Experimental investigation to study the effects of AFF process on direct injection (DI) diesel engine fuel injector nozzle is done by Jung et al. [52]. EDM process is mainly used to drill micro holes in fuel injector nozzles. Typical EDM for the injector nozzle leaves burrs and a rough surface along the hole wall. AFF process increases the performance of the nozzles by removing burrs and provides a smooth internal surface. Zhang et al. [53] used one way AFF process for finishing of microholes and studied the effect of medium viscosity and abrasive particle size on MMR. Li et al. [54] tried to increase the accuracy and efficiency of AFF process during finishing of microholes. Authors developed a system to control the piston speed during AFF process, which in turn determines the medium flow rate through the workpiece. Venkatesh et al. [55] finished microchannels with AFF process and concluded that extrusion pressure and medium viscosity are significant process parameters compared to processing time.

1.4.3 Medium development and its rheological study

AFF medium plays a vital role in the finishing of the workpiece. It is the rheology of the medium which determines pattern and aggressiveness of the abrasive action. Abrasive particle size in combination with extrusion pressure influences their depth of indentation into the workpiece surface, which in turn determines the workpiece surface roughness. Researchers developed various AFF medium compositions depending on the dimensions of the workpieces to be finished. High viscous medium is preferred for finishing workpieces with macro features while moderate to low viscous medium are appropriate to finish micro features.

i. Development and rheological study of medium for finishing macro featured components

Rheological study of the commonly used polyborosiloxane (PBS) as base polymer during AFF finishing operation is done by Hull et al. [56]. From the study author concluded that medium shows time dependent rheological behavior. Davies and Fletcher [57] did rheological study on three types of PBS base medium (low viscosity (LV), medium viscosity (MV) and high viscosity (HV). Fletcher and Firovanti [58] experimentally determined thermal conductivity, specific heat capacity and surface heat transfer coefficient

for various PBS and SiC abrasive particles mixtures. Viscosity of medium used during AFF process plays a vital role in determining the material removal and surface finish. Jain et al. [59] demonstrated the same by conducting AFF experiments at different medium viscosities. Author concluded that abrasive particle size, abrasive concentration and temperature significantly affect the medium viscosity. Abrasive polishing composition for finishing of complex workpieces produced by casting, forging, machining and like is developed by Gilmore [60]. Wang et al. [61, 62] developed abrasive medium to finish complex chain holes. Two types of polymer are used in the study, pure silicon rubber (P-silicon) and silicon rubber with additives (A-silicon). Later on, a numerical model is also developed using CFD-ACE software to predict the flow of abrasive medium in the complex hole. Lunn [63] emphasized the need for incorporating at least one thermoplastic polymer in the abrasive medium. The objective of adding thermoplastic polymer (styrene polymers) is to enhance the elastomer properties which help in achieving uniform surface roughness in passageways having large length/diameter ratio. Kar et al. [64, 65] attempted to replace costly commercially used base polymers during AFF process. Experiments are carriedout with five types of base polymers viz. natural rubber (NR), ethylene propylene diene monomer (EPDM) rubber, butyl rubber (IIR), silicone rubber (Si) and styrene butadiene rubber (SBR). Each medium is characterized in terms of mechanical as well as rheological properties. A natural polymer based AFF medium is developed by Rajesha et al. [66]. Thermogravimetric analysis (TGA) showed that the developed medium can withstand a temperature upto 71°C without changing its properties. Seng et al. [67] developed a low cost medium for low pressure AFF system. The rheological properties of the newly developed medium without adding abrasive particles are studied using rotational rheometer. Cheng et al. [68] studied the rheological properties of the A-silicon rubber and showed that medium viscosity decreases with shear rate. Gao et al. [69] used SBR as AFF finishing medium for finishing of complex parts used in the aerospace industry made up of titanium and aluminium alloy. Authors reported that SBR has good finishing efficiency.

ii. Development and rheological study of medium for finishing micro featured components

Rhoades [70] developed the medium for abrading and deburring inaccessible openings of workpieces. The chief characteristic of medium is that it can be easily modified according to the characteristic of the workpiece to be finished by adding water to it. Perry [71] developed the medium that can be used for honing, abrading, deburring or polishing the

internal surfaces of workpieces. Base polymer (silicon) of medium is mixed with a gel composed of metallic soap (e.g. aluminium stearates) and hydrocarbon oil (e.g. aliphatic oil, naphthenic oil). The amount of gel added to the base medium can be varied according to the use of abrasive composition, whether is it required in a soft or stiffer state. Perry [72] developed abrasive liquid slurry for polishing and radiusing a microhole. The slurry consists of the liquid material (naphthenic mineral oil), a theological additive (polyethylene) for creating the thixotropic slurry and abrasive particles. Tzeng et al. [73] performed AFF process on the micro parts fabricated by using EDM process. Authors developed medium composed of polymer, wax, silicon oil and SiC abrasive particles.

1.4.4 Modeling of abrasive flow finishing process

To perform any process successfully, the foremost thing is to understand physics of the process. With the proper understanding of the process, further improvements in the same can be done to achieve optimum results with minimum efforts. Process modeling can be done in following ways.

i. Theoretical modeling

Theoretical model of radial and axial forces acting on a single abrasive particle is developed by Gorana et al. [74]. Scratching experiments are performed to see the mechanism of material removal during AFF process. Experiments are conducted to verify the theoretical results. Axial force, radial force, active abrasive particle density and abrasive particle depth of indentation, have a significant influence on the scale of material deformation. Later, Gorana et al. [75] developed an analytical model to simulate surface roughness generated during AFF process. Theoretical models for determination of specific energy, heat transfer and temperature produced during the AFF process are developed by Jain and Jain [76]. Abrasive particle movement pattern during AFF process is predicted by the Fang et al. [77]. The effect of normal load, abrasive particle size and hardness of machined part are taken as the input parameters for deciding abrasive particle movement.

ii. Numerical/simulation modeling

Jain et al. [78, 79] modeled the stresses and forces generated during the AFF process using finite element (FE) method. Later, these forces are used as input in the theoretical models to predict the surface roughness and material removal during the AFF process. Authors considered triangular based uniform roughness profile as workpiece initial surface roughness profile. Later, Jain and Jain [80] carriedout simulations of final surface

roughness obtained during AFF process and found that simulated results are in good agreement with experimental results. Partial error between experimental and simulated results is because of not considering real abrasive particles shape, wear of abrasive particles and workpiece actual surface roughness profile. Jain and Jain [81] further used the same numerical approach to determine the effect of percent abrasive concentration as well as mesh size on active abrasive particles density and verified the same experimentally. Author considered abrasive particles with single cutting edge and assumed that the abrasive particle size (radius) follows normal distribution about the mean particle radius. Jain et al. [82] extended the FE analysis of AFF process for complex workpiece and assumed medium as Bingham plastic fluid. The governing equations (conservation of mass, balance of momentum, and conservation of energy) are modified accordingly and theoretical model was developed for volume of material removed during AFF process. Wang et al. [83] attempted to achieve uniform surface roughness across complex holes surface during finishing with AFF process. CFD is used to determine the velocity, strain rates and shear forces acting on the workpiece surface at constant pressure condition. Their objective is to design an appropriate passageway in the workpiece core to have the same shear force that results in uniform surface roughness. Wan et al. [84] did CFD simulation of the AFF process while finishing straight tubes with ellipsoidal cross-sections. In order to predict accurately the finishing forces and other output responses of the AFF process, it is necessary to model the physical behavior of abrasive medium as exact as possible. Uhlmann et al. [85] laid emphasis on the above stated concept and found that standard Maxwell model (when extended to generalize Maxwell model) can more accurately model the AFF medium in terms of storage and loss modulus.

1.4.5 Gaps in the literature

Based on the literature survey on AFF process in various fields, major gaps are:-

1. Development of AFF process setup and experimental study of the process

Researchers developed various AFF setups but flexibility of using same setup for finishing of macro featured and micro featured components is limited. Major shortcomings of the developed setups are:-

i. Most of the set-ups are designed for finishing workpieces with macro features. Hence, high viscous medium is used. While, the medium used for finishing micro features of workpieces is less viscous. This increases the chance of medium leakage during the AFF experiments.

ii. Also, not much attention is paid on finishing surgical stainless steel (SS 316L) cylindrical tubes with the help of AFF process.

iii. Limited literature is available on finishing of micro features (microholes and microslots) by AFF process. While, detailed parametric study of AFF process during finishing of micro features still needs to be done.

2. Development of economical medium and its rheological study

A well prepared medium with good rheological properties helps in achieving fine surface roughness uniformly on the workpiece. Majority of the researchers used the commercially expensive AFF medium. So, major short comings related to the medium development are:-

i. Very few researchers develop in house medium and tune the same by checking the rheological properties.

ii. Extensive rheology (static and dynamic) of developed medium and its utilization in modeling is not carriedout much.

3. Modeling of the AFF process

Modeling is necessary for understanding the physics of the AFF process. However, still there are number of gaps related to the modeling of the porcess:-

i. Limited literature on the modeling of AFF process during finishing of macro features is available.

ii. No literature is found that includes modeling of AFF process during finishing of micro features.

iii. There is a lack of studies involving the finishing forces modeling using medium rheological properties. It is the rheological properties of the medium along with the extrusion pressure, decides the magnitude of forces generated during AFF process.

1.5 Motivation and objectives of the present work

Main motivation is to develop economic AFF system (experimental setup, tooling and medium) that can able to finish macro to micro features. The broad objectives of the current research work:-

1. Design and development AFF process setup. To make sure the structural stability of the developed AFF setup, its static structural FE analysis will be carriedout in Ansys®.
2. Fabrication of economic in-house medium by blending various polymers for finishing of macro and micro features as well as its rheological characterization.
3. To carry out finishing of the SS 316L workpieces (tubes, microslots, and microholes) with the help of developed AFF process setup and medium. To study the effects of AFF

process input parameters (numbers of cycles, extrusion pressure, mesh size of the abrasive particles and wt. % of the abrasive particles in the AFF medium) on AFF process output responses (percentage change in surface roughness, percentage change in maximum height of the roughness profile).

4. To study the finishing mechanism of AFF process during finishing the workpieces with macro to micro features and its surface morphology as well as topography characterization.
5. Modeling of AFF process in Ansys® Polyflow by using experimentally evaluated rheological properties of the medium as input. The outcome of the modeling is the finishing stresses generated on the workpiece surfaces during the AFF process.
6. To develop the simulation model for predicting the final surface roughness achieved on the workpiece surface during AFF process by reducing the number of assumptions. Also, to perform 1-D as well as 2-D simulation of the surface roughness.

1.6 Organization of the thesis

Current thesis is organized into 8 chapters with references and appendices at the end. **Chapter 1** discusses the need of finishing and various traditional to advanced abrasive finishing processes. The shortcomings of the traditional finishing processes regarding workpiece hardness and shape could be minimized by the advanced abrasive finishing processes. Most of the advanced finishing process uses abrasive fluids. Broadly these processes are three type viz. electrorheological, magnetorheological and polymer rheological abrasive fluids. Since electrorheological fluids require heavy electrical power supply requirements, these are used rarely. So, commonly used fluids are magnetic and polymer rheological abrasive fluids. Later, AFF process is discussed in detail with working principle and its important elements. Relevant literature on AFF process in the areas of design and development of setups, experimental study, medium development, medium rheological characterization, modeling and simulation of AFF process is presented.

Chapter 2 presents the design and development of the AFF setup. AFF setup when combined with appropriate tooling can be used for finishing workpieces with macro and micro features. Various key components of the setup are designed on strength criteria by using fundamental design theories. In order to check the reliability of the developed AFF setup, static structural FE analysis is done in the Ansys® workbench. All the components of AFF setup are modeled and assembled in Ansys® design modeler. FE analysis results show that the designed setup is safe to operate from the strength and rigidity point of view.

Chapter 3 includes the in-house developed economic polymer rheological abrasive medium (medium). Different medium with varying viscoelastic properties are developed based on the geometric dimensions of the workpieces (tubes, microslots, and microholes) to be finished. Medium with dominating elastic properties are developed for finishing tubes while medium with dominating viscous nature is used during finishing of and microholes. Various ingredients of the medium such as the base polymer, abrasive particles, plasticizers, and softeners are mixed properly with the help of two-roll mill setup. Detailed rheological (static and dynamic) study of the medium is done using MCR- 101 parallel plate rheometer.

Finishing of SS 316L tubes with the AFF process is presented in **Chapter 4**. Preliminary experiments are carriedout to study the effective ranges of the AFF input parameters (extrusion pressure, number of AFF cycles, abrasive particle size, and wt. % of the abrasive particles). Later on, the detailed parametric study of the AFF process during finishing of SS 316L is presented.

To prove the capability of the developed AFF setup for finishing of microslots, detailed experimental study is presented in **Chapter 5**. Microslots on SS 316L workpieces are made with the help of electric discharge micromachining (EDµM) process. Preliminary experiments followed by the complete parametric study of AFF process during finishing the microslots are presented.

In **Chapter 6,** finishing of microholes is carriedout with the help of AFF process**.** Microholes are initially machined on SS 316L workpieces by using die-sinking electric discharge micromachining (Die-sink EDµM) process. Microholes offer more resistance to the medium flow as compared to microslots. Thus, low viscous medium with partial elastic nature with reference to the medium used for finishing of microslots is prepared in-house. Effect of AFF input parameters on AFF output responses is studied by conducting AFF experiments.

Modeling of AFF process during finishing of tubes, microslots, and microholes with their respective simulation of the surface roughness generated on the workpiece surface is presented in **Chapter 7**. 2-D FE analysis of AFF process during finishing of cylindrical tubes, while 3-D FE analysis of AFF process during finishing of microslots and microholes is carriedout in Ansys® Polyflow. The developed FE model uses rheological properties of the medium as input which increases its accuracy in predicting finishing forces acting on the abrasive particles. By using the results of FE analysis as input, surface roughness simulation

models are proposed for predicting the final surface roughness generated on the surface of tube, microslot and microhole. At last comparative study between the experimental and simulated obtained results of percentage change in surface roughness is presented. There is a good agreement between the experimental and simulated results.

Chapter 8 represents the main findings of the present work, important conclusions and future scope in the field of AFF process. The outcome of the present work in the form of various journal papers, book chapters, and conferences is reported.

References and appendices are added at the last.

Chapter 2

DESIGN AND DEVELOPMENT OF ABRASIVE FLOW FINISHING PROCESS EXPERIMENTAL SETUP

2.1 Introduction about the developed abrasive flow finishing process setup

2.2 Design methodology

2.2.1 Specifications of setup

2.2.2 Medium cylinder

2.2.2.1 Thickness of medium cylinder wall

2.2.2.2 Length of medium cylinder

2.2.2.3 Flange dimensions

2.2.3 Piston

2.2.3.1 Piston (piston nut) thickness

2.2.3.2 Teflon piston ring

2.2.3.3 Total length of the piston

2.2.3.4 Gudgeon pin

2.2.4 Connecting rod

2.2.5 Frame and housing

2.2.5.1 Supporting plates

2.2.5.2 Supporting rods

2.2.5.3 Design of the bolts

2.2.5.4 Spacer

2.3 Finite element analysis of abrasive flow finishing setup

2.3.1 Pre-processing

2.3.1.1 Model the geometry

2.3.1.2 Assign material properties to different components

2.3.1.3 Mesh the geometry

2.3.1.4 Boundary conditions

2.3.2 Solution

2.3.3 Post-processing

2.3.3.1 Equivalent stress

2.3.3.2 Total deformation

Chapter two contains the detailed design methodology, calculations and fabrication of AFF experimental setup. It also includes the static structural analysis of designed AFF setup which is carried out in Ansys® workbench.

2.1 Introduction about the developed abrasive flow finishing process setup

As found out from literature survey (chapter 1) several AFF setups are developed by researchers for finishing components with macro features. Few attempts are also made to design the AFF setups for finishing components with micro features. However, each AFF setup mainly developed for a particular component to be finished. This can range from internal finishing of tubes to microholes. The basic design of AFF setup is based on the component geometric dimensions, shape. The medium composition is determined by dimensions of the component to be finished, e.g., components in macro dimensions requires the high viscous medium while components with micro dimensions requires a low viscous (easily flowable) medium for finishing operation. High viscous medium possesses more elastic component and requires high extrusion pressure for its extrusion. On the other hand low viscous medium flow easily, however there are high chances of leakage. This is due to the restrictions provided to the medium during its passage by the micro openings in the component undergoing finishing operation. Thus, keeping in mind the above points, an AFF setup is designed that can not only withstand high to low extrusion pressure as well as leak proof for low viscous medium.

The current AFF setup is designed and developed to withstand extrusion pressure upto 12 MPa. Thus, the developed AFF setup can be used for finishing macro components that require high viscous and elastic dominant medium. Also, the same setup can be effectively and efficiently used for finishing components with micro features. Later, to further check the reliability of designed AFF setup, static structural finite element (FE) analysis is done using the Ansys® workbench. Various components are modeled and assembled in Ansys® design modeler. After assembly various loads and boundary conditions are applied to the AFF developed model, resembling the experimental conditions. Analysis result showed that the designed AFF setup is safe from the strength and rigidity point of view.

2.2 Design methodology

The AFF experimental setup is designed by keeping in view the basic requirements and fundamental mechanism of the process. Various key components are designed based on

strength criteria by using fundamental design theories and some simplified assumptions. Key elements of the AFF setup are:-

1. Hydraulic cylinder
2. Medium cylinder
3. Piston
4. Workpiece fixture
5. Frame and housing (supporting rods, supporting plates etc.)

Some of the design considerations on which the AFF setup is designed are:-

1. Loads are static in nature.
2. Self-weight of components are neglected.
3. Considering strength as the most important requirement for setup, it is used as the design criteria.

2.2.1 Specifications of setup

An economic laboratory level AFF experimental setup is designed and developed. The basic specifications on which the complete setup is designed are:-

1. Maximum working pressure: 12 MPa.
2. Maximum stroke length: 68 mm.
3. Inner diameter of medium cylinder: 60 mm.

2.2.2 Medium cylinder

Medium cylinder serves mainly two functions. First, to contain sufficient quantity of abrasive medium in it and second is to guide the same through the tooling as well as workpiece by the motion of the piston due to extrusion pressure. Medium cylinder is considered as an open ended pressure vessel during its design. Medium cylinder is a casted component and thus it contains blow holes with the rough surface. To make a high wear resistant medium cylinder sliding inner surface, it is fitted with a stainless steel cylinder liner.

Material selected- Grey cast iron (FG 300)

Ultimate tensile strength, σ_{um} =300 MPa (as per IS 210: 1993)

Factor of safety = 8, as cast iron is non-homogeneous in nature, thus factor of safety is high [86].

2.2.2.1 Thickness of medium cylinder wall

Thickness of cylinder as given by thin cylinder theory:-

Medium cylinder is an open ended pressure vessel. Thus, circumferential stress is the criteria for determining the cylinder wall thickness. According to the thin cylinder theory, the wall thickness of medium cylinder (t_m) is given by [86]:-

$$t_m = \frac{P d_{im}}{2\sigma_{dm}} \tag{2.1}$$

where,

$P =$ internal pressure acting on medium cylinder wall=12 MPa,

$d_{im} =$ internal diameter of medium cylinder = 60 mm,

$\sigma_{dm} =$ design stress for medium cylinder material.

Now,

$$\sigma_{dm} = \frac{\sigma_{um}}{F.S.} \tag{2.2}$$

$$= \frac{300}{8} = 37.5\,\text{MPa}$$

Putting the values p, d_{im} and σ_{tm} in eq. 2.1, t_m is given as:-

$$t_m = \frac{12 \times 60}{2 \times 37.5} = 9.6\,\text{mm} \tag{2.3}$$

Thickness of cylinder wall as given by thick cylinder theory:-

Cylinder material is brittle in nature so lame's theory which is based on maximum principle stress theory of failure is used [86]. According to the lame's equation t_m is given as:-

$$t_m = \frac{d_{im}}{2}\left[\sqrt{\frac{\sigma_{tm}+P}{\sigma_{tm}-P}} - 1\right] \tag{2.4}$$

$$= \frac{60}{2}\left[\sqrt{\frac{37.5+12}{37.5-12}} - 1\right] = 11.80 \cong 12 \text{ mm}$$

Inner surface of medium cylinder is fitted with stainless steel liner of thickness 1 mm and for reconditioning in future, 2 mm additional thickness is kept.

So, total thickness of medium cylinder is:-

$$t_m = 12 + 1 + 2 = 15 \text{ mm} \tag{2.5}$$

Thus, the outer diameter of the medium cylinder (d_{om}) is:-

$$d_{om} = 60 + 2(15) = 90 \text{ mm} \tag{2.6}$$

2.2.2.2 Length of medium cylinder

Medium cylinder length (L_m) is the sum of piston length, stroke length and allowance i.e.:-

$$L_m = 80 + 68 + 2 = 150 \text{ mm} \tag{2.7}$$

2.2.2.3 Flange dimensions

Let d_{hm} be the diameter of the holes in the medium cylinder flange for properly fixing it to the supporting plate and hydraulic cylinder. Then pitch circle diameter (PCD) (d_{pm}) of the holes is given as [87]:-

$$d_{pm} = d_{im} + 2t_m + 3d_{hm} \tag{2.8}$$

$$= 60 + 2(15) + 3(12) = 126 \text{ mm}$$

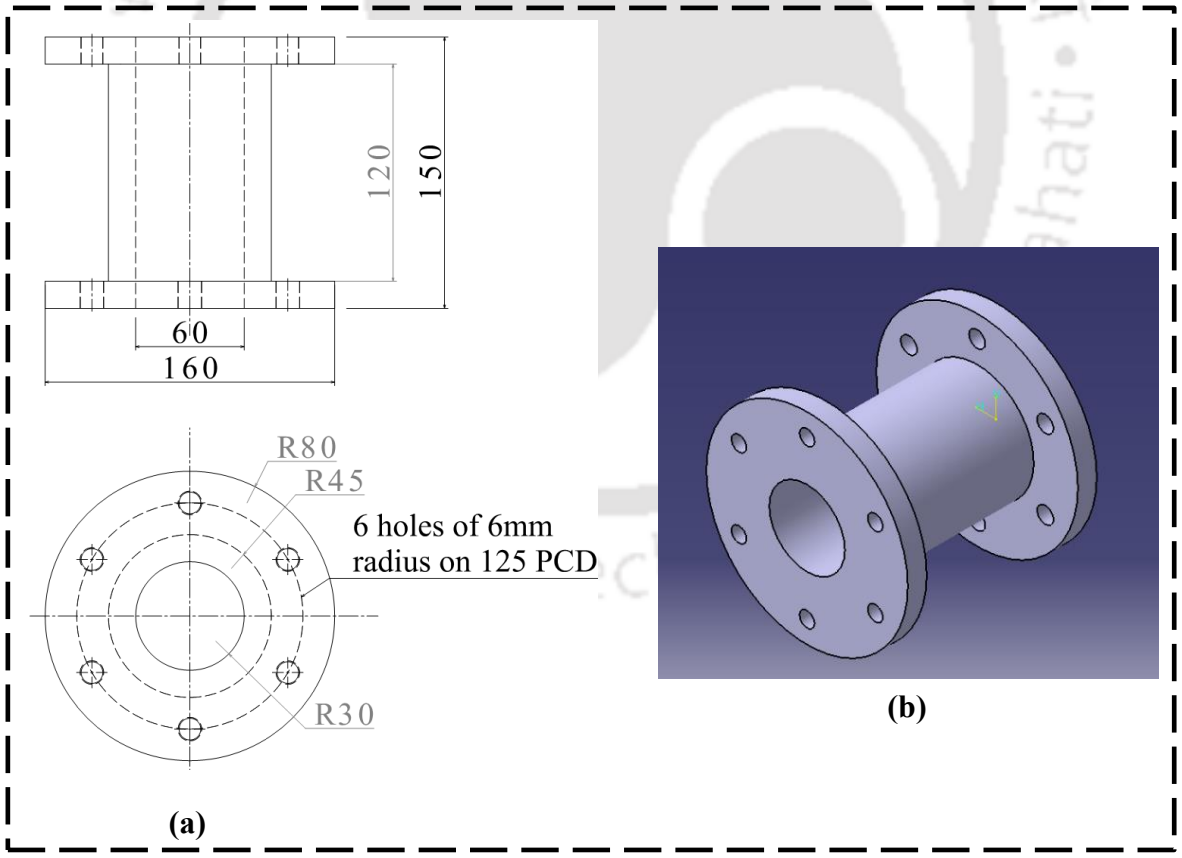

Fig. 2.1 (a) *2-D drawing of medium cylinder with dimensions* ***(b)*** *3-D model of medium cylinder (All dimensions are in mm).*

Outside diameter of the medium cylinder flange (d_{om}) and thickness of the flange (t_{fm}) is given as [87]:-

$$d_{om} = d_{pm} + 3d_{hm} \tag{2.9}$$

$$= 125 + 3(12) = 161 \cong 160 \text{ mm}$$

Also,

$$t_{fm} = 1.25 d_{hm} \text{ to } 1.5 d_{hm} = 1.25 \times 12 \text{ to } 1.5 \times 12 \tag{2.10}$$

= 15 mm to 18 mm

In the current design medium cylinder is casted with d_{pm} as 125 mm, d_{om} as 160 mm and t_{fm} as 15 mm.

The detailed drawing of medium cylinder is shown in Fig. 2.1

2.2.3 Piston

The primarily function of the medium cylinder piston (piston) is to transmit the extrusion force of the hydraulic cylinder piston rod to the abrasive medium. Each medium cylinder on either side of workpiece contains piston which guides the medium to and fro from the medium cylinder through the workpiece. Piston is made up of aluminium alloy due to its light weight and good strength. The detail drawing of piston with its 3-D model geometry is in Fig. 2.2(a-b)

Material selected- Aluminium alloy 2011

Yield strength, σ_{yp} = 270 MPa

Factor of safety = 3,

2.2.3.1 Piston (piston nut) thickness

Piston head thickness (t_{hp}) according to Grashoff's formula is given as [87]:-

$$t_{hp} = \sqrt{\frac{3pd_{im}^{\ 2}}{16\sigma_{dp}}} \tag{2.11}$$

where,

p = internal pressure acting on medium cylinder wall =12 MPa,

d_{im} = internal diameter of the medium cylinder = 60 mm,

σ_{dp} =design stress for piston material.

Now,

$$\sigma_{dp} = \frac{\sigma_{yp}}{F.S.} \tag{2.12}$$

$$= \frac{270}{3} = 90\,\text{MPa}$$

Putting the values p , d_{im} and σ_{tp} in eq. 2.11, t_{hp} is given as:

$$t_{hp} = \sqrt{\frac{3 \times 12 \times 60^2}{16 \times 90}} = 9.49\,\text{mm} \tag{2.13}$$

So value of t_{hp} is taken as 10 mm.

Fig. 2.2(c) shows the detailed drawing of the piston nut.

2.2.3.2 Teflon piston ring

In order to prevent the leakage of the abrasive medium, piston head is mounted with a piston ring. Teflon is used as the ring material due to its good resistance to wear and having low coefficient of friction. Radial thickness of the piston ring (t_{rp}) is given by the empirical relation [87]:-

$$t_{rp} = \frac{d_{im}}{25} \times F.S \tag{2.14}$$

$$= \frac{60}{25} \times 6 = 14.4 \cong 15\,\text{mm}$$

As, teflon is a soft material a high factor of safety is taken.

Axial thickness of the piston ring (t_{ap}) is given as [87]:-

$$t_{ap} = \frac{d_{im}}{10 \times n_r} \times F.S \tag{2.15}$$

$$= \frac{60}{10 \times 1} \times 6 = 36\,\text{mm}$$

where n_r is the number of rings = 1

Fig. 2.2(d) shows the detailed drawing of the teflon piston ring.

2.2.3.3 Total length of the piston

Total length of the piston (l_p) is given by empirical relation [87]:-

$$l_p = d_{im}\, to 1.5 \times d_{im} \tag{2.16}$$

$$= 60 \text{ to } 90 \text{ mm}$$

In the present case it is taken as 80 mm so design is safe.

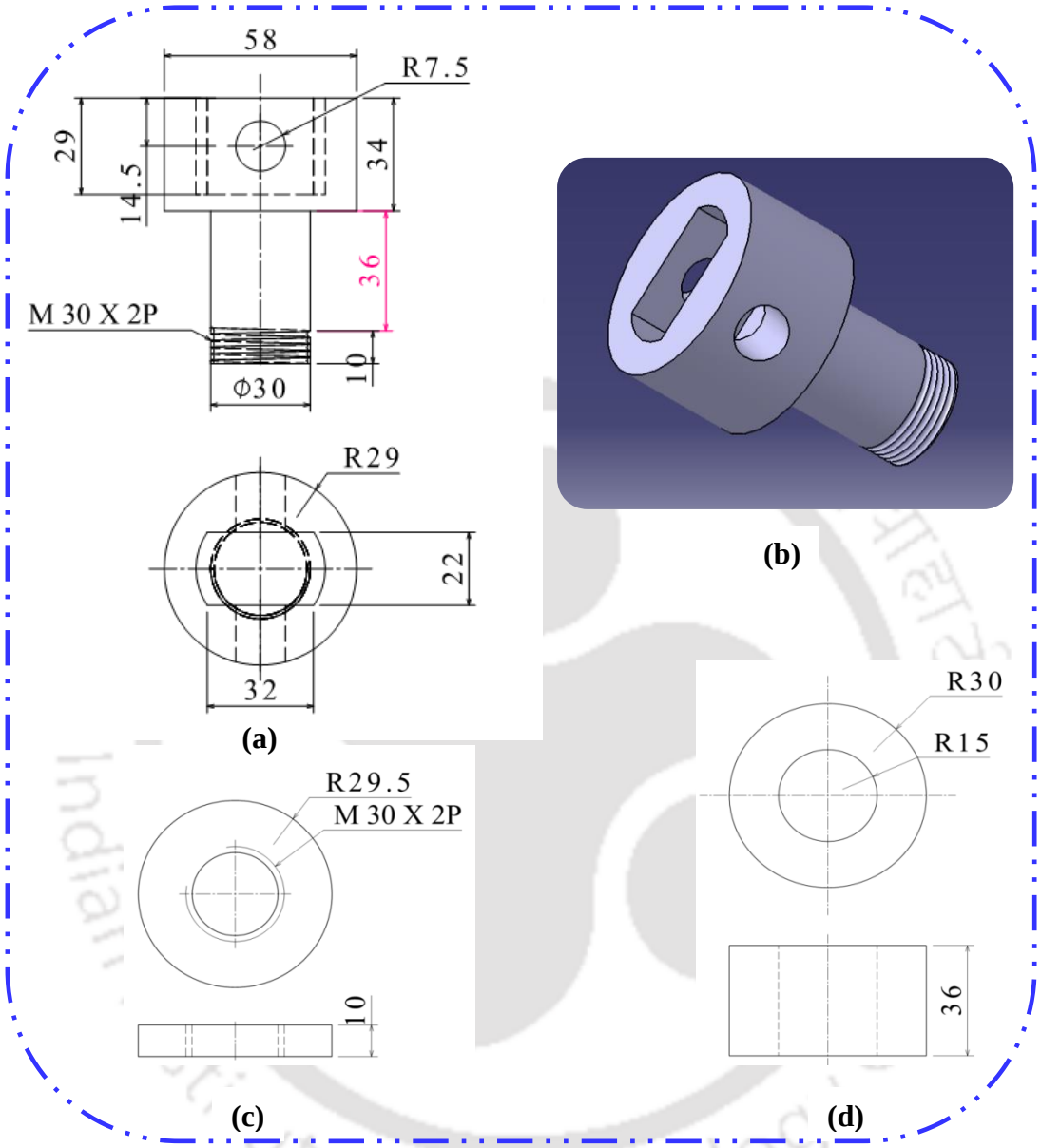

Fig. 2.2 (a) *2-D drawing of piston with dimensions* ***(b)*** *3-D model of piston* ***(c)*** *2-D drawing of piston nut with dimensions* ***(d)*** *2-D drawing of teflon piston ring with dimensions (All dimensions are in mm).*

2.2.3.4 Gudgeon pin

Gudgeon pin which is used in 2-stroke automobile engine piston is considered as it is fulfilling functional requirements. Specifications of the gudgeon pin are:-

Outer diameter = 15 mm

Inner diameter = 10 mm

Length = 45 mm

2.2.4 Connecting rod

Connecting rod is used to connect the hydraulic cylinder piston rod to the medium cylinder piston (Fig. 2.3). The hydraulic cylinder piston rod consists of M 24 x 2P threads. Thus, connecting rod end towards the hydraulic cylinder requires the same size hole. Therefore, hole dimension at the hydraulic cylinder rod end = M 24 x 2P

Outer diameter of the connecting rod at the hydraulic cylinder rod end (d_{ocr}) given by the empirical relation is [87]:-

$$d_{ocr} = 1.5 \text{ to } 2 \times \text{inner hole diameter} \qquad (2.17)$$

$$= 36 \text{ to } 48 \text{ mm}$$

In the current design it is considered as 50 mm.

Also, hole diameter in the connecting rod at the medium cylinder piston end = 15 mm

So width of that section = 2 × hole diameter = 2 ×15 = 30 mm.

In the present case it is 35 mm so considered design is safe.

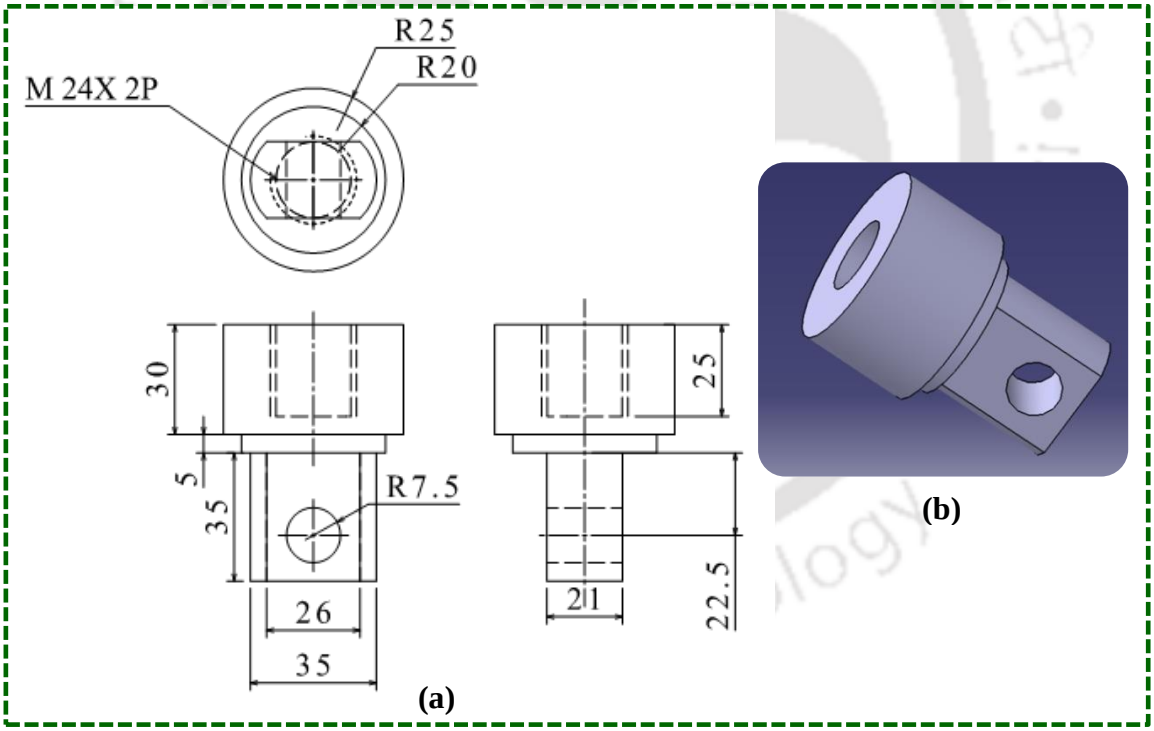

Fig. 2.3 (a) *2-D drawing of connecting rod with dimensions* ***(b)*** *3-D model of connecting rod (All dimensions are in mm).*

2.2.5 Frame and housing

Frame and housing are necessary to accommodate and connect different components of AFF setup for its working as a single unit. A vertical drilling machine base and pillar are used as

the support for mounting AFF setup components. Various supporting members of the setup are designed by calculating the forces which are generated during the working condition. The major force which is generated during the experimental setup operation is due to the pressurized oil in the hydraulic cylinder. This force produces action and reaction forces in all other components of the experimental setup. Fig. 2.4(a-c) shows the free body diagram (FBD) of the hydraulic system. As shown in Fig. 2.4(a-c) forces generated in the hydraulic system goes to the hydraulic cylinder and to counter those forces, flange of the hydraulic cylinder is screwed to the frame by bolts. These forces are then transmitted to the frame. As all the forces are axial, the frame must be rigid enough to counter axial forces.

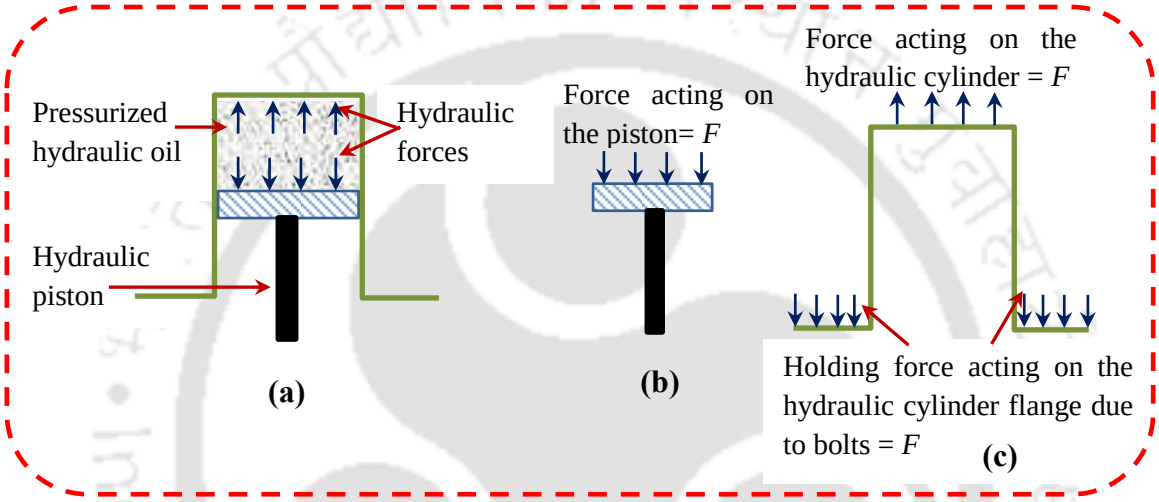

Fig. 2.4 (a) *Forces acting inside hydraulic system* ***(b)*** *free body diagram of hydraulic piston* ***(c)*** *free body diagram of hydraulic cylinder.*

Maximum hydraulic pressure, P = 12 MPa.

Cross-sectional area of the hydraulic cylinder having inner diameter 63 mm, is given as:

$$A = \pi r^2 \tag{2.18}$$

$$= \pi \times (31.5)^2 = 3117.25\,\text{mm}^2$$

Thus, maximum force on the flange of the hydraulic cylinder is:-

$$F = P \times A = 12 \times 10^6 \times 3117.25 \times 10^{-6} = 37407\,\text{N} \tag{2.19}$$

2.2.5.1 Supporting plates

Two main functions of the supporting plate are first to hold and locate the medium cylinders. Second is to resist and transmit the structural forces to the supporting rods which are generated during AFF process.

Material selected = AISI 1040 steel

Young's modulus, E_s = 205 GPa

Yield strength, σ_{ys} = 465 MPa

Factor of safety = 4, a high factor of safety is considered to counter the stress concentration which is due to holes which are machined in the plate for holding various AFF setup components.

Assumptions:-

1. Plate is considered as a fixed beam carrying a point load at the middle.
2. The maximum force generated on the flange of hydraulic cylinder is transmitted in the same magnitude to the supporting plate. Also, it is considered as a point load that is acting in the middle of the plate (beam).
3. The length of plate (L_{sp}) is considered equal to its breadth (B_s) i.e., $L_s = B_s$ = 360 mm

Maximum bending moment that acts at the centre of the beam is given as [88]:-

$$M_{\max} = \frac{FL_{sp}}{8} \tag{2.20}$$

Section modulus is,

$$Z_s = \frac{B_s H_s^{\,2}}{6} \tag{2.21}$$

where, H_s is the height of the plate.

Allowable bending stress is,

$$\sigma_{ab} = \frac{\sigma_{ys}}{4} \tag{2.22}$$

To ensure the safety of the beam, bending stresses generated in the beam should be less than the allowable bending stress. Therefore, section modulus of the beam (Z_s) should be greater than the following value:-

$$Z_s = \frac{M_{\max}}{\sigma_{ab}} \tag{2.23}$$

Using eq. 2.21, eq. 2.22 in eq. 2.23

$$Z_s = \frac{FL_{sp}4}{8\sigma_{ys}} = \frac{37407\times360\times10^{-3}\times4}{8\times465\times10^{6}} = 1.45\times10^{-5}\,\mathrm{m}^3 \tag{2.24}$$

Comparing eq. 2.24 and eq. 2.21, the value of H_s is:-

$$H_s = \sqrt{\frac{6Z_s}{B_s}} = \sqrt{\frac{6\times1.45\times10^{-5}}{360\times10^{-3}}}\text{m} = 15.55\,\text{mm} \tag{2.25}$$

Thickness of the plate should be greater than 15.55 mm. So, it is considered as H_s =16 mm.

Maximum deflection (y_{max}) is given as [88]:-

$$y_{\max} = \frac{FL_{sp}^{\ 3}}{192E_sI_s} \tag{2.26}$$

where, I_s is the moment of inertia of the supporting rod given as:-

$$I_s = \frac{B_sH_s^{\ 3}}{12} \tag{2.27}$$

$$= \frac{(360\times10^{-3})\times(16\times10^{-3})^3}{12} = 1.228\times10^{-7}\,\text{m}^4$$

Considering the values of F, L_{sp}, E_s and I_s in eq. 2.26, y_{max} is calculated as:-

$$y_{\max} = \frac{37407\times(360\times10^{-3})^3}{192\times(205\times10^9)\times(1.228\times10^{-7})} = 3.61\times10^{-4}\,\text{m} \tag{2.28}$$

This deflection is negligible so design is safe.

Both upper and lower supporting plate possesses same dimensions but with respect to their position their holes feature are different. The detailed drawings of upper plate and lower plate are shown in Fig. 2.5(a-b).

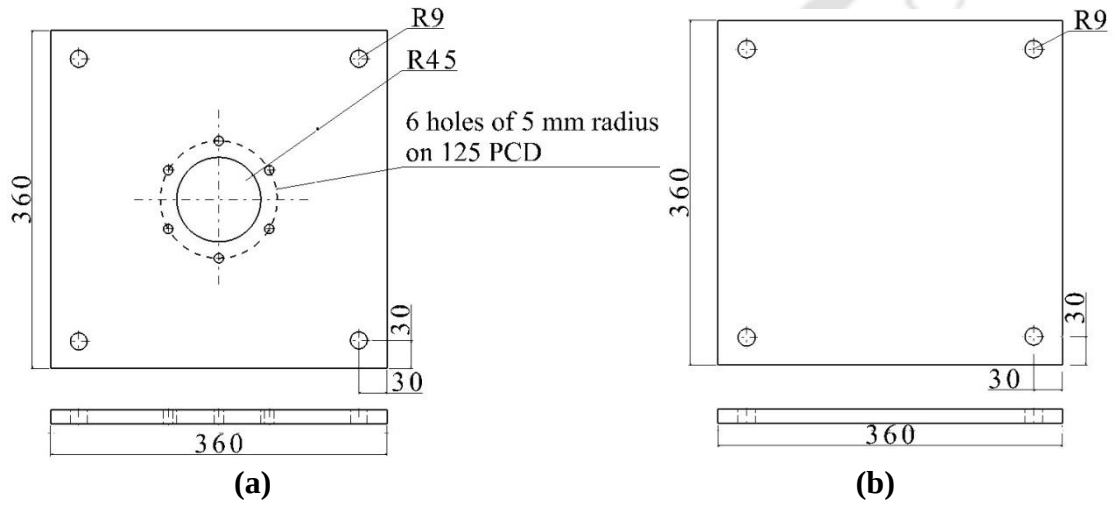

Fig. 2.5 *Detailed 2-D drawing of* ***(a)*** *upper supporting plate* ***(b)*** *lower supporting plate (All dimensions are in mm).*

2.2.5.2 Supporting rods

The main function of the supporting rod is to hold and provide stability to the lower unit that consists of supporting plate, fixture, lower medium cylinder and lower hydraulic cylinder. Supporting rods also assist in transmitting the forces generated during AFF process to the supporting pillar. There are four rods used on which lower unit is supported.

Material selected = AISI 1040 steel

Young's modulus, E_s = 205 GPa

Yield strength, σ_{ys} = 465 MPa

Factor of safety = 4.

Assumptions:-

1. Each supporting rod is considered as a column with both ends fixed.
2. Most of the load is taken by the bolts connecting hydraulic cylinder, medium cylinder to the supporting plate and a high factor of safety is considered. Thus, to simplify the calculations it is assumed that the load acting on each column passes directly through the centroidal axis without any eccentricity.
3. Supporting rod with internal diameter ($I.D._{sr}$) 18 mm, outer diameter ($O.D._{sr}$) 27 mm and length (L_{sr}) 530 mm are considered.

Safety of supporting rod is checked from crippling load (long column) as well as crushing load (short column) criteria.

Maximum crippling load (P_{cl}) carried by the supporting rod fixed at both the ends is given as [88]:-

$$P_{cl} = \frac{4\pi^2 E_s I_{sr}}{L_{sr}^{\ 2}} \tag{2.29}$$

where, I_{sr} is the moment of inertia of the circular cross-section of the supporting rod and is given as:-

$$I_{sr} = \frac{\pi}{64} \times (O.D._{sr}^{\ 4} - I.D._{sr}^{\ 4}) \tag{2.30}$$

$$= 20934.05 \times 10^{-12}\,\mathrm{m}^4$$

Putting values of E_s, I_{sr} and L_{sr} in eq. 2.29, P_{cl} is given as:-

$$P_{cl} = \frac{4 \times \pi^2 \times 205 \times 10^9 \times 20934.05 \times 10^{-12}}{(530 \times 10^{-3})^2} = 603.14\,\mathrm{KN} \tag{2.31}$$

Allowing a factor of safety of 4, safe crippling load (P_{safe}) is:-

$$P_{safe} = \frac{P_{cl}}{4} \tag{2.32}$$

$$= \frac{603.14}{4} = 150.8\,\text{KN}$$

Also, tensile load acting on each supporting rod is given as:-

$$P_{acting} = \frac{F}{4} \text{ (Number of rods = 4)} \tag{2.33}$$

$$= \frac{37407}{4} = 9.35\,\text{KN}$$

As the tensile load is much less than the safe crippling load value, so the supporting rod will not fail due to crippling.

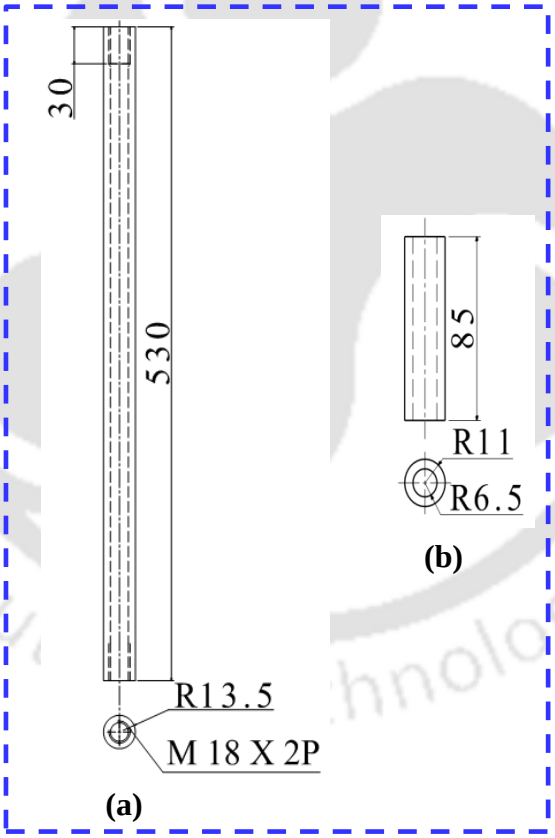

Fig. 2.6 *Detailed 2-D drawing of* ***(a)*** *supporting rod* ***(b)*** *spacer (All dimensions are in mm).*

Also, crushing stress ($P_{crushing}$) generated due to the tensile load on each rod is given as [88]:-

$$P_{crushing} = \frac{P_{acting}}{\frac{\pi}{4} \times (O.D._{sr}{}^2 - I.D._{sr}{}^2)} \tag{2.34}$$

$$= \frac{9.35\times10^{3}}{\frac{\pi}{4}\times(27^{2}-18^{2})\times10^{-6}} = 29.4\,\text{MPa}$$

As, $P_{crushing}$ is much less than the yield stress of the supporting rod material so the rod will not fail by crushing. Detailed drawing of the supporting rod is shown in Fig. 2.6(a).

2.2.5.3 Design of the bolt

Bolts connecting hydraulic cylinder to medium cylinder and medium cylinder to upper supporting plate are M10 high tensile bolt (make: TVS company).

Assumptions:-

1. Bolt used are having major diameter, d_{major} = 10 mm and minor diameter, d_{minor} = 8.876 mm [87].
2. The bolts are free from initial pre-tension.
3. Maximum tensile stress on each bolt should not exceed 100 MPa.

Maximum load ($P_{bcarried}$) that can be carried by the bolts (N_{bolts}) is given as [87]:-

$$P_{bcarried} = N_{bolt}\frac{\pi}{4}d_{minor}^{2}\sigma_{tbolt} \tag{2.35}$$

where,

σ_{tbolt} = Maximum tensile stress on each bolt.

Also, tensile load applied to the bolts is (described later in section):-

$$P_{bapplied} = F = 37407\,\text{N} \tag{2.36}$$

Now from eq. 2.11 and eq. 2.12, N_{bolt} is calculated as:-

$$N_{bolt} = \frac{37407}{\frac{\pi}{4}d_{minor}^{2}\sigma_{tbolt}} = \frac{37407}{\frac{\pi}{4}\times(8.876\times10^{-3})^{2}\times100\times10^{6}} = 6.05 \tag{2.37}$$

Thus, N_{bolts} = 6 are used.

2.2.5.4 **Spacer**

The main function of the spacer is to provide space between the medium cylinder and the hydraulic cylinder. In this space connecting rod is accommodated. Also, the bolt that connects the medium cylinder to the respective hydraulic cylinder is passed through these spacers. Thus, the details of the spacer can be given as:-

Number of spacers = number of bolts = 6.

Length of spacer (l_{spacer}) should be greater than the length of connecting rod which is 70 mm. Thus, in the present case l_{spacer} is considered as 85 mm. Internal diameter of the spacer ($I.\ D._s$) should be greater than the d_{major} of the bolts which is 10 mm. In the present case, it is taken as 13 mm. Also, outer diameter of the spacer ($O.\ D._s$) is 22 mm (Fig. 2.6(b)).

2.3 Finite element analysis of abrasive flow finishing setup

Static structural FE analysis of the designed and developed AFF setup is carried out to check its overall strength as well as rigidity under working conditions. 3-D model of AFF setup components is designed and assembled in Ansys® design modeler, to resemble like the actual AFF setup. Theoretically, AFF setup is designed for a maximum operating pressure (12 MPa). So, taking a factor of safety 2 for the overall setup under operating conditions, its FE analysis is done for the operating pressure of 24 MPa. The following steps constitute the static structural FE analysis of the AFF setup:-

2.3.1 Pre–processing

2.3.1.1 Model the geometry

All the components of AFF setup such as upper-lower hydraulic cylinder, upper-lower medium cylinder, frame-housing are modeled and assembled in the Ansys® workbench design modeler. The 3-D model of AFF setup is as shown in Fig. 2.7.

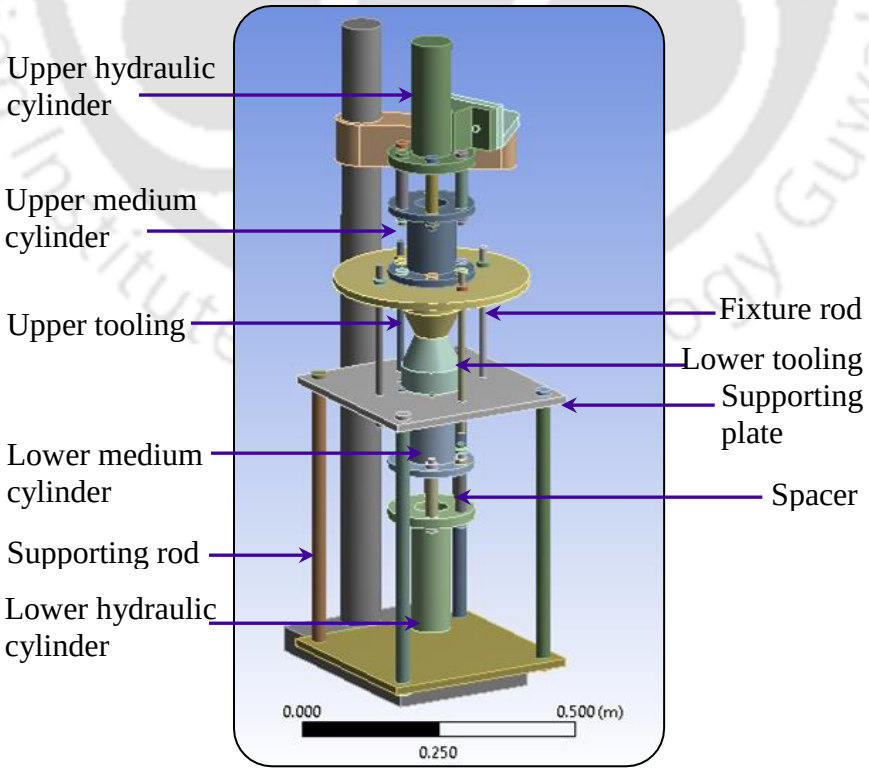

Fig. 2.7 *3-D model of the abrasive flow finishing setup.*

2.3.1.2 Assign material properties to different components

According to the material of different AFF setup components, properties are assigned to each component in Ansys®. Different materials and their properties are added in Ansys® workbench through its engineering data section. Some of the major component and their material properties used in structural analysis are given in table 2.1:-

Table 2.1 *Properties of various materials used in AFF setup.*

S. No.	Component name	Material	Young's modulus	Poisson's ratio
1.	Medium cylinder	Cast Iron	135 (GPa)	0.26
2.	Hydraulic cylinder and frame -housing	AISI 1040	205 (GPa)	0.29

2.3.1.3 Mesh the geometry

In this step geometry is discretized into a number of small elements. Each element is characterized by a number of points called nodes and the complete system of elements is called a mesh. Automatic meshing method with advanced sizing function is applied to do the meshing of the whole assembly. It toggles between tetrahedral (patch conforming) and swept meshing, depending upon whether the body is sweepable or not.

Table 2.2 *Statistics of the mesh used in finite element modeling of the AFF setup.*

Number of elements	108136
Number of nodes	256322
Average skewness	0.2767
Average aspect ratio	1.9194

On critical parts such as hydraulic cylinder, medium cylinder local body sizing is done. Some of the important statistics of the mesh are given in table. 2.2. Value of the average skewness and the average aspect ratio indicates that the generated mesh is of good quality [89]. Hence, further analysis can be done on the modeled and meshed AFF setup geometry. Fig. 2.8 shows the meshed AFF setup assembly.

2.3.1.4 Boundary conditions

In order to simulate the real working environment of the AFF setup, different loads and boundary conditions are applied to each component (Fig. 2.9). In accordance with the AFF experimental setup, types of contacts (fixed, no separation etc.) between various components are defined.

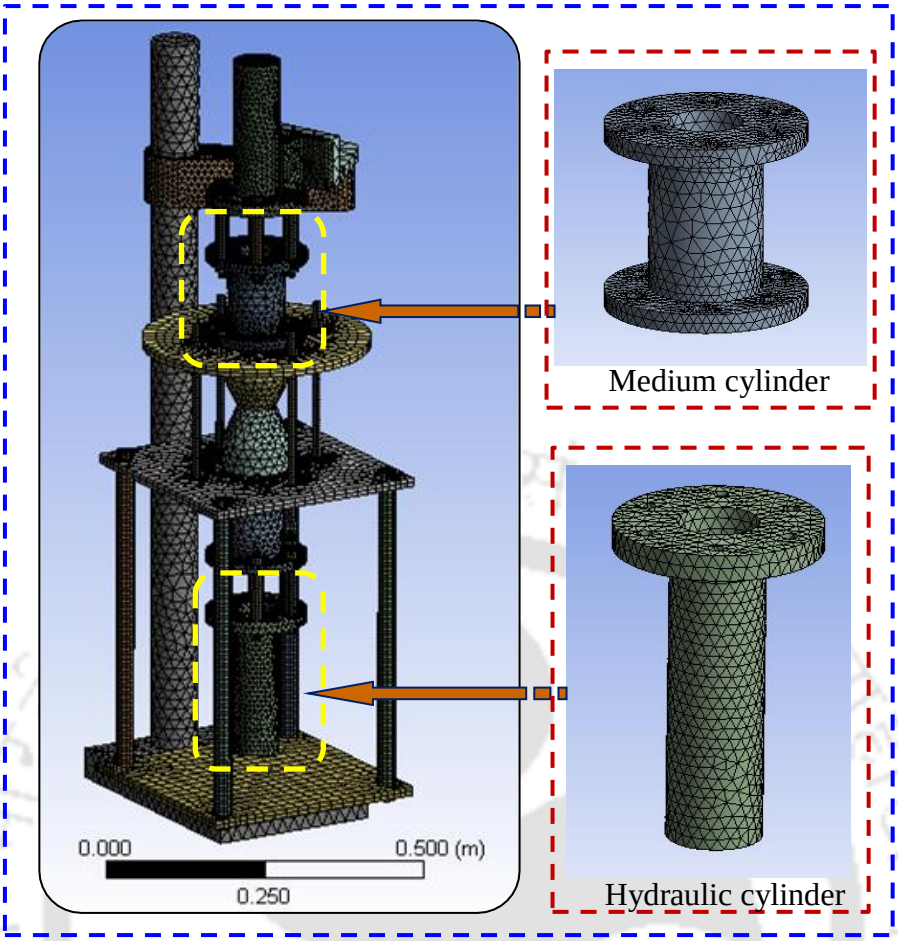

Fig. 2.8 *3-D view of the meshed abrasive flow finishing setup.*

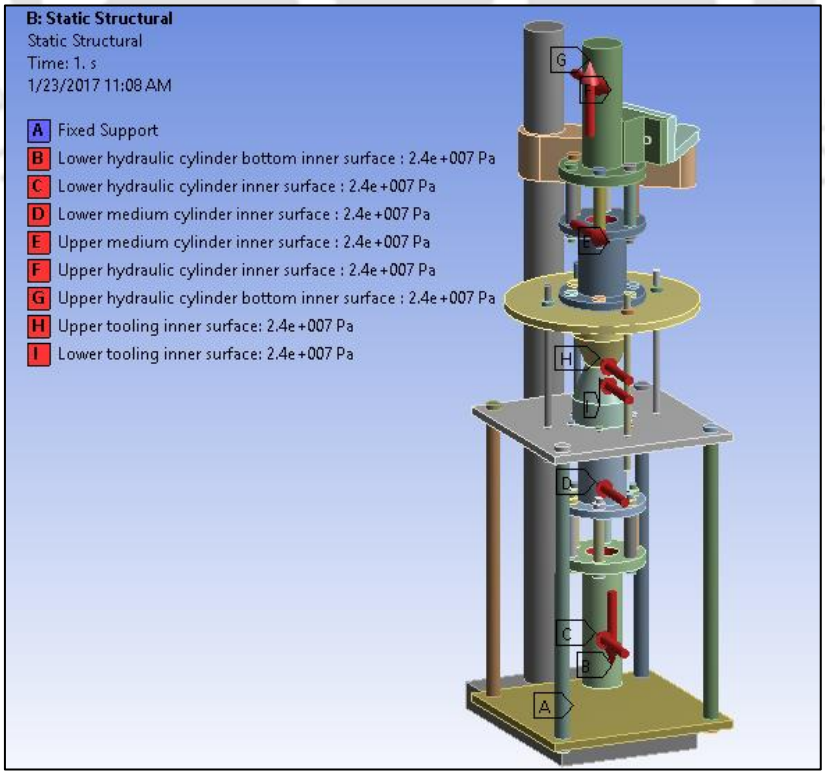

Fig. 2.9 *3-D view of the abrasive flow finishing setup with loads and boundary conditions.*

2.3.2 Solution

After properly defining the problem in terms of geometry, material properties, contact between different components, loads and boundary conditions, solution is done by using Ansys® workbench. Requested output results are generated at the end of analysis.

2.3.3 Post-processing

To study the overall strength and rigidity of AFF setup, two main results are required during the post-processing phase.

2.3.3.1 Equivalent stress

As shown in Fig. 2.10, the maximum equivalent stress generated in the whole assembly is 229.02 MPa. It is generated in the spacer made up of AISI 1040 steel whose yield strength is 465 MPa. So, design is safe from strength point of view.

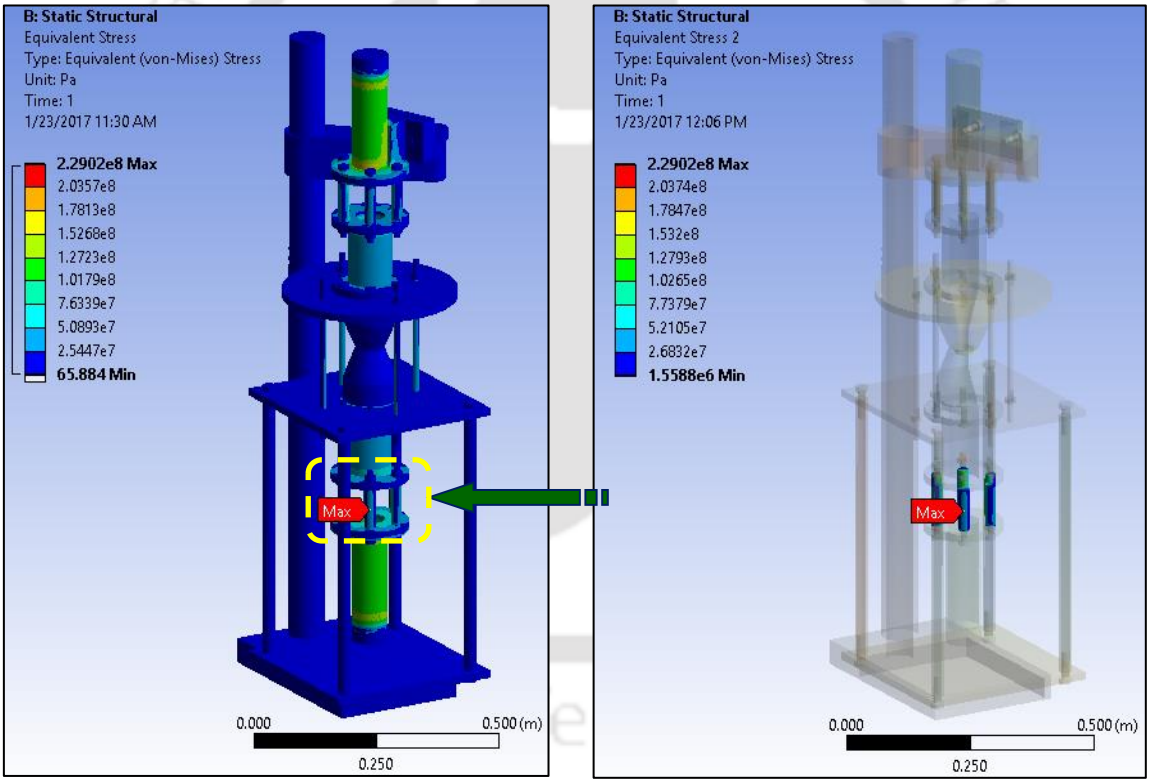

Fig. 2.10 *Equivalent stress distribution in the abrasive flow finishing setup.*

2.3.3.2 Total deformation

Maximum total deformation (Fig. 2.11) generated within AFF setup is 276.32 µm which can be neglected during the operating conditions of the AFF setup.

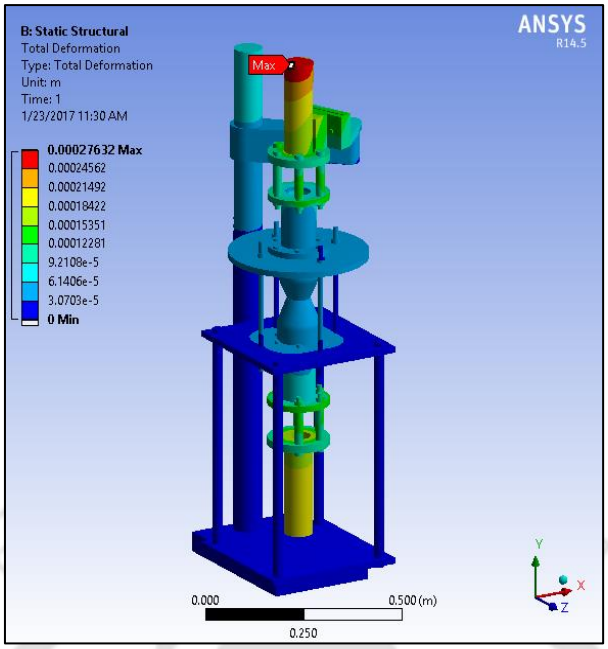

Fig. 2.11 *Total deformation distribution in the abrasive flow finishing setup.*

By considering all design condition, the AFF experimental setup is developed (Fig. 2.12).

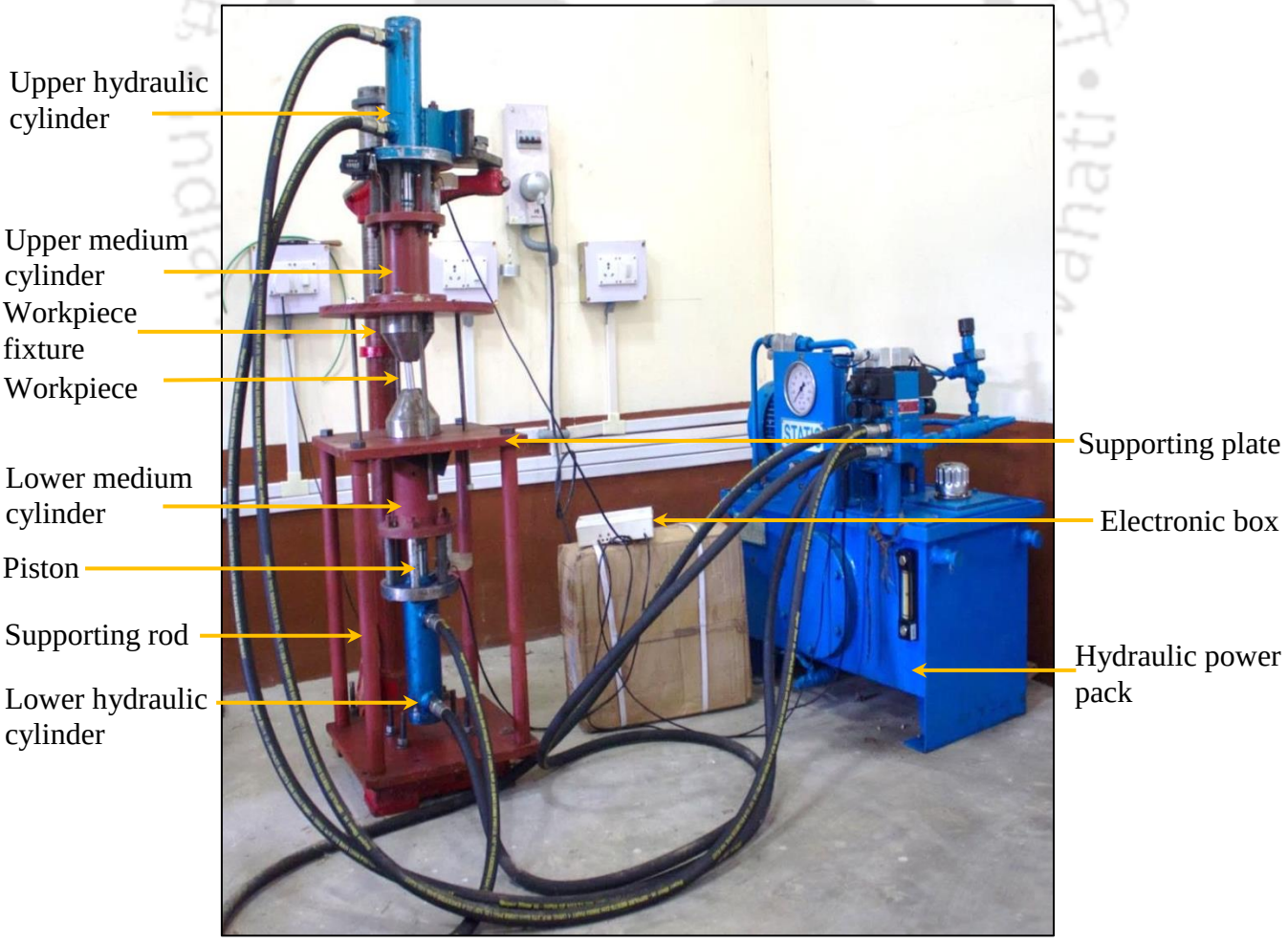

Fig. 2.12 *Abrasive flow finishing experimental setup.*

2.4 Conclusions

In the current chapter, dimensions of the various components of the AFF setup are calculated using fundamental design theories. Later, complete AFF setup is fabricated at IIT Guwahati. In order to ensure the safety of the complete AFF setup, its static structural FE analysis is carried out in Ansys® workbench. Some of the important conclusions are:-

1. Economic AFF setup that can finish macro and micro features of the workpieces is successfully designed and fabricated at IIT Guwahati.
2. The basic specifications on which the complete AFF setup is designed are maximum 12 MPa of extrusion pressure, maximum stroke length of 68 mm and inner diameter of the medium cylinder is 60 mm.
3. Maximum equivalent stress of 229.02 MPa is generated in the AFF setup. It is generated in the spacer made up of AISI 1040 steel whose yield strength is 465 MPa. So, design is safe from strength point of view
4. Maximum total deformation generated within AFF setup is 276.32 µm. This small deformation can be neglected during the working of the AFF setup.

Chapter 3

PREPARATION AND RHEOLOGICAL CHARACTERIZATION OF ABRASIVE FLOW FINISHING MEDIUM FOR FINISHING MACRO AND MICRO FEATURES

3.1 Introduction to abrasive flow finishing medium

Medium is one of the most important constituent of AFF process. It mainly comprises of the base polymer which is viscoelastic in nature, additives (plasticizers, softeners) and abrasive particles. A good AFF medium possesses properties such as mechanically stable, chemically non-reactive, self-deformable, good fluidity and better abrading ability. Based on the

workpiece to be finished, the non-newtonian base polymer is chosen which can be of nature such as shear thinning, shear thickening, bingham plastic, etc. (Fig. 3.1)

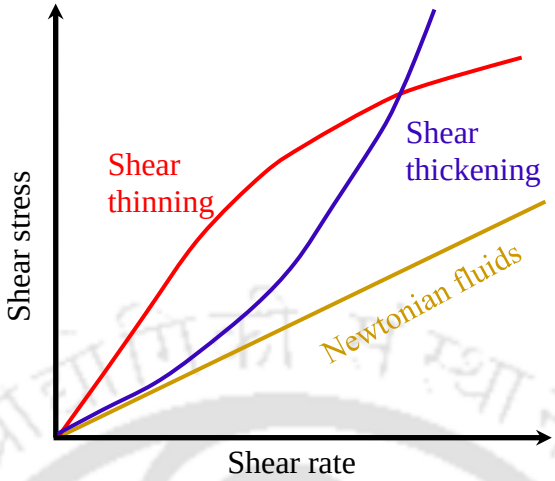

Fig. 3.1 *Types of flow behaviour.*

It is the rheology of medium which determines pattern and aggressiveness of the abrasive action. The base polymer acts as a main matrix for holding the abrasive particles during finishing operation. Most of the base polymers are elastic dominant in nature so to improve their viscous properties (to make viscoelastic) various additives such as plasticizers and softeners are blended to the base medium. This creates the flexibility in polymer chains resulting in better flowability and self-deformability of the medium. Abrasive particles from coarse to fine size in varying concentration are added to the base polymer blend (base polymer + plasticizer + softener) depending upon the workpiece dimensions to be finished. Commercial medium viscosity levels are specified using number systems. Medium viscosity can vary from 10 (less stiff – low viscosity) to base number 70 (very stiff – high viscosity) Fig. 3.2.

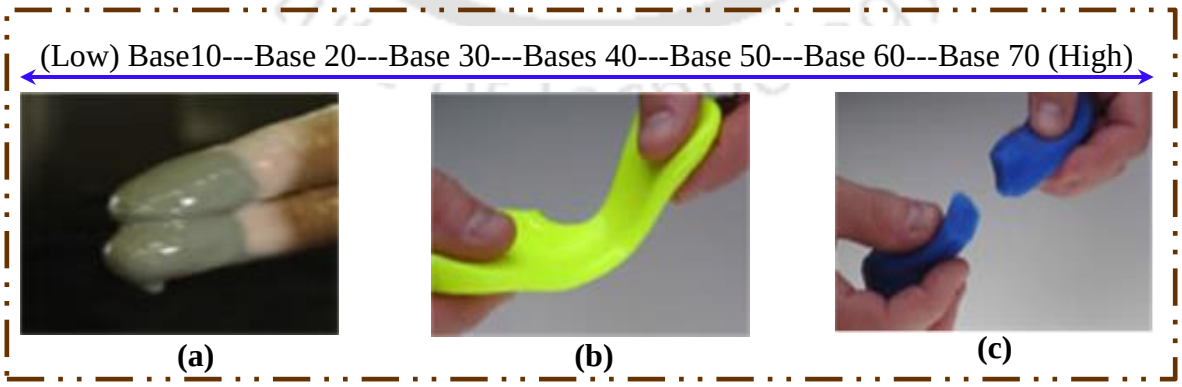

Fig. 3.2 *Medium classification* ***(a)*** *low viscous* ***(b)*** *moderate viscous* ***(c)*** *high viscous (Courtesy: Kennametal extrude hone).*

At the start of AFF experiments medium is filled in the lower medium cylinder. Thereafter, hydraulic pressure is applied by the lower piston to push the medium from the lower medium cylinder to the upper medium cylinder via the workpiece openings (Fig. 3.3).

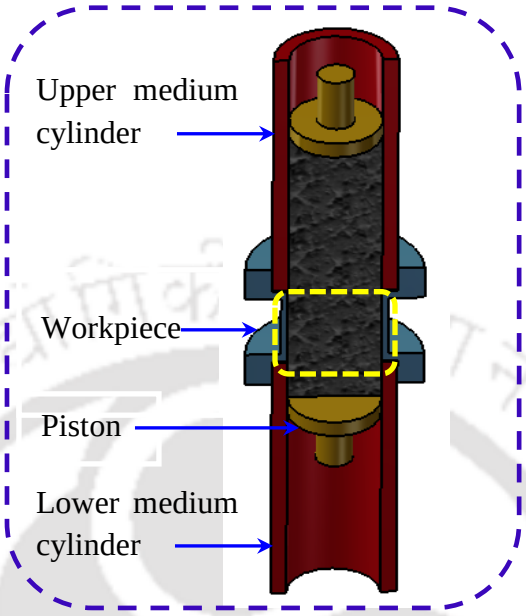

Fig. 3.3 *Schematic diagram of the abrasive flow finishing process showing AFF process working principle.*

As found out from the literature review (Chapter 1) several researchers had made attempts to study the rheology of the medium. Few authors also tried to replace the commercially used expensive medium by economic medium. Pure silicon rubber, silicon rubber with additives, styrene polymers, natural rubber, ethylene propylene diene monomer rubber and butyl rubber are some of the proposed economic base polymer for the AFF medium. In the current chapter, various medium compositions are prepared for finishing of tubes, microslots and microholes. Detailed rheological study (static and dynamic) of the developed medium is done with the help of parallel plate rheometer (make: Anton Paar; series: MCR-101 series).

3.1.1 Rheology of the viscoelastic medium

Rheology is the study of flow and deformation of matters. Rheology in case of non-newtonian fluids describes their flow behaviour by relating strain rates (rate of change of strain) with stresses. Non-newtonian behaviour can further be categorized as viscoelastic, time dependent viscosity and time independent viscosity. Medium used in AFF process is generally composed of base polymer with viscoelastic nature. Finishing efficiency of AFF process mainly relies on the medium rheological properties. When extrusion pressure (P) is

applied on the AFF medium, molecular rearrangement, i.e. change in position of polymer chains in the base polymer takes place to accompany applied stresses. As the medium rearranges itself (viscous nature), it creates back stresses (elastic nature) and as soon as this back stress equals to applied stress no rearrangement of polymer chains take place. In normal state (no extrusion pressure is applied) base polymer chains are randomly entangled and coiled with each other (Fig. 3.4(a)). As extrusion pressure is applied, in AFF process polymer chains begins to uncoil and gradually start to flow through workpiece passage. While flowing through the restricted passage, the polymer chains align themselves in the direction of flow through the workpiece (Fig. 3.4(b)).

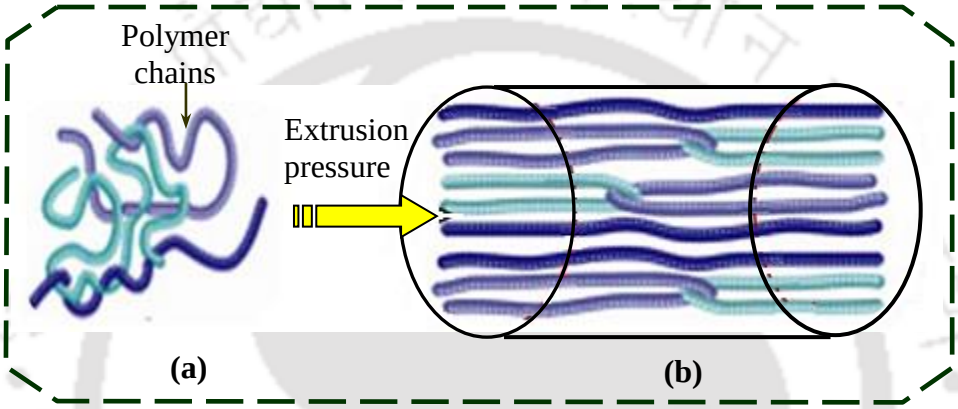

Fig. 3.4 *Polymer chains* ***(a)*** *coiled at rest* ***(b)*** *uncoiled polymer chains aligned through restricted workpiece passage when the extrusion pressure is applied [90].*

3.1.2 Role of viscoelasticity in determining finishing forces

Base polymer for AFF medium should possess viscoelastic properties. As shown in Fig. 3.5, as extrusion pressure (P) is applied to the medium, the elastic component of medium result in generation of radial force (F_R) while viscous component generates axial force (F_A) [91].

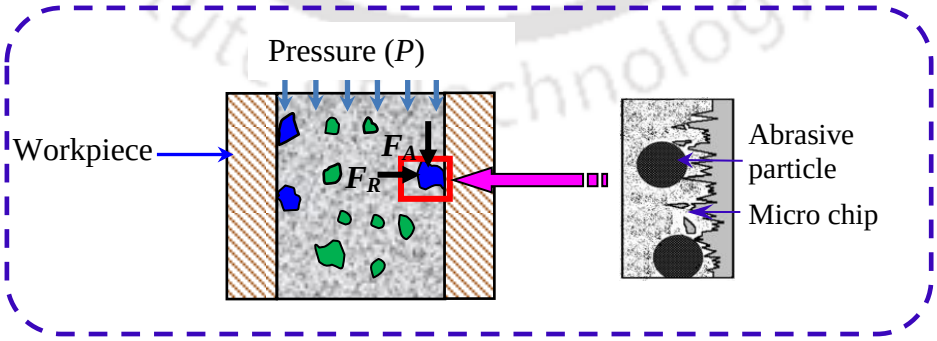

Fig. 3.5 *Forces acting on abrasive particle during abrasive flow finishing process.*

The base polymer with other additives acts as a flexible binder to hold the abrasive particles and transmit the forces developed in the medium to the active abrasive particles.

Initially, due to the F_R, abrasive particles are indented into the workpiece surface. Afterwards, F_A pushes the indented abrasive particle in the axial direction to remove the material in the form of micro/nano sized chips. Abrasive particles that take part in material removal during AFF process are known as active abrasive particles. While, the ones that don't take part in the material removal process are called inactive abrasive particles. During the preparation of medium proper balance is maintained between the elastic and viscous component of the medium. Viscoelastic medium with dominating elastic component is not able to deform itself properly while extruding through workpiece passage. It results in causing problems during extrusion. Also, large elastic force can cause the abrasive particle to hit the workpiece surface with high F_R. This can cause severe indentation on the workpiece surface which distorts the final surface roughness of the workpiece surface. On the other hand, if the medium has dominating viscous component, it flows freely through workpiece passageway without having sufficient F_R forces for the shearing of surface roughness peaks by abrasive particles.

3.2 Development of viscoelastic abrasive medium

In the present experimental work, indigenously developed economic medium is used for carrying out AFF experiments.

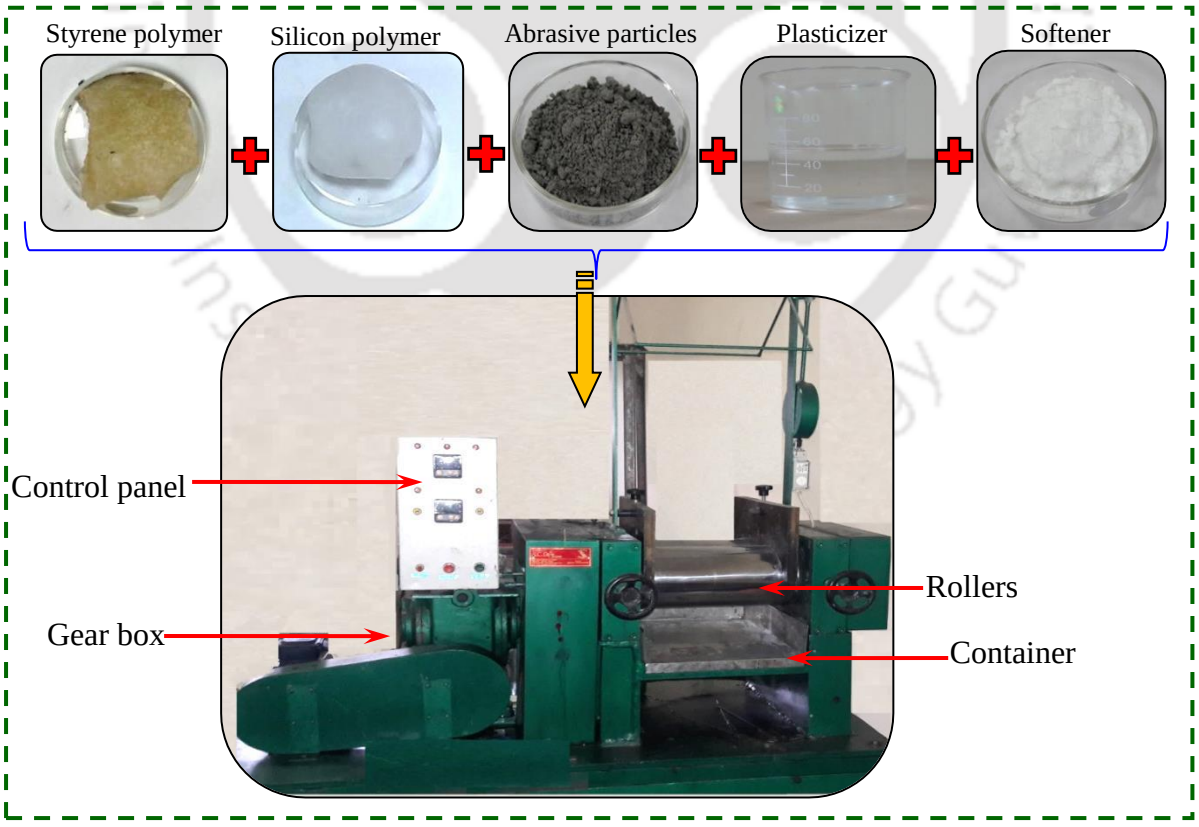

Fig. 3.6 *Various ingredients with two roll mill machine used for developing in-house medium.*

All the medium constituents are mixed properly with the help of two-roll mill. The two-roll mill consists of two chromium plated roller separated by a small gap. As the rollers start rolling, medium constituents are allowed to pass through the gap again and again until all ingredients are mixed properly. Initially, polymers that are making the base medium are mixed properly. Later, in appropriate quantities various additives and abrasive particles are added to the mixture (Fig. 3.6). Static and dynamic rheological study of the developed medium is done on MCR- 101 parallel plate rheometer (Fig. 3.7(a)). Rheometer consists of a rotating top plate (tool master) and bottom stationary plate (base plate). For properly holding the semisolid medium samples, ends of both the plates are provided with the diamond cone pattern and the sample is kept between them (Fig. 3.7(b)). Rheometer is also provided with thermoelectric temperature control (Peltier thermostat). This helps in studying the medium rheological properties at constant as well as varying temperatures.

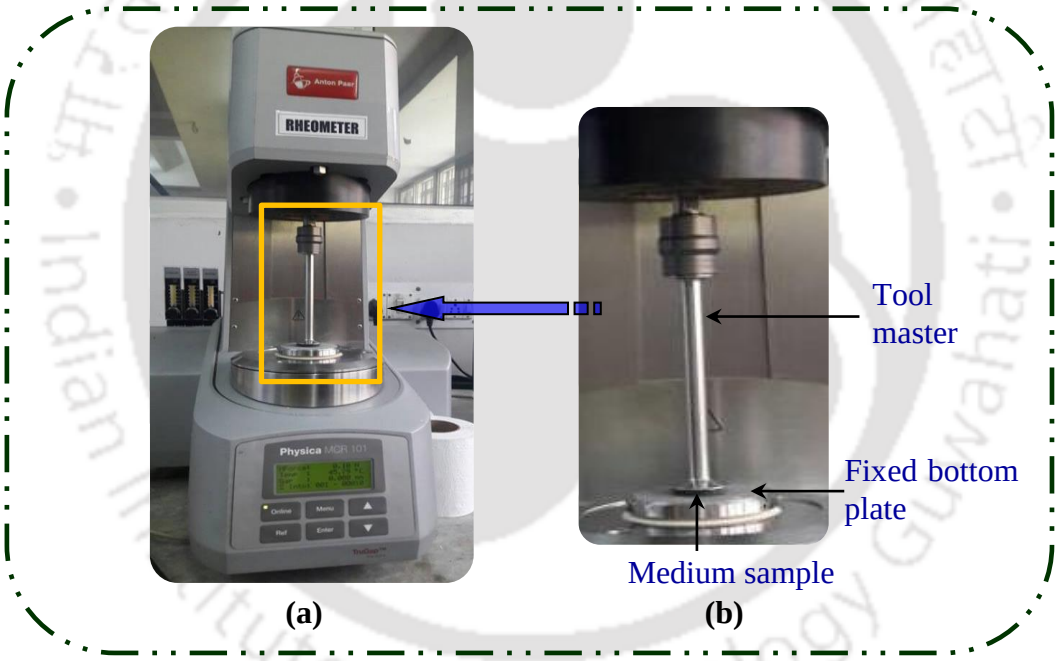

Fig. 3.7 *Rheological characterization of medium* ***(a)*** *overview of rheometer used for measuring static and dynamic rheology (Anton Paar-MCR-101 series)* ***(b)*** *sample between top and bottom plate.*

3.2.1 Medium ingredients

Medium used for finishing of workpieces with AFF process mainly consists of base polymers, various additives (plasticizers and softeners) and abrasive particles. In literatures, several researchers attempted to replace the commercially expensive AFF medium with economic in-house developed medium. In the current thesis, various mixtures of styrene

butadiene polymer (SBP) and silicon polymer (SP) based base polymers blended medium is used for carrying out AFF experiments. The weight percentages of the different medium ingredients are varied according to workpiece dimensions to be finished (macro or micro passage).

3.2.1.1 Base polymer

Styrene butadiene polymer (SBP) is a synthetic polymer derived from two monomers, styrene and butadiene (Fig. 3.8). SBP is one of the economic synthetic general purpose elastomer. The main reason of using SBP as a constituent of the medium is due to its good abrasion resistance and ageing properties. So, the medium can be used for a longer period without degrading its properties. In the present work, SBP consists of 75 % butadiene (CH_2=CH-CH=CH_2) and 25% styrene (CH_2=CHC_6H_5) by weight. Styrene monomer makes SBP more elastic in nature, while butadiene monomer imparts the viscous nature. The amorphous nature of the SBP provides flexibility to the polymer chains. Polymer chains are held together by the weakest intermolecular forces. These weak binding forces permit polymers to stretch or compress under the action of external forces. Styrene monomer possesses branched structure with phenyl ring acting as the branch, while butadiene has a linear structure. These polymer branches resist the easy movement of the polymer chains which enhances the elasticity of SBP. Butadiene polymer chain is flexible in nature because of its linear repeating units joined in a single chain by weak intermolecular forces.

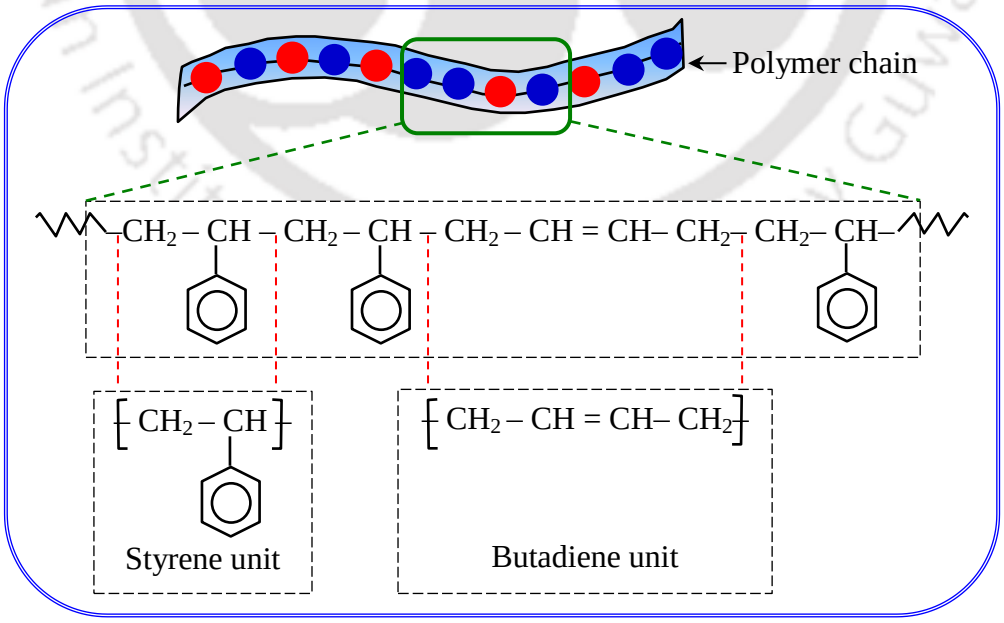

Fig. 3.8 *Random copolymer arrangement of styrene butadiene polymer.*

The other base polymer used is soft silicone polymer (Fig. 3.9). This soft silicone based polymer is cured to enhance its mechanical properties (toughness, hardening). Silicone based polymer is a chain of alternating silicon atoms and oxygen atoms (⋯-Si-O-Si-O-Si-O-⋯). Soft silicone base polymer is non-reactive, stable, and resistant to extreme environments and temperatures. This polymer is very flexible due to the presence of silicon and oxygen bond with large bond angles and bond lengths. Due to large bond length polymer chains can easily stretch in the direction of applied stress and change conformation easily (i.e., good flexibility).

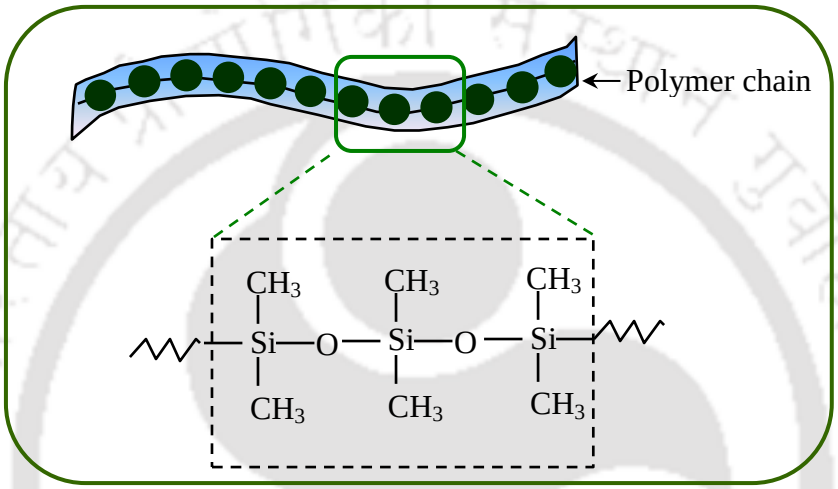

Fig. 3.9 *Chemical structure of the soft silicone polymer.*

3.2.1.2 Abrasive particles

During the AFF process, abrasive particles with multiple cutting edges act as miniature cutting tools. In the literature, it is found that researchers mainly used abrasive particles of boron carbide, silicon carbide, aluminium oxide, and diamond. Choice of the abrasive particle depends on the workpiece hardness to be finished. While, the size of abrasive particle depends on the workpiece surface roughness before AFF process and the workpiece surface roughness required after the AFF process. During the current experiments, silicon carbide (SiC) abrasive particles are mixed in the medium for shearing the surface roughness peaks. To study the effect of abrasive particle size and their concentration on the final surface roughness, SiC particles of various mesh size (#180, #220, #400, #600 and #1000) and in different wt. % are mixed in the medium.

3.2.1.3 Plasticizers

For finishing components with macro features, moderate to high viscous medium can serve the purpose. On the other hand, as the dimensions of the components to be finished by the

AFF process decreases, low viscous medium is preferred. Medium viscosity can be reduced by increasing the plasticizer content [91]. Plasticizers (processing oils or dispersants) are small molecules (low molecular weight materials) and do not have long chains. Being small in size, plasticizer's diffuse between long polymer chains (high molecular weight materials), thus increasing the gap between the long polymer chains which results in increased mobility/flexibility and the reduced viscosity of the medium (Fig. 3.10).

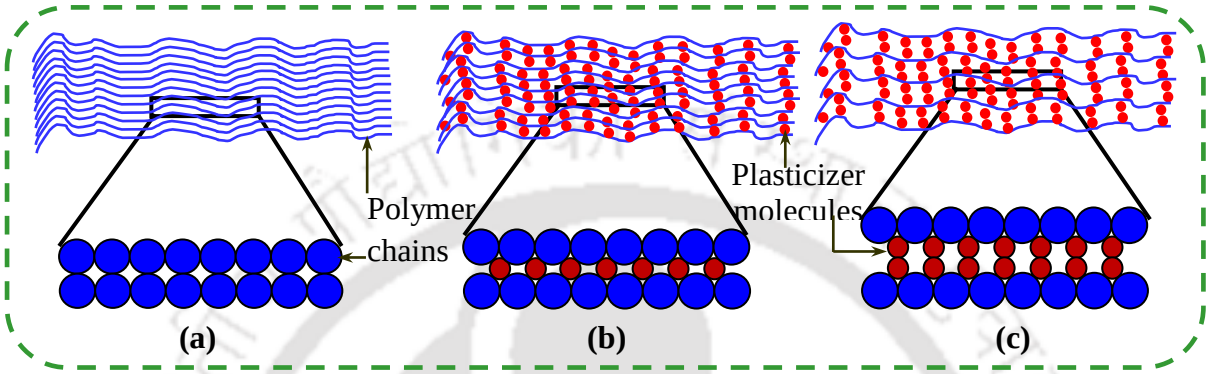

Fig. 3.10 *Diffusion phenomenon of low molecular weight plasticizer in between polymer chains* ***(a)*** *polymer chains with no plasticizer molecules* ***(b)*** *low volume of plasticizer molecules getting diffused between polymer chains* ***(c)*** *high volume of plasticizer molecules getting diffused between polymer chains [91].*

3.2.1.4 Softeners

Addition of plasticizers decreases the medium viscosity. However, above a critical wt. % it imparts sticky nature to medium. As a result, during the AFF experiments medium starts to stick on the workpiece surface wall, thus reduces the finishing efficiency of the AFF process. Softeners are organic compounds available in micro to nano powder which promotes the flexibility to the polymer chains.

3.2.2 Medium composition

Medium used for finishing tubes, microslots and microholes is prepared in-house. The base polymer is a mixture of styrene butadiene polymer (SBP) and silicone polymer (SP). Among the workpieces finished by AFF process in the current thesis work tubes possess dimension in macro range followed by micro range dimensions of microslot and microhole workpieces (Fig. 3.11). During the finishing of workpieces with macro dimensions medium doesn't undergo large deformation while extruding through the workpiece passageway. Therefore, for finishing such workpieces high viscous medium with dominating elastic nature is needed. This leads to the generation of sufficient amount of radial stresses even for a small

deformation which helps the abrasive particles to shear the surface roughness peaks. Considering the above reason (dominating elastic component), the wt. % of SBP polymer is kept higher than wt. % of SP in all the medium compositions prepared for finishing tubes (Table 3.1).

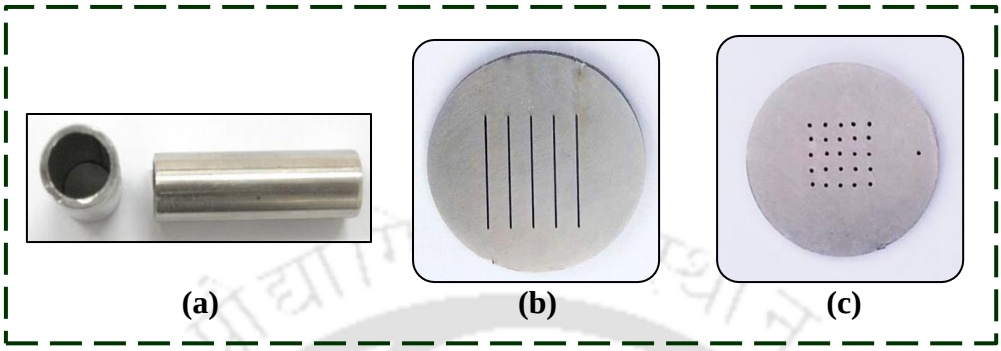

Fig. 3.11 *Various workpieces finished by the abrasive flow finishing process (a) tubes having inner diameter 12.7 mm (b) microslots having length 20 mm and width 450 µm (c) microhole having radius 425 µm.*

Table 3.1 *Various AFF medium compositions (wt. %) prepared for finishing tubes.*

Medium composition	SBP	Silicon polymer	Abrasive particles	Plasticizers	Softeners
1.	28.22	19.47	41.60	4.87	5.84
2.	26.58	18.33	45.00	4.58	5.50
3.	24.12	16.67	50.00	4.17	5.00
4.	21.75	15.00	55.00	3.75	4.50
5.	20.11	13.87	58.40	3.47	4.16

Table 3.2 *Various AFF medium compositions (wt. %) prepared for finishing microslots.*

Medium composition	SBP	Silicon polymer	Abrasive particles	Plasticizers	Softeners
1.	21.13	26.42	36.60	8.45	7.40
2.	20.00	25.00	40.00	8.00	7.00
3.	18.33	22.92	45.00	7.33	6.42
4.	16.67	20.83	50.00	6.67	5.83
5.	15.53	19.42	53.40	6.21	5.44

Passageway of the microslots through which medium is extruded during the AFF experiments is very narrow due to the micro dimensions of microslots. Thus, the medium need to undergo large deformation during its extrusion through the microslot passageway. So,

to assist for easy flow, medium with low viscosity and minimal elasticity is prepared. As shown in table 3.2, higher wt. % of the SP than the wt. % of the SBP ensures that the medium prepared for finishing microslots is less viscous in nature as compared to the medium prepared for finishing tubes.

Workpiece with microholes provides still more resistance to the medium during its extrusion compared to microslots. This is due to the comparatively smaller cross-sectional area of the microholes through which the medium extrudes. Thus, various compositions of the medium prepared for finishing microholes are decreased in viscosity by increasing the wt. % of the SP and decreasing the wt. % of the SBP (table 3.3). To further decrease the viscosity of the microhole medium wt. % of softeners is increased.

Table 3.3 *Various AFF medium compositions (wt. %) prepared for finishing microholes.*

Medium composition	SBP	Silicon polymer	Abrasive particles	Plasticizers	Softeners
1.	15.60	29.26	36.60	8.78	9.75
2.	14.77	27.69	40.00	8.31	9.23
3.	13.59	25.38	45.00	7.66	8.47
4.	12.31	23.08	50.00	6.92	7.69
5.	11.47	21.51	53.40	6.45	7.17

3.3 Rheological Characterization

To examine various properties of the developed medium prepared for conducting AFF experiments, its rheological study is carried out. Type and amount of various ingredients added in the medium preparation plays a vital role during the finishing action of AFF process. Hence, to understand flow and deformation of the medium during AFF process it is necessary to understand the rheological properties of the developed medium. Static and dynamic rheological characterization of the medium help in understanding the pattern and aggressiveness of the abrasive action during AFF process, i.e. how other medium ingredients assist the abrasive particles to shear workpiece surface peaks.

3.3.1 Static rheology

3.3.1.1 Flow characterization

In AFF process, medium flows with assistance of extrusion pressure. The flow characterization decides the finishing action. So, first flow characterization is performed. During the flow test, the variable shear rate is applied by the rotating tool master on the

medium sample which is placed in between the upper and bottom rheometer plate (Fig. 3.12(a)). Initially, polymer chains are randomly aligned (Fig. 3.12(b)). As the shear rate is applied by the rheometer tool master on the medium, the tool master starts rotating. This applies shear stress on polymer chains. Then polymer chains start moving. At low shear rate the top layer of polymer chains start climb one over another. This increases polymer chains density at tool master interface (Fig. 3.12(c)). So, the resistance to the tool master gradually increase (i.e. shear stress gradually increase). On application of more shear rate the polymer chains start breaking (Fig. 3.12(d)). As a result, polymer molecular entanglement density starts decreasing and the alignment of the polymer chains takes place (Fig. 3.12(e)).

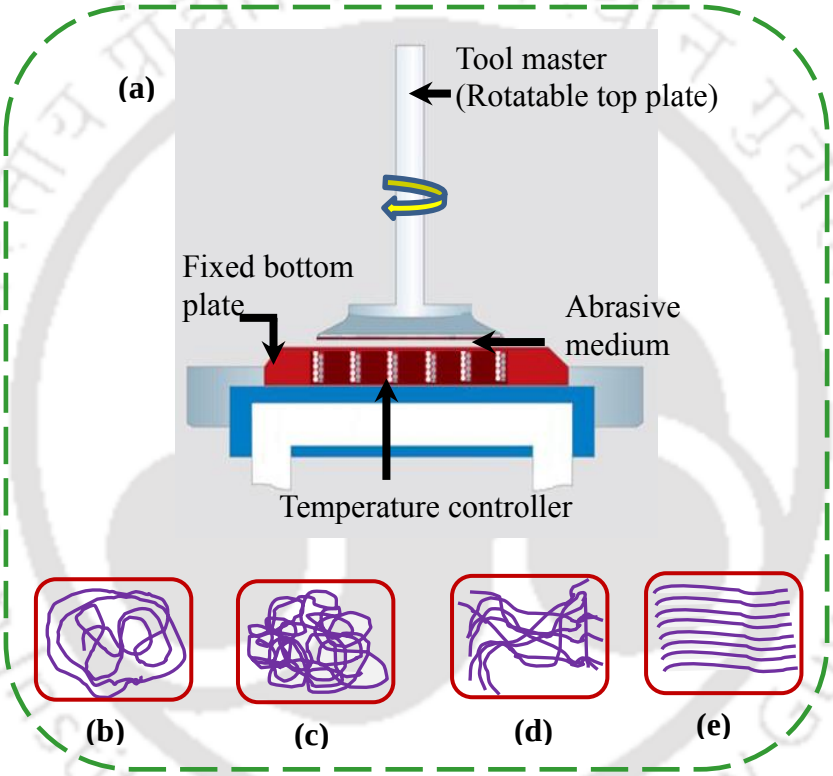

Fig. 3.12 (a) *Rheometer schematic, polymer chain structure at* ***(b)*** *rest* ***(c)*** *low shear rate* ***(d-e)*** *high shear rate.*

Initially at low shear rate due to the increase in density of the polymer chains shear stress increases. However, beyond a critical value of shear rate (0.30 s^{-1}) due to the breaking of the polymer chains shear stress value decreases (Fig. 3.13). In the literature, Jain et al. [59] reported the shear rate in the range of 0.04 s^{-1} - 0.24 s^{-1} during AFF experiments. Sankar et al. [92] reported the range of shear rate as 0.02 s^{-1} - 0.10 s^{-1}. Thus, in the reported shear rate range breaking of the polymer chains doesn't take place. So, in the current work for performing the flow characterization test, maximum shear rate value is taken approximately

0.30 s^{-1}. The slight variation in the shear rate value may be due to the change in compositions with above mentioned authors. In this shear rate region breaking of the polymer chains and hence decrease in the shear stress value with increasing shear rate doesn't take place.

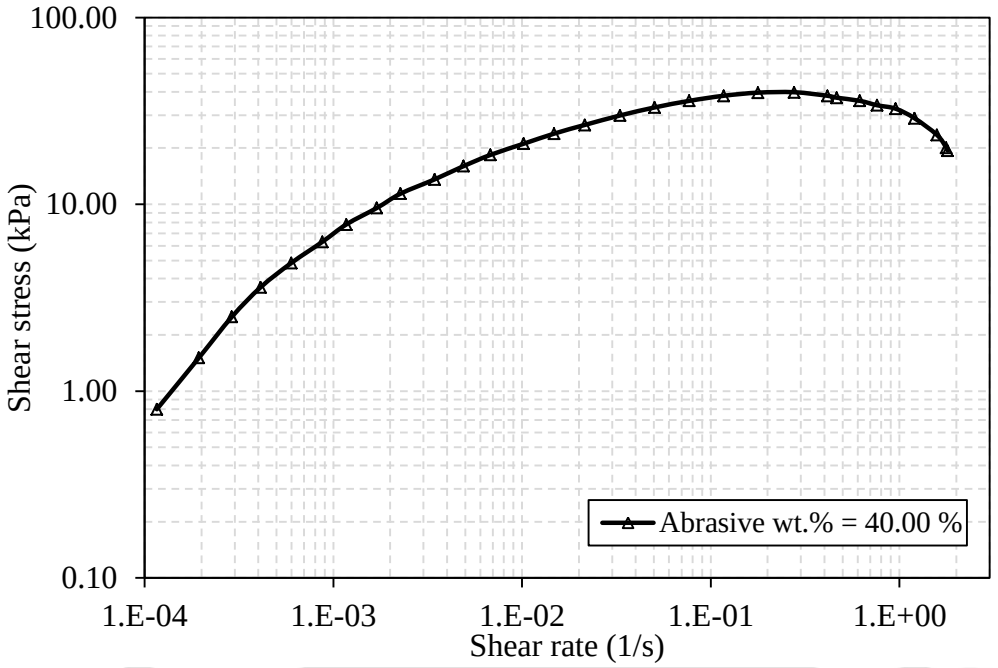

Fig. 3.13 *Effect of shear rate on shear stress of medium prepared for finishing of tube.*

The variation of shear stress with shear rate for different medium compositions prepared for finishing tubes, microslots and microholes are shown in Fig. 3.14.

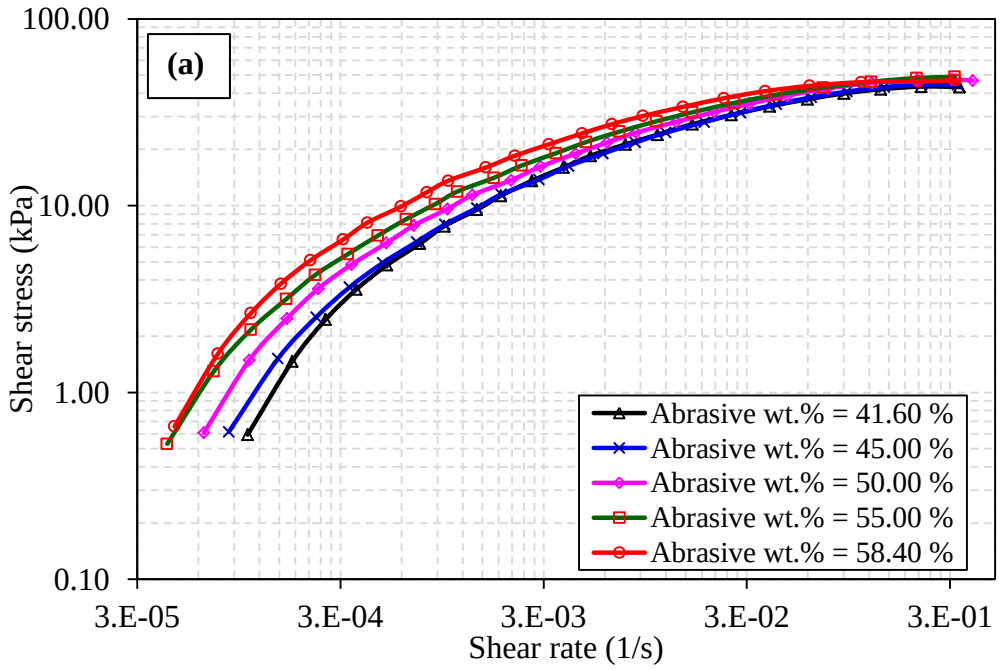

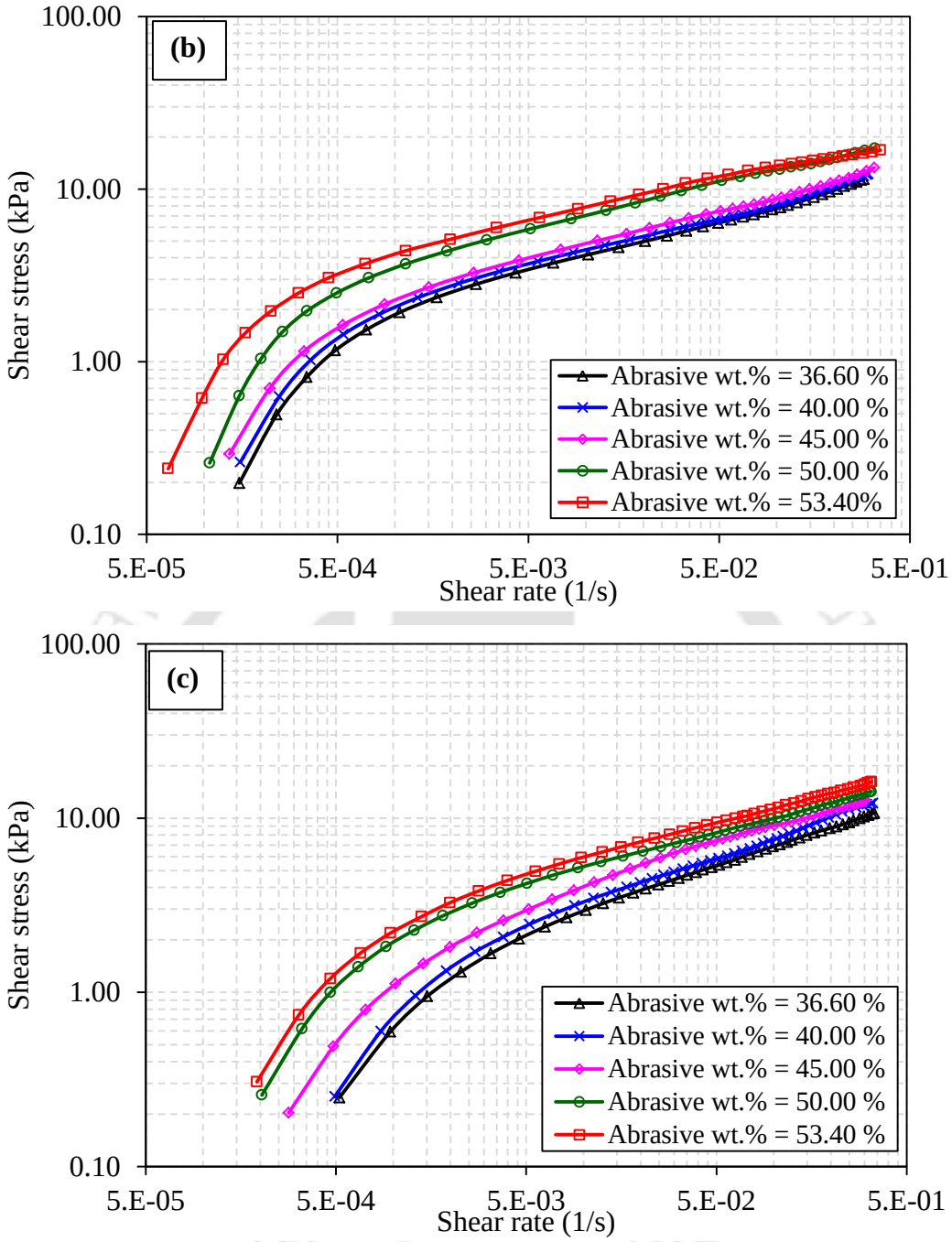

Fig. 3.14 *Effect of shear rate on shear stress of medium prepared for finishing of* ***(a)*** *tube* ***(b)*** *microslot* ***(c)*** microhole *(Logarithmic scale on both X and Y axis).*

3.3.1.2 Strain sweep and stress relaxation

The main purpose of conducting strain sweep test is to study the elongation/stretching behaviour of the base polymer chains of the medium. Polymer chains are stretched by varying % strain and the "range in which the polymer chains are in stretch without breaking is known as its linear viscoelastic range (LVE range)". In LVE range, change in % strain, doesn't cause any change in medium storage modulus (i.e. storage modulus remains

independent of applied % strain). During the strain sweep test, polymer chains are subjected to a range of % strain and the corresponding change in storage modulus is monitored. It is found that LVE range in case of various medium compositions developed to finish tubes is 0.016 % - 0.056% (Fig. 3.15(a)). In case of microslots and microholes, LVE range is observed in between 0.021% - 0.042 % and 0.015 % - 0.030 % respectively (Fig. 3.15(b-c)). The LVE range is highest in case of medium prepared for tube which becomes less in microslot medium and least in microhole medium. This shows the elastic component of viscoelastic medium prepared for tubes finishing is dominant because of more SBP and less SP. Thus, it can sustain high % strain without breaking the polymer chains.

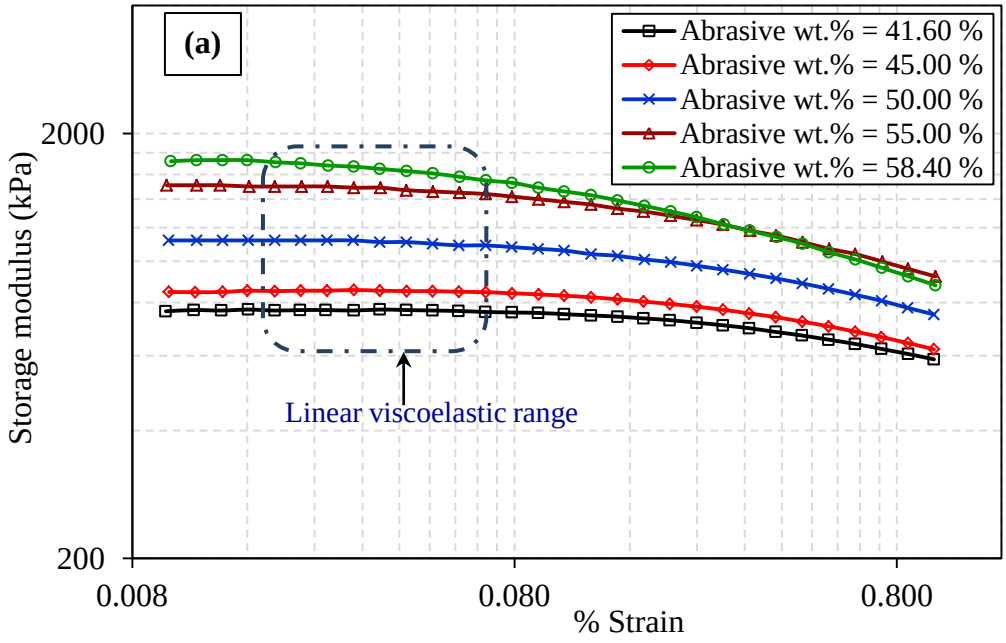

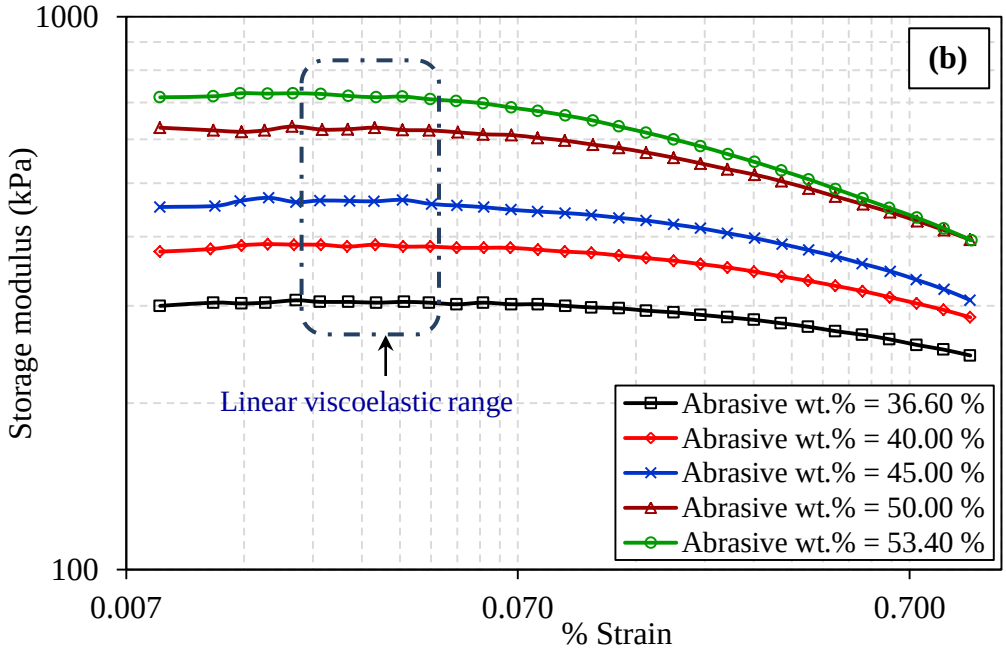

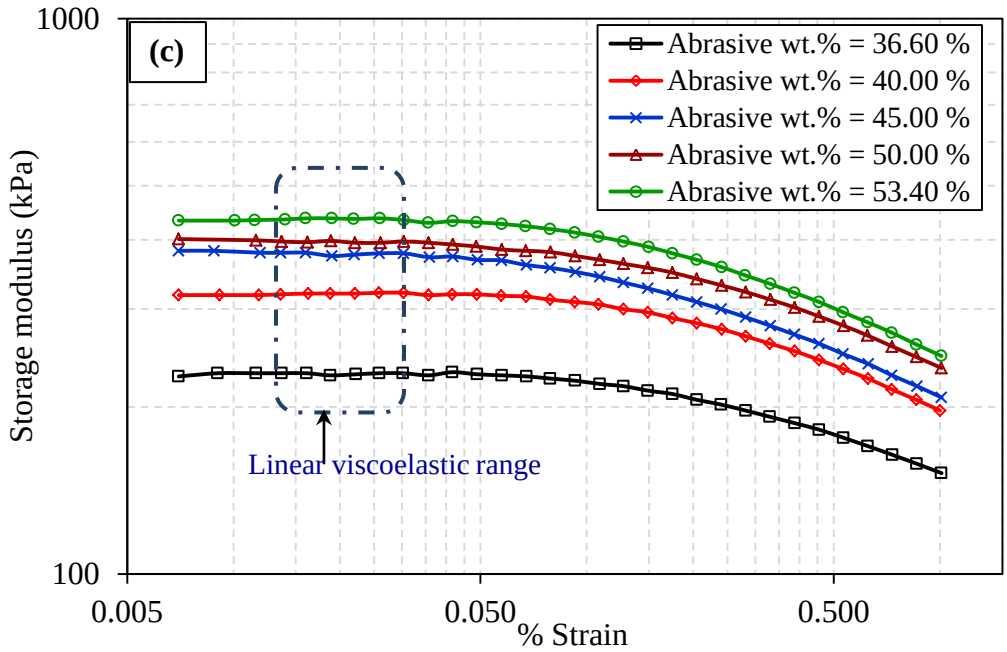

Fig. 3.15 *Variation of storage modulus with percentage strain of medium prepared for finishing of* ***(a)*** *tube* ***(b)*** *microslot* ***(c)*** microhole *(Logarithmic scale on both X and Y axis).*

Medium prepared for finishing microslots and microholes are viscous component dominant because of more silicone based polymer. Thus, polymer chains making the base medium can't be stretched to high strain rates without breaking. This is indicated by the decrease of LVE range in various compositions of microslot and microhole medium.

Behaviour of the medium under the action of constant strain is studied by carrying out the stress relaxation test. During the test, the medium is subjected to a constant % strain, whose value is taken from the LVE region that obtained from amplitude sweep test (Fig. 3.15). Relaxation modulus is given as:

$$\text{Relaxation modulus} = \frac{\text{Stress(t)}}{\text{Applied strain}} \tag{3.1}$$

where, stress(t) is the difference in the stress values acting on polymer chains at different time interval. As the strain is applied for a time period of 300 s, change in stress is calculated for the same time period i.e.:

$$\text{Stress(t)} = \text{Stress}_{t=0s} - \text{Stress}_{t=300s} \tag{3.2}$$

Viscoelastic polymers when subjected to an applied % strain, chains may deform by either or both fundamentally different molecular mechanisms. The lengths and angles of the chemical bonds connecting the atoms may distort, moving the atoms to new positions of

greater internal energy. This is a small motion and occurs very quickly, this corresponds to elastic nature. If the polymer has sufficient molecular mobility, larger-scale rearrangements of the atoms are possible i.e. viscous fluidity. Initially, on the sudden application of strain on medium, polymer chains accommodates the applied strain by stretching of bonds and behave as an elastic dominant material with high relaxation modulus. But as the time progresses, polymer molecules gradually accommodate the strain by conformational extension rather than bond distortion and exhibits the relaxation modulus of a material with viscous dominant nature [93]. Thus, relaxation modulus decreases with time (Fig. 3.16(a-c)).

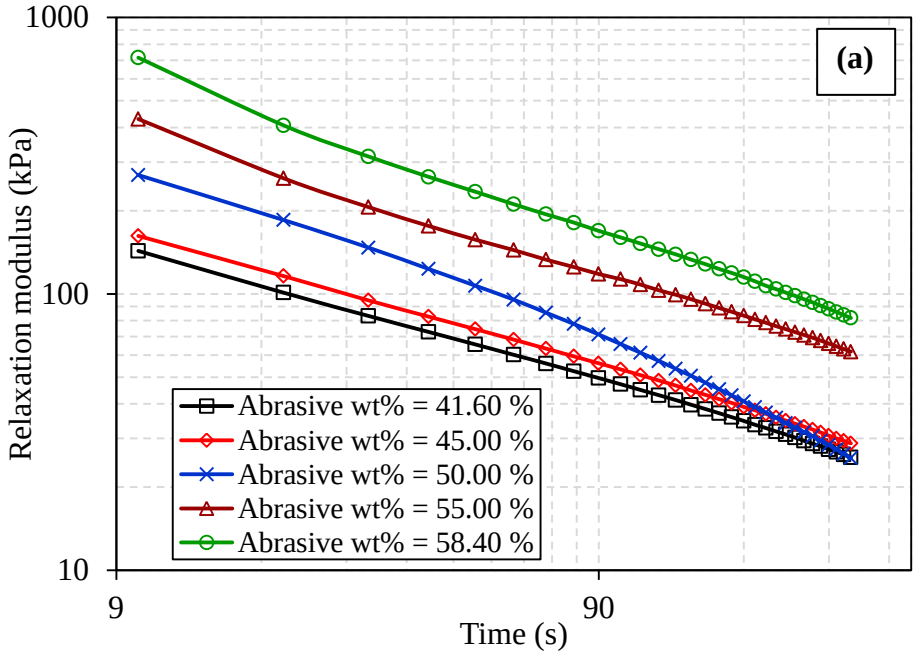

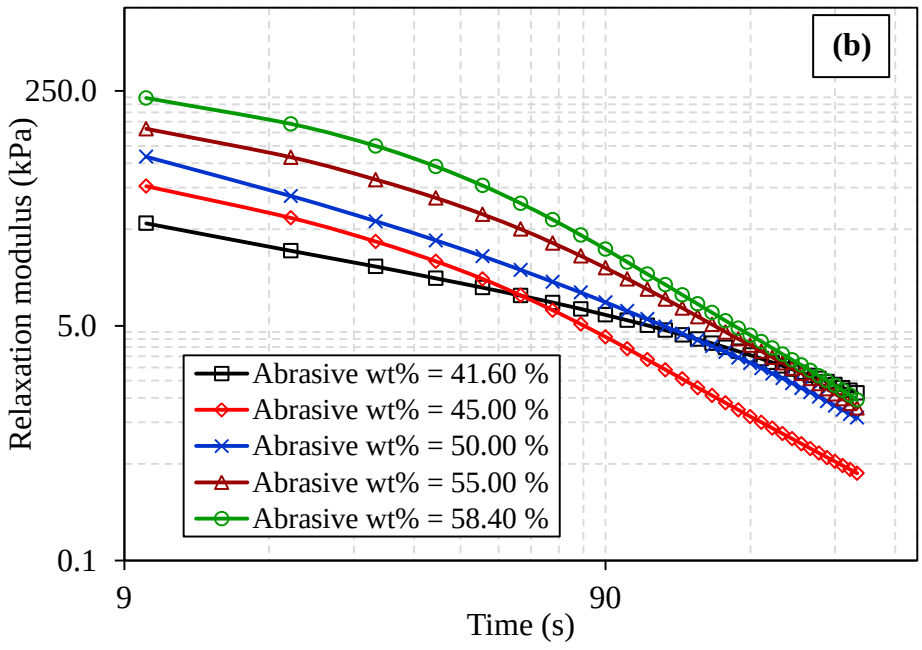

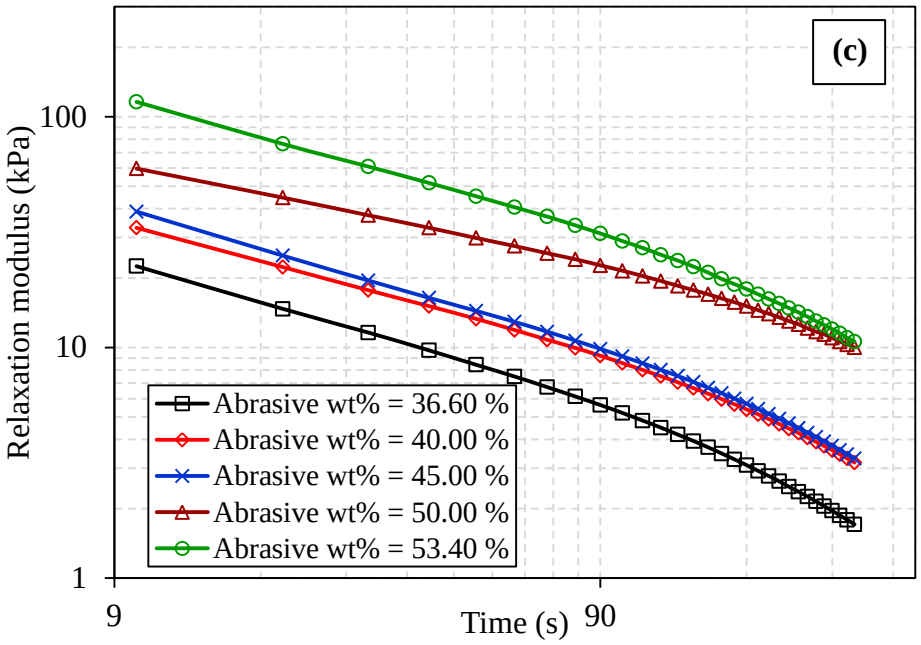

Fig. 3.16 *Variation of stress relaxation modulus with time of medium prepared for finishing of* ***(a)*** *tube* ***(b)*** *microslot* ***(c)*** *microhole (Logarithmic scale on both X and Y axes).*

Stretched bonds between styrene atoms retract at faster rate as compared to the bonds between silicon atoms. As a result, rate of decreases of relaxation modulus of the styrene dominant base medium of tube (Fig. 3.16(a)) is more as compared to silicon base polymer dominant medium for microslot (Fig. 3.16(b)) and microhole (Fig. 3.16(c)).

3.3.1.3 Stress sweep and creep recovery

Stress sweep test is performed to find the variation of storage modulus of medium with the change of stress. The stress range in which there is not much change in storage modulus, this range is called linear viscoelastic (LVE) range. In LVE range, the probability of medium polymer chains doesn't stretch or break is high. This is shown by their constant storage modulus value for a range of stress. LVE range of shear stress for tube medium is around 150-500 Pa (Fig. 3.17(a)). While, for microslots and microhole LVE range is 100-300 Pa and 50-160 Pa respectively (Fig. 3.17(b-c)). This clearly shows that tube medium can resist deformation at higher stress values. As the viscosity of the medium decreases, resisting to external deformation also decreases and hence the value of LVE range decreases. After performing the stress sweep test, a constant value of stress is considered from the measured LVE region and creep recovery test is performed. The main aim to choose stress value from the LVE range is to ensure that the applied stress during the creep test won't damage the polymer chains. Creep test is performed to investigate about the percentage of elastic and

viscous component in the viscoelastic medium. During creep recovery test, the medium is subjected to a constant stress and hold for a fixed amount of time. As a result of the applied stress, medium deforms which consist of both elastic and viscous deformation. Later, the stress is removed and the medium is allowed to recover from the deformation. During the recovery phase, only the elastic deformation of the medium recovers. In current creep recovery test, a constant shear stress is applied for a period of 50 s and thereafter it is removed allowing the medium to recover the deformation.

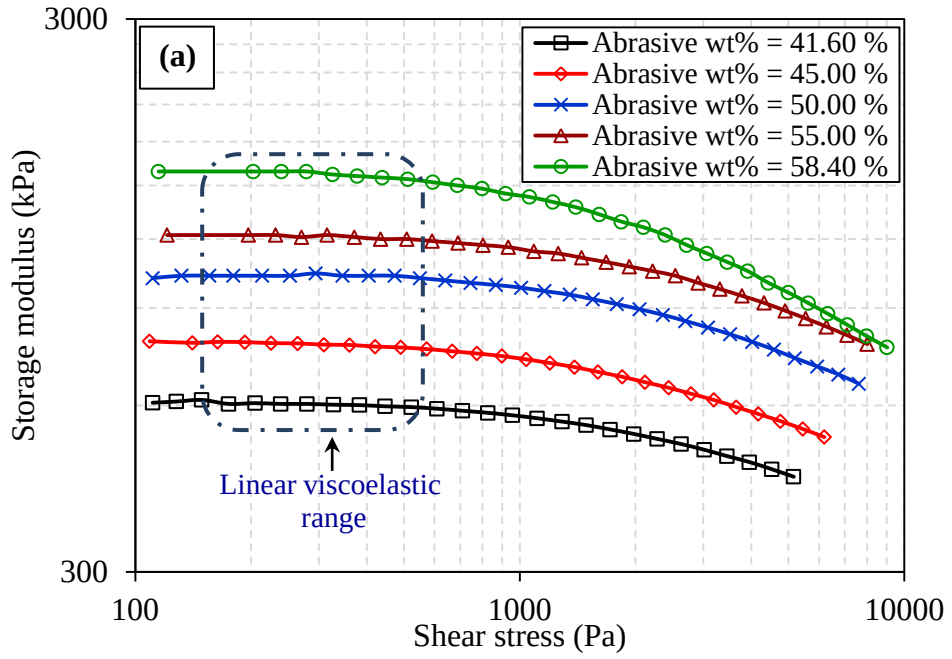

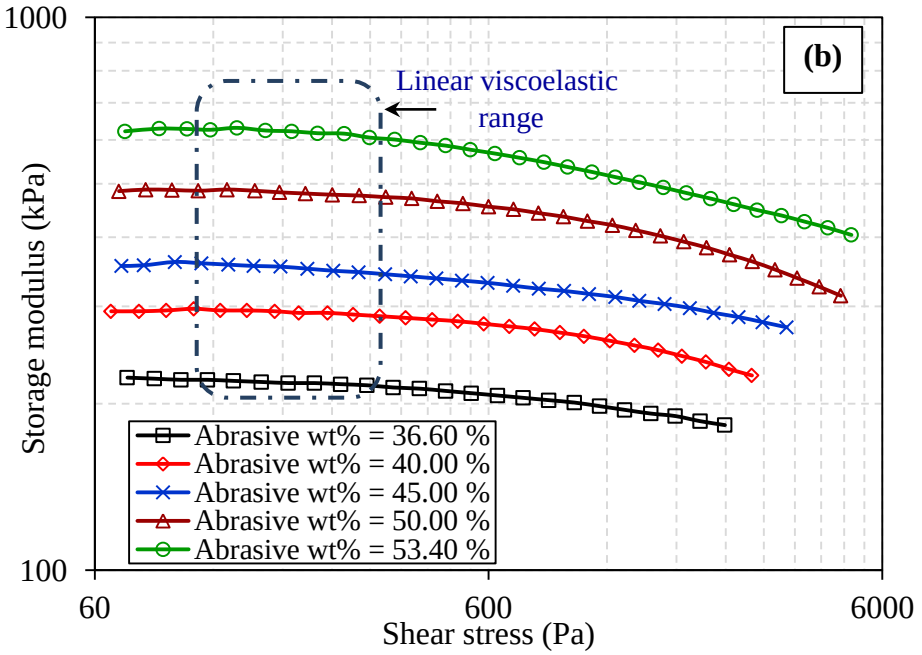

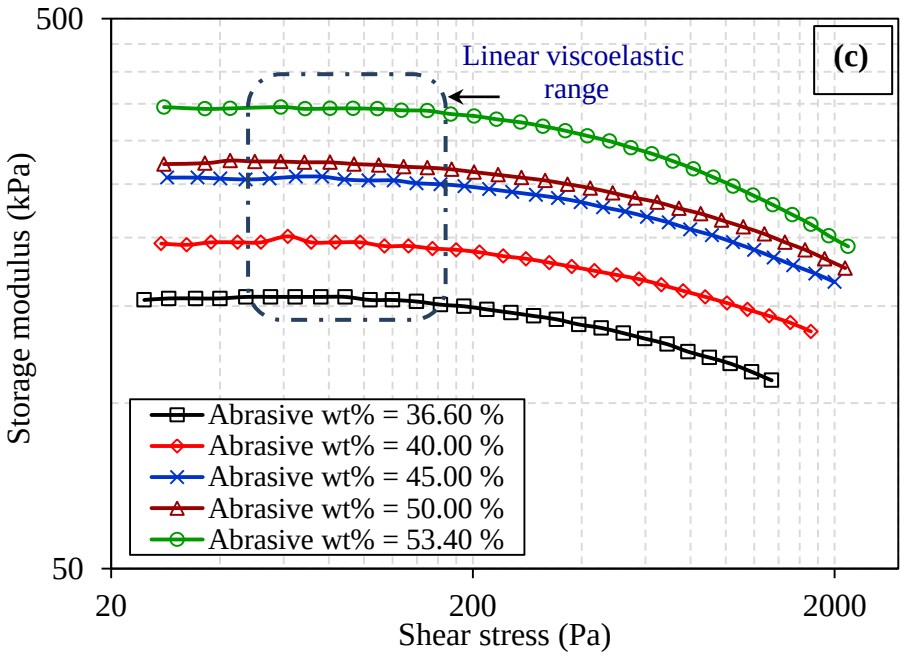

Fig. 3.17 *Effect of shear stress on storage modulus of medium prepared for finishing of* ***(a)*** *tube* ***(b)*** *microslot* ***(c)*** microhole *(Logarithmic scale on both X and Y axis).*

At the start of the creep phase the polymer chains with plasticizers molecules and abrasive particles are at rest. As the stress applied, the viscoelastic polymer chains along with viscous (plasticizers and softeners) molecules undergo deformation. Strain from point A to B in Fig. 3.18 shows total viscoelastic deformation medium undergoes during the creep phase.

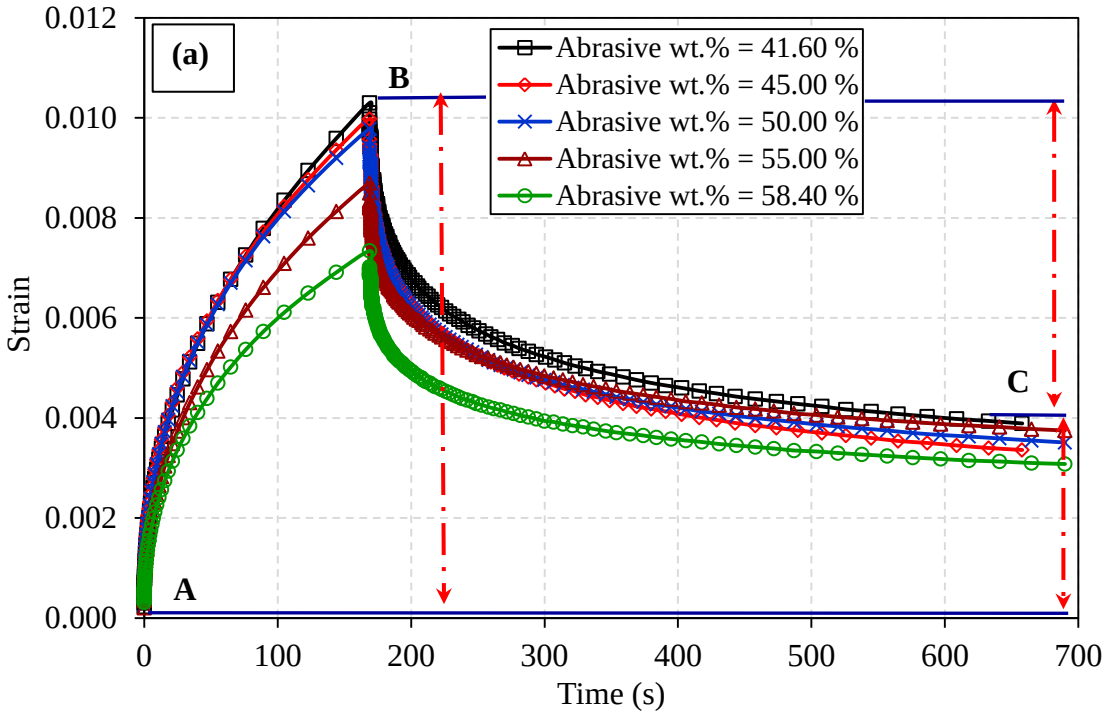

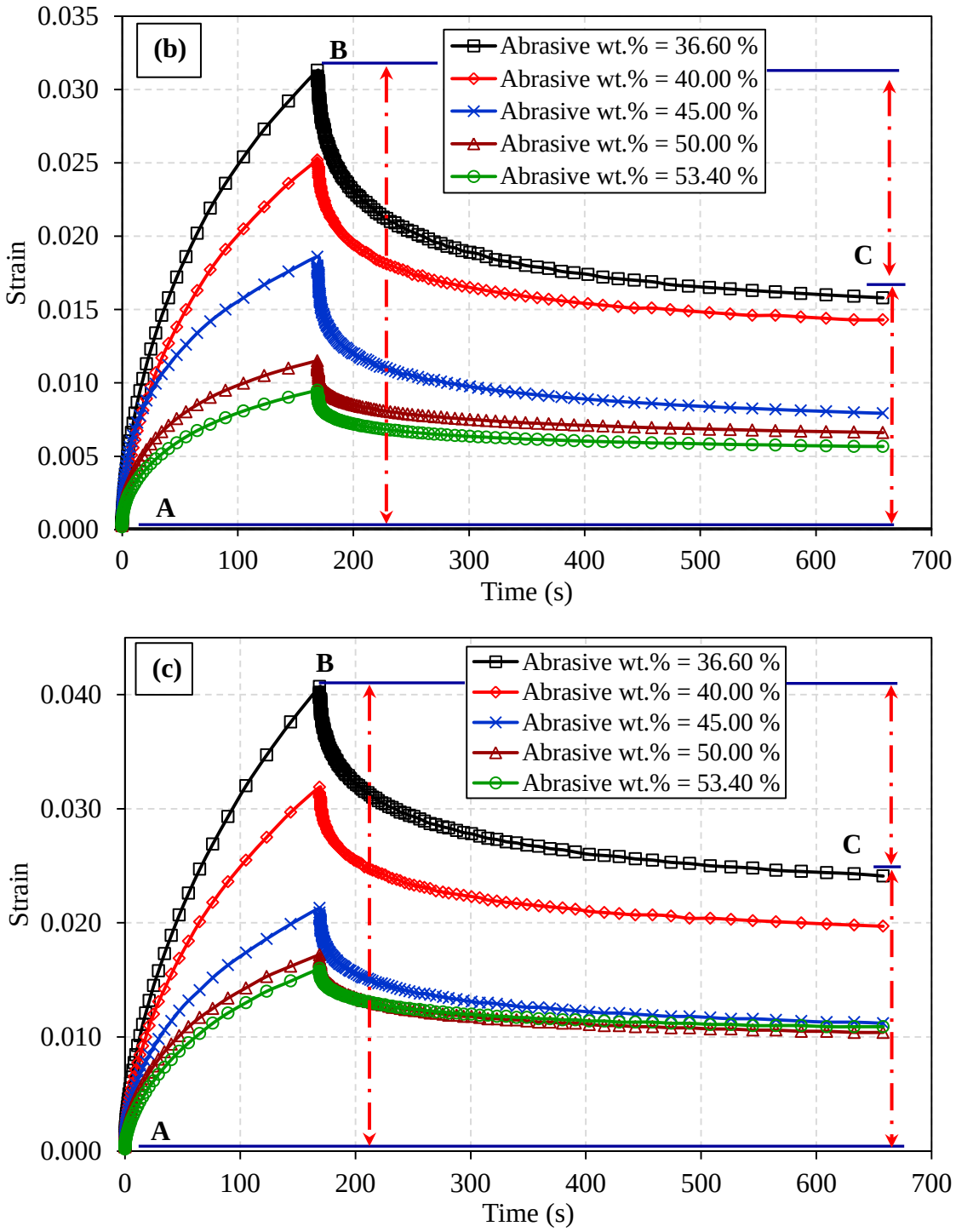

Fig. 3.18 *Variation of strain with time in medium prepared for finishing of* ***(a)*** *tube* ***(b)*** *microslot* ***(c)*** *microhole.*

During the recovery phase (after the release of shear stress) elastic deformation of the medium recovers leaving the viscous deformation permanently in the medium. In Fig. 3.18, BC shows the recovered elastic component of the medium while AC corresponds to the unrecovered viscous component of the viscoelastic medium. Higher the elasticity in medium, more it resists the deformation it has to undergo during its extrusion through the fine

openings of microslots and microholes. Thus, to assist the easy flow of medium through micro openings the viscous component of the medium prepared for finishing microslots and microholes enhanced. Hence, during the recovery phase of the microslot medium (Fig. 3.18(b)), the considerable amount of unrecoverable strain remains in the medium, which further increases in case of microhole medium (Fig. 3.18(c)). Thus, the medium prepared for finishing microslots and microholes fulfills the flow characteristics required during finishing components with micro features by AFF process.

3.3.1.4 Variation of viscosity with temperature

Temperature is an important parameter that affects the viscosity of the medium which in turn decides its finishing capability. As the extrusion pressure during AFF experiments increases, the hydraulic cylinder piston velocity increases, thus number of AFF cycles per unit time increases. Due to this, medium doesn't have sufficient time for releasing the heat which is generated due to continuous shearing of the surface roughness peaks and the friction between medium and the workpiece surface. Base polymer of the medium is very sensitive to the change in temperature. Hence, the role of temperature in deciding shear viscosity of the medium is studied in this section. Polymers are large molecules with long chains formed by repeating units called monomers. These monomers are joined by bonding to form polymers. At normal temperature, the polymer chains are long with original structures. As the temperature increases, thermal energy is gradually added to the medium which results in the movement of bulky side groups and decreases the cohesive forces between polymer molecules. As the temperature of the medium increases, beyond critical these polymer chains of base polymer start vibrating. Further increase in temperature, provides enough energy between interlinks and they start moving apart with respect to each other. Thus, monomer molecules start translating rather than vibrating at high amplitude. Therefore, at high temperature medium becomes low viscous because of more distance relative motion of the monomers within polymer chains. Also, with an increase in temperature, long polymer chains of base polymer disintegrate into smaller segments which assist in their easy movement.

With the decrease in viscosity, the amount of finishing forces acting in the medium decreases as well as medium loses its capacity to hold the abrasive particles effectively. Thus, the finishing capability of the medium reduces at high temperature. The presence of bulky side groups and the double bond between the monomers in SBP provides strong cohesive inter actions and thus less free movement of the polymer chains. Hence, higher the SBP content in the medium more temperature is needed to allow for the free movement of

polymer chains due to strong bonding. Elastic component dominant SBP medium used for finishing of tubes provides more resistance to temperature change as compared to the viscous component dominant medium of microslots and microholes. Therefore, at low temperatures the slope of the shear viscosity-temperature graph is less in case of SBP used to finish tubes (Fig. 3.19(a)) and increases SP used to finish microslots (Fig. 3.19(b)) and microholes (Fig. 3.19(c)).

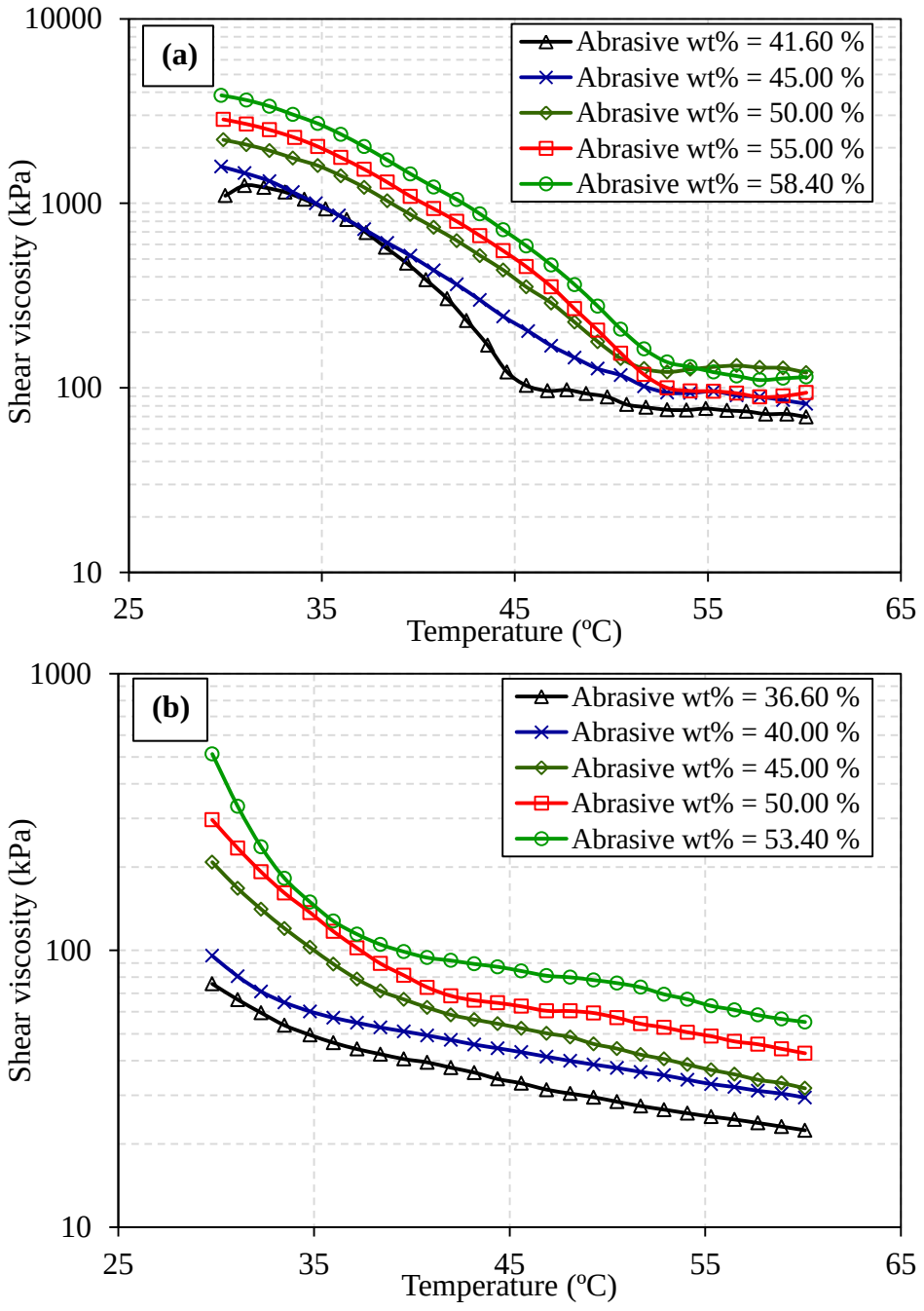

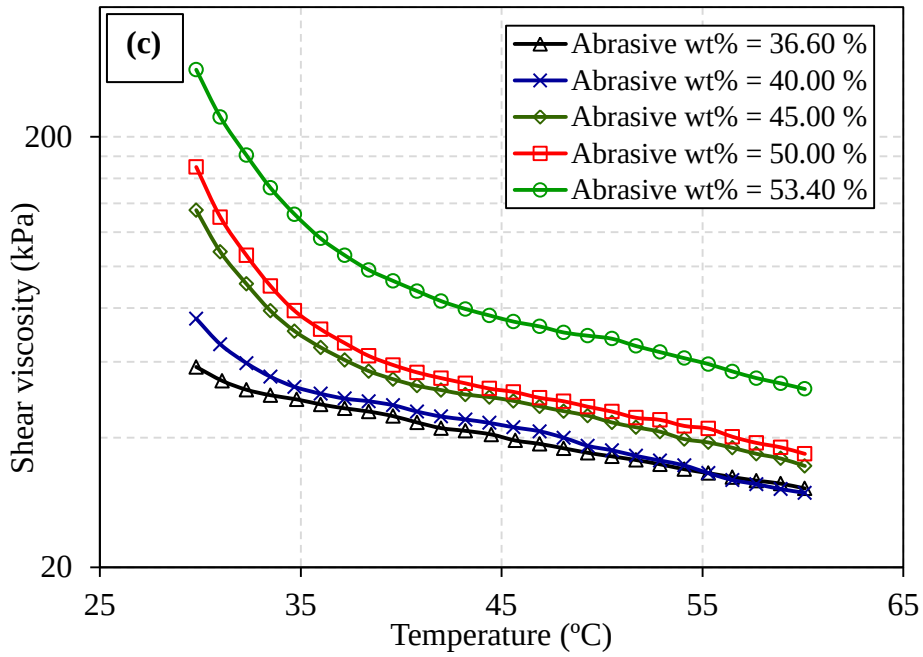

Fig. 3.19 *Effect of temperature on shear viscosity for different weight percentage of abrasive particles in the medium* ***(a)*** *tube* ***(b)*** *microslot* ***(c)*** microhole *(Logarithmic scale on X axis).*

Also, medium with higher wt. % of abrasive particles possesses more viscosity because of more solid content in the medium. Higher the amount of abrasive in the medium, more restriction to the free movement of polymer chains which increases the medium viscosity (Fig. 3.19).

3.3.2 Dynamic rheology

3.3.2.1 Frequency sweep

To study the viscoelastic nature of the medium under oscillatory conditions (which is analogues to the reciprocating motion during the AFF experiments) frequency sweep test is carried out. During frequency sweep test, storage and loss modulus at varying frequency is observed. Storage modulus indicates the elastic component and loss modulus indicates the viscous nature of the medium. Under the action of external force, the amount of energy that can be stored by the medium is represented by storage modulus while the dissipated energy is indicated by the loss modulus. At higher frequencies, there is not enough time between two successive oscillations for the polymer chains to relax and come back to original. Therefore, as the frequency increases, the medium is sheared at a very high rate. Also, higher the frequency, more is the amount of energy applied by the external source on the medium for its shearing. Thus, the storage modulus of the medium increases at increased frequency. This trend is similar in all the medium compositions prepared for finishing of tubes (Fig. 3.20(a)),

microslots (Fig. 3. 20(b)) and microholes (Fig. 3. 20(c)). During AFF experiments extrusion pressure is the external force. Thus, with an increase in extrusion pressure, medium storage modulus increases. This increase the amount of energy is transferred by polymer chains to the abrasive particles during the shearing of roughness peaks. This results in an increase in efficiency of abrasive particles for shearing of the surface roughness peaks effectively. As a result, surface roughness on the workpiece surface improves with an increase in extrusion pressure in case of finishing tubes (Chapter 4), microslots (Chapter 5) and microholes (Chapter 6).

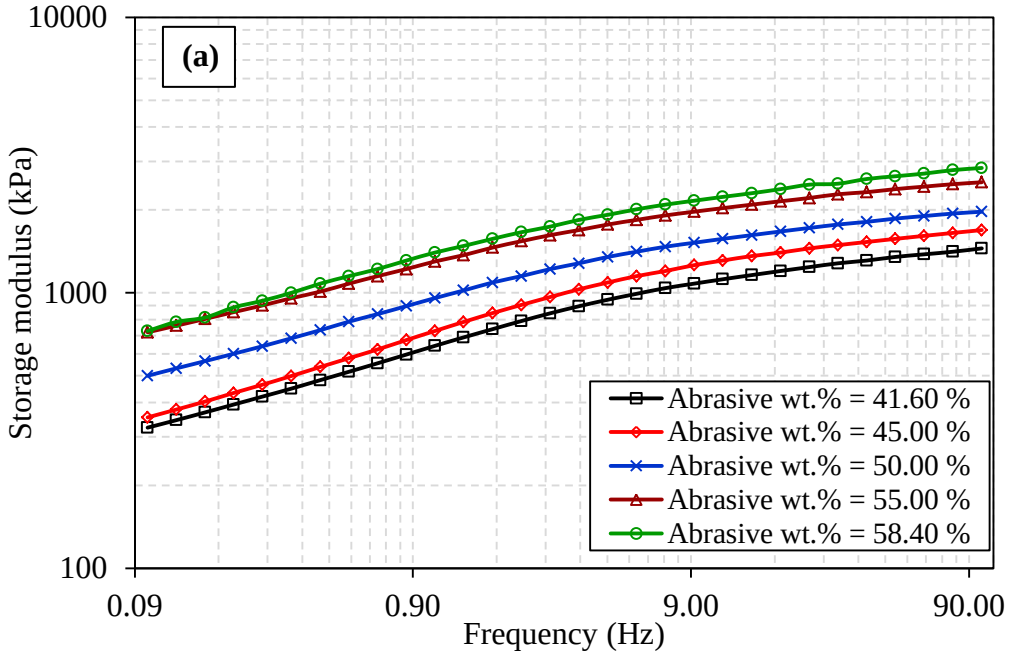

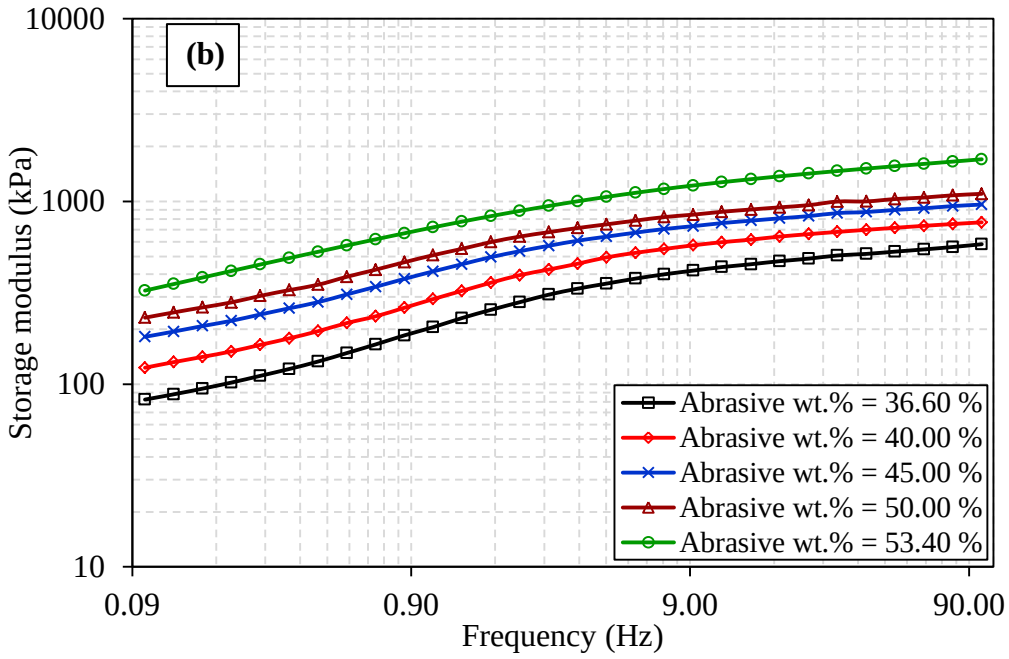

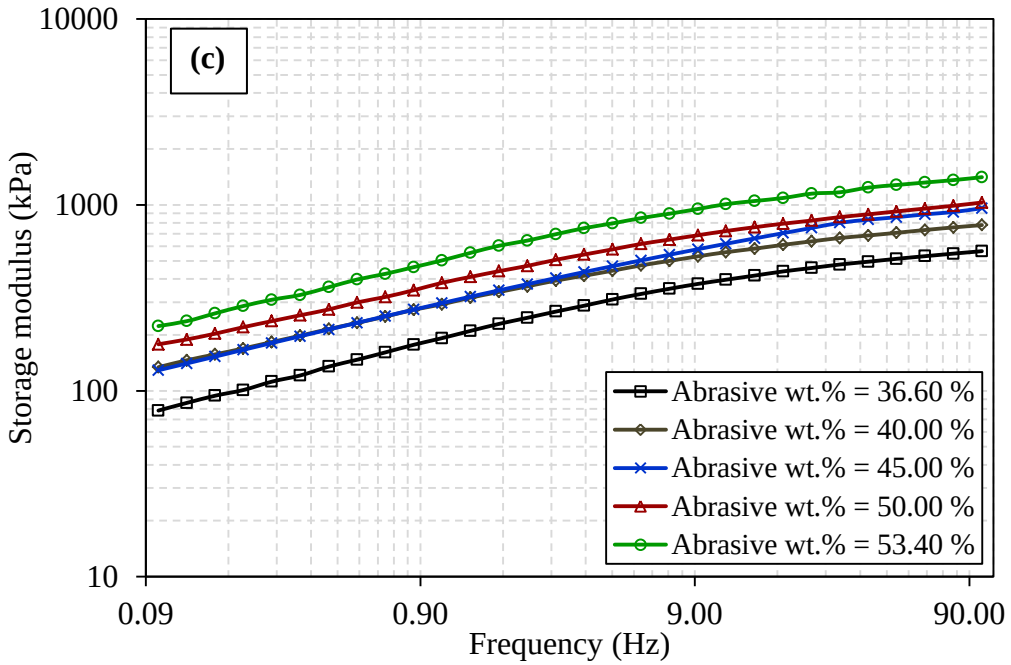

Fig. 3.20 *Effect of frequency on storage modulus of the medium used to finish* ***(a)*** *tube* ***(b)*** *microslot* ***(c)*** *microhole (Logarithmic scale on both X and Y axis).*

Energy dissipated by the medium is generally a natural phenomenon and depends on material properties. Thus, as shown in Fig. 3.21(a-c), there is a marginal increase in the loss modulus with the increase in frequency.

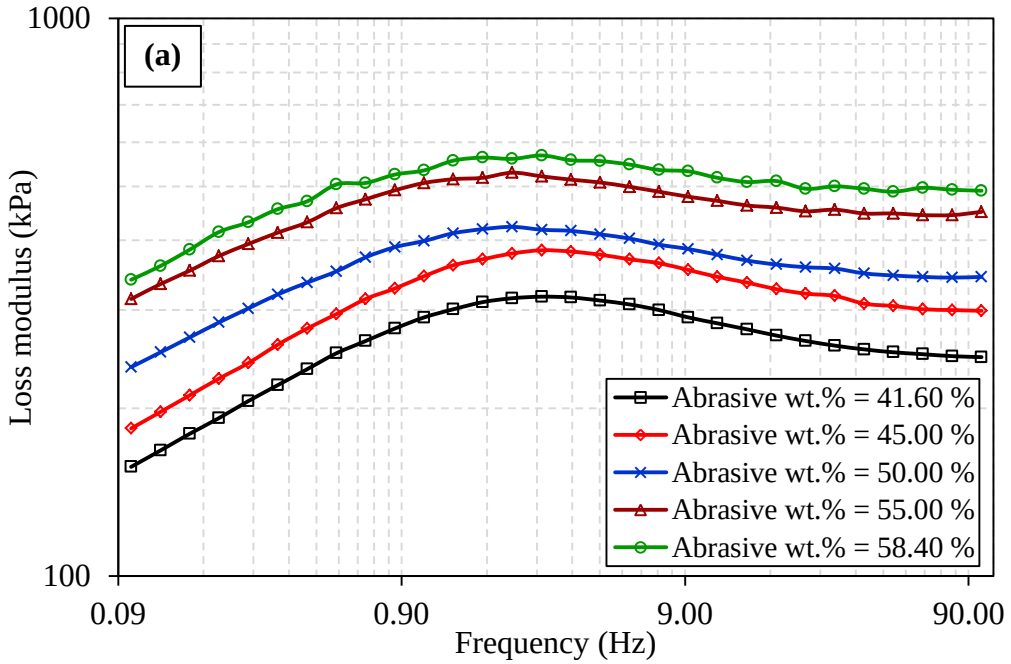

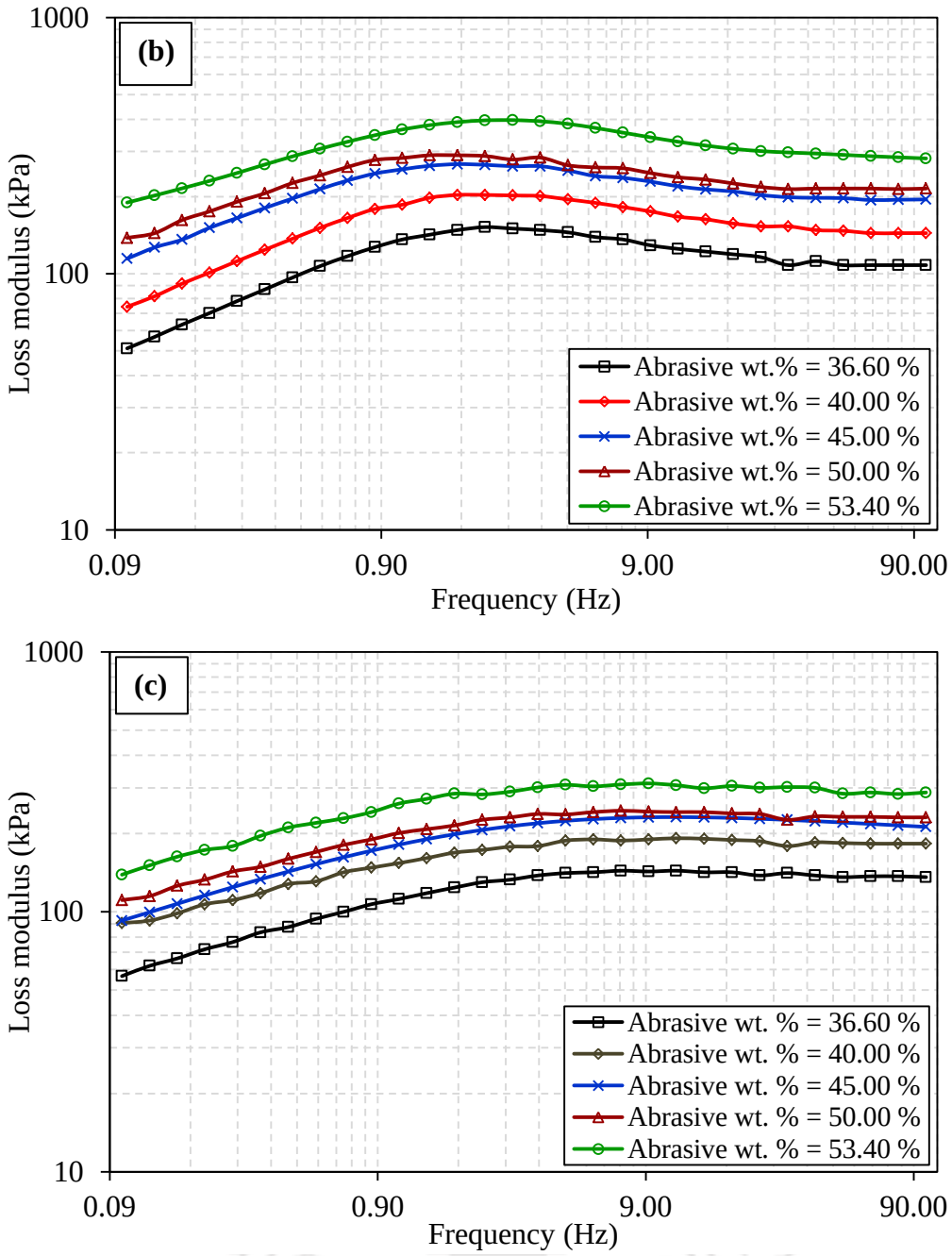

Fig. 3.21 *Effect of frequency on loss modulus of the medium used to finish* ***(a)*** *tube* ***(b)*** *microslot* ***(c)*** microhole *(Logarithmic scale on both X and Y axis).*

As frequency continues to increase above the critical value friction between polymer chains decreases, less energy is dissipated and the loss modulus again decreases. This is due to the fact that dissipated energy increases the temperature of the medium and above a critical value of frequency, the increase in temperature resulted in increased mobility of polymer chains and reducing friction. SBP content is more in the tube medium which resulted in high energy losses due to high friction between polymer chains with dominant elastic component.

The magnitude of loss modulus decreases with the reduction in SBP content in the medium prepared to finish microslot and microhole.

3.3.2.2 Complex viscosity

With an increase in frequency or shear rate of the medium, complex viscosity of medium decreases which represents its shear thinning behaviour (Fig. 3.22(a-c)). This is the most desirable medium property required for finishing of micro features by the AFF process. The narrow passageway of the micro features offers high resistance to the medium during the extrusion. As a result, the medium has to undergo a considerable amount of deformation or in other words, the shear rate of the medium increases during its extrusion through the fine micro features passageway in the workpieces. With an increase of shear rate, the viscosity of the medium decreases which aids in its easy extrusion through the workpieces during the AFF process. Also for the same frequency, the medium with higher wt. % of the abrasive particles possesses higher complex viscosity as compared to the medium with lower wt. % of abrasive particles. This is due to the fact that with the addition of the abrasive particles in the medium the density of medium increases. Polymer chains free movement is restricted by the abrasive particles and the medium becomes stiffer as wt. % of abrasive particles in the medium increases.

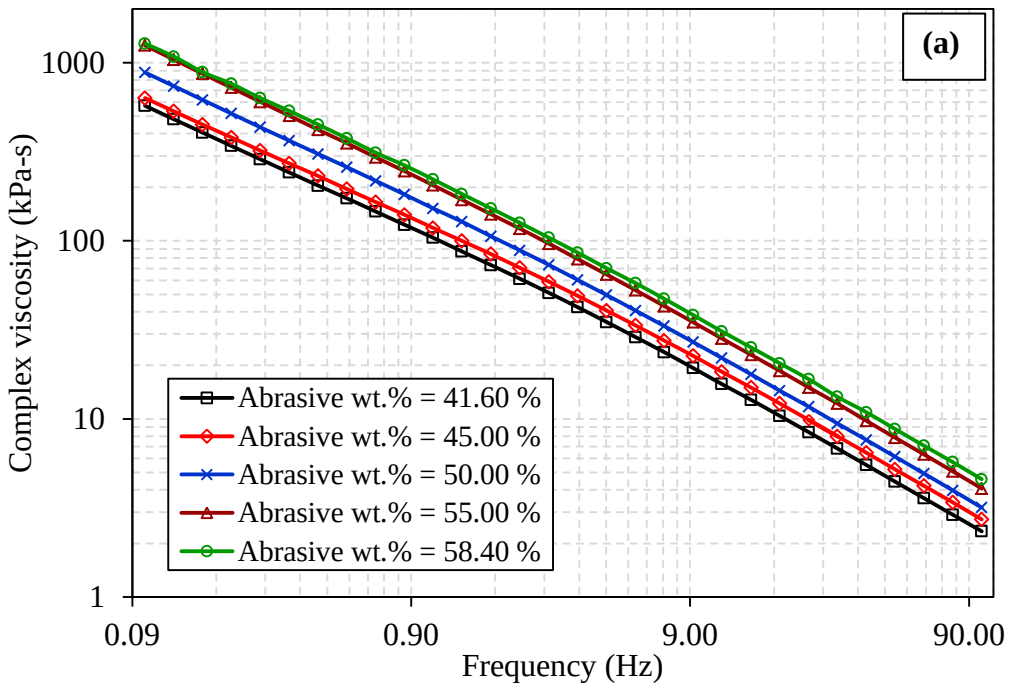

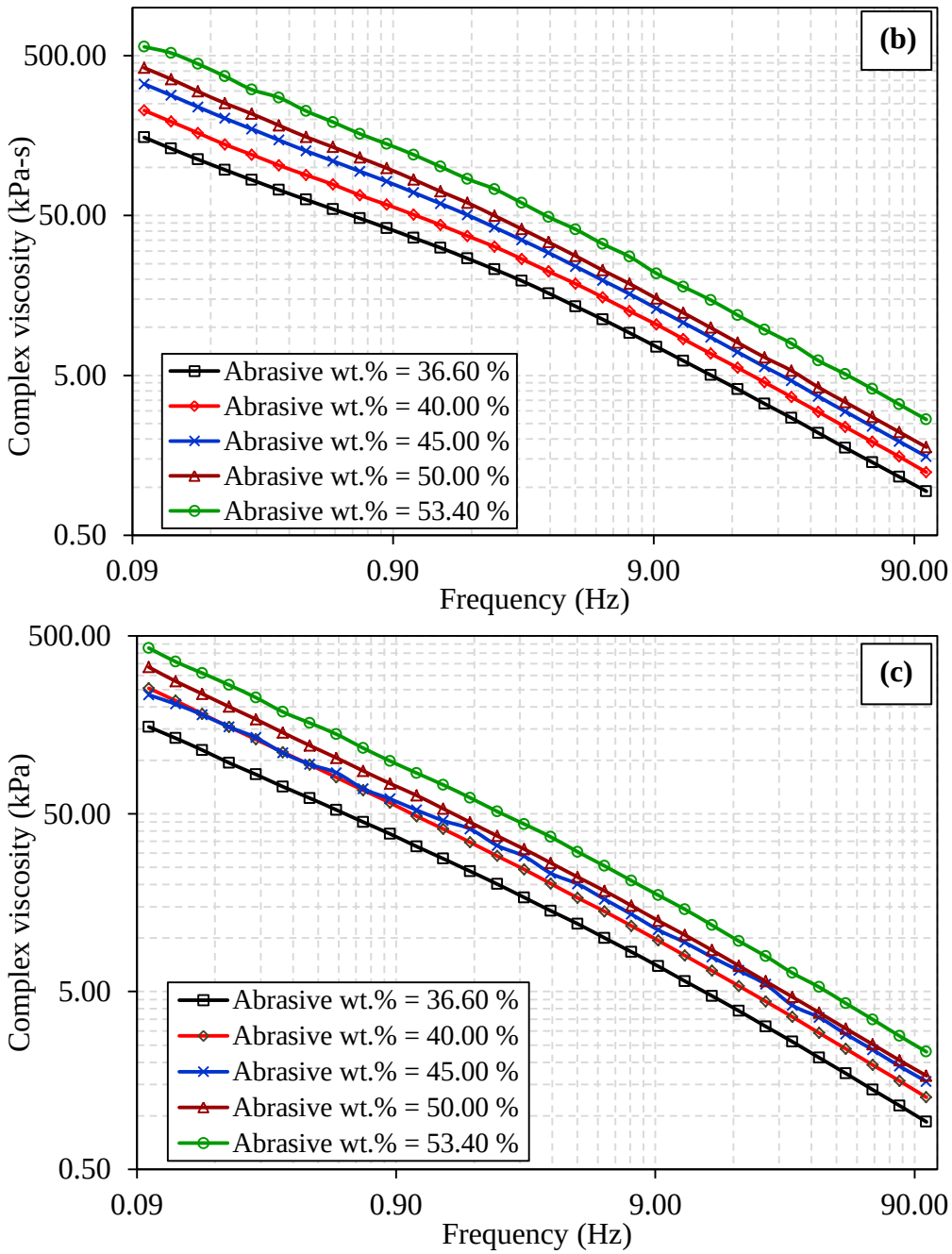

Fig. 3.22 *Effect of frequency on complex viscosity* ***(a)*** *tube* ***(b)*** *microslot* ***(c)*** microhole *(Logarithmic scale on both X and Y axis).*

3.4 Rheological properties comparison among three developed medium

In the above section (3.3), rheological characterization of each medium is individually carried out. To understand the variation among rheological properties of the medium developed for finishing various workpieces (tubes, microslots and microholes), their comparison is carried out.

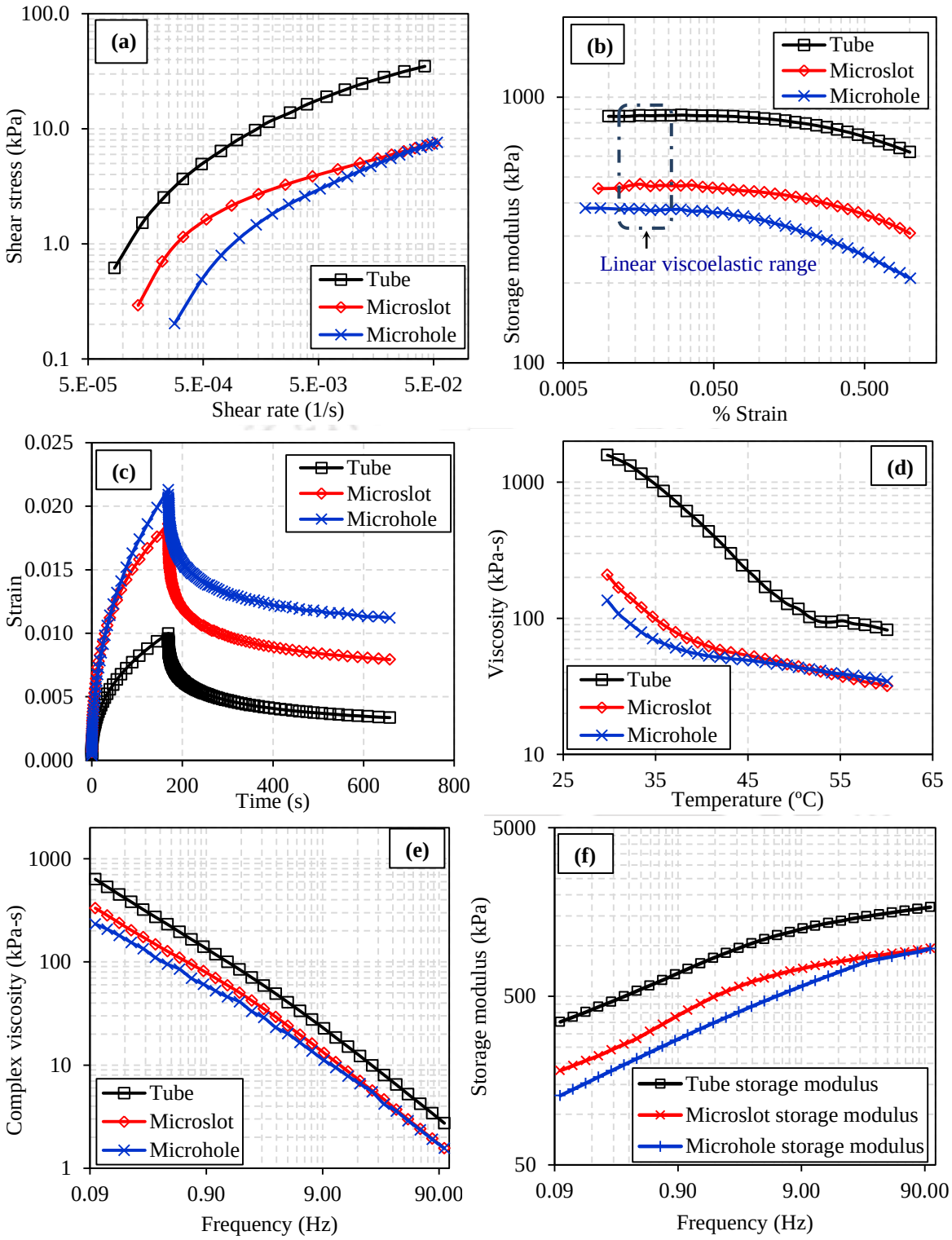

Fig. 3.23 *Comparisons of various rheological properties of the medium developed for finishing tubes, microslots and microholes* ***(a)*** *effect of shear rate on shear stress* ***(b)*** *effect of % strain on storage modulus* ***(c)*** *effect of time on strain* ***(d)*** *effect of temperature on viscosity* ***(e)*** *effect of frequency on complex viscosity* ***(f)*** *effect of frequency on storage modulus (wt. %.* of abrasive particle = 45 %).

Higher the elastic component in the AFF viscoelastic medium more is the resistance against the deformation process. Hence, for the same shear rates, the medium prepared for finishing tubes offers a higher amount of shear stress as compared to the medium prepared for finishing microslots and microholes (Fig. 3.23(a)). Amplitude sweep test (Fig. 3.23(b)) further shows that elastically dominant tube medium polymer chains can sustain higher % strain ranges without breaking. Through the creep test it is found that the deformation (elastic + viscous) of low viscous microhole medium is more than the elastically dominant tube medium because of low viscous nature, for the same stress, strain is high in microhole medium followed by microslot medium. In the recovery phase, high amount of viscous deformation is left in the microhole medium as compared to the tube medium (Fig. 3.23(c)). Since, temperature plays an important role in determining the viscosity of the medium. For the same temperature range, change in viscosity of the tube medium is more as compared to microslot medium and microhole medium (Fig. 3.23(d)). The major reason is that the tube medium mainly consists of SBP. Due to the presence of bulky side groups and double bond between the polymer atoms in SBP, it restricts the free movement of the polymer chains. This results in high viscosity of the tube medium. As the SBP enriched medium gains the thermal energy due to the increase in temperature, local agitation and movement of polymer molecule start. Therefore, the viscosity of tube medium decreases in considerable amount compared to the viscosity of microslot medium and microhole medium. Complex viscosity is an indicator of resistance to deformation of the material under the external forces. Tube medium shows the highest complex viscosity of around 6.33×10^5 Pa-s. For the easy flow of medium through the micro features (microslots and microholes) the elastic nature of the viscoelastic medium is decreased. Thus, the maximum value of complex viscosity achieved in microslot medium is 3.22×10^5 Pa-s which is further lowered to 2.33×10^5 Pa-s for the microhole medium (Fig. 3.23(e)). Fig. 3.23(f) shows the comparison between storage modulus of the various medium. Higher the amount of elastic content in the medium more is the amount of energy it can store. Hence, the storage modulus of the medium prepared for finishing tube is very high as compared to the other medium. To ensure the smooth flow of the medium through the micro features (microslot, microhole), the elastic nature of the medium is decreased. This is shown by the considerable amount of decrease in the storage modulus of medium prepared for finishing microslots and microholes.

3.5 Conclusions

Various compositions of the AFF medium are prepared in-house for finishing of tubes, microslots and microholes. The main aim of developing in-house medium is to replace the commercially used expensive AFF medium. To ensure that the developed medium possesses sufficient and necessary rheological properties needed during the finishing of workpieces their detailed rheological study is done. Based on the rheological study following conclusions are made:

1. Medium prepared are viscoelastic in nature with shear thinning property.
2. Shear stress increases with an increase in shear rate for all the mediums.
3. From the creep recovery test, it is observed that elastic component of the medium is highest in the tube medium, while it is least in microhole medium.
4. Viscosity of the medium decreases with increase in temperature. This is mainly due to the motion of polymer molecules and breaking of polymer chains because of the addition of thermal energy. In the range of 30º C to 60º C the viscosity of the tube medium decreases from 1.58 x 10^6 Pa-s to 8.20 x 10^4 Pa-s. While, for microslot and microhole medium it decreases from 2.08 x 10^5 Pa-s to 3.17 x 10^4 Pa-s and 1.35 x 10^5 Pa-s to 3.44 x 10^4 Pa-s respectively.
5. With an increase in frequency, storage modulus of medium increases. Higher the external forces acting on the medium, more energy it stores during the deformation process.
6. Tube medium with 45 wt. % of abrasive particles shows the highest complex viscosity of around 6.33 x 10^5 Pa-s. The decrease in the elastic component of the viscoelastic medium results in easy flow of medium through the micro features (microslots and microholes). The maximum value of complex viscosity of the medium for the finishing of the microslot is 3.22 x 10^5 Pa-s whereas this value was 2.33 x 10^5 Pa-s during finishing of the microholes.

Chapter 4

NANOFINISHING OF CYLINDRICAL STAINLESS STEEL TUBES

4.1 Introduction to finishing of cylindrical tubes

Stainless steel (SS) due to its resistant to corrosion, staining and low maintenance cost is the most commonly used material in industries. SS tubes are mostly used for laying the piping system in various industries such as power plants, petrochemical, aerospace, marine and medical for carrying high purity gasses and liquids. In the above applications, the internal surface roughness of tube is one of the most important parameters in deciding their overall performance. Tubes having a low internal surface roughness prevent contamination of the flowing substance and reduce the flow losses. From the literature review, it is evident that not much attention paid towards abrasive flow finishing of surgical or bio-steel cylindrical workpieces. Complete experimental parametric study helps in understanding the individual and interaction effect of various AFF input parameters on the finishing output responses.

In view of the above gaps and importance of SS 316L cylindrical tubes finishing, first preliminary experiments are carried out followed by the detailed parametric study of AFF process during finishing of SS 316L tubes is done in the present chapter. Designed and developed AFF setup (Chapter 2) and indigenously developed polymer rheological abrasive medium (Chapter 3) is used for finishing of SS316L cylindrical tubes in this chapter. Experiments are designed by using the central composite rotatable design (CCRD) method. Analysis of variance is carried out for finding the percentage contribution of each input parameter on the output responses. Initial surface roughness on the internal surface of SS 316L workpiece varies in the range of 0.57 ± 0.07 µm. The best surface roughness of 48 nm (0.048µm) is achieved after finishing the workpiece with AFF process.

4.2 Experimental details

The three main components of the AFF process are experimental setup, tooling/fixture and medium.

4.2.1 Abrasive flow finishing setup and tooling

In the current experimentation, AFF process is used. AFF experimental setup consists of hydraulic power pack, two hydraulic cylinders, two medium cylinders structural frame and piston.

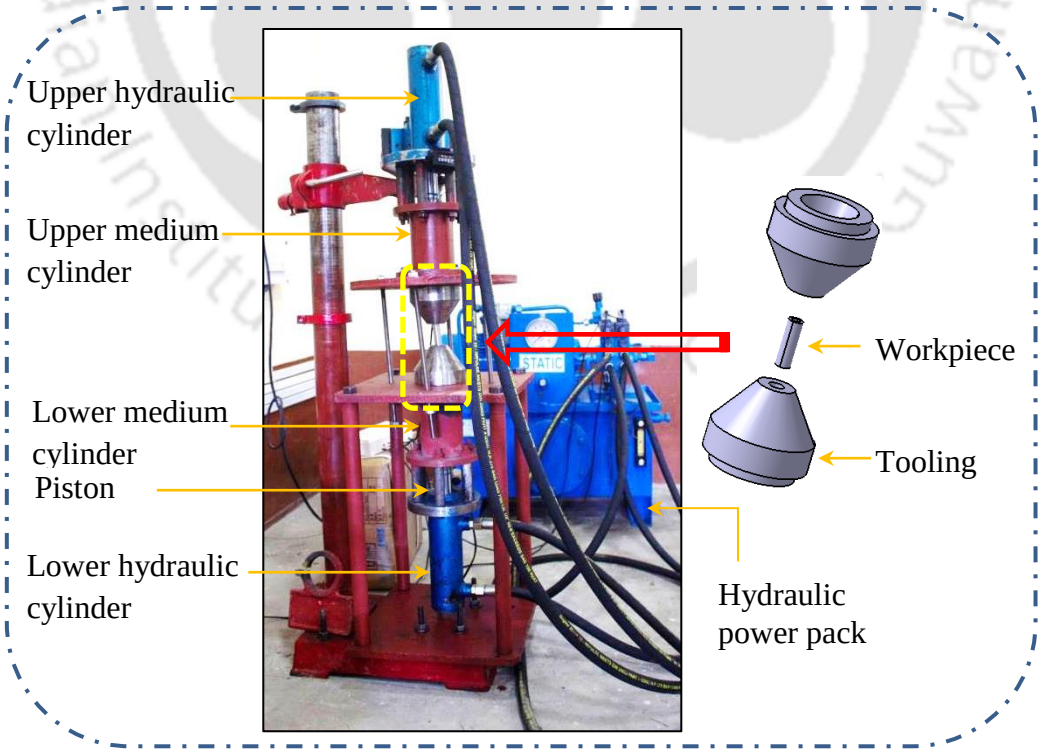

Fig. 4.1 *Abrasive flow finishing experimental setup.*

Complete assembly of the AFF setup with tooling and cylindrical workpiece as shown in Fig. 4.1. At the start of AFF experiments, the medium is filled in the lower medium cylinder. Workpiece is placed in the tooling/fixture and held securely in position by tightening the fixture rods. Medium is then pushed from lower medium cylinder to upper medium cylinder by lower hydraulic cylinder piston with the help of hydraulic power pack. The to-fro motion of the medium via the workpiece internal surface continues till the desired surface roughness on workpiece surface is achieved. The internal diameter of the SS 316L tubes used during the experiments is small. So to ensure a smooth flow of medium from medium cylinder to the workpiece tooling is made of the conical profile. Detailed drawing of the tooling is shown in Fig. 4.2.

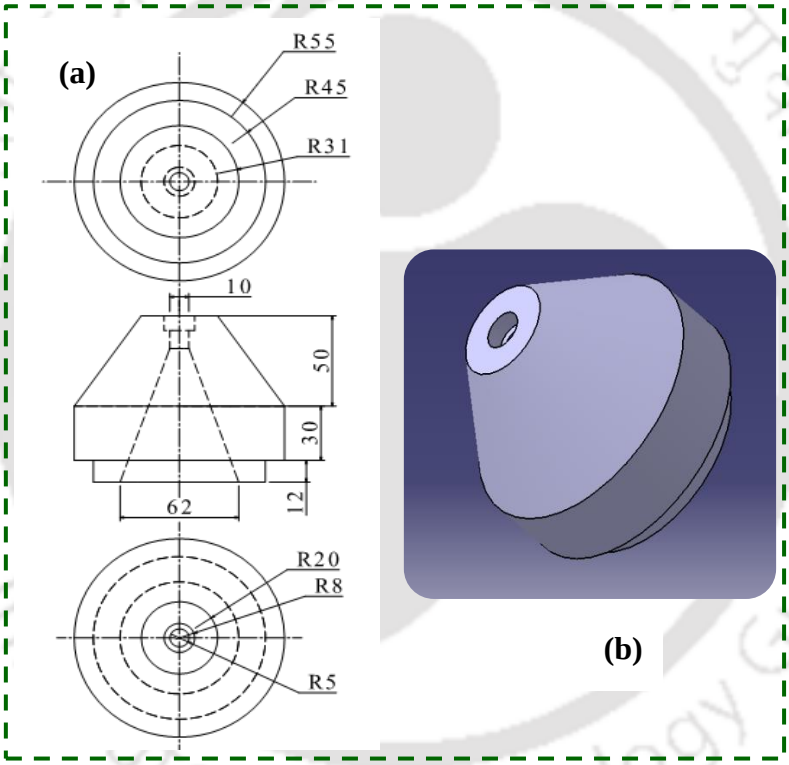

Fig. 4.2 (a) *2-D drawing of workpiece fixture with dimensions* ***(b)*** *3-D model of workpiece fixture (All dimensions are in mm).*

4.2.2 Workpiece

SS 316L tubes (length = 50 mm, external diameter = 15.78 mm and internal diameter = 12.70 mm) are finished in the current experiments using AFF process. Chemical composition of SS 316L is shown in table 4.1. To have a uniform initial surface roughness the tubes are internally bored using a precision lathe. To measure the initial surface roughness of SS 316L tubes internal surface, the workpiece samples are cut with the help of wire electrical

discharge machining (wire-EDM) process. To maintain the accuracy during the measurement of surface roughness, total 18 measurements at 6 different locations (3 measurements at each location) are taken for each tube. Similar procedure of surface roughness measurement is followed after AFF process also. Surface roughness value before and after the AFF experiments were measured by using non-contact type profilometer (make: Taylor Hobson).

Table 4.1 *Chemical composition (in wt. %) of stainless steel 316L.*

C	Cr	Ni	Mo	Mn	Si	P	S	N	Fe
<0.03	16-18	10-14	2-3	<2	<1	<0.045	<0.03	<0.1	balance

4.2.3 Polymer rheological abrasive medium (medium)

Medium used for finishing SS 316L tubes are explained in chapter 3. In house prepared styrene butadiene polymer, silicone polymer, plasticizer and abrasive particles based medium is used to finish SS 316L tubes. Various compositions of the medium are prepared by varying mesh size and wt. % of abrasive particles.

4.3 Preliminary experiments

Preliminary experiments are conducted to find the suitable ranges of AFF input parameters for achieving better surface roughness (low surface roughness) in SS 316L tubes. During the preliminary experiments, the percentage change in roughness ($\% \Delta R_a$) is calculated for various input conditions and is given as:-

$$\% \Delta R_a = \frac{Initial\ surface\ roughness - Final\ surface\ roughness}{Initial\ surface\ roughness} \times 100 \qquad (4.1)$$

Suitable input ranges are used to carry out the design of experiments for complete parametric study of the AFF process.

4.3.1 Effect of extrusion pressure

Extrusion pressure is one of the main input parameters of AFF process. This is the pressure exerted by hydraulic piston on the medium, so that medium starts flowing across the workpiece surface to be finished. Because of extrusion pressure, viscoelastic medium exerts axial force (F_A) and radial force (F_R) on the workpiece surface. As extrusion pressure increases finishing forces (F_R, F_A) on the workpiece gradually increases. F_R, F_A shears the roughness peaks as well as generate smooth surface. Thus, $\% \Delta R_a$ increases with an increase in extrusion pressure (Fig. 4.3).

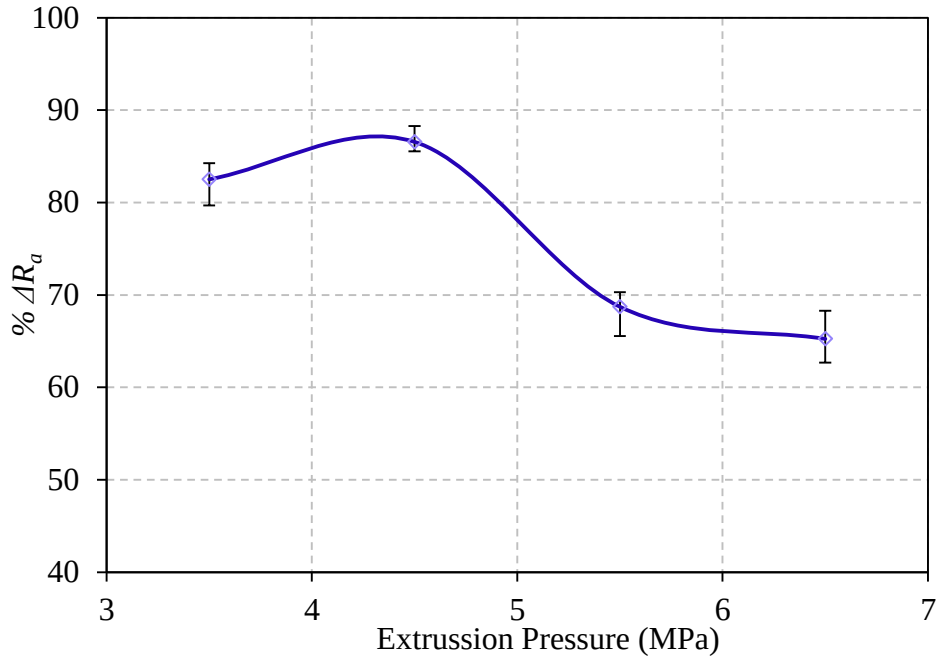

Fig. 4.3 *Variation of the percentage change in surface roughness with extrusion pressure (500 cycles, # 400, 40 wt. % abrasives).*

However, at higher extrusion pressure, increase of F_R is high compared to F_A and causes deep indentation on the workpiece surface. Thus, the final surface roughness above the critical value of extrusion pressure decreases with an increase in extrusion pressure. The suitable range of extrusion pressure varies in the range 4-5 MPa. Suitable amount of extrusion pressure should be applied such that sufficient amount of F_A is required to remove material in the form of microchips. As the extrusion pressure gradually increases, F_R, F_A tries to shear the initial surface roughness (lathe boring marks) peaks and smooth surface is achieved (Fig. 4.4(a-b)). Increase in the extrusion pressure beyond the critical value starts deteriorating the final surface roughness of the workpiece surface. At the high magnitude of extrusion pressure, the rate of increase in F_R is more as compared to F_A [38]. Due to the increased amount of F_R, the abrasive particles penetrate deeper into the workpiece surface. At this increased depth, if the axial force (F_A) acting on abrasive particle is smaller than the resistance of workpiece to remove material in the form of the microchip, then the abrasive particles rotate to decrease the depth of penetration [44] and leave the indentation marks at that location. Also in some cases, abrasive particles may remain intact into the workpiece surface and remove material in the following cycles because of the decrease in penetration depth. This also results in partial bluntness of the abrasive particle cutting edge [94]. As a

result, the ability of the abrasive particle to act as effective cutting tool decreases and initial lathe boring marks are not removed completely (Fig. 4.4(c)).

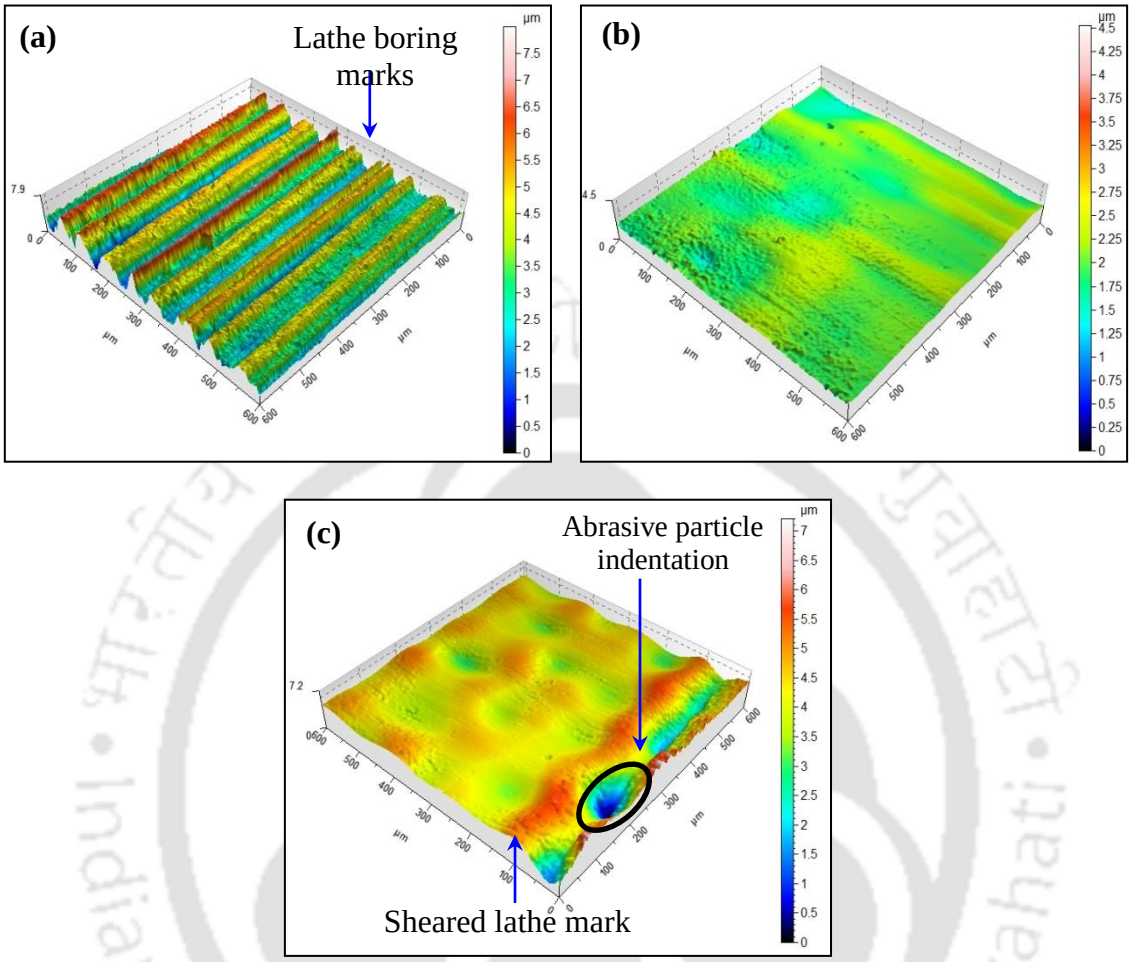

Fig. 4.4 *Workpiece surface at various extrusion pressure* ***(a)*** *initial workpiece surface* ***(b)*** *4.5 MPa* ***(c)*** *5.5 MPa (500 cycles, # 400, 40 wt. % abrasives).*

4.3.2 Effect of number of abrasive flow finishing cycles

Finishing of the workpiece surface takes place because of the repetitive indentation of the abrasive particle and shearing of the surface roughness peaks on the workpiece surface. $\% \Delta R_a$ increases upto 500 AFF cycles and gradually decreases with the increase in the number of AFF cycles (Fig. 4.5). It is found from the 3-D surface profiles that the initial lathe boring marks are sheared around 500 AFF cycles and smooth surface is achieved. Since $\% \Delta R_a$ starts decreasing beyond 500 cycles, this might be the critical surface roughness. As the number of AFF cycles increases beyond 500, abrasive particles starts indenting the finished surface and create its own indentation marks. From the 3-D surface profile (Fig. 4.5), with an increase in AFF cycles due to the repetitive striking of the abrasive particle the indentation marks increases which further add to the deterioration of the final surface roughness.

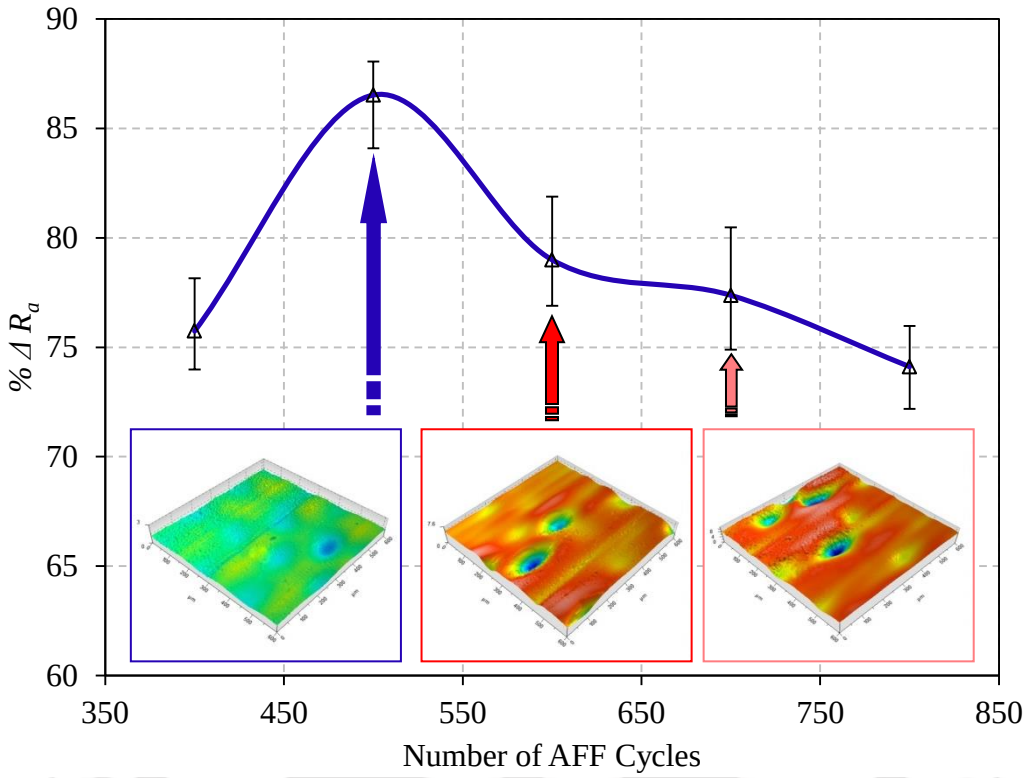

Fig. 4.5 *Variation of the percentage change in surface roughness with number of abrasive flow finishing cycles (4.5 MPa, # 400, 40 wt. % abrasives).*

4.3.3 Effect of mesh size of abrasive particles

Mesh size of abrasive particle plays a vital role in deciding the final surface roughness on the workpiece surface. The abrasive particle cutting edges shear the roughness peaks on the workpiece surface. So, AFF experiments are conducted to study the effect of abrasive mesh size (#) on the final surface roughness. The relation between mesh size (M) and abrasive particle size (R_g radius of the abrasive particle) is given as:-

$$R_g\,(mm) = \frac{7.62}{M} \tag{4.2}$$

As the mesh size increases, the abrasive particle size decreases and in turn its cutting edges drastically reduces. As a result, the depth and width of abrasive particle penetration into the workpiece surface decreases [34]. Since the abrasive particles are part of soft medium, there is chance that these may push back during their interaction with the workpiece surface. So, small abrasive particle (higher mesh size) will have more chance to embed back into medium. For the same amount of embedding, bigger abrasive particles (lower mesh size) still may possess their sharp cutting edges in contact with workpiece surface. So, finishing ability of lower mesh size (#180, #220) is observed higher.

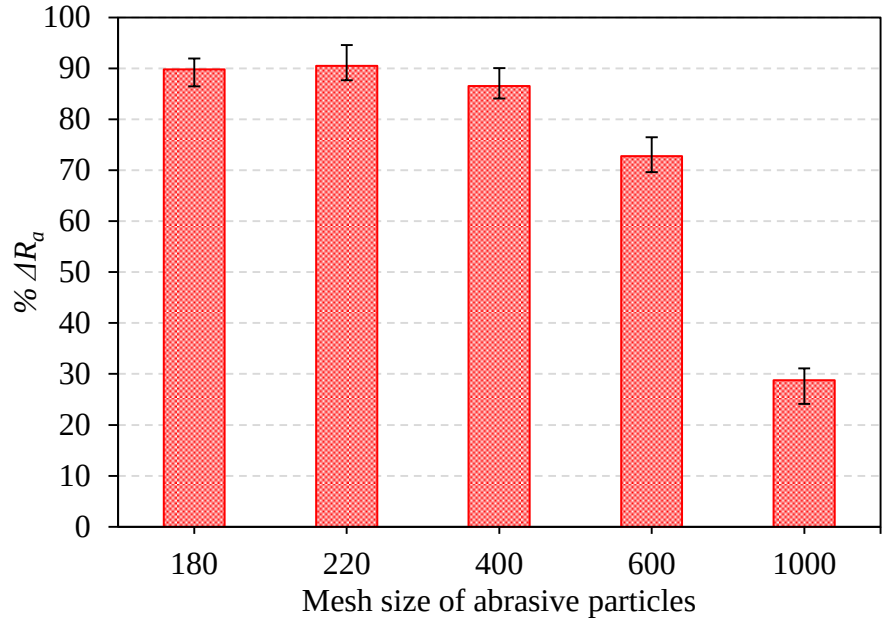

Fig. 4.6 *Variation of the percentage change in surface roughness with mesh size (500 cycles, 4.5 MPa, 40 wt. % abrasives).*

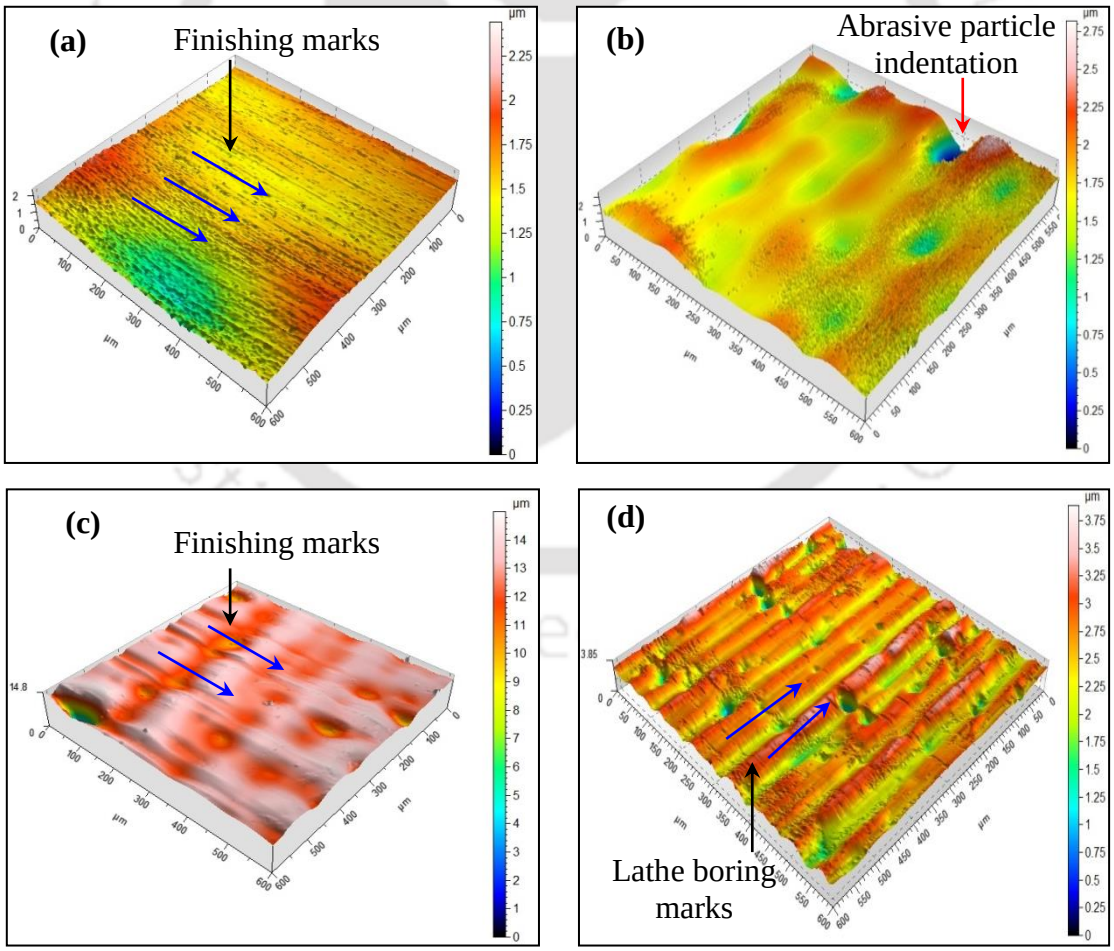

Fig. 4.7 *Workpiece surface topography at different mesh sizes* ***(a)*** *# 220* ***(b)*** *# 400* ***(c)*** *# 600* ***(d)*** *# 1000 (500 cycles, 4.5 MPa, 40 wt. % abrasives).*

Keeping all other AFF input parameters constant during the experiments, $\% \Delta R_a$ is minimal for the # 1000 abrasive particle (Fig. 4.6). As shown in Fig. 4.7(a) majority of lathe marks are removed after performing AFF experiments by using # 220 abrasive particles. At few places on the workpiece surface, blunt lathe marks appears after finishing with # 400 abrasive particles (Fig. 4.7(b)) which become more visible for # 600 (Fig. 4.7(c)) and higher for # 1000 abrasive particles (Fig. 4.7(d)) because of incomplete removal of initial surface (lathe boring) marks. Lathe boring marks might be too big for small abrasive particles (# 600, # 1000) to shear. Approximately, the similar average surface roughness is obtained at # 220 and # 180 abrasive particles. The error bar shows best $\% \Delta R_a$ for # 220. Since best surface roughness is achieved at # 220 and abrasive particles sizes cannot be varied continuously the complete parametric study of AFF process is conducted by using # 220 abrasive particles.

4.3.4 Effect of weight percentage of abrasive particles

As the wt. % of the abrasive particles in the medium increases (for the same mesh size) the number of abrasive particles increases in the medium. So, for same number of AFF cycles number of abrasive particles involving in finishing operation increases. Thus, $\% \Delta R_a$ gradually increases with wt. % of abrasive particles in medium (Fig. 4.8).

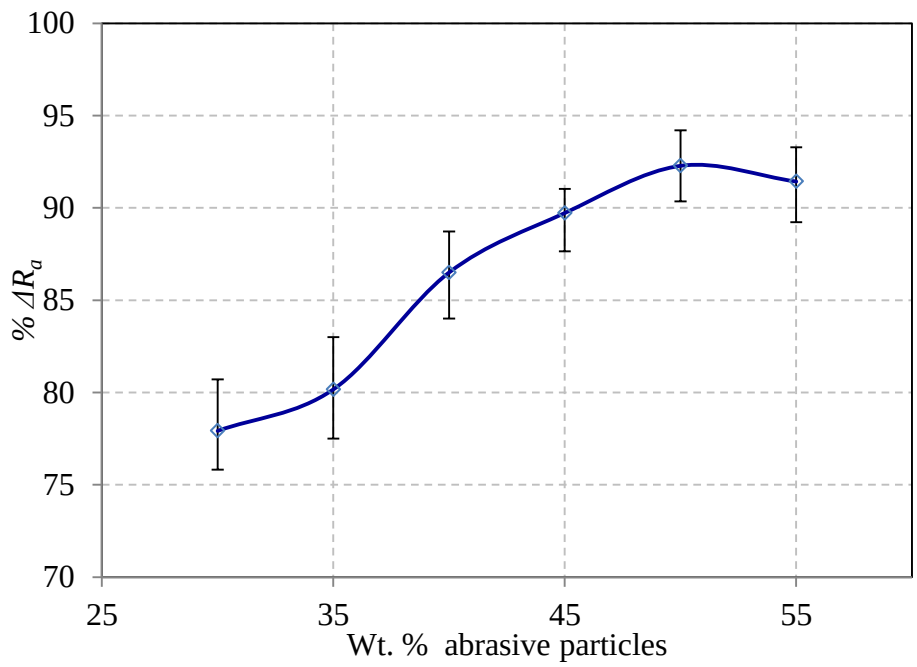

Fig. 4.8 *Variation of the percentage change in surface roughness with wt. % of the abrasive particles in the medium (4.5 MPa, # 220, 500 AFF cycles).*

Surface topographic images and corresponding 2-D surface roughness profile shows that alternate roughness peaks and valleys due to lathe boring marks are completely removed at higher wt. % of the abrasives (Fig. 4.9(a-c)).

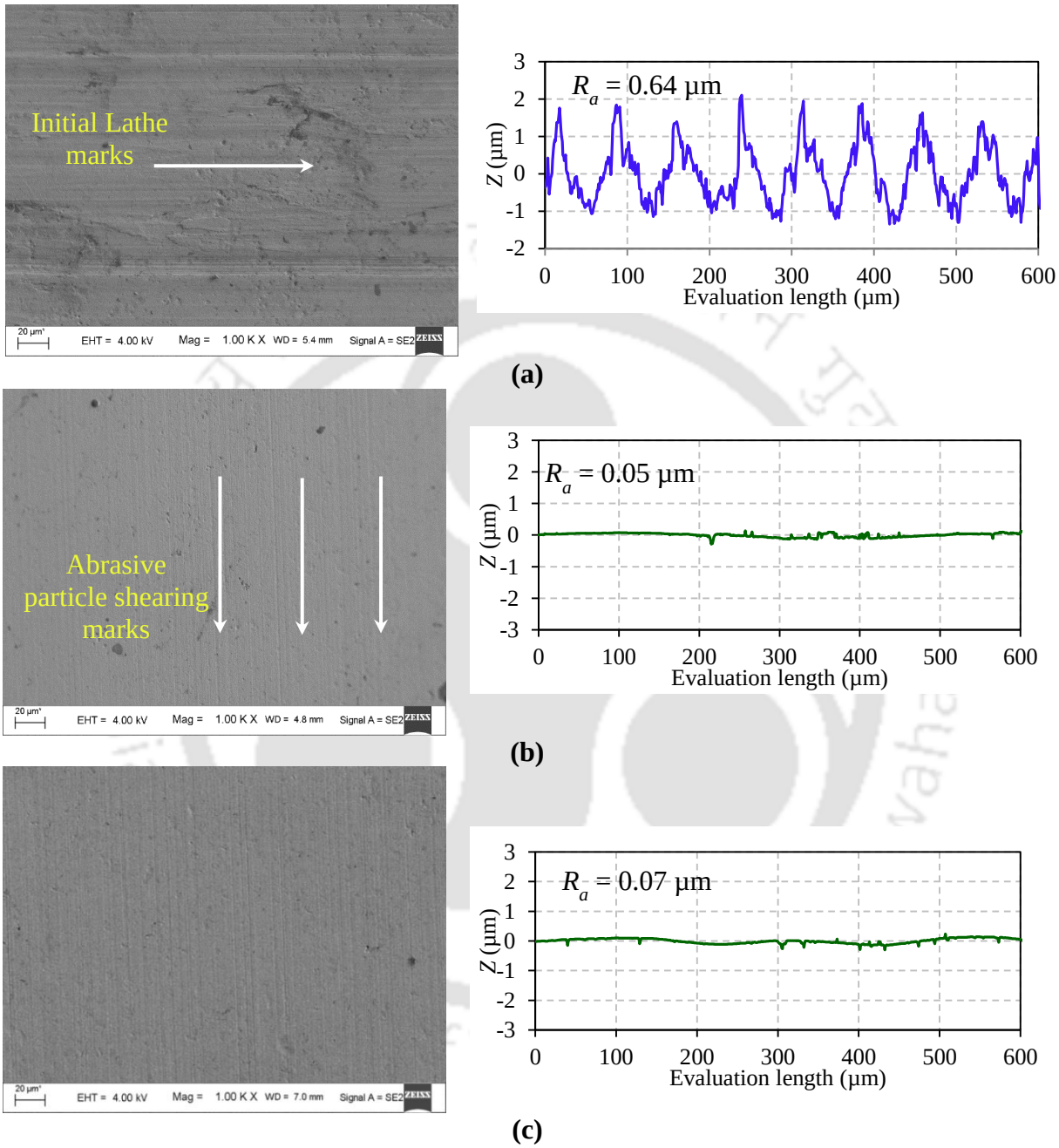

Fig. 4.9 *Workpiece surface topography at various wt. % of the abrasive particles in the abrasive flow finishing medium* ***(a)*** *initial* ***(b)*** *45 %* ***(c)*** *55 % (4.5 MPa, # 220, 500 AFF cycles).*

Increasing wt. % of abrasive particles beyond a critical value leads to a slight decrease in *% ΔR_a* (4.9(c)). This is due to the fact that at higher wt. % of abrasive particles in the

medium, there are not enough polymer chains left to hold the increased number of abrasive particles. As a result, the bonding strength of polymer chains to hold the abrasive particles together decreases. Thus, the amount of finishing forces (F_R, F_A) generated in the medium are not effectively transferred to the abrasive particles that shear the surface roughness peaks. On the other hand, the probability of collision among the abrasive particles increases as wt. % of abrasive particles in the medium increases. So, this collision among abrasive particles in the medium might blunt the sharp cutting edges. Therefore, surface roughness improvement decreases beyond a threshold value of wt. % of abrasive particles.

4.4 Design of experiments

Detailed experimental study on the effect of AFF process input parameters on the output responses during AFF process is carried out by using the central composite rotatable design (CCRD) method. Table 4.2 shows the coded and absolute values of the AFF process input parameters and its levels.

Table 4.2 *Abrasive flow finishing input parameters their coded and absolute values.*

S. No.	AFF input parameter	Unit	Levels				
			-1.682	**-1.000**	**0.000**	**1.000**	**1.682**
1.	Pressure (P)	MPa	3.70	4.00	4.50	5.00	5.30
2.	No. of AFF cycles (N)	-	416	450	500	550	584
3.	Wt. % of abrasives (W)	%	41.6	45.0	50.0	55.0	58.4

The effect of three AFF input parameters (extrusion pressure, number of AFF cycles and weight percentage of abrasive particle in the medium) is studied on output responses *% ΔR_a* (eq. 4.1) and percentage change in maximum height of the roughness profile (*% ΔR_z*) given as:-

$$\% \ \Delta R_z = \frac{Initial\ maximum\ height - Final\ maximum\ height}{Initial\ maximum\ height} \times 100 \qquad (4.3)$$

The detailed experimental plan with the summary of input parameters and output responses is shown in Table 4.3. A total of 20 experiments are carried out with 6 central runs and 6 axial runs.

Table 4.3 *Plan of experiments and summary of abrasive flow finishing output responses.*

Std. order	Exp. No.	Factors			Surface roughness			Maximum height of the roughness profile		
		P	N	W	Initial R_a (µm)	Final R_a (µm)	% ΔR_a	Initial R_z (µm)	Final R_z (µm)	% ΔR_z
1	4	5.0	550	45.0	0.602	0.066	89.037	3.663	0.531	85.504
2	15	4.5	500	50.0	0.646	0.060	90.712	3.744	0.470	87.447
3	9	3.7	500	50.0	0.572	0.199	65.210	3.392	1.092	67.807
4	13	4.5	500	41.6	0.516	0.101	80.426	2.675	0.492	81.607
5	20	4.5	500	50.0	0.515	0.060	88.350	3.124	0.390	87.516
6	8	5.0	550	55.0	0.616	0.048	92.208	4.191	0.346	91.744
7	6	5.0	450	55.0	0.577	0.082	85.789	3.214	0.471	85.345
8	19	4.5	500	50.0	0.540	0.070	87.037	3.840	0.460	88.020
9	18	4.5	500	50.0	0.503	0.056	88.867	3.238	0.451	86.072
10	11	4.5	416	50.0	0.533	0.140	73.734	4.108	1.133	72.420
11	5	4.0	450	55.0	0.582	0.141	75.773	4.287	1.128	73.688
12	7	4.0	550	55.0	0.567	0.096	83.069	3.933	0.722	81.643
13	12	4.5	584	50.0	0.632	0.091	85.601	3.889	0.600	84.572
14	14	4.5	500	58.4	0.573	0.072	87.435	3.456	0.388	88.773
15	16	4.5	500	50.0	0.517	0.052	89.942	2.792	0.409	85.351
16	10	5.3	500	50.0	0.619	0.071	88.530	3.318	0.479	85.564
17	17	4.5	500	50.0	0.634	0.062	90.221	3.789	0.448	88.176
18	1	4.0	450	45.0	0.533	0.192	63.977	2.604	0.856	67.127
19	2	5.0	450	45.0	0.589	0.108	81.664	3.789	0.698	81.578
20	3	4.0	550	45.0	0.523	0.130	75.143	2.642	0.673	74.527

Analysis of the experimental results is carried out by response surface methodology (RSM). Table 4.4 shows the analysis of variance (ANOVA) for $\% \Delta R_a$ and $\% \Delta R_z$. The model p-value Prob > F for both $\% \Delta R_a$ and $\% \Delta R_z$ is 0.0001 i.e., less than 0.05 (significance level, α for 95% confidence interval) implies that both model are significant. It is found from the significant model terms extrusion pressure ($P + P^2$) has the highest contribution (61.88 %) followed by the contribution of number of cycles ($N + N^2$) (25.12 %) and weight percent of abrasive particles ($W + W^2$) (10.92 %) for $\% \Delta R_a$. Same trend follows in case of $\% \Delta R_z$ with the % contribution of P ($P + P^2$), N ($N + N^2$), W ($W + W^2$) of 61.62 %, 27.91 % and 9.77 % respectively.

Table 4.4 *Analysis of variance for output responses of abrasive flow finishing.*

Source	$\% \Delta R_a$			$\% \Delta R_z$		
	F-Value	**p-value Prob > F**	**% Contribution**	**F-Value**	**p-value Prob > F**	**% Contribution**
Model	62.84	< 0.0001*		93.27	< 0.0001*	
A-P	260.07	< 0.0001*	43.94	374.99	< 0.0001*	43.19
B-N	87.61	< 0.0001*	14.80	134.34	< 0.0001*	15.47
C-W	48.40	< 0.0001*	8.18	80.66	< 0.0001*	9.29
AB	1.20	0.2997	0.20	2.73	0.1296	0.31
AC	8.47	0.0155*	1.43	1.45	0.2559	0.17
BC	1.28	0.2849	0.22	0.99	0.3435	0.11
A^2	106.16	< 0.0001*	17.94	159.99	< 0.0001*	18.43
B^2	61.09	< 0.0001*	10.32	107.99	< 0.0001*	12.44
C^2	16.20	0.0024*	2.74	4.19	0.0678	0.48
Lack of Fit	1.43	0.3532		0.81	0.5899	

*Significant terms

4.5 Results and discussion

Results of AFF process parametric analysis during the finishing of SS 316L cylindrical tubes are discussed in the present section. To improve the accuracy of regression equations, all the model terms are considered upto 2^{nd} order in the present regression model. From the experimental study ANOVA, the final output responses equations in terms of input parameters can be written as:-

$$\%\Delta R_a = -1092.06 + 203.40P + 1.55N + 10.97W - 0.02PN - 0.62PW - 2.41\times10^{-3}NW - 16.39P^2 - 1.24\times10^{-3}N^2 - 0.06W^2 \quad (4.4)$$

$$\%\Delta R_z = -727.02 + 162.18P + 1.28N + 2.91W - 0.03PN - 0.18PW - 1.54\times10^{-3}NW - 14.35P^2 - 1.18\times10^{-3}N^2 - 0.02W^2 \quad (4.5)$$

4.5.1 Regression model validation by confirmation tests

Results of the regression model for $\% \Delta R_a$ and $\% \Delta R_z$ are confirmed by carrying out the confirmation test. Confirmation test are performed by choosing the random values of the different AFF input parameters within their ranges given is table 4.2. Comparative analysis between the experimental results and the results obtained by the regression (eq. 4.4, eq. 4.5 and eq. 4.6) shows the maximum % error of - 3.54 % for $\% \Delta R_a$ while 5.84 % for $\% \Delta R_z$. % error is given as:-

$$\% \text{ error} = \frac{\text{Experimental value} - \text{Predicted value from regression eq.}}{\text{Experimental value}} \times 100 \qquad (4.6)$$

Table 4.5 *Various combinations of AFF confirmation tests for validation of regression equations*

S. No.	Input conditions			Surface roughness			Maximum height of the roughness profile		
	P	N	W	Experimental % ΔR_a	Predicted % ΔR_a	% error	Experimental % ΔR_z	Predicted % ΔR_z	% error
1	4.00	450	50	74.22	70.95	3.27	76.74	70.90	5.84
2	5.00	500	45	87.16	88.74	-1.58	89.24	86.39	2.85
3	4.50	550	55	88.98	90.50	-1.52	88.75	89.93	-1.18
4	4.80	525	55	89.05	92.59	-3.54	90.29	91.88	-1.59

4.5.2 Extrusion pressure

Analysis of variance (ANOVA) shows extrusion pressure is the most significant AFF process input parameter in deciding $\% \Delta R_a$ and $\% \Delta R_z$. With an increase in the extrusion pressure upto 5 MPa, the magnitude of F_R *and* F_A both increase gradually. An increase in F_R results in greater depth of indentation while the increased F_A makes it possible to remove the material in the form of micro chip. Thus, the surface roughness value decreases with an increase in extrusion pressure at higher finishing rate upto a certain value, say, upto 5 MPa. Beyond this value, the finishing rate and percentage improvement in maximum height decrease that is the value of $\% \Delta R_a$ and $\% \Delta R_z$ decreases (Fig. 4.10(a-b)).

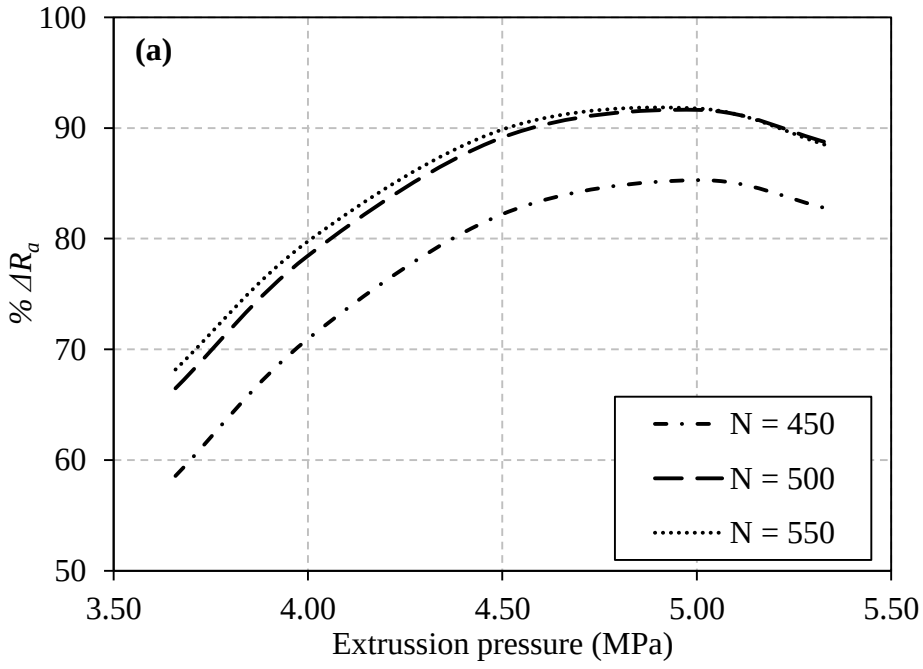

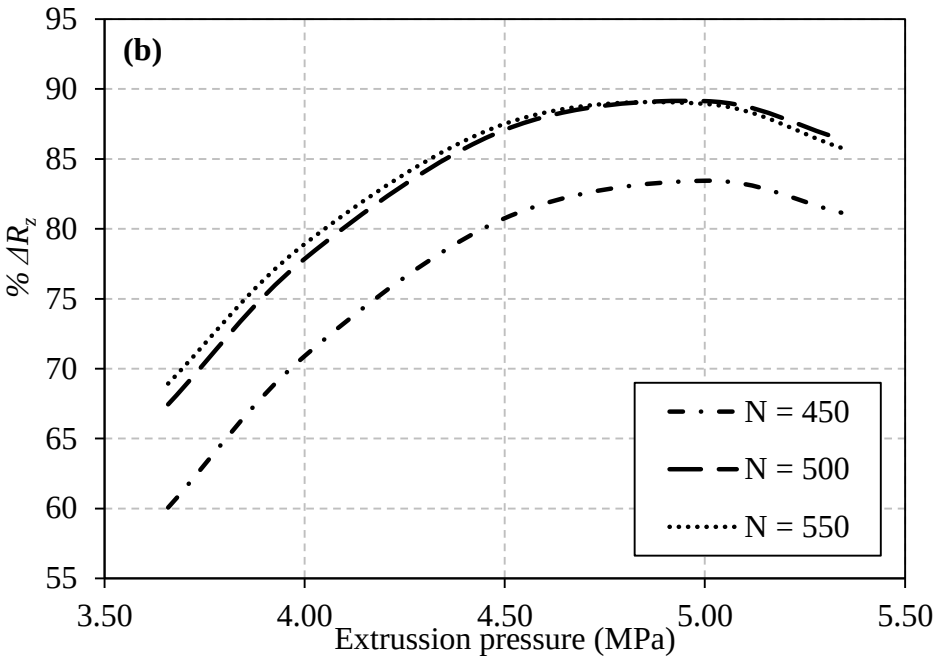

Fig. 4.10 *Effect of extrusion pressure at different number of cycles (wt. % of abrasives = 50 %) on* ***(a)*** *% ΔR_a,* ***(b)*** *% ΔR_z.*

As extrusion pressure increases, the shear rate at which the medium is extruded through the workpiece also increases. From the medium rheological characterization (frequency sweep test), storage modulus of AFF medium increases with an increase in frequency. However, the loss modulus remain approximately same. Storage modulus shows the energy storing capacity of the medium under deformation due to an external load. As frequency increases the number of shearing oscillations per unit time increases. Higher the frequency more is the stretching of the polymer chains and larger is the amount of energy stored in them (Fig. 3.20(a)). Therefore, as the extrusion pressure increases in AFF process the more amount of energy is stored in the medium. This stored energy in the medium is transferred to the abrasive particles to finish the workpiece surface.

At low extrusion pressure, (3.7 MPa) the storage modulus attain by medium is less. So indentation by abrasive particles is low. Thus, finishing of deep surface profiles during generated boring process cannot be achieved (Fig. 4.11(a)). Gradual increase of extrusion pressure increases the storage modulus and thus medium finishing ability increases. So *% ΔR_a* and *% ΔR_z* is high at 5.0 MPa. However, increasing of extrusion pressure beyond 5.0 MPa, the storage modulus of medium increases, which increase F_R. Therefore, indentation depth of abrasive particles on workpiece surface increases. Thus, abrasive particles not only

finish but also create its own scratches marks (Fig. 4.11(b)). This results in the decrease of $\% \Delta R_a$ and $\% \Delta R_z$ beyond 5.0 MPa extrusion pressure.

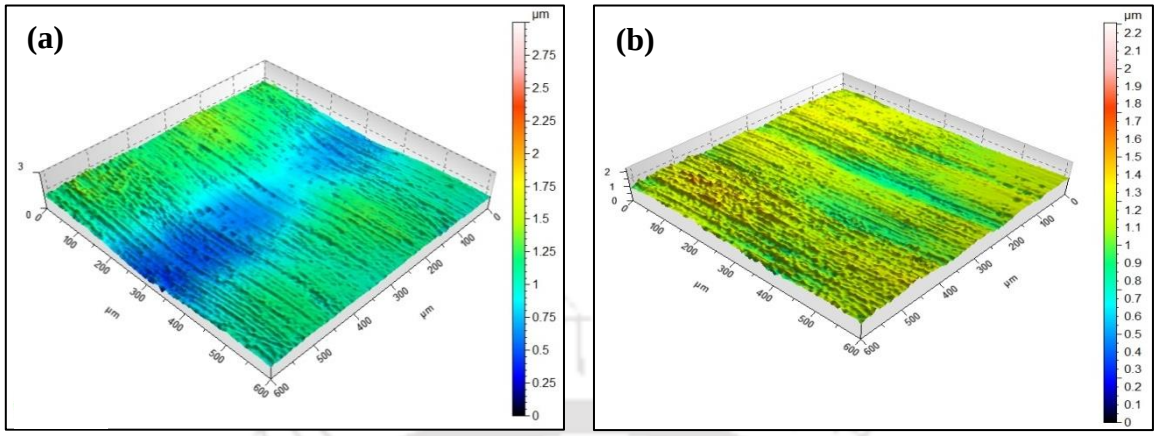

Fig. 4.11 *Workpiece surface topography after finishing at extrusion pressure* ***(a)*** *3.7 MPa* ***(b)*** *5.3 MPa (500 AFF cycles, 50 % wt. % of the abrasive particles, # 220).*

4.5.3 Number of abrasive flow finishing cycles

The $\% \Delta R_a$ increases at faster rate in first few hundred number of AFF cycles, due to the presence of large number of sharp roughness peaks on the workpiece surface by abrasive particles. Beyond 500 cycles the rate of change in $\% \Delta R_a$ is low and approximately constant (Fig. 4.12(a)). The probable reason seems that the total number of blunt (round off) surface peaks to be sheared by the abrasive particles decreases at the higher number of AFF cycles. As the number of AFF cycle increases beyond a threshold value (550) the abrasive particle scratches the finished surface and creates indentation marks on the finished surface. This results in deterioration of the final surface roughness.

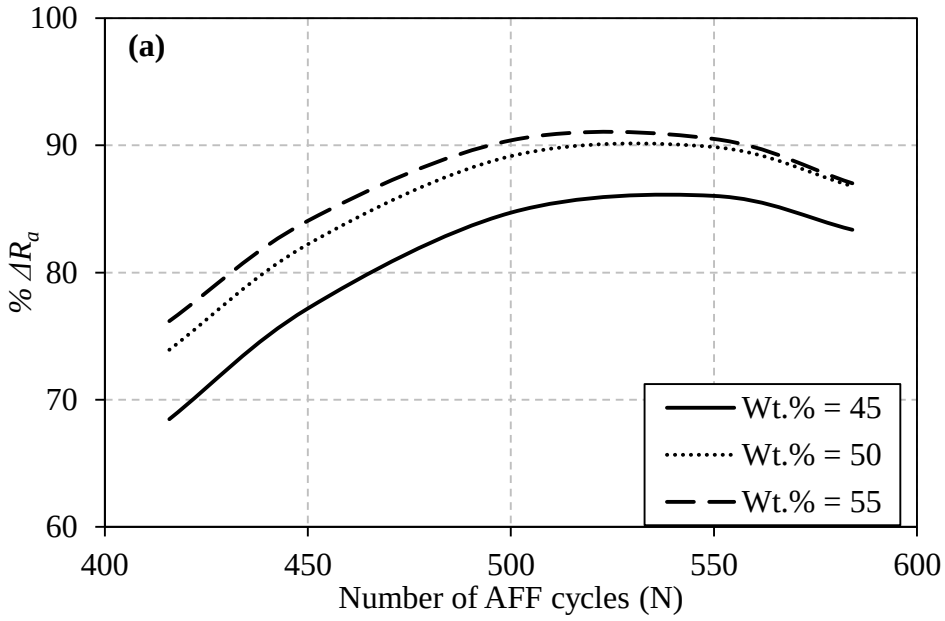

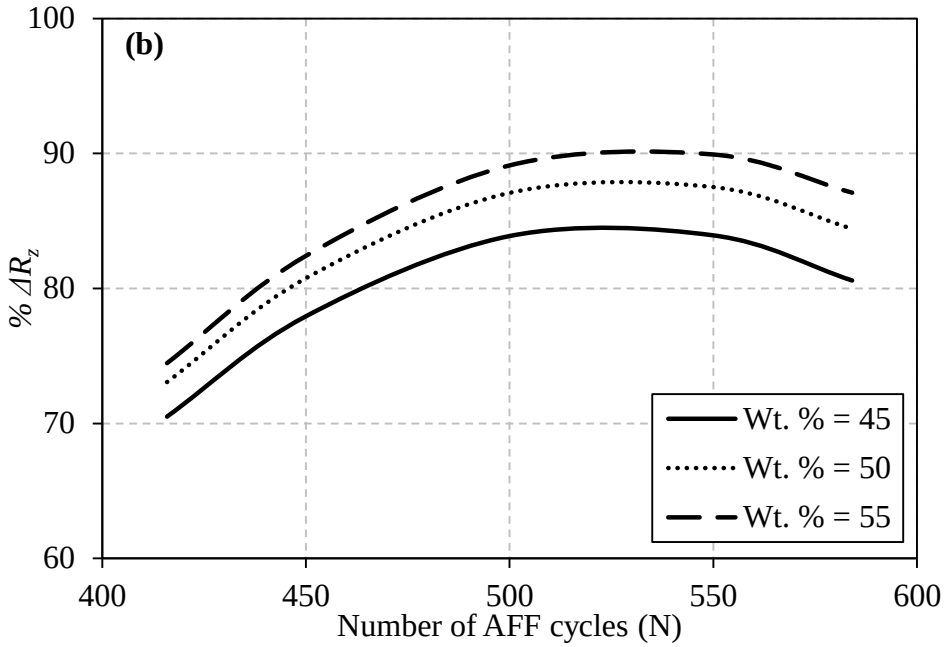

Fig. 4.12 *Effect of number of abrasive flow finishing cycles at various wt. % of abrasive particle (extrusion pressure = 4.5 MPa) on* ***(a)*** *% ΔR_a,* ***(b)*** *% ΔR_z.*

As the number of AFF cycles increases, more number of times the peaks and valleys of the surface roughness on the workpiece surface are sheared by the abrasive particle. All the roughness peaks of the lathe boring marks are partially removed from the workpiece surface in the initial AFF cycles (Fig. 4.13(a)).

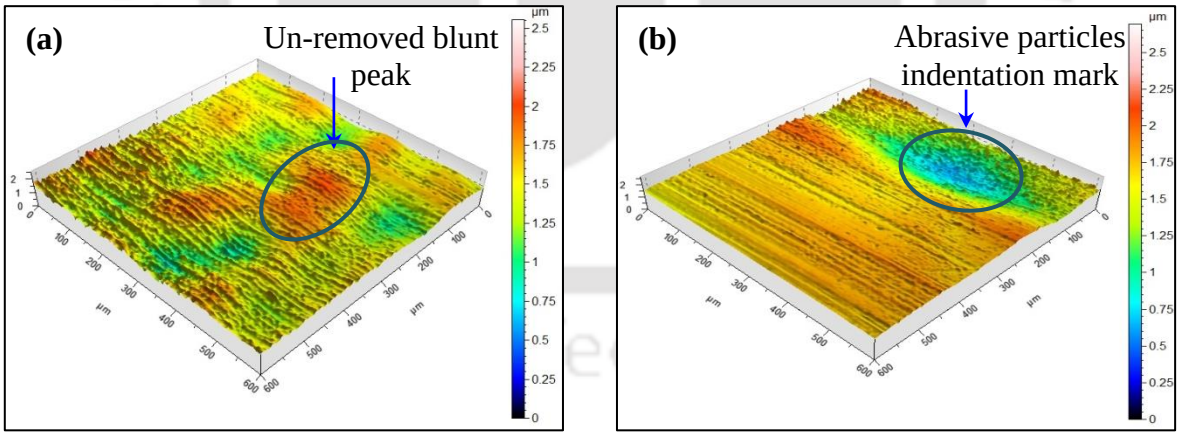

Fig. 4.13 *Workpiece surface topography after finishing at AFF cycles* ***(a)*** *416* ***(b)*** *584 (4.5 MPa, 50 % wt. % of the abrasive particles, # 220).*

As shown in Fig. 4.12(b) the value of *% ΔR_z* initially increase with an increase in AFF cycles due to the reduction in height of the roughness peaks. But as the AFF cycles increases beyond a critical value (550) abrasive particles makes their own indentation on the workpiece surface (Fig. 4.13(b)). This results in an increase in depth of the valleys created by abrasive

shearing marks. The depth of these valleys further increases with an increase in AFF cycles due to repetitive indentation of the abrasive particles. Thus, the value of $\% \Delta R_z$ decreases at higher number of AFF cycles.

4.5.4 Weight percentage of abrasive particles

As the wt. % of abrasive particles in the medium increases, $\% \Delta R_a$, $\% \Delta R_z$ gradually increases (Fig. 4.14).

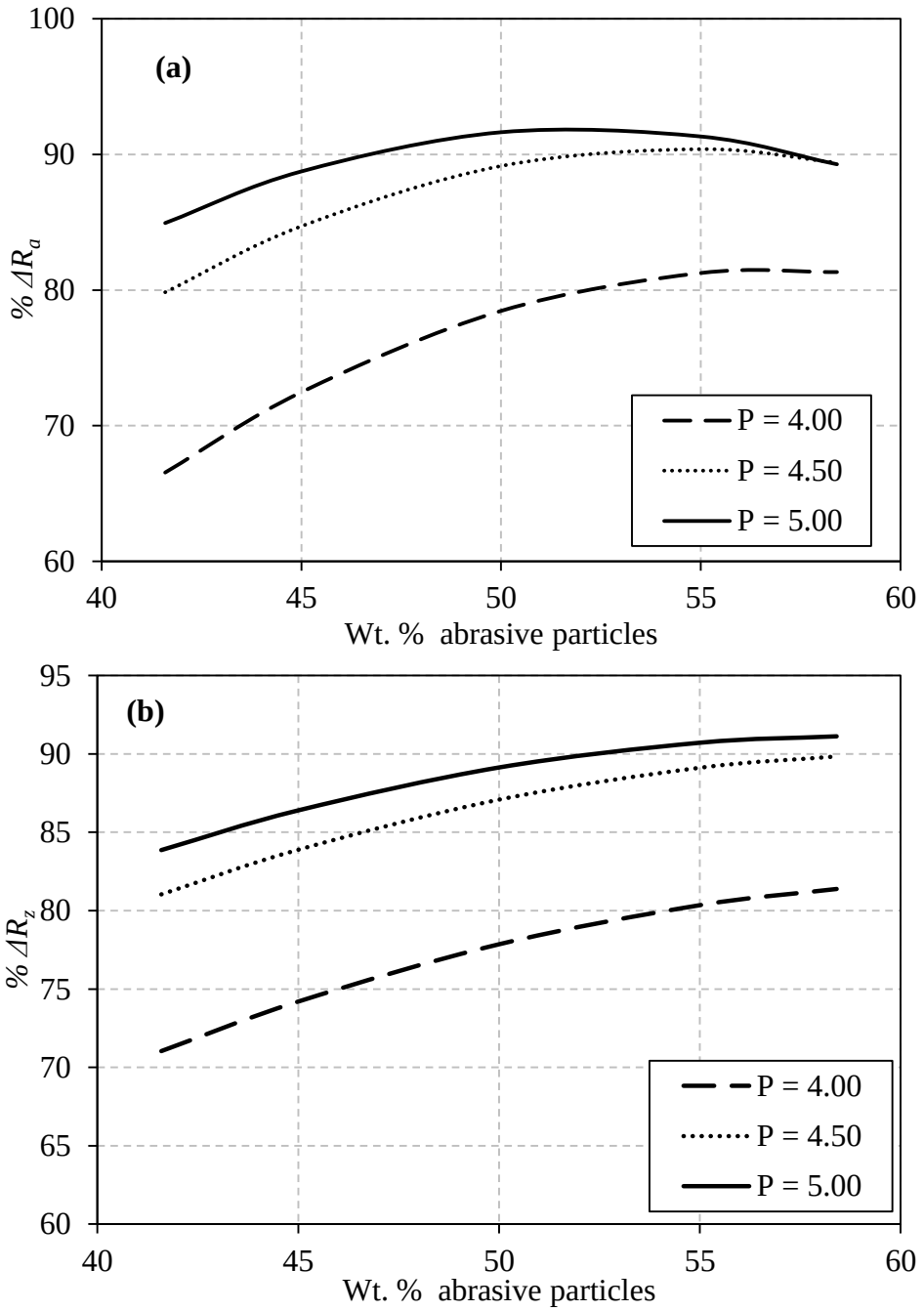

Fig. 4.14 *Effect of wt. % of abrasives particles at different extrusion pressure (number of AFF cycles = 500) on* ***(a)*** $\% \Delta R_a$, ***(b)*** $\% \Delta R_z$.

The number of abrasive particles interacting with surface roughness peaks per unit time increases with the increase in wt. % of abrasive particles in AFF medium. Therefore, for the same extrusion pressures and number of cycles higher number of abrasive particles take part in finishing. On other hand, as wt. % of abrasive particles increases, the viscosity of the medium increases for the same shear rate (Fig. 3.22(a)). Higher the viscosity of the medium, more effectively it can hold the abrasive particles against the workpiece surface during finishing operation. These two reasons assists in improving the final surface roughness. Thus, the value of $\% \Delta R_a$ and $\% \Delta R_z$ increases with an increase in wt. % of abrasive particles in medium (Fig. 4.14).

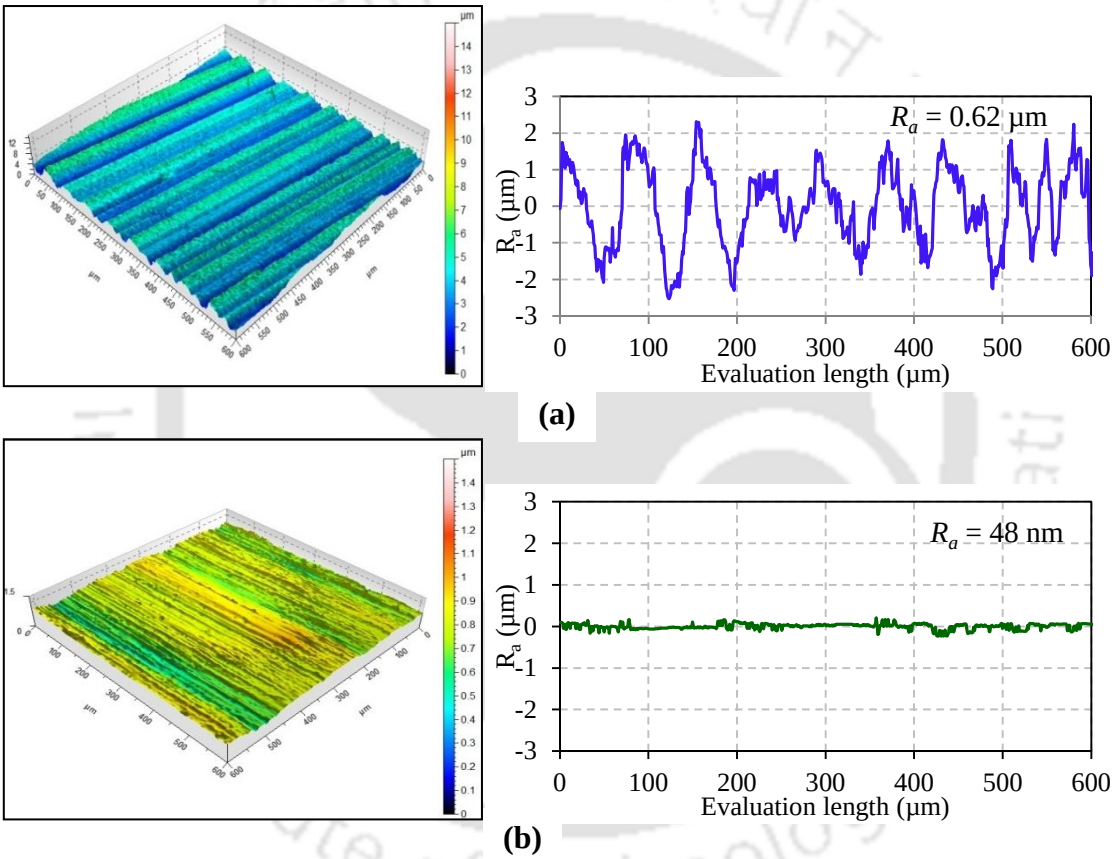

Fig. 4.15 *Workpiece surface topography and corresponding 2-D surface roughness* ***(a)*** *initial workpiece surface,* R_a *= 0.62 µm* ***(b)*** *finished surface,* R_a *=0.048 µm (5 MPa, 550 AFF cycles, 55 % wt. % of abrasive particles).*

The best surface roughness obtained during AFF experiments is 48 nm with % improvement of 92.24 % in $\% \Delta R_a$ and 91.75 % in $\% \Delta R_z$. The AFF process input parameters for achieving the same are 5 MPa (extrusion pressure), 550 (numbers of AFF cycles) and 55 % (wt. % of abrasive particles in the AFF medium). Fig. 4.15(a) shows surface peaks and

valleys due to the initial internal boring that are clearly visible on the workpiece surface. These boring surface marks are sheared by AFF process (Fig. 4.15(b)).

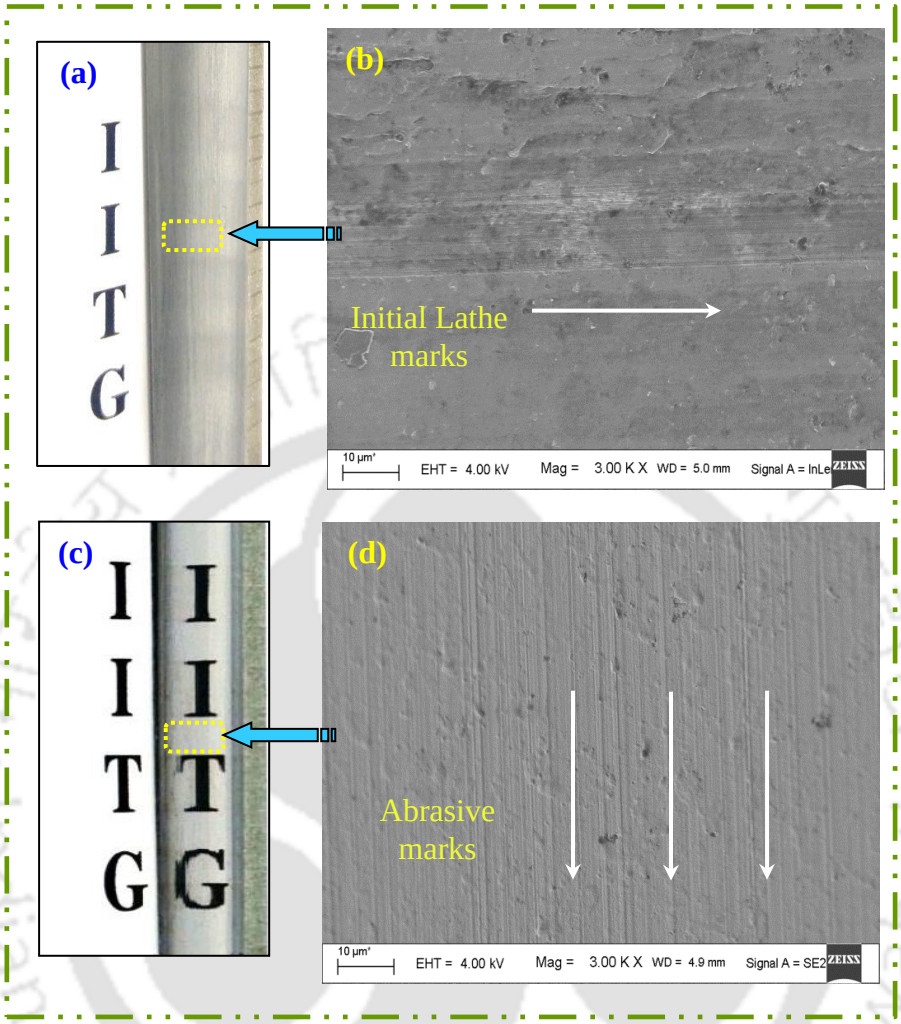

Fig. 4.16 *Initial workpiece surface* ***(a)*** *photograph of initial surface* ***(b)*** *topography images, finished workpiece surface* ***(c)*** *photograph of final surface* ***(d)*** *topography images (5 MPa, 550 AFF cycles, 55 % wt. % of abrasive particles).*

As shown in Fig. 4.16(a) the word “IITG” is not reflected by the tube internal surface because of high surface roughness. The surface topography of unfinished surface is too rough and clearly shows the boring marks (Fig. 4.16(b)). This roughness is removed by shearing after performing the AFF finishing operation. Final surface achieves the mirror like finish, thus producing the clear reflection of “IITG” (Fig. 4.16(c)). Finishing the workpiece surface by using AFF process removes the initial lathe internal boring marks. The direction of flow of AFF medium containing abrasive particle is perpendicular to the direction of initial lathe boring marks. Therefore, abrasive particles shearing marks perpendicular to the lathe boring marks are clearly visible in Fig. 4.16(d). Hence, the AFF process can be used to finish the SS tubes to nano scale (i.e., mirror finish).

4.6 Conclusions

In the current chapter experimental study of AFF process during finishing of SS 316L cylindrical tubes is carried out. Based on the above studies following conclusions are drawn:-

1. AFF process successfully finishes the internal surfaces of the SS 316L cylindrical tubes with in house developed economic polymer rheological abrasive medium (medium).
2. From the ANOVA, it is found that in the case of $\% \Delta R_a$, the percentage contribution of extrusion pressure is 61.88 %, number of AFF cycles and wt. % of abrasives particles in the medium has a contribution of 25.12 % and 10.92 % respectively.
3. Similar trend is followed in case of $\% \Delta R_z$ also with the % contribution of extrusion pressure, number of cycles and wt. % of abrasives 61.62 %, 27.91 % and 9.77 % respectively.
4. From the surface topography study, it is observed that the abrasive shearing marks generate straight lines in the direction of flow of the medium (perpendicular to the initial internal boring marks).
5. With a 92.24 % improvement in surface roughness, the best surface roughness obtained during the current set of AFF experiments is 48 nm.

Chapter 5

ABRASIVE FLOW FINISHING OF MICROSLOTS: EXPERIMENTAL STUDY

5.1 Introduction

Today's technological advancement needs the miniaturization of the components without compromising their efficiency. The size variation in modern manufacturing industries is shifted from macro and milli level to micro level and further to nano as well as sub-atomic level. The aim behind such a motive is "doing more with less" in other words, to precisely develop a complex system made up of a large number of parts fitted in the least possible space. The role of big computers can now be handled by laptops, big bulky machines of the 1980-90's are replaced by the light weight CNC machines. All there are possible because of technological advancement and miniaturization of the components. Some of the advantages achieved from the miniaturization of the components are these require less space, mass produced in batches and can be moved easily from one place to another as well as less prone

to mechanical vibration. However, machining and finishing of such components is the biggest challenge for the modern manufacturing industries. The role of surface roughness becomes more prominent as the geometric dimensions of the component decreases. As found out from the literature survey (chapter 1), very little attention is paid towards the finishing of micro feature components with AFF process.

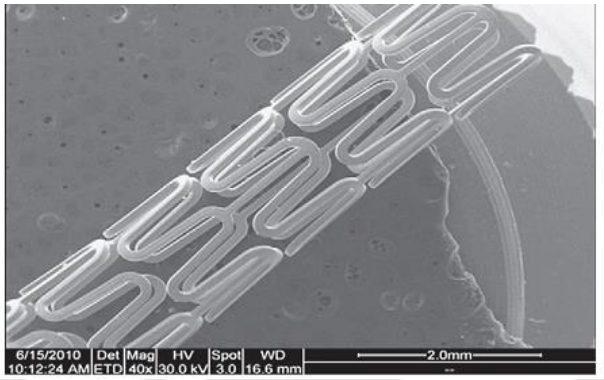

Fig. 5.1 *Overview of metallic stent [95].*

In the present chapter finishing of microslots is carried out. One of many applications of the microslots is in the medical field for manufacturing of coronary metallic stents (Fig. 5.1). Mostly surgical steel (SS 316L) material are used in metallic stent applications where in microslots are fabricated by thermal based micro manufacturing processes such as micromachining, electrical discharge micromachining (EDμM) because of thermal based micromachining, these microslots is metallurgical deteriorated/change having recast layer with loosely bonded metal debris. These metallurgically changed layers and loosely bonded resolidified metal debris contamination with body fluids can adversely affect patient.

5.2 Experimentation

5.2.1 Abrasive flow finishing setup and tooling

AFF experimental setup, which is used for finishing cylindrical tubes (Chapter 4), is used for finishing microslots. However, a new tooling is designed and fabricated for finishing workpiece with microslots. As the start of AFF process starts, the medium is extruded from lower medium cylinder to upper medium cylinder across microslots which are in workpieces (Fig. 5.2). This result in shearing of the roughness peaks on microslot surface by abrasive particles in the medium. Once the medium reaches to upper medium cylinder, the motion of the piston reverses and AFF cycles continue.

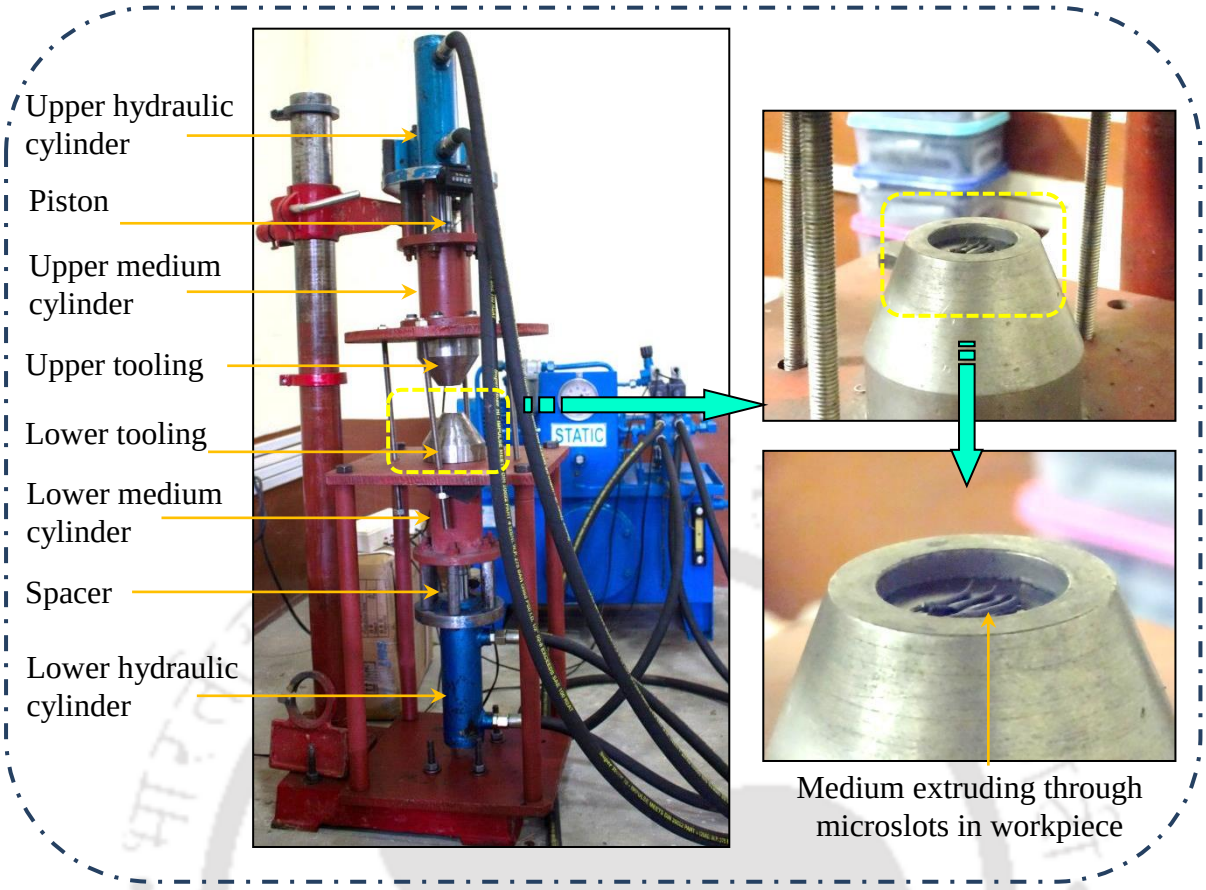

Fig 5.2 *Overview of abrasive flow finishing process setup showing the extrusion of medium through microslots.*

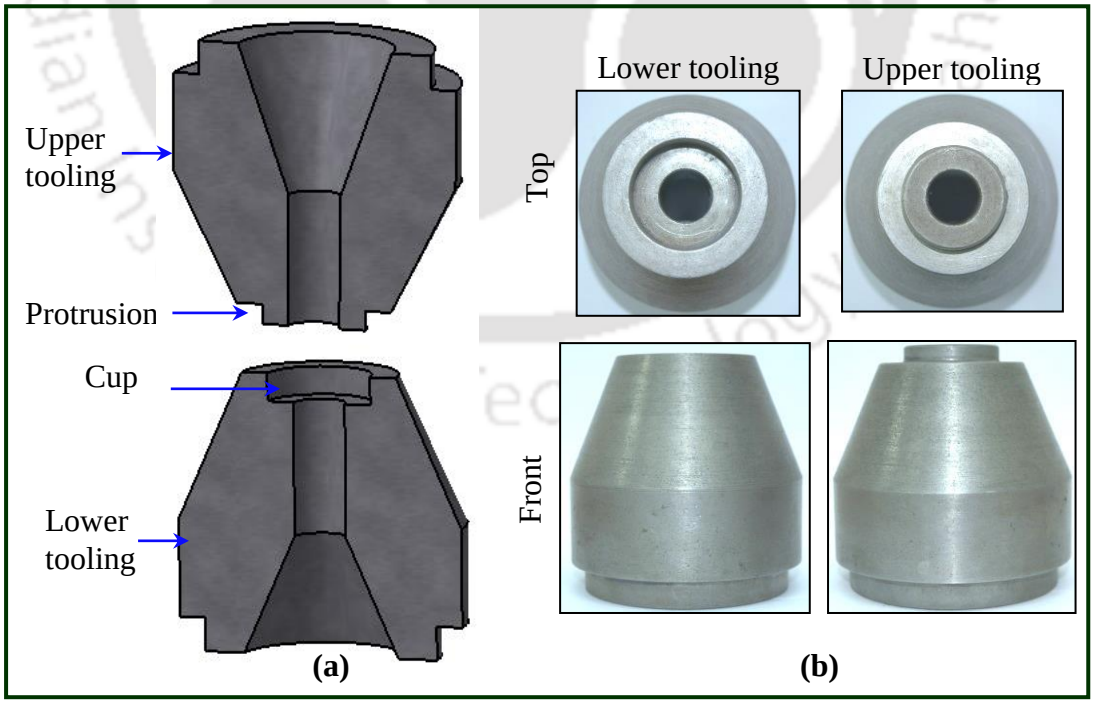

Fig. 5.3 (a) *3-D model showing the cross section of the tooling* ***(b)*** *tooling to hold the workpiece.*

Tooling is specially designed to hold the workpiece in place properly and to assist the medium to flow across workpiece uniformly without leakage. As shown in Fig. 5.3(a), cup shape arrangement is provided in lower tooling to hold the workpiece properly in place. The protrusion in upper tooling locks the workpiece in position and prevents leakage of the medium during experiments. A conic section is provided at the start of upper and lower tooling to ensure a smooth flow of the medium through the workpiece from the medium cylinder without much resistance by the narrow passageway of microslots. Front and top view of upper and lower tooling is shown in Fig 5.3(b).

5.2.2 Workpiece and its surface topography

In the current AFF experiments, microslots in SS316L workpiece are finished. First, microslots of width 440 ± 10 µm and 20 mm length are micro machined on SS 316L circular workpieces of 3 mm thickness using electrical discharge micromachining (EDµM) process.

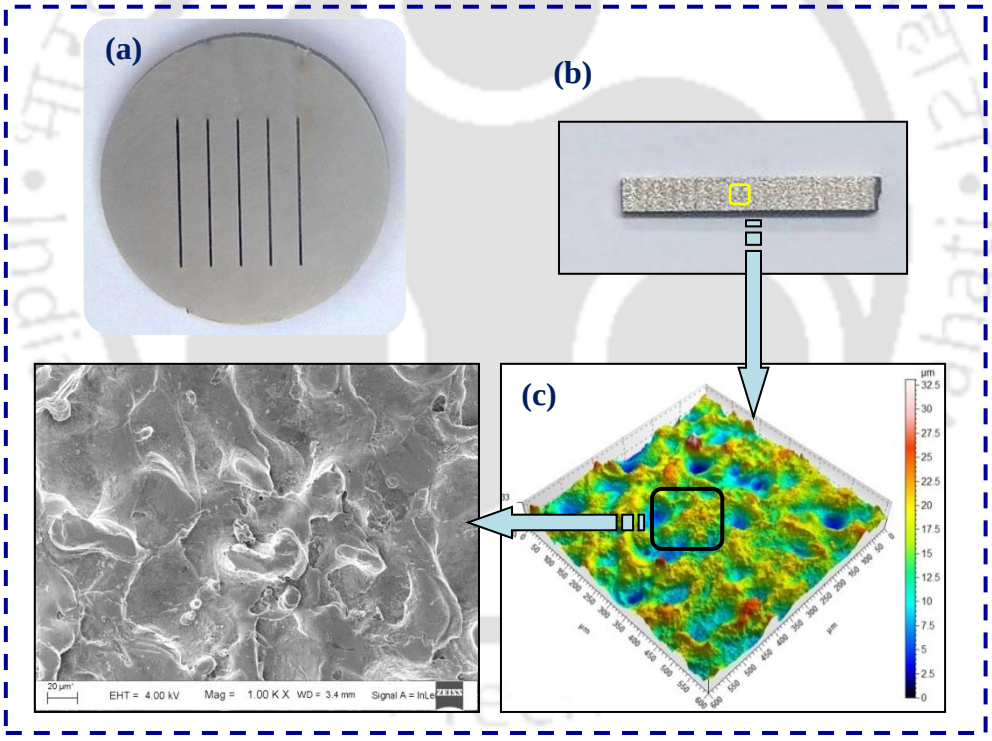

Fig. 5.4 (a) *Workpiece with microslots for abrasive flow finishing* ***(b)*** *surface of machined microslot* ***(c)*** *topographic image of the microslot surface.*

For measuring average surface roughness, (R_a) workpieces are cut again by the EDµM process and strips between two microslots are taken out (Fig. 5.4(b)). These microslot surfaces are initial surface that are to be finished by AFF process. To maintain the accuracy, a total of 24 measurements of R_a are taken on 4 strips with 6 measurements on each strip. Microslot initial surface is very rough due to the solidification of un-vaporised molten

material during machining of microslots with the EDµM process (Fig. 5.4(c)). The initial surface roughness of microslots is in the range of 3.50 ± 0.10 µm.

5.2.3 Medium

The development and rheological study of medium used for finishing of microslots is carried out in chapter 3. Medium is composed of styrene base soft polymer and silicon base polymer, mixed with a suitable amount of plasticizers and softeners along with SiC abrasive particles.

5.3 Preliminary experiments

During preliminary experiments, the effect of AFF process input parameters (extrusion pressure, numbers of AFF cycles, mesh size of abrasive particles and wt. % of abrasive particles in the medium) are studied on AFF process output response (average surface roughness). Optimum input parameters range is found out from the preliminary experiments. These ranges are later used during the parametric study of central composite rotatable design AFF process during finishing of microslots.

5.3.1 Variation of surface roughness with extrusion pressure

With the increase in extrusion pressure surface roughness of the workpiece improves upto a critical value of extrusion pressure. However, increasing the extrusion pressure beyond critical value leads negligible improvement in surface roughness (Fig. 5.5).

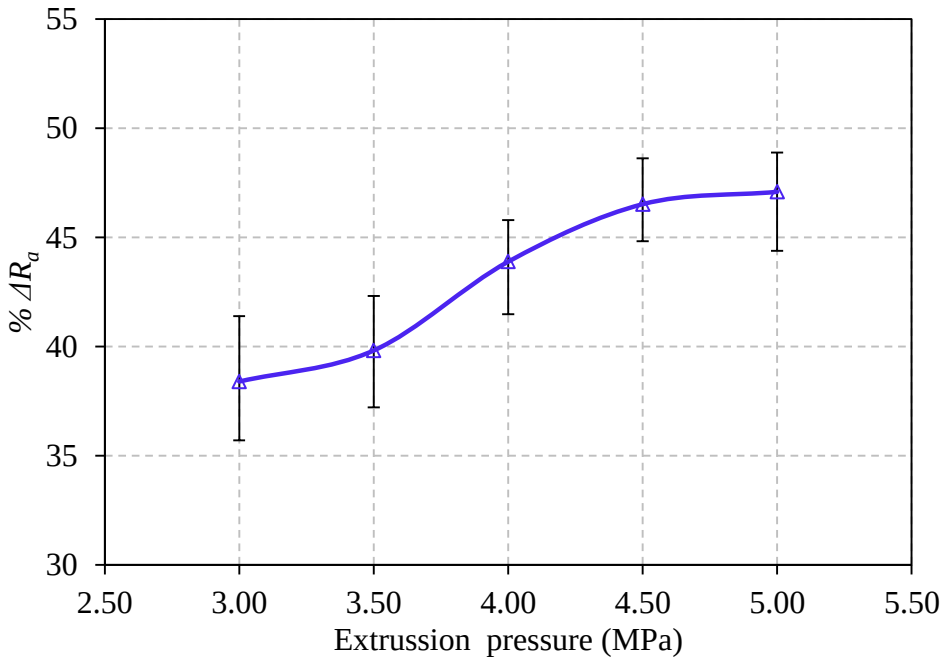

Fig. 5.5 *Variation of percentage change in surface roughness with extrusion pressure (5 cycles, # 400, 40 wt. % abrasives).*

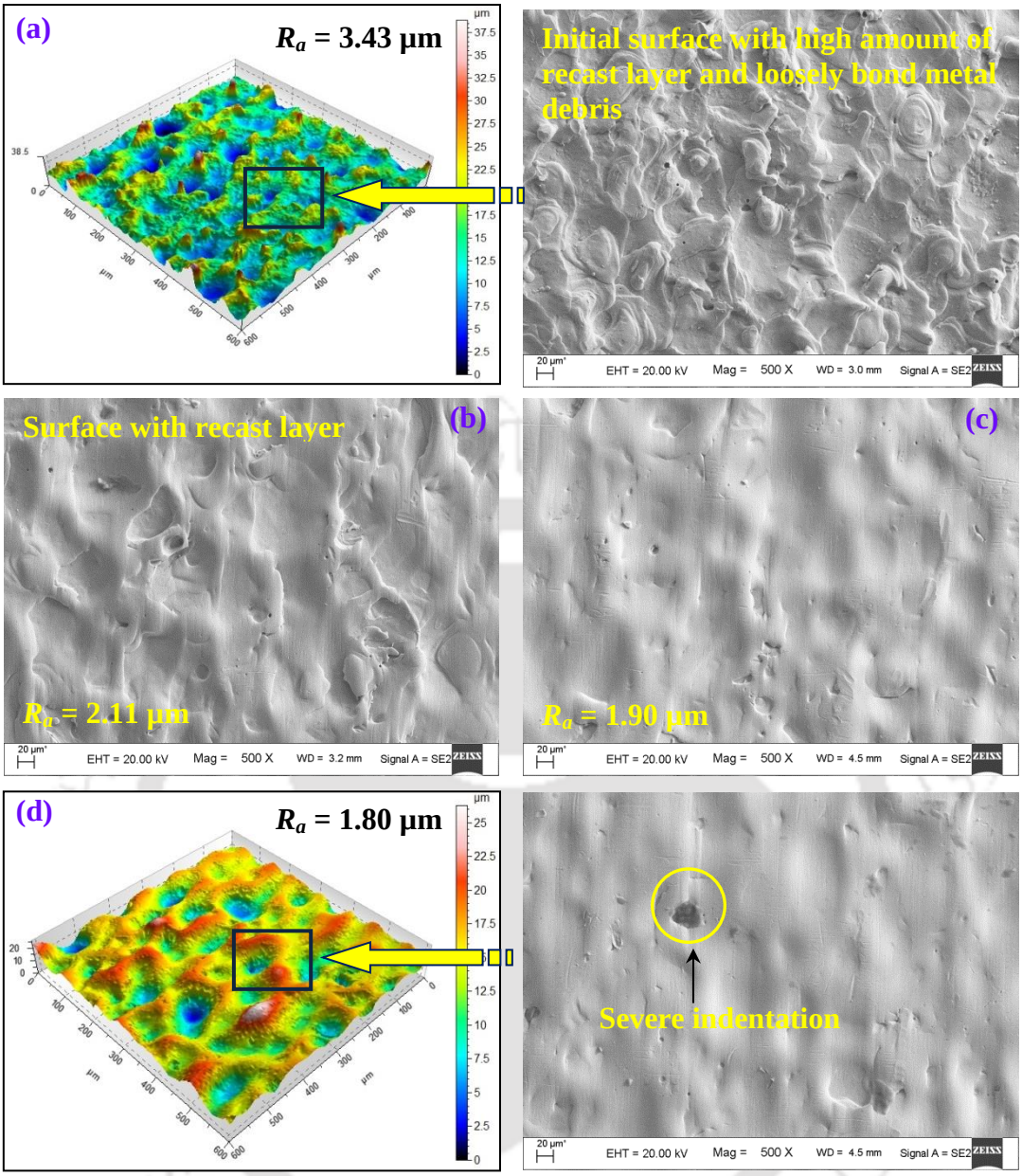

Fig. 5.6 *Workpiece surface topography at different extrusion pressure* ***(a)*** *initial* ***(b)*** *3 MPa* ***(c)*** *4 MPa* ***(d)*** *5 MPa (5 cycles, # 400, 40 wt. % abrasives).*

Initial surface of the microslot contains several high surface roughness peaks and deep valleys which result in high initial surface roughness (Fig. 5.6(a)). As the extrusion pressure increases, the amount of finishing forces (F_R, F_A) acting on the workpiece surface by medium increases. Initial workpiece surface also contains loosely bonded metal debris. These are easily removed at low extrusion pressure which results in a sharp improvement in surface roughness at 3 MPa (Fig. 5.6(b)). Higher the magnitude of finishing force exerts by the abrasive particles, deeper is the indent on the workpiece surface. Thus, amount of material removal and change in surface roughness improves at higher extrusion pressure (Fig. 5.6(c-

d)). Improvement in surface roughness occurs at a slow rate at a higher magnitude of extrusion pressure. This is due to exposure of the hard recast layer. This layer provides high resistance to shearing by abrasive particles during the material removal process. At high extrusion pressure increase of F_R is high compare to F_A. Therefore, dominant indentation on workpiece surface takes place.

5.3.2 Variation of surface roughness with number of finishing cycles

As the medium is extruded to and fro through the workpieces passage, surface roughness peaks come in contact with abrasive particles. Due to continuous hitting by abrasive particles, these surface peaks are sheared in the form of micro/nano chips. This results in improvement of surface roughness (Fig. 5.7). As the number of AFF cycles increases, number of times the surface roughness peak are sheared by the abrasive particles increases. Workpiece surface topography shows that as the AFF cycle increases the workpiece surface becomes more finished and the surface roughness decreases (Fig. 5.8(a-c)).

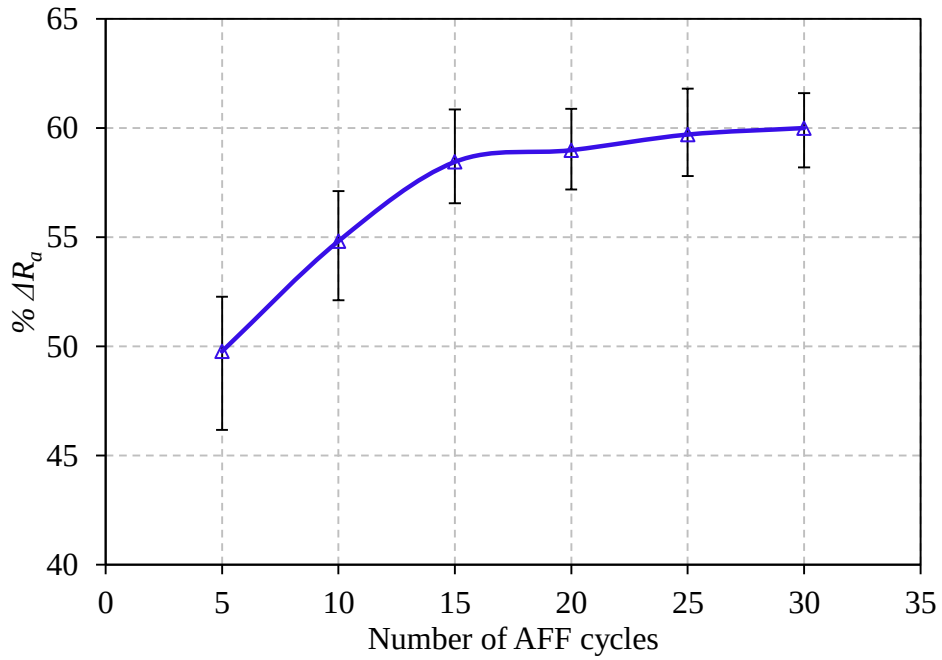

Fig. 5.7 *Variation of percentage change in surface roughness with the number of abrasive flow finishing cycles (4.5 MPa, # 400, 40 wt. % abrasive particle).*

The decrease in height of the surface roughness peaks with an increase in AFF cycles is clearly shown by 2-D surface roughness profile (Fig. 5.8(a-c)). There is a sharp surface improvement during the initial AFF cycles because of the presence of loosely bounded surface roughness peaks. The height of roughness peaks decreases in a considerable amount up to 15 AFF cycles. As the number of cycle increases further, there is not much

improvement in surface roughness values. This shows that 1.42 µm is the best surface roughness that can be achieved with the current set of AFF process input parameters and the medium composition.

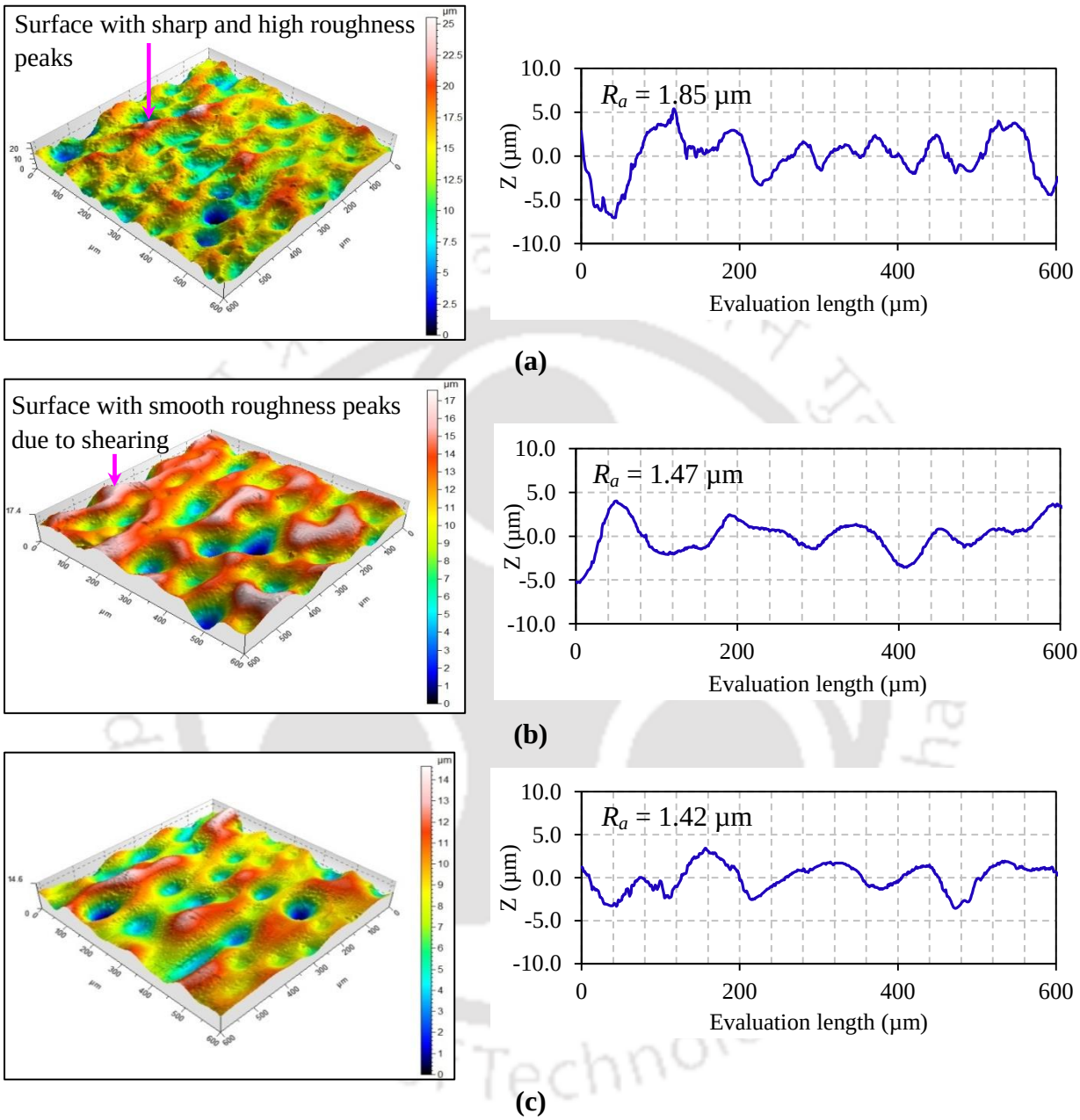

Fig. 5.8 *Workpiece surface topography and corresponding 2-D surface roughness profile at various AFF cycles* ***(a)*** *5* ***(b)*** *15* ***(c)*** *25 (4.5 MPa, # 400, 40 wt. % abrasive particle).*

5.3.3 Variation of surface roughness with abrasive particle size

After getting the better operating ranges of AFF input parameters (extrusion pressure and number of AFF cycles), next step is to improve the medium composition for removal of leftover recast layer on the workpiece surface. With all AFF input parameters constant, the effect of abrasive particle size (diameter of the abrasive particle) on the surface roughness

improvement is studied. Sometimes mesh size is also used to describe the size of the abrasive particle. Relation between mesh size and the diameter of abrasive particle is given by eq. 4.2 (chapter 4). As shown by the surface topography, workpiece surface contains few shearing marks of the abrasive particles.

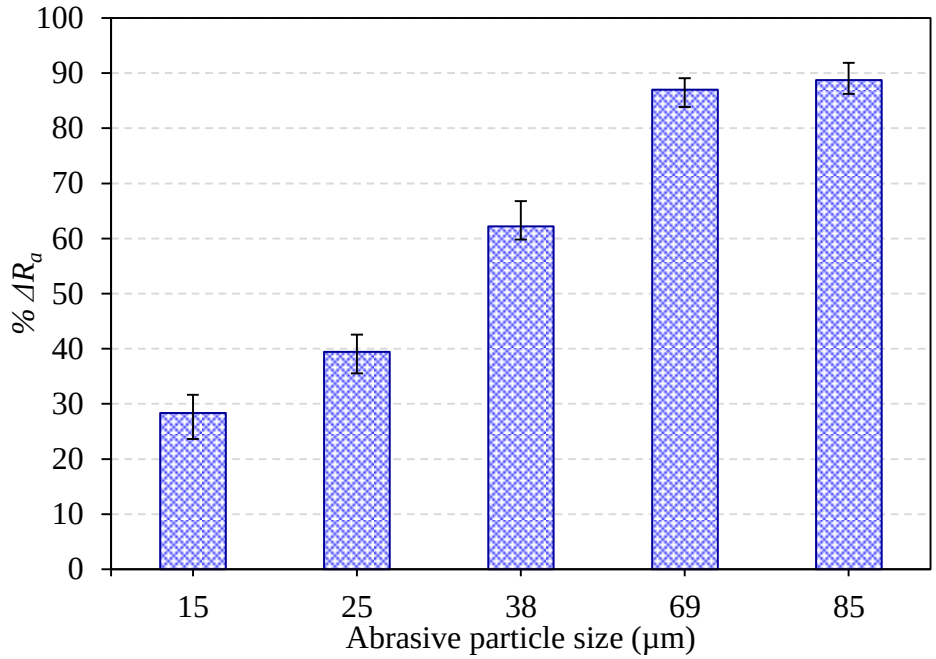

Fig. 5.9 *Variation of percentage change in surface roughness with size (diameter) of abrasive particles (25 cycles, 4.5 MPa, 40 wt. % abrasives).*

As the size of the abrasive particles increases, it improves the shearing process in two ways. Firstly, bigger the size of the abrasive particle, larger is its cutting edge. Secondly, for the same magnitude of finishing stresses transferred by the medium, the amount of finishing force generated on bigger size abrasives is more as compared to smaller size abrasive particle. Thus, a big abrasive particle with the large cutting edge and high magnitude of finishing forces indent into the workpiece to a greater depth. This results in an improved surface roughness with an increase in abrasive particle size (Fig. 5.9). As shown in Fig. 5.10(a), workpiece surface obtained after finishing with 15.24 µm diameter abrasive particles (# 1000) has a large amount of recast layer. Finishing microslots with 38.10 µm diameter abrasive particles (# 400) produces a surface free from recast layer having few valleys (Fig. 5.10(b)). Also, the abrasive particle's shearing marks become dominant because of an increase in abrasive particle size. Surface roughness deep valleys are effectively removed with AFF process by using medium containing 84.67 µm diameter abrasive particles (#180) (Fig. 5.10(c)).

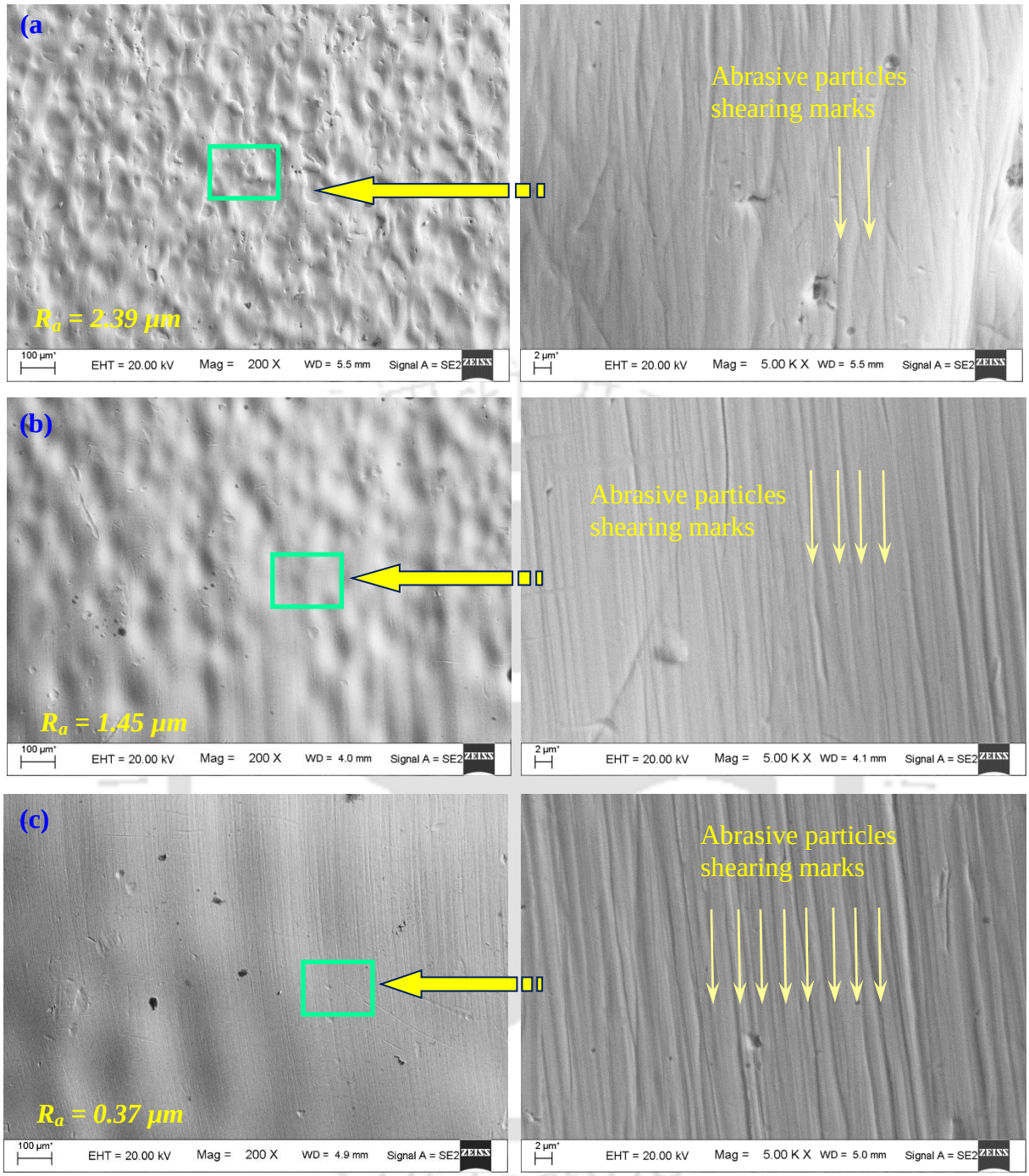

Fig. 5.10 *Workpiece surface topography at different abrasive particle sizes* ***(a)*** *15.24µm* ***(b)*** *38.10 µm* ***(c)*** *84.67µm (25 cycles, 4.5 MPa, 40 wt. % abrasives).*

5.3.4 Variation of surface roughness with weight percentage of abrasive particle

Under same experimental conditions, with an increase in wt. % of abrasive particles in the medium % ΔR_a increases (Fig. 5.11). Topographic images of workpiece surface clearly show that as wt. % of abrasive increases, the surface becomes more and more uniform, free from surface roughness peaks (Fig. 5.12(a-c)). At the wt. % of the abrasive particles in the medium

increases, 2-D surface roughness profiles of workpiece surface become gradually flat and start reducing from R_a value 0.53 µm.

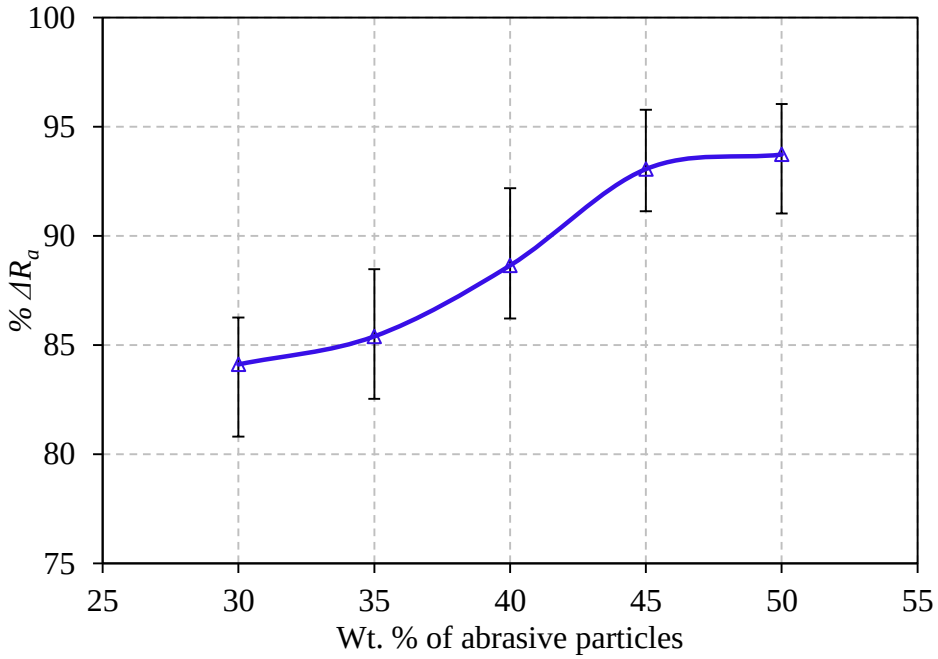

Fig. 5.11 *Variation of percentage change in surface roughness with wt. % of abrasive particles (25 cycles, # 180, 4.5 MPa).*

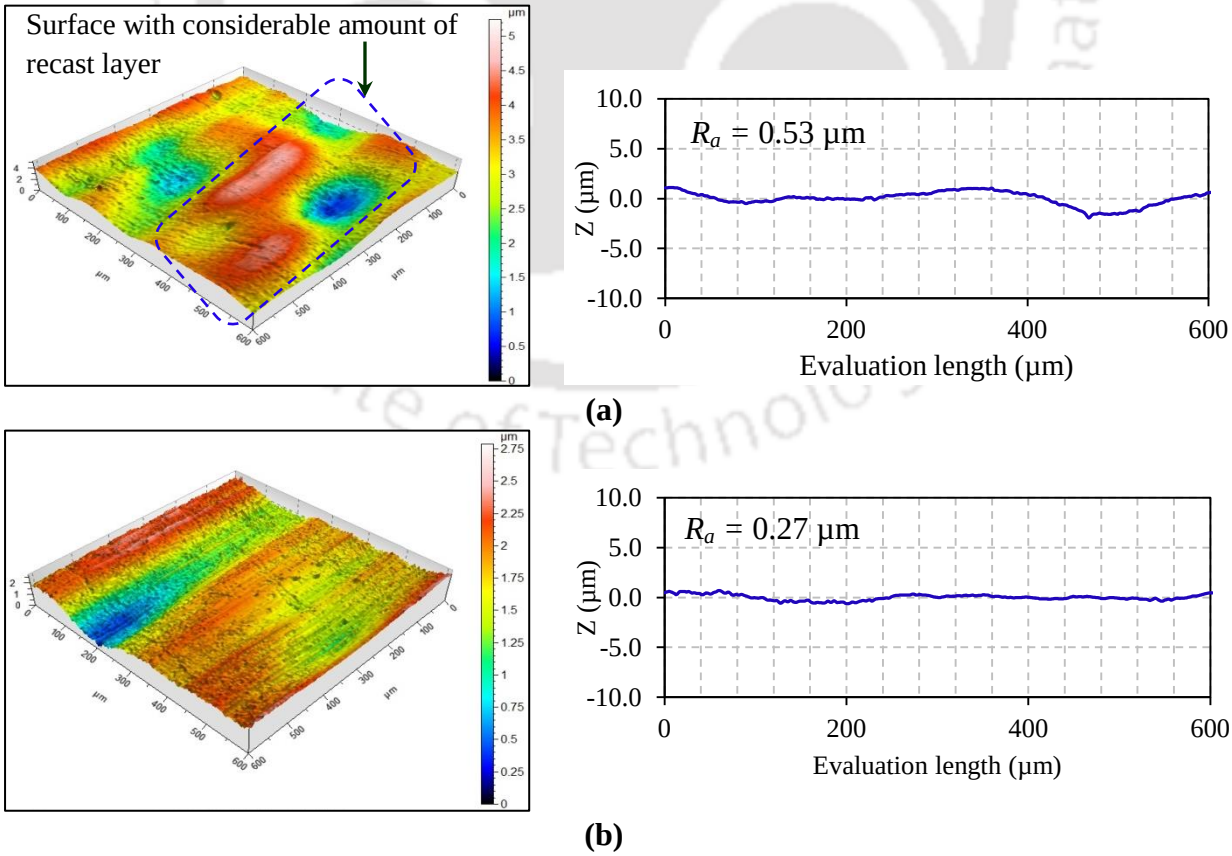

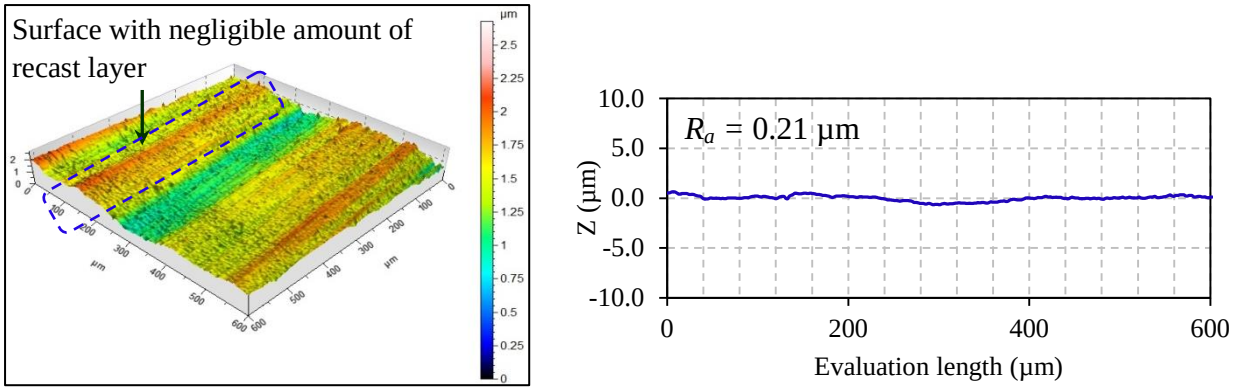

(c)

Fig. 5.12 *Workpiece surface topography and corresponding 2-D surface roughness profile at different wt. % of abrasive particles in the medium* ***(a)*** *35 %* ***(b)*** *45 %* ***(c)*** *50 % (25 cycles, # 180, 4.5 MPa).*

With an increase in wt. % of abrasive particles, the number of abrasive particles taking part per unit time in the shearing process of roughness peaks increases. Thus, for a given number of AFF cycles, extrusion pressure and mesh size of the abrasive particles, medium with higher wt. % of abrasive particles achieves an improved surface roughness as compared to the medium with lower wt. % of abrasive particles. However, increasing wt. % of abrasive particles beyond the critical value (45.00 %) improvement in surface roughness is negligible (Fig. 5.12(c)). This is mainly because there are not enough polymer chains left to hold the abrasive particles at higher wt. % of abrasive particles. Due to this, there is a weak bonding between the polymer chains and abrasive particles. Thus, the finishing forces generated in the medium are not properly transferred to the abrasive particles which adversely affect their finishing capabilities.

5.4 Experimental parametric design and analysis

In order to save the experimental resources and productive time, a design of experiment method is used. Study gives the interaction effect between input variables on output responses.

Table 5.1 *Abrasive flow finishing input parameters their coded and absolute values.*

S. No.	AFF input parameter	Unit	Levels				
			-1.682	**-1.000**	**0.000**	**1.000**	**1.682**
1.	Extrusion pressure (P)	MPa	~3.70	4.00	4.50	5.00	~5.30
2.	No. of AFF cycles (N)	-	~17	20	25	30	~33
3.	Wt. % of abrasives (W)	%	36.60	40.00	45.00	50.00	53.40

Table 5.2 *Plan of experiments and summary of output responses during microslots finishing.*

Std. order	Exp. No.	Factors			Surface roughness			Maximum height of the roughness profile		
		P	N	W	Initial R_a (µm)	Final R_a (µm)	% ΔR_a	Initial R_z (µm)	Final R_z (µm)	% ΔR_z
1	11	4.50	17	45.00	3.48	0.46	86.78	15.05	2.05	86.38
2	9	3.66	25	45.00	3.55	0.68	80.85	15.74	2.59	83.55
3	14	4.50	25	53.41	3.52	0.20	94.32	16.47	1.17	92.90
4	13	4.50	25	36.59	3.46	0.62	82.08	15.59	2.46	84.22
5	18	4.50	25	45.00	3.51	0.25	92.88	14.98	1.34	91.05
6	8	5.00	30	50.00	3.49	0.19	94.56	16.43	0.90	94.52
7	17	4.50	25	45.00	3.43	0.31	90.96	15.03	1.45	90.35
8	6	5.00	20	50.00	3.56	0.24	93.26	15.77	1.38	91.25
9	10	5.34	25	45.00	3.47	0.21	93.95	16.75	1.59	90.51
10	15	4.50	25	45.00	3.46	0.21	93.93	15.33	1.27	91.72
11	16	4.50	25	45.00	3.45	0.29	91.59	15.91	1.69	89.38
12	7	4.00	30	50.00	3.49	0.39	88.83	16.83	1.69	89.96
13	5	4.00	20	50.00	3.44	0.51	85.17	16.65	2.12	87.27
14	4	5.00	30	40.00	3.53	0.45	87.25	16.09	1.89	88.25
15	2	5.00	20	40.00	3.49	0.53	84.81	15.99	2.26	85.87
16	3	4.00	30	40.00	3.42	0.70	79.53	15.40	2.75	82.14
17	20	4.50	25	45.00	3.59	0.27	92.48	16.10	1.36	91.55
18	12	4.50	33	45.00	3.42	0.26	92.40	16.79	1.29	92.32
19	1	4.00	20	40.00	3.49	0.84	75.93	15.82	3.41	78.45
20	19	4.50	25	45.00	3.49	0.29	91.69	16.80	1.44	91.43

Effective ranges of input parameters that are found out after conducting a preliminary study of AFF process is used to design the experiments by CCRD method. Table 5.1 shows coded levels (-1.682 to 1.682) and actual values of the AFF input parameters. A total of 20 experiments are designed using the CCRD method. Two level full factorial design consists of 8 factorial runs (2^k), 6 axial runs (2k) and 6 central runs. Where "k" is the number of input parameters used during the design of experiments (k = 3 in the current case). Table 5.2 shows the detailed plan of experiments with AFF output responses (% ΔR_a, % ΔR_z).

The CCRD experimental results are analyzed by using response surface methodology. To find the significant input parameters and their % contribution on output responses, analysis of variance (ANOVA) is carried out (Table 5.3). The model p-value, Prob > F of <.0001 for

% ΔR_a and *% ΔR_z* being less than 0.05 (significance level, α for 95% confidence interval) implies that both models are significant. Analysis results show that all the AFF process input terms have an effect on output responses. In both output responses (*% ΔR_a, % ΔR_z*) the significant model terms are P, N, W, P^2, N^2 and W^2.

Table 5.3 *Analysis of variance for abrasive flow finishing of microslots.*

Source	*% ΔR_a*			*% ΔR_z*		
	F-Value	**p-value Prob > F**	**% Contribution**	**F-Value**	**p-value Prob > F**	**% Contribution**
Model	31.45	< 0.0001*		28.32	< 0.0001*	
P	98.98	< 0.0001*	33.30	69.27	< 0.0001*	26.23
N	15.38	0.0029*	5.18	29.26	0.0003*	11.08
W	107.40	< 0.0001*	36.14	111.53	< 0.0001*	42.24
PN	0.56	0.4726	0.19	0.05	0.8214	0.02
PW	0.55	0.4754	0.19	2.58	0.1393	0.98
NW	0.11	0.7461	0.04	0.00	0.9695	0.00
P^2	33.24	0.0002*	11.19	29.63	0.0003*	11.22
N^2	13.29	0.0045*	4.47	6.85	0.0257*	2.59
W^2	24.75	0.0006*	8.33	12.75	0.0051*	4.83
Lack of Fit	2.94	0.1311		2.12	0.2151	

*Significant terms

Among the significant terms found out from ANOVA, the contribution of P and P^2 (44.49 %) is highest followed by the contribution of W and W^2 (44.47 %), N and N^2 (9.65 %) in deciding *% ΔR_a*. While in the case of *% ΔR_z*, it is observed that among the significant terms, the contribution of W and W^2 (47.07 %) is highest followed by the contribution of P and P^2 (37.46 %) and N and N^2 (13.67 %).

5.5 Results and discussion

In this section, the parametric study of AFF process during the finishing of microslots is represented. The effect of AFF process input parameters (extrusion pressure, no. of AFF cycles and wt. % of abrasive particles in the medium) on AFF output responses (*% ΔR_a* and *% ΔR_z*) are discussed. As found out from the ANOVA, equations of the output responses in terms of input parameters based on the experimental are :-

$$\%\Delta R_a = -399.20 + 95.67P + 4.00N + 8.33W - 0.15PN - 0.15PW - 6.68\times10^{-3}NW - 8.62P^2 - 0.05N^2 - 0.07W^2 \quad (5.1)$$

$$\%\Delta R_z = -253.14 + 73.80P + 2.07N + 5.49W - 0.04PN - 0.25PW - 6.09\times10^{-4}NW - 6.30P^2 - 0.03N^2 - 0.04W^2 \quad (5.2)$$

5.5.1 Validation of the regression model

To validate the model developed from the regression analysis, four confirmation tests are carried out at AFF input parameter chosen randomly within the experimental plan as presented in table 5.4. The predicted responses are calculated from the regression equations (eq. (5.1)–(5.2)) for each case. After that percentage error between the actual (experimental) and predicted results are calculated. Good agreements between the experimental and predicted responses with % errors less than 5% are observed for both the output responses plotted in Fig. 5.13.

Table 5.4 *Experimental input conditions for validation of output responses regression model obtained for finishing of microslots by AFF process.*

Experiment number	Input conditions		
	P	N	W
1	4.50	30	50.00
2	4.00	20	45.00
3	4.00	20	36.66
4	4.00	25	40.00

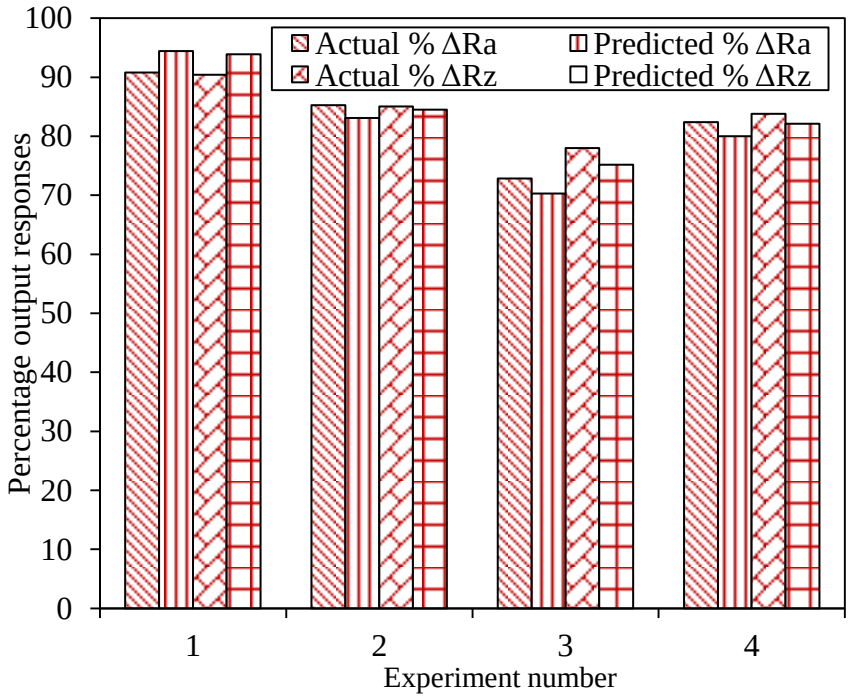

Fig. 5.13 *Validation tests with the predicted and experimental output responses (% ΔR_a* and *% ΔR_z) at various combinations of AFF input parameters.*

5.5.2 Extrusion pressure

ANOVA of AFF output responses show that extrusion pressure is the most significant parameter in deciding $\% \Delta R_a$ and $\% \Delta R_z$. It is extrusion pressure which is responsible for the generation of finishing forces (F_A and F_R) in the medium. F_R helps in the indentation of abrasive particles into workpiece surface, while F_A helps in the movement of the indented abrasive particle in the axial direction through fine openings of microslot. As shown in Fig. 3.20(b) storage modulus of the medium increases with an increase in frequency (higher the frequency more is the shear rate). Thus, the amount of energy added to the medium per unit time increases with an increase of external forces. Similarly, as extrusion pressure increases medium is sheared at higher rate and it stores a large amount of energy. This energy is released by polymer chains in the form of finishing forces to the abrasive particles during the shearing of roughness peaks which enhances their finishing capabilities. Thus, $\% \Delta R_a$ increase with an increase in extrusion pressure (Fig. 5.14(a)). The improvement in surface roughness is mainly due to the shearing of the high roughness peaks which is indicated by an increase of $\% \Delta R_z$ at a higher magnitude of extrusion pressure (Fig. 5.14(b)). However, increasing the extrusion pressure beyond a critical value leads to a slight decrease in $\% \Delta R_a$ and $\% \Delta R_z$.

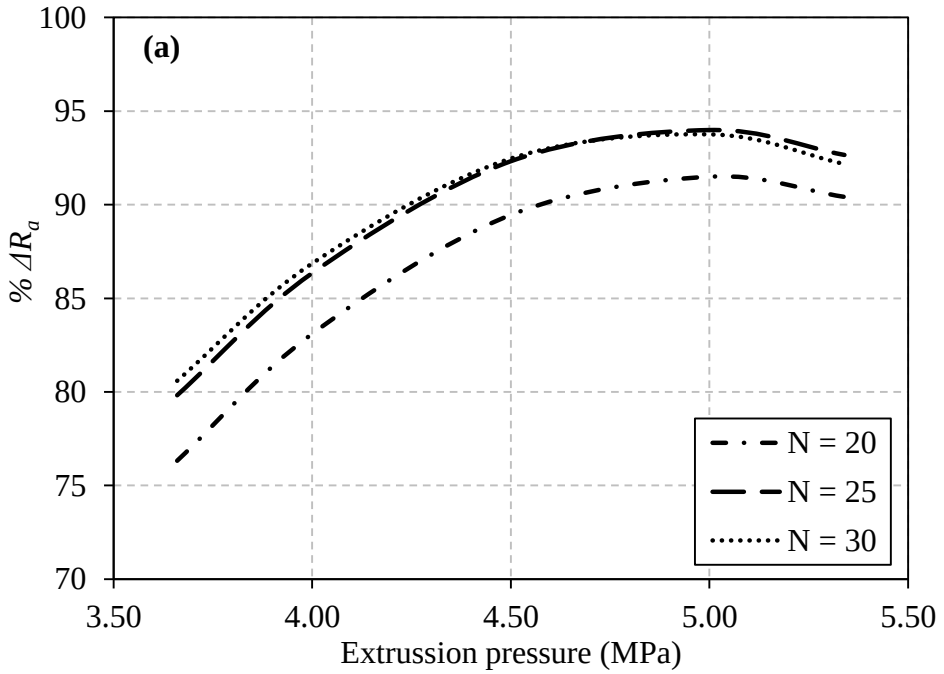

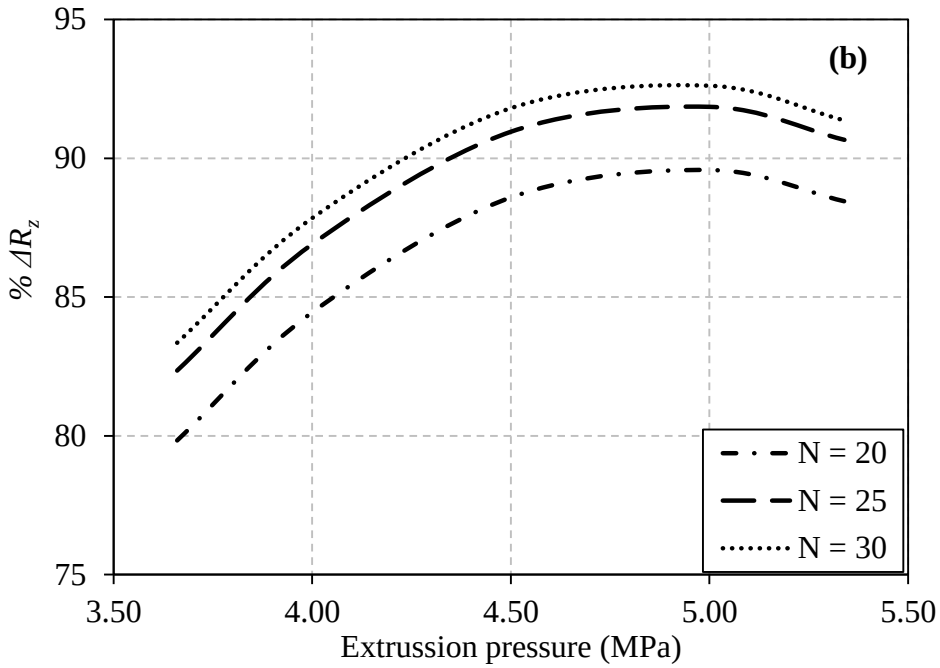

Fig. 5.14 *Effect of extrusion pressure at different number of AFF cycles on (wt. % of abrasives = 45 %)* ***(a)*** *% ΔR_a* ***(b)*** *% ΔR_z.*

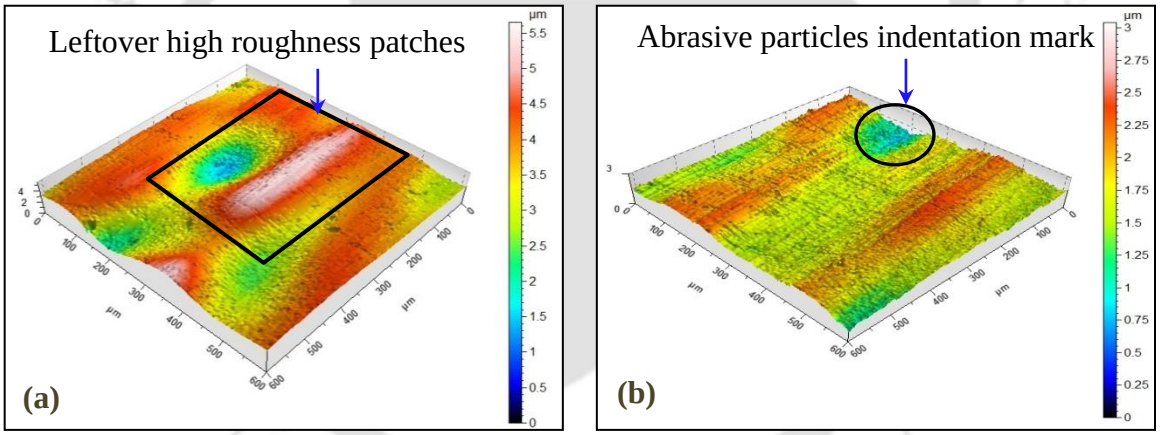

Fig. 5.15 *Workpiece surface topography after finishing at extrusion pressure* ***(a)*** *3.70 MPa* ***(b)*** *5.30 MPa (25 AFF cycles, 45 % wt. % of the abrasive particles, # 180).*

At high extrusion pressure, the medium had a large amount of stored energy (storage modulus) which is released by the polymer chains to the abrasive particles. Abrasive particles, in turn, indent into the workpiece surface with high F_R. However, at high extrusion pressure, increase in the amount of F_R is large as compared to F_A. Thus, there is no sufficient amount of F_A available in the medium to move the indented abrasive particle in the axial direction for removal of extra material in the form of micro/nano chips. The indented abrasive particle gets removed from workpiece surface in the upcoming cycles. This not only creates the indentation on the workpiece surface but also results in the breaking of sharp

cutting edges of the abrasive particles. Thus, final surface roughness is distorted by increasing the extrusion pressure beyond the critical value.

As shown in Fig. 5.15(a) the finished surface of microslot wall at 3.7 MPa of extrusion pressure consist of few roughness peaks and valleys because of insufficient extrusion pressure. At high extrusion pressure, such leftover roughness peaks and valley are removed by abrasive particles. However, increasing the extrusion pressure around 5.30 MPa results in indentation marks of the abrasive particles on the finished workpiece surface (Fig. 5.15(b)).

5.5.3 Number of abrasive flow finishing cycles

As the number of AFF cycles increase, number of times the medium is reciprocation through the workpiece surface increases. Therefore, with an increase in the number of AFF cycles, the interaction between abrasive particles and roughness peaks increases. Thus, surface roughness improves which is indicated by an increase in $\% \Delta R_a$ and $\% \Delta R_z$ with an increase in the number of AFF cycles (Fig. 5.16(a-b)). For a particular number of cycles, surface improvement in the case of medium with higher wt. % of abrasive particle is more as compared to medium with lower wt. % of abrasive particles. This is because with an increase in wt. % of abrasives the number of abrasive particles shearing the roughness peaks per unit time increases. Thus, $\% \Delta R_a$ and $\% \Delta R_z$ for the same number of AFF cycles is more for the medium with higher wt. % abrasive particles. Further, increasing the AFF cycles beyond a threshold value leads to decrease in $\% \Delta R_a$, but the value of $\% \Delta R_z$ almost remains constant.

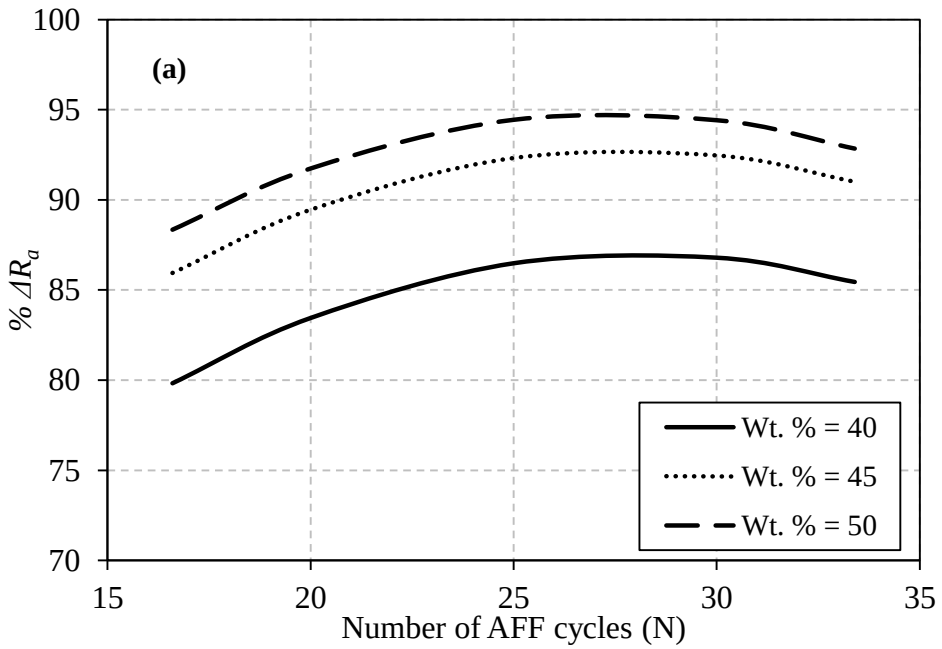

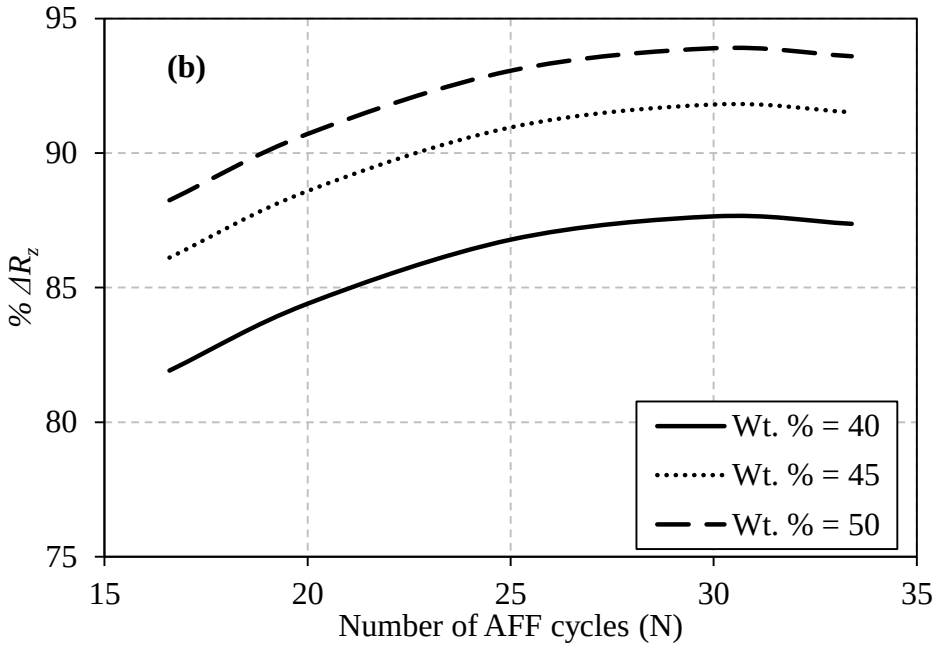

Fig. 5.16 *Effect of number of AFF cycles at different wt. % of abrasives particles (extrusion pressure = 4.5 MPa) on* ***(a)*** *% ΔR_a* ***(b)*** *% ΔR_z.*

Few hard roughness peaks and valleys are left on the microslots surface after finishing for 17 AFF cycles, 45 % wt. % of the abrasive particle (Fig. 5.17(a)). Increasing the number of AFF cycle beyond 17 cycles leads to a small improvement in % ΔR_a.

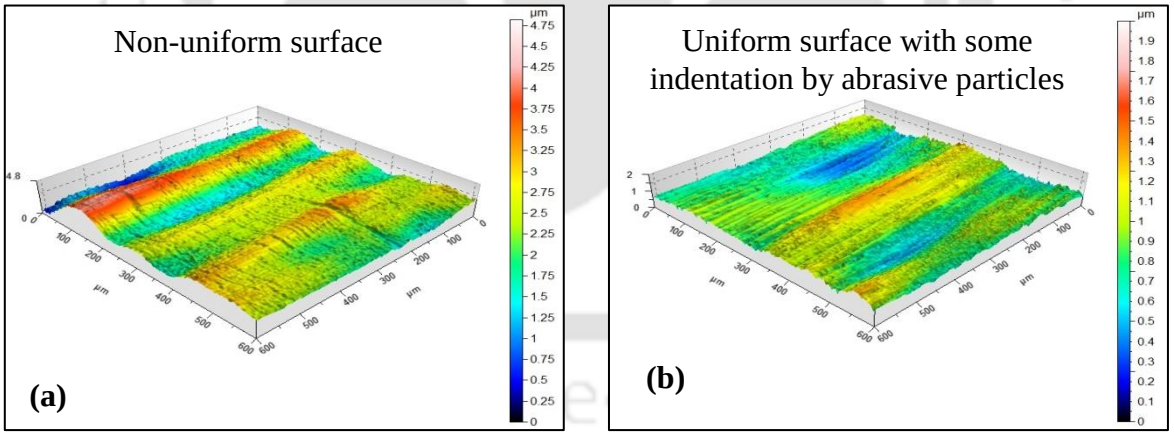

Fig. 5.17 *Workpiece surface topography after finishing at AFF cycles* ***(a)*** *17* ***(b)*** *33 (4.5 MPa, 45 % wt. % of the abrasive particles, # 180).*

Microslots are machined with the help of EDµM process and the surface obtained possesses high roughness peaks and deep valleys. Initially, shearing of roughness peaks takes place but few deep valleys remain on the workpiece surface in the blunt form. Increasing AFF cycles beyond a critical value leads to the creation of indentation marks of the abrasive particle on the finished workpiece surface. Secondly, the width of blunt roughness valleys

increases with repetitive indentation of abrasive particles (Fig. 5.17(b)). Thus, $\% \Delta R_a$ decreases but $\% \Delta R_z$ almost remains constant with the increasing AFF cycles above a critical value.

5.5.4 Weight percentage of abrasive particles

With an increase in wt. % of abrasive particles in the medium, there is an improvement in surface roughness which is indicated by an increase in $\% \Delta R_a$ and $\% \Delta R_z$ (Fig. 5.18(a-b)). As wt. % of abrasive particles in the medium increases, it enhances the finishing performance of the medium in two ways. Firstly, the number of abrasive particles per unit time that are taking part in the shearing action of roughness peak increases with an increase in wt. % of abrasive particles. Secondly, it is found out by conducting the rheological study of the medium, that medium with higher wt. % of abrasive particles possess higher viscosity (Fig. 3.22(b)). The medium with higher viscosity serves as a strong backing for the abrasive particles during the shearing action of roughness peaks. Thus, abrasive particles indent to a larger depth at high wt. % of abrasive particles. As a result the value of $\% \Delta R_a$ and $\% \Delta R_z$ increases with an increase in wt. % of abrasive particles in the medium.

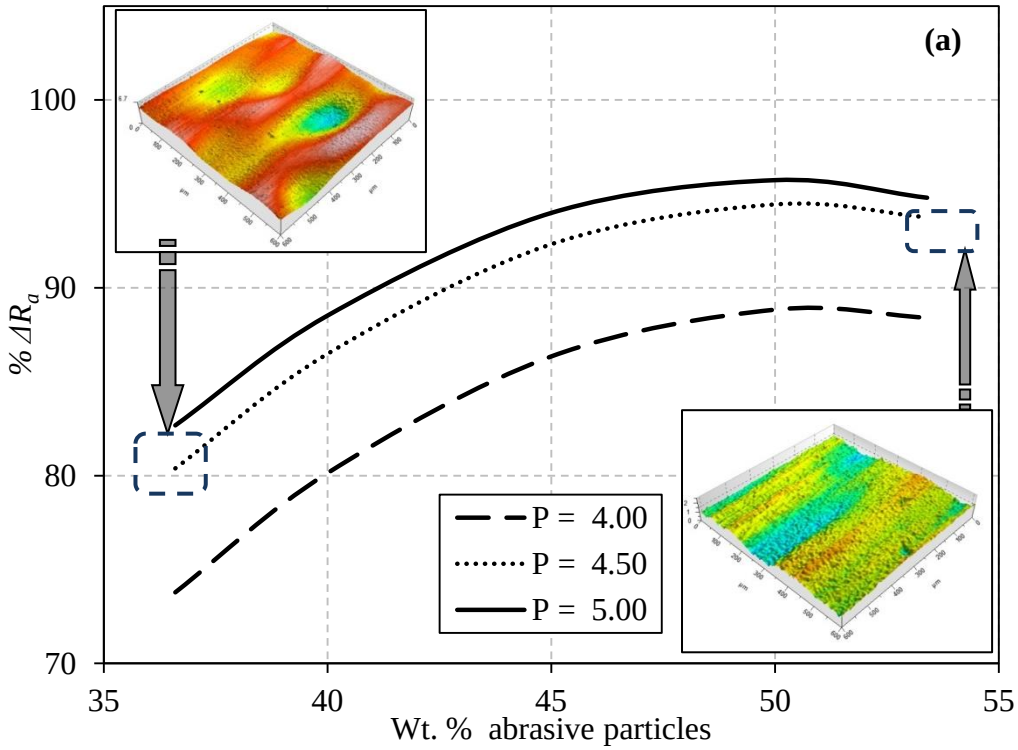

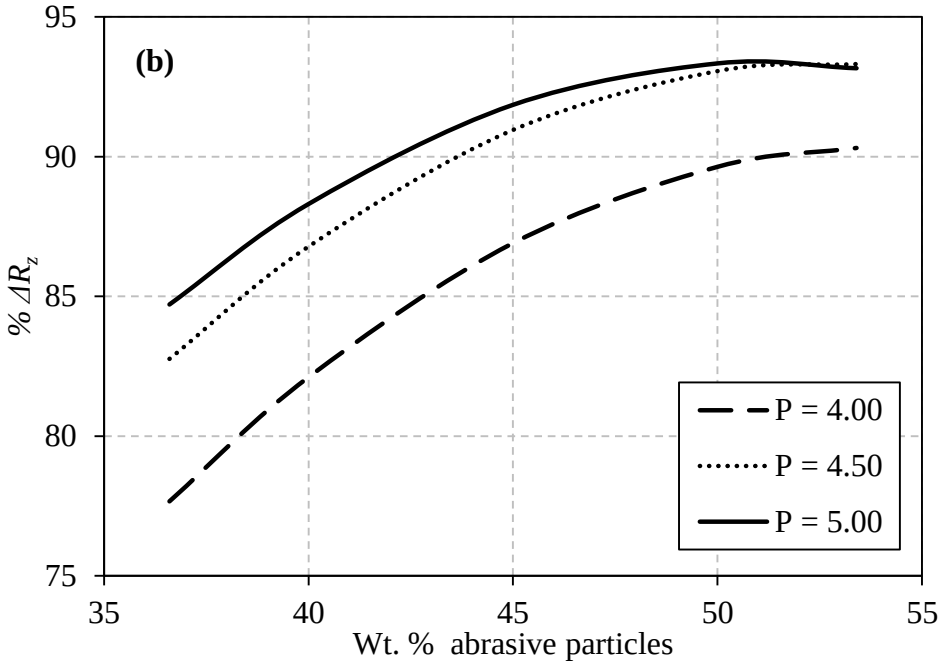

Fig. 5.18 *Effect of wt. % of abrasives particles at different extrusion pressure (number of AFF cycles = 25) on* ***(a)*** *% ΔR_a* ***(b)*** *% ΔR_z.*

The best combination of AFF process input parameters for getting the minimum surface roughness as found out by conducting AFF experiments during finishing microslots is 5 MPa extrusion pressure, 30 number of AFF cycles and 50 % of abrasive particles in the medium. With these input parameters, the percentage improvement of 94.56 % in *% ΔR_a*, is achieved by reducing initial roughness of 3.49 µm to 0.19 µm. As shown in Fig. 5.19(a), initial surface of the workpiece is very rough. This is due to the presence of recast layer with high roughness peaks and deep valleys formed on workpiece surface during the EDµM process. After finishing the same by AFF process most of the peaks, valleys are removed, and a finished surface is obtained (Fig. 5.19(b)).

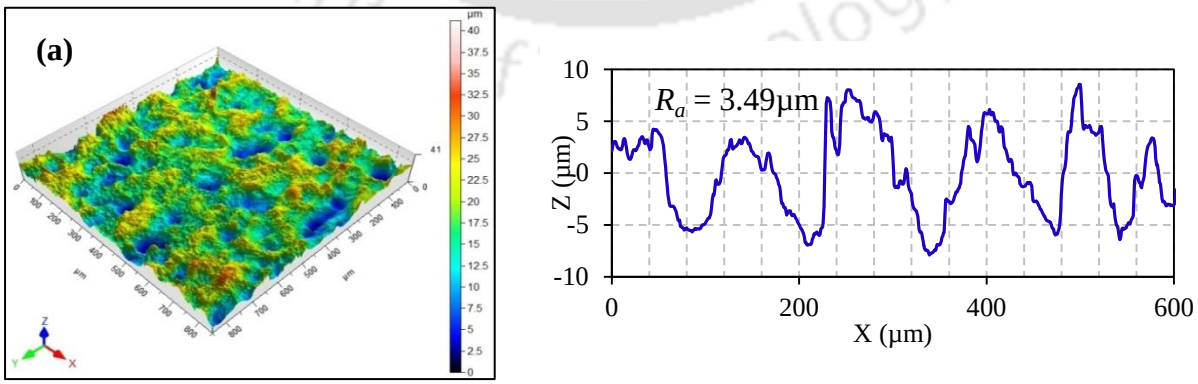

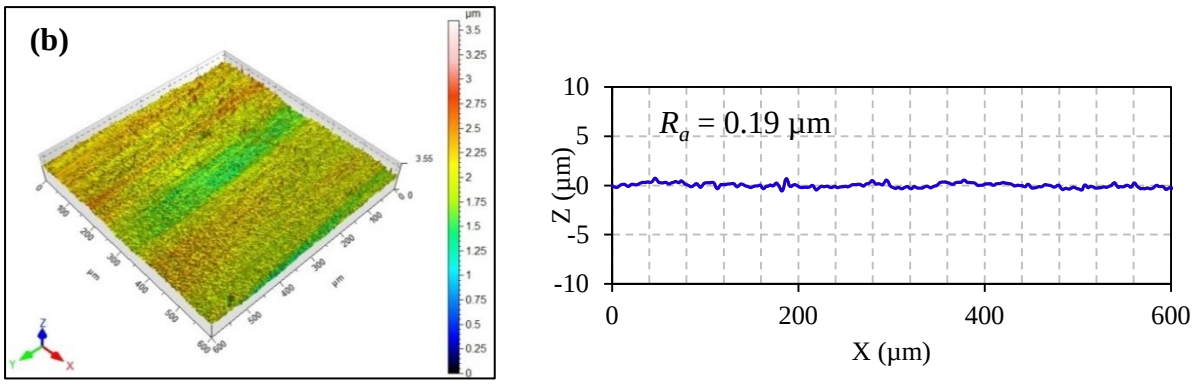

Fig. 5.19 *Workpiece surface topography and its 2-D surface roughness profile* ***(a)*** *initial workpiece surface* ***(b)*** *finished workpiece surface (30 cycles, # 180, 5 MPa, 50 wt. % abrasives particles).*

In the literature, researchers reported the material removal mechanism during finishing of components with macro features by abrasive particles in three ways i.e. microploughing, micro cutting or a combination of both [78]. However, no such literature is found for the AFF process regarding the material removal process during finishing components with micro features. Therefore, the surface topography of initial and final workpiece surface is studied.

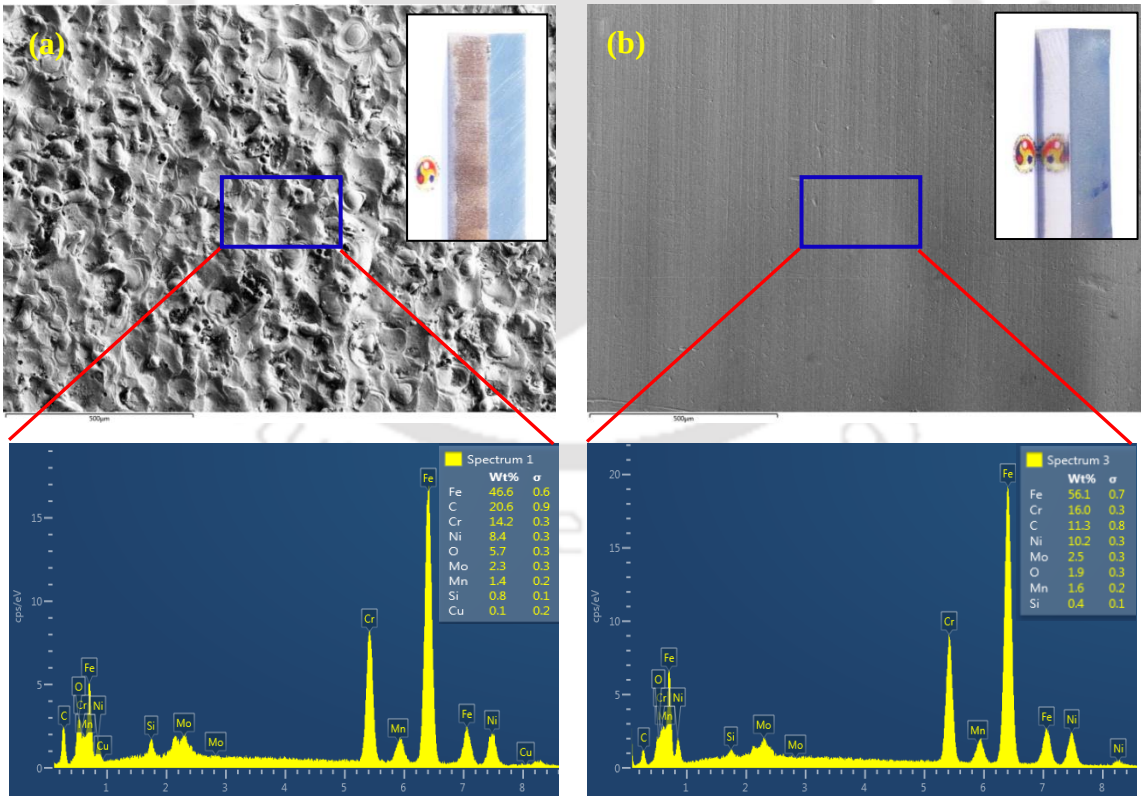

Fig. 5.20 *Workpiece surface topography with corresponding energy-dispersive X-ray spectroscopy* ***(a)*** *before finishing* ***(b)*** *after finishing (30 cycles, # 180, 5 MPa, 50 % wt. % abrasives particles).*

Initial surface roughness peaks and valleys (Fig. 5.20(a)) are removed by AFF process and the sharp shearing marks of abrasive particles are visible on finished workpiece surface (Fig. 5.20(b)). This confirms that material removal mechanism in the current set of experiments is micro cutting of roughness peaks by abrasive particles. Energy-dispersive X-ray spectroscopy (EDX) images of the initial microslot surface show that surface contains very less percentage of the SS 316L alloying elements due to the presence of unwanted recast layer (carbides) (Fig. 5.20(a)). However, in the current chapter with the help of developed AFF setup, tooling and medium, microslots are finished to the in the nanometer range. Finishing microslots by AFF process removes the recast layer. This is also indicated by EDX analysis showing the increase in percentage of SS 316L alloying elements (Fig. 5. 20(b)).

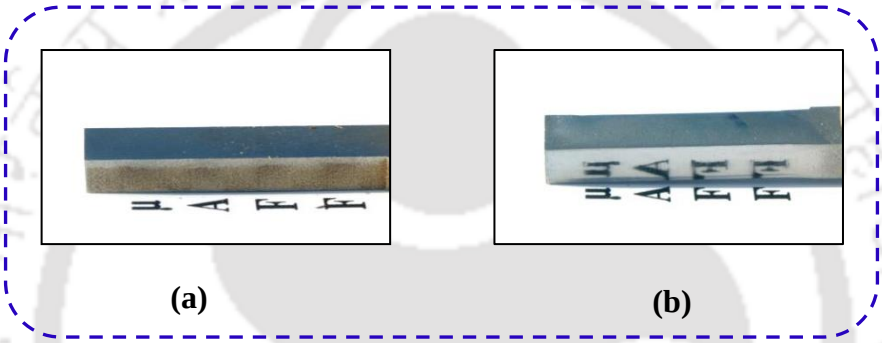

Fig. 5.21 *Workpiece microslot surface* ***(a)*** *initial workpiece surface that doesn't reflect the letters µAFF* ***(b)*** *final workpiece surface after finishing showing µAFF.*

Workpiece surface obtained after finishing microslots with AFF process achieves a mirror finish. As shown in Fig. 5.21(a) the initial surface of microslot doesn't show any reflection due to the rough surface, but after finishing the same with AFF process the letters "µAFF" are clearly reflected on the workpiece surface (Fig. 5.21(b)).

5.6 Conclusions

In the current chapter, initially preliminary experiments are conducted to study the effective ranges of AFF process. Later, a detailed parametric study of AFF process during finishing of microslots is carried out. Finishing of microslots is carried out by using indigenously developed AFF process and medium. Based on the study following important conclusions are made:-

1. Indigenously developed AFF medium and tooling is suitable for finishing microslots.
2. In-house developed medium successfully reduced the surface roughness on the microslots wall to nanometer ranges.

3. From the ANOVA, it is found that extrusion pressure is the most significant term affecting the AFF output responses. During the experimental analysis, the contribution of P and P^2 (44.49 %) is the highest followed by the contribution of W and W^2 (44.47 %), N and N^2 (9.65 %) in deciding $\% \Delta R_a$.
4. In the case of $\% \Delta R_z$, it is observed that among the significant terms the contribution of the combination of W and W^2 (47.07 %) is the highest followed by the combination of P and P^2 (37.46 %) and N and N^2 (13.67 %).
5. The best experimental surface roughness of 192 nm with a surface improvement of 94.56 % is achieved on the microslots surface.

Chapter 6

ABRASIVE FLOW FINISHING OF MICROHOLES

6.1 Introduction

Microholes are one of the most common features in many applications such as drug eluting stents (DES), high-pressure orifices, ink-jet printer nozzles, turbine blades and fuel injection nozzles. Finishing of microholes plays an important role in deciding the component performance. Microholes are normally fabricated by thermal based micromachining process such as electric discharge micromachining (EDµM), or laser micromachining process. The microholes surface that generated from EDµM is very rough due to re-solidification of the molten layer. Depending on the end use of the product, surface roughness in some fields hampers the proper functioning of the product. i.e., in case of fuel injector nozzle, surface roughness causes the change in fuel flow rate. This not only decreases the efficiency of the vehicle but also generates unwanted pollution due to improper air-fuel mixing. AFF finished fuel injector nozzles possess a smoother surface and a definite exit radius. This leads to required amount of fuel flow rate which increases engine performance, power and reduction of emissions as well as crack propagation. As found from the literature, very few attempts are

made by researchers for finishing of microholes with the help of AFF process. Microholes are machined on surgical steel (SS 316L) specimens such as metallic coronary DES for delivering the drug. If microholes in DES possess high surface roughness with loosely bonded metal debris, there are high chances of drug contamination. Also, drug delivery at required flow rate is not possible due to obstruction of drug by high surface peaks and retention of the drug in deep roughness valleys. As a result, cells do not receive the proper amount of drug, which may harmer the curing process (Fig. 6.1(a)). To avoid these problems, nanofinishing of microholes can be carried out. Since size of microhole is too small, finishing can be carried out by AFF process. Nanofinished microholes in DES can deliver drug at required flow rate (Fig. 6.1(b)). Similar applications of nanofinishing of microholes exist in many sectors. Therefore, there is a need of nanofinishing of microholes in many manufacturing fields.

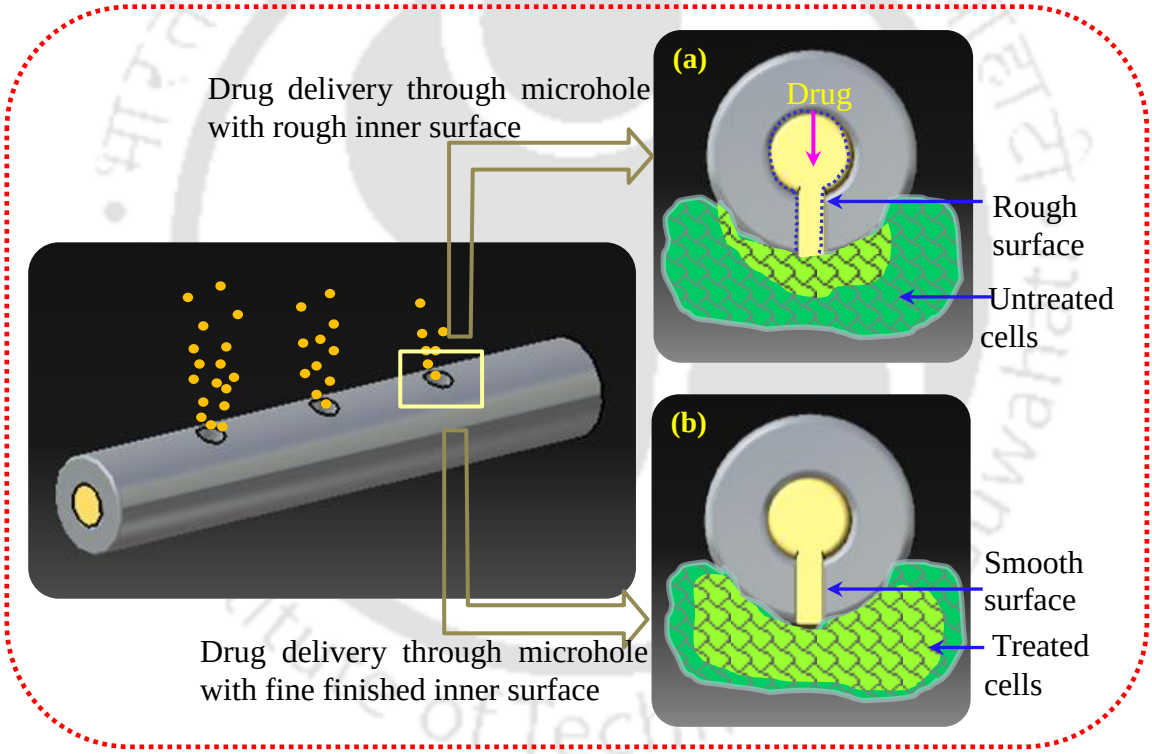

Fig. 6.1 *Schematic of drug elution from microholes of metallic drug eluting stents* ***(a)*** *before finishing* ***(b)*** *after finishing.*

An attempt to finish microholes in SS 316L with the help of AFF process is made in the current chapter. First microholes are machined in SS 316L steel using EDµM process. Later, preliminary experiments are carried out to find various ranges of input variables (extrusion pressure, number of cycles, mesh size and weight percentage of abrasive particles). Then

complete experimental parametric study of AFF process during finishing of microholes is carried out using design of experiment (central composite rotatable design) technique.

6.2 Experimentation

Microholes are machined by EDµM and same are finished by AFF process. Surface roughness and morphology of microhole is characterized before and after AFF process.

6.2.1 Micromachining of microholes

Surgical stainless steel (SS 316L) plate of thickness 3 mm is chosen as the workpiece material in the present work. Microholes with a radius of 425 ± 15 µm are machined with the help of EDµM (Fig. 6.2(a)) process. A special tool is designed for micromachining (Fig. 6.2(b)), and 25 microholes are fabricated simultaneously on each specimen (Fig. 6.2(c)). Before and after finishing of the workpiece by AFF process, surface roughness is measured with the help of Taylor Hobson non-contact type profilometer.

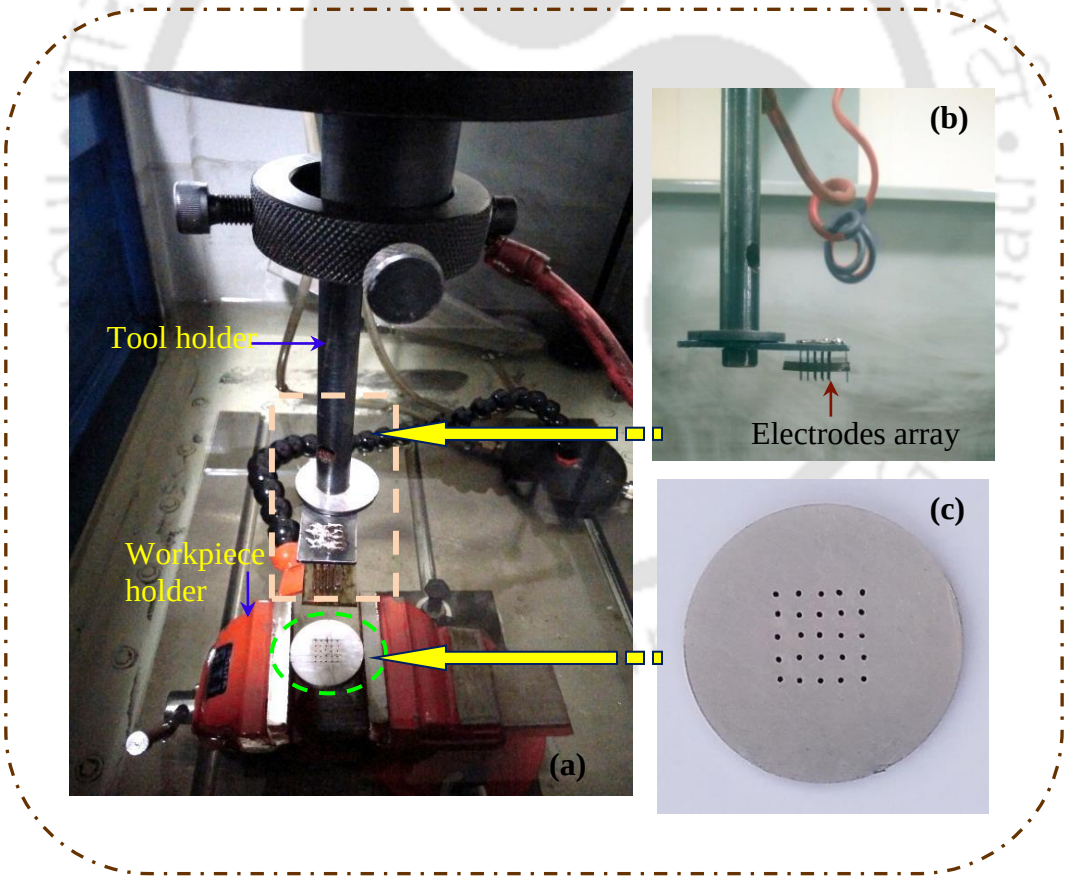

Fig. 6.2 (a) *Overview of electric discharge micromachining setup and tooling used for machining microholes* ***(b)*** *tooling* ***(c)*** *micromachined workpiece.*

From the workpiece, a small strip is taken out containing microhole with the help of wire electric discharge machining (WEDM) process (Fig. 6.3(a-b)). Using non-contact type profilometer, 3-D surface topography (Area of 130 µm x 130 µm) of microhole finished region is obtained. 2-D surface roughness profile data in the circumferential direction (along the line drawn in the center half of the image) from the 3-D image is extracted in the form of *X* and *Z* coordinates (Fig. 6.3(c)).

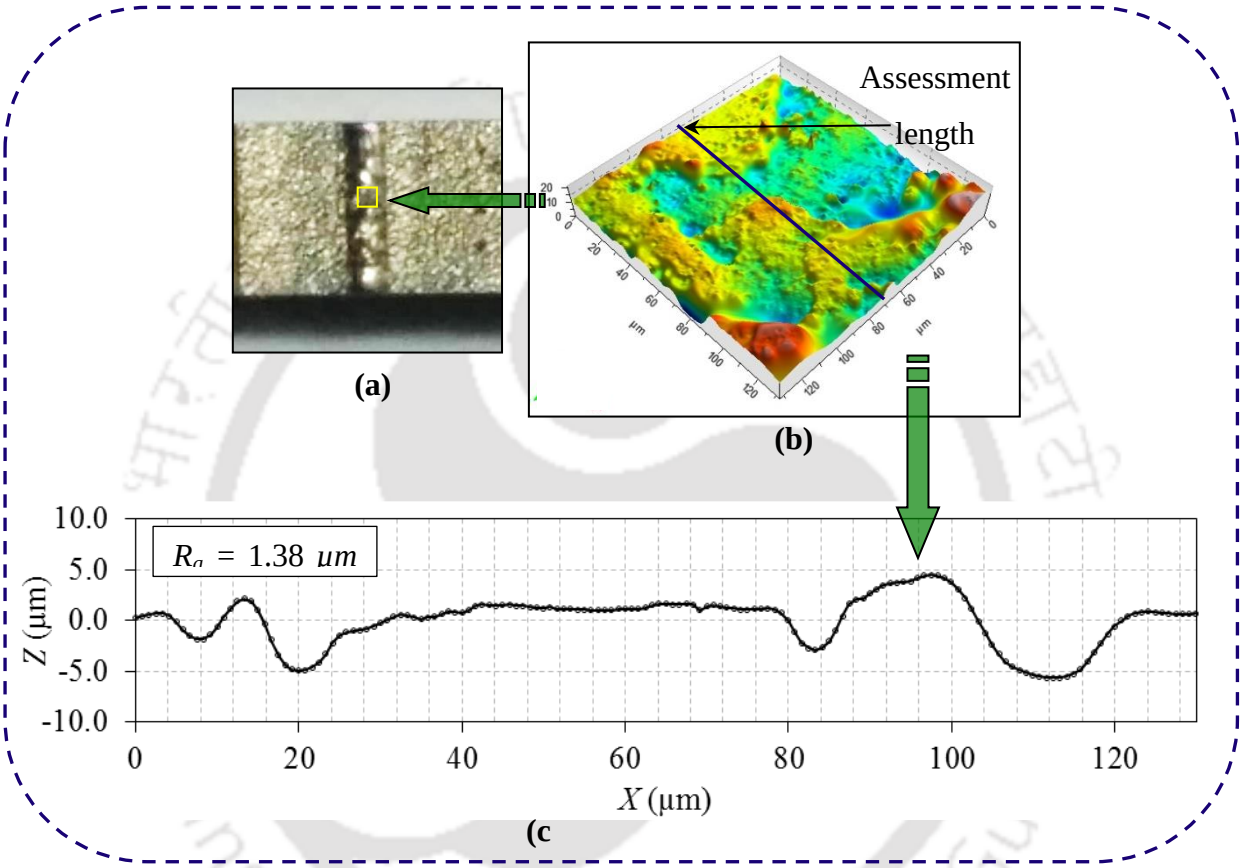

Fig. 6.3 (a) *workpiece* ***(b)*** *cut surface of the microhole* ***(c)*** *3-D surface topography of the workpiece* ***(d)*** *2-D roughness profile of the workpiece surface (R_a = 1.38 µm).*

6.2.2 Abrasive flow finishing tooling and medium

Tooling fabricated for finishing microslots in chapter 5 is used for finishing of microholes. Effective passage area for the medium to extrude across microholes is less compared to microslots. As a result, there is more restriction offered to the medium during extrusion through microholes. Therefore, to ensure a smooth flow of medium through fine openings in workpiece, medium with low viscosity compared to microslot is used for finishing microholes. Medium preparation for finishing microholes and its rheological study is

prepared in chapter 3. Fig. 6.4 shows the extrusion of the medium through the fine openings of microholes machined in the SS 316L workpiece.

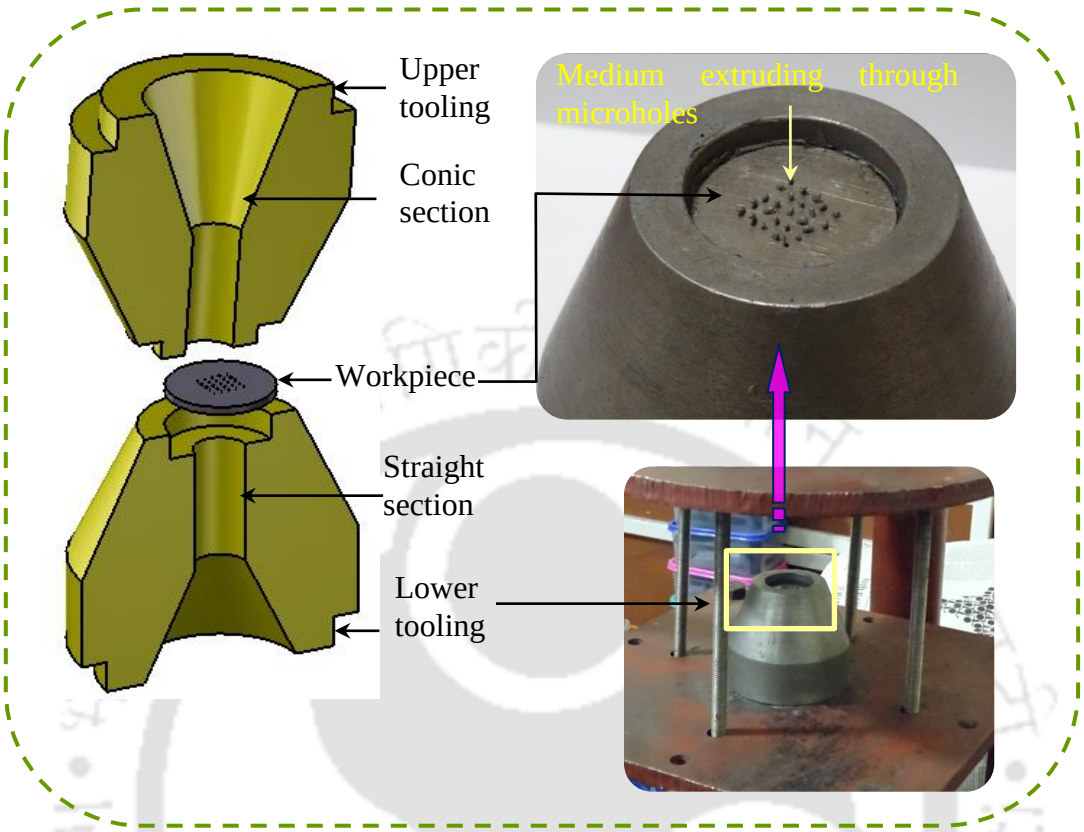

Fig. 6.4 *Overview of the tooling used for finishing of the microholes.*

6.3 Preliminary experimental study

The main objective of preliminary experimentation is to find effective ranges of AFF process input parameters for best values of output responses. The effect of various AFF process input parameters (i.e., extrusion pressure, number of AFF cycles, mesh size of abrasive particle and wt. % of the abrasive particles in the medium) on the output response (i.e., surface roughness) is studied.

6.3.1 Extrusion pressure

As the magnitude of extrusion pressure increases, the amount of finishing forces generated in the medium increases. With an increase in the finishing forces, the abrasive particle indents deeper into the workpiece surface. Due to this, the amount of material removed in a given number of AFF cycles increases with an increase in extrusion pressure. Therefore, surface roughness improves with an increase in extrusion pressure (Fig. 6.5).

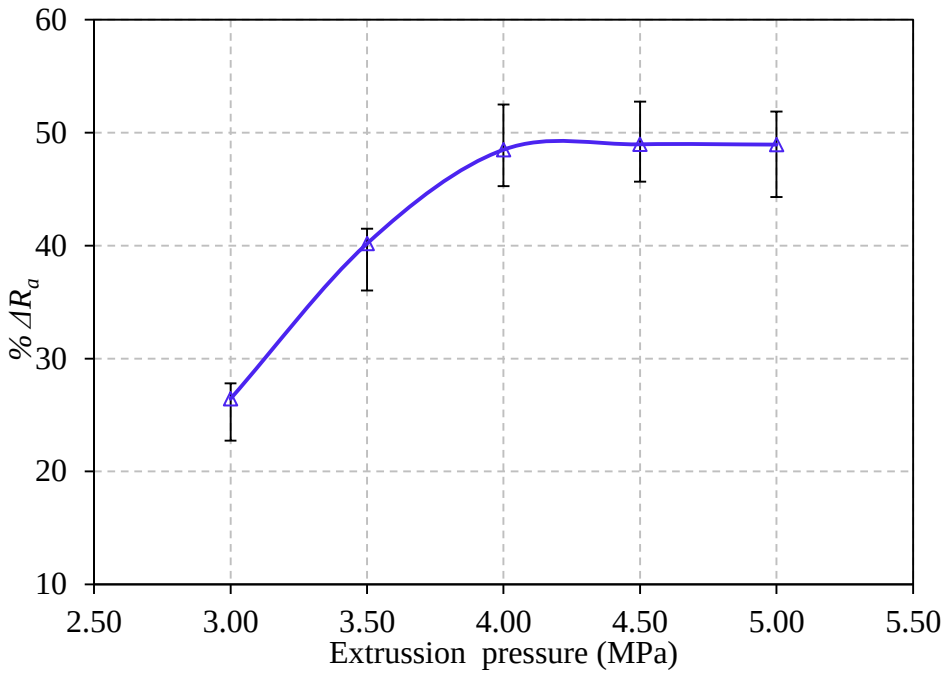

Fig. 6.5 *Variation of the percentage change in surface roughness with extrusion pressure (6 cycles, # 400, 35 wt. % abrasives).*

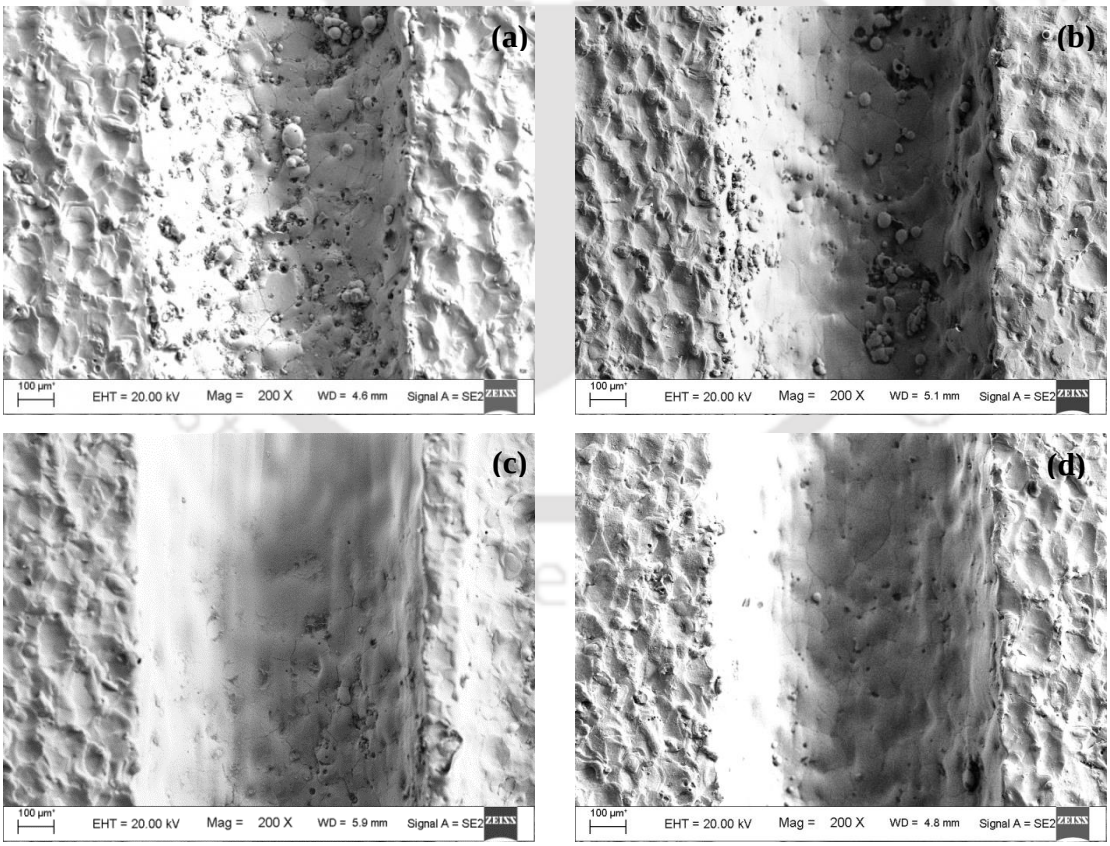

Fig. 6.6 *Workpiece surface topography at various extrusion pressure* ***(a)*** *initial (R_a = 1.47 µm)* ***(b)*** *3 MPa (R_a = 1.03 µm)* ***(c)*** *4 MPa (R_a = 0.69 µm)* ***(d)*** *5 MPa (R_a = 0.65 µm) (6 cycles, # 400, 35 wt. % abrasives).*

As seen from the surface morphology of unfinished surface, the workpiece surface is too rough due to the formation of recast layer along with solidified spheroids (Fig. 6.6(a)). As the extrusion pressure increases, the force ratio (F_R/F_A) increases which results in effective shearing of surface roughness peaks by abrasive particles. With the increase in extrusion pressure, surface roughness improves sharply upto 4 MPa (Fig. 6.6(b-c)). Increasing the extrusion pressure beyond the critical value (4 MPa), not much improvement in surface roughness is observed. This is due to start of indentation effect by abrasive particle due to high F_R at high extrusion pressure, since F_R/F_A increases with extrusion pressure, at high extrusion pressure F_R dominates. Therefore, indentation depth increases but F_A remains approximately same. Thus, the ability of medium to provide axial motion to highly indented abrasive particle reduces. Hence, the abrasive particle creates indentation along with finishing. Therefore, $\% \Delta R_a$ is approximately same after critical value of extrusion pressure (4 MPa).

6.3.2 Number of abrasive flow finishing cycles

As the number of AFF cycles increases, more number of times surface roughness peaks are sheared by abrasive particles. Thus, the value of $\% \Delta R_a$ increases, with an increase in number of AFF cycles (Fig. 6.7).

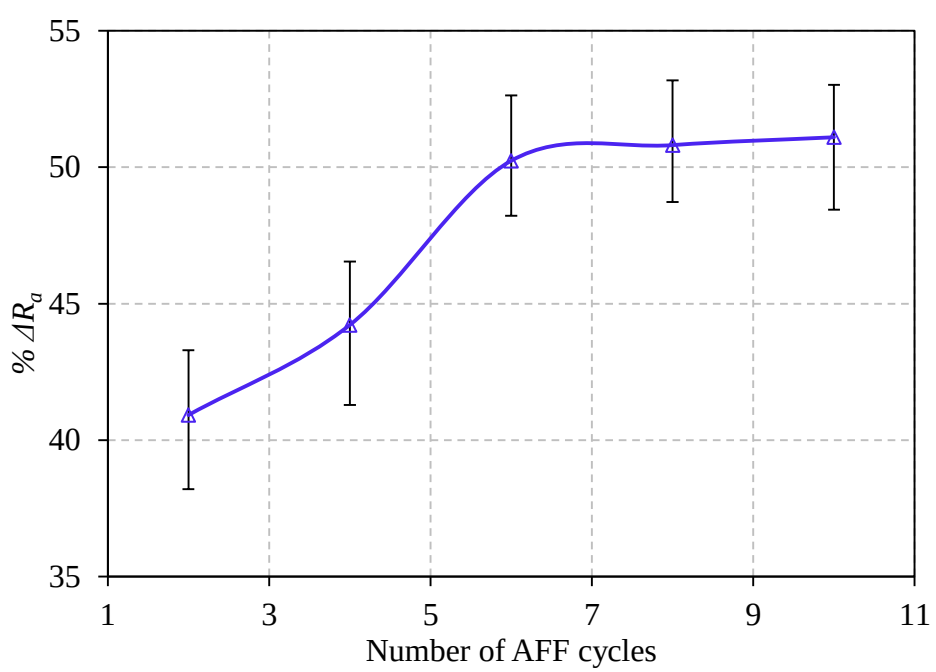

Fig. 6.7 *Variation of percentage change in surface roughness with number of abrasive flow finishing cycles (4 MPa, # 400, 35 wt. % abrasives).*

Topography and the corresponding 2-D surface roughness profile shows that during the initial AFF cycles the rate of change of % ΔR_a is more (Fig. 6.8(a-b)). However, as the number of AFF cycles increases there is very less or no improvement in the surface roughness. This is due to the fact that loosely held surface roughness peaks are sheared by roughness particles in the early AFF cycles. Hard surface left after the initial AFF cycles provide high resistance to the abrasive particles during shearing process. Thus, there is no or very little surface improvement at higher number of AFF cycles (Fig. 6.8(c)).

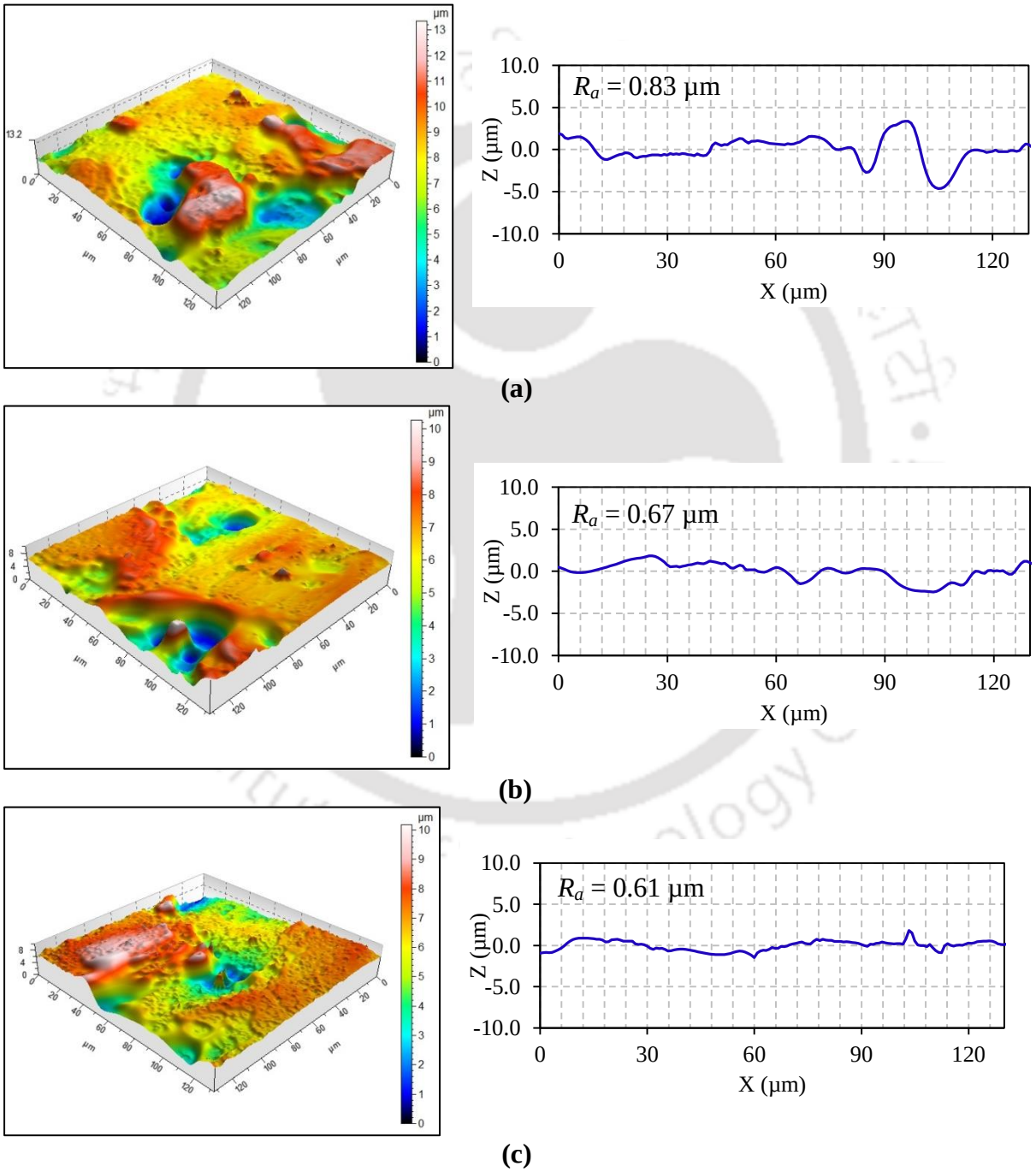

Fig. 6.8 *Workpiece surface topography and corresponding 2-D surface roughness profile at various AFF cycles* ***(a)*** *2* ***(b)*** *8* ***(c)*** *10 (4 MPa, # 400, 35 wt. % abrasives).*

6.3.3 Mesh size of abrasive particle

After studying the effect of extrusion pressure, number of AFF cycles and finding their optimum ranges, the medium composition is varied to give a better surface roughness. Mesh is inversely proportional to size of abrasive particles i.e. larger the mesh size, smaller the abrasive particle and vice versa. Larger the abrasive particle (low mesh size) more is the magnitude of finishing forces acting on it. Thus, for a given set of experimental conditions, as the mesh size of the abrasive particle decreases $\% \Delta R_a$ increases (Fig. 6.9). Amount of the recast layer left on the microhole wall decreases as the size of abrasive particle increases, which improves the surface roughness.

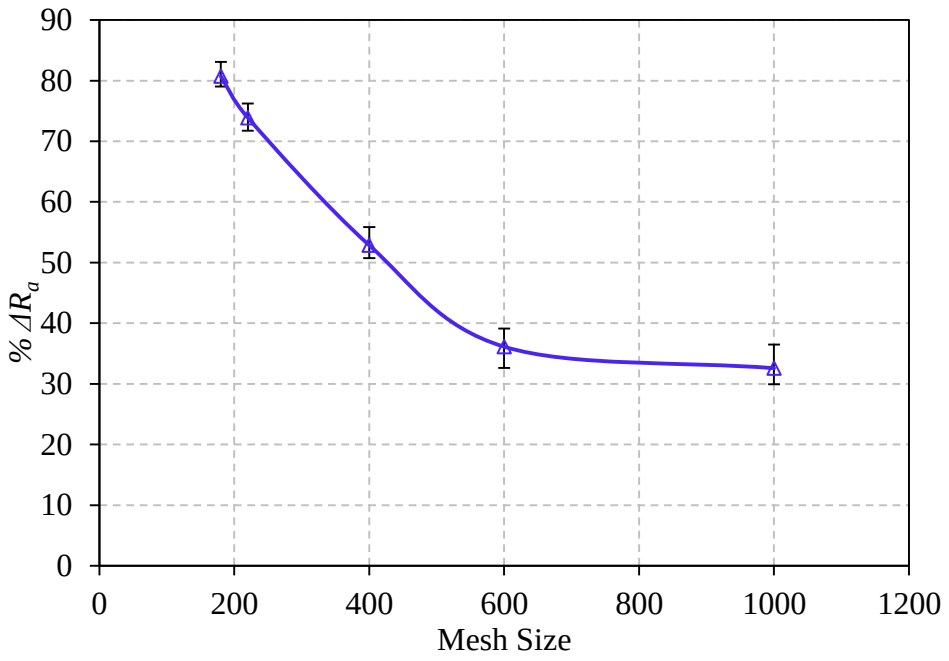

Fig. 6.9 *Variation of the percentage change in surface roughness with mesh size (8 cycles, 4 MPa, 35 wt. % abrasives).*

As the size of abrasive particle increases, its cutting edge also becomes big. Thus, bigger abrasive particle with the high magnitude of cutting force indents deeper into the workpiece surface. Initially, for # 1000 abrasive particles, considerable amount of recast layer is left on the workpiece surface (Fig. 6.10(a)). As the mesh size decreases, the amount of recast layer on the workpiece surface decreases due to the effective shearing of roughness peaks by lower mesh size abrasive particles (Fig. 6.10(b-d)). After finishing the microhole with # 180 abrasive particles there is very less or no amount of recast layer left on the workpiece surface.

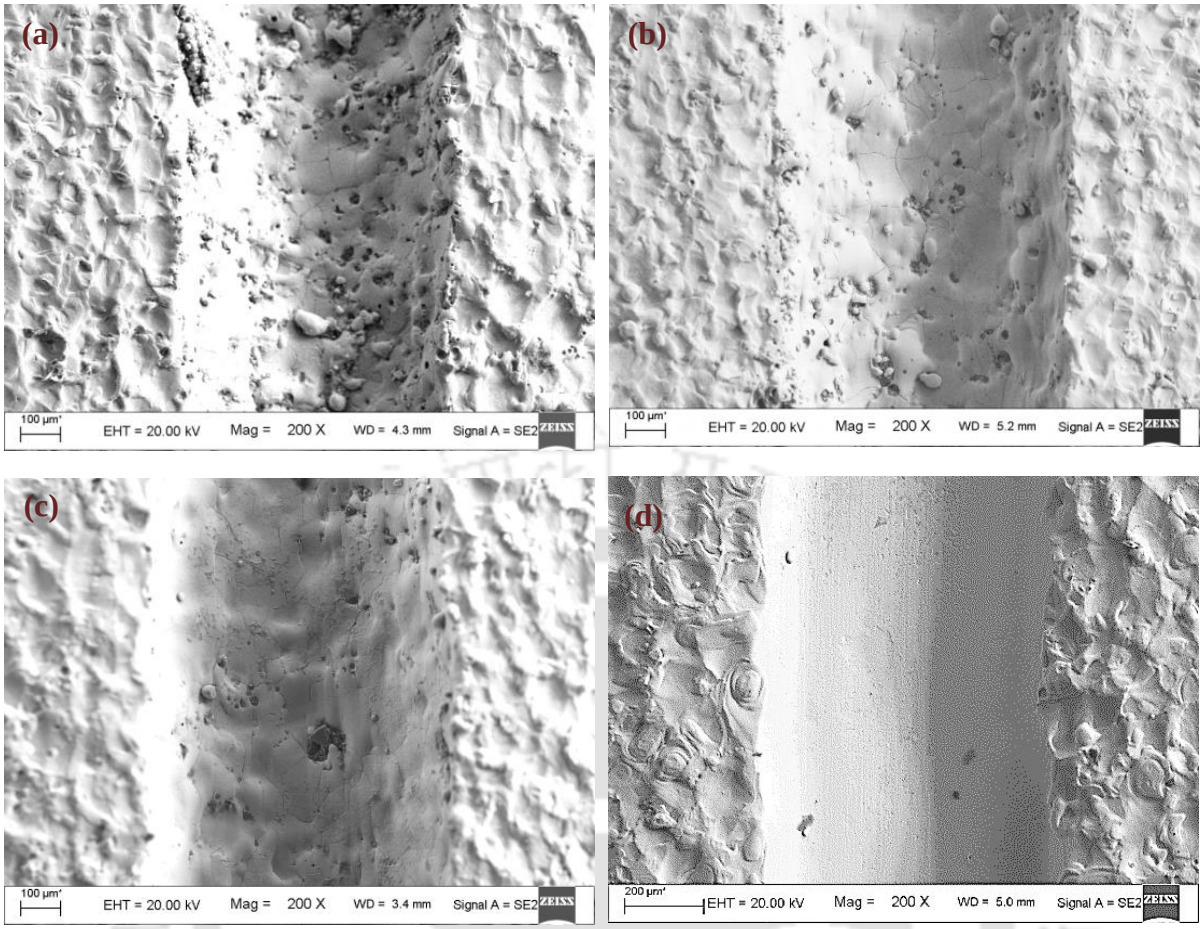

Fig. 6.10 *Workpiece surface topography at various mesh size* ***(a)*** *1000 (R_a = 0.98 µm)* ***(b)*** *600 (R_a = 0.79 µm)* ***(c)*** *400 (R_a = 0.66 µm)* ***(d)*** *180 (R_a = 0.26 µm) (8 cycles, 4 MPa, 35 wt. % abrasives).*

6.3.4 Weight percentage of abrasive particle

As wt. % of abrasive particles in the medium increases, *% ΔR_a* gradually increases (Fig. 6.11). As the wt. % of abrasive particle increases in the medium, the number of cutting edges in the medium for shearing of roughness peaks increases. Thus, number of times surface roughness peaks undergoing shearing increases with an increase in wt. % of abrasive particles for a given number of AFF cycles. The finishing of the workpiece surface is shown by 2-D roughness profile which becomes gradually smooth as wt. % of abrasive particles increases in the medium (Fig. 6.12(a-c)). This is due to the effective removal of roughness peaks at higher abrasives content.

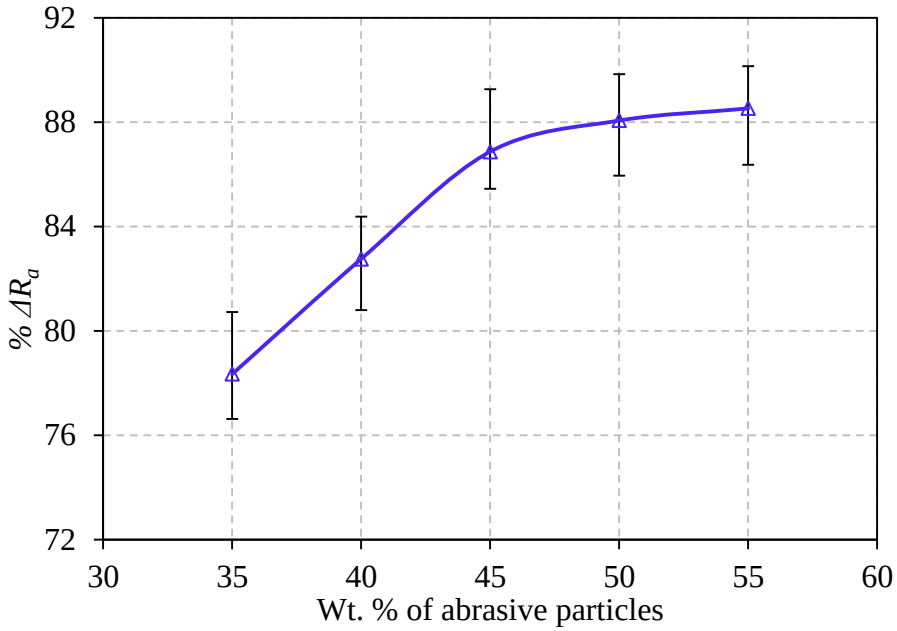

Fig. 6.11 *Variation of the percentage change in surface roughness with wt. % of the abrasive particles in the medium (4 MPa, # 180, 8 AFF cycles).*

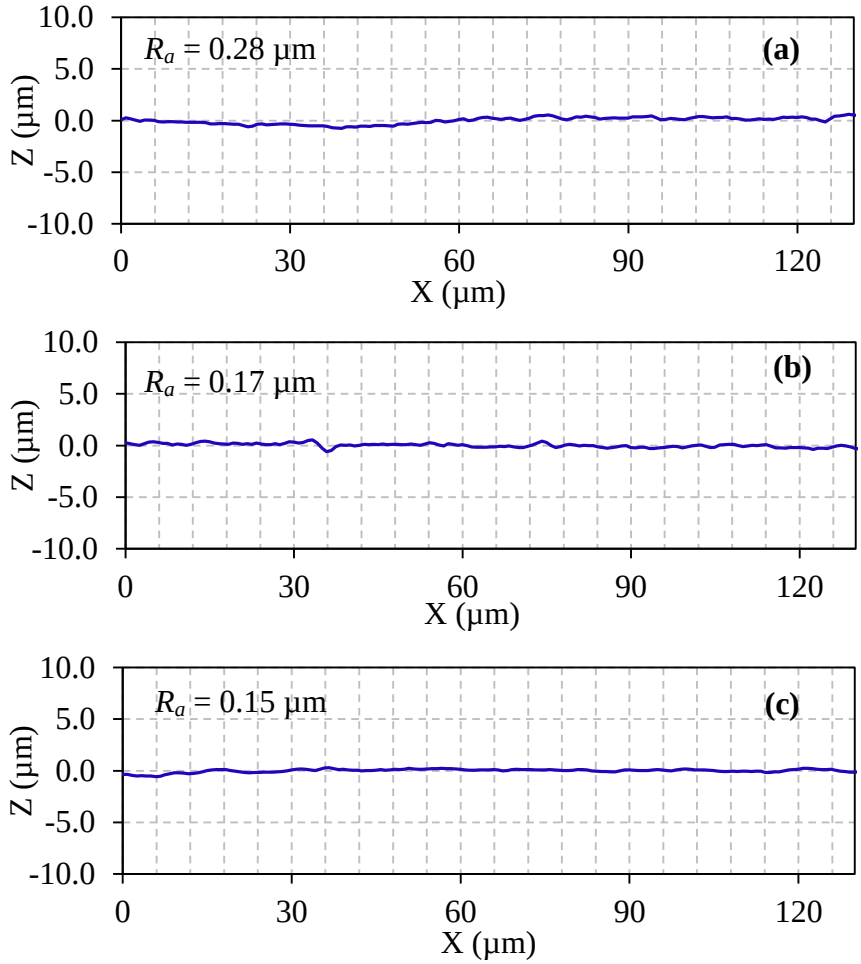

Fig. 6.12 *2-D surface roughness profile at different wt. % of abrasive particles in the medium* ***(a)*** *35 %* ***(b)*** *45 %* ***(c)*** *50 % (8 cycles, # 180, 4 MPa).*

6.4 Experimentation for parametric analysis

After getting the ranges of various input parameters from preliminary experimental study complete parametric study of AFF process is carried out. Parametric study of AFF process is done by using CCRD method. The main motive behind conducting the CCRD is to study the effect of process input parameters (extrusion pressure, number of AFF cycles and wt. % of the abrasive particles) and their interaction on the output response ($\% \Delta R_a$ *and* $\% \Delta R_z$) of AFF process. CCRD also gives the best combination of the various input parameters across which the minimum final surface roughness is obtained. The coded levels (-1.682 to 1.682) and their corresponding actual values of the input parameters are shown in table 6.1.

Table 6.1 *AFF input parameters with its coded and actual values.*

S. No.	AFF input parameter	Unit	Levels				
			-1.682	**-1.000**	**0.000**	**1.000**	**1.682**
1.	Extrusion pressure (P)	MPa	~3.20	3.50	4.00	4.50	~4.90
2.	No. of AFF cycles (N)	-	~5	6	8	10	~11
3.	Wt. % of abrasives (W)	%	36.60	40.00	45.00	50.00	53.40

Table 6.2 shows the detailed plan of 20 experiments with the combination of input parameters and the corresponding output responses. As seen from the table 6.2, the best surface roughness obtained is 130 nm with $\% \Delta R_a$ of 91.16 % and $\% \Delta R_z$ of 89.97 %. After performing designed CCRD experiments, the results are analysed by using response surface methodology. Later, analysis of variance (ANOVA) is carried out to study the percent contribution of input parameters on output response.

As shown in the table 6.3 model p-value Prob > F of <.0001 for $\% \Delta R_a$ and $\% \Delta R_z$ being less than 0.05 (significance level, α for 95 % confidence interval) imply that both models are significant. From the ANOVA analysis it is found that all input parameters plays a significant role on output responses. Model terms in decreasing order of significance are W, P, N, P^2, N^2, and W^2. While deciding the value of $\% \Delta R_a$ the highest percent contribution is of the combined model terms P and P^2 (42.81 %) followed by the contribution of the W and W^2 (40.74 %), N and N^2 (14.72 %). Similarly, in case of $\% \Delta R_z$ model term P and P^2 (41.81 %) dominates followed by W and W^2 (38.18 %), N and N^2 (14.73 %).

Table 6.2 *Plan of experiments and summary of AFF output responses.*

Std. order	Exp. No.	Factors			Surface roughness			Maximum height of the roughness profile		
		P	N	W	Initial R_a (µm)	Final R_a (µm)	% ΔR_a	Initial R_z (µm)	Final R_z (µm)	% ΔR_z
1	14	4.00	8	53.40	1.47	0.13	91.16	6.18	0.62	89.97
2	10	4.90	8	45.00	1.48	0.15	89.86	5.45	0.79	85.50
3	8	4.50	10	50.00	1.4	0.14	90.00	6.37	0.60	90.58
4	9	3.20	8	45.00	1.42	0.31	78.17	5.62	1.44	74.38
5	4	4.50	10	40.00	1.33	0.18	86.47	7.22	1.01	86.01
6	12	4.00	11	45.00	1.32	0.16	87.88	5.23	0.82	84.32
7	11	4.00	5	45.00	1.44	0.25	82.64	6.32	1.22	80.70
8	6	4.50	6	50.00	1.34	0.15	88.81	5.57	0.76	86.36
9	3	3.50	10	40.00	1.34	0.29	78.36	6.87	1.34	80.49
10	18	4.00	8	45.00	1.35	0.14	89.63	6.02	0.74	87.71
11	16	4.00	8	45.00	1.44	0.18	87.50	6.99	0.96	86.27
12	2	4.50	6	40.00	1.32	0.25	81.06	6.94	1.16	83.29
13	15	4.00	8	45.00	1.37	0.16	88.32	6.24	0.90	85.58
14	20	4.00	8	45.00	1.37	0.18	86.86	5.27	0.76	85.58
15	7	3.50	10	50.00	1.37	0.18	86.86	6.92	0.85	87.72
16	5	3.50	6	50.00	1.4	0.26	81.43	6.40	1.15	82.03
17	17	4.00	8	45.00	1.39	0.19	86.33	5.87	0.89	84.84
18	1	3.50	6	40.00	1.35	0.35	74.07	5.97	1.60	73.20
19	13	4.00	8	36.60	1.47	0.30	79.59	6.37	1.44	77.39
20	19	4.00	8	45.00	1.33	0.18	86.47	6.05	0.98	83.80

Table 6.3 *Analysis of variance for % ΔR_a and % ΔR_z.*

Source	% ΔR_a			% ΔR_z		
	F-Value	p-value Prob > F	% Contri-bution	F-Value	p-value Prob > F	% Contri-bution
Model	25.11	< 0.0001*		14.15	0.0001*	
A-P	81.57	< 0.0001*	35.03	42.34	< 0.0001*	32.25
B-N	25.13	0.0005*	10.79	16.85	0.0021*	12.84
C-W	86.39	< 0.0001*	37.10	49.74	< 0.0001*	37.88
AB	0.66	0.4351	0.28	1.52	0.2456	1.16
AC	1.42	0.2602	0.61	2.82	0.1241	2.15
BC	0.64	0.4408	0.28	0.00	0.9587	0.00

A^2	18.13	0.0017*	7.78	12.55	0.0053*	9.56
B^2	9.16	0.0128*	3.93	2.49	0.1459	1.89
C^2	8.48	0.0155*	3.64	0.40	0.5421	0.30
Lack of Fit	1.29	0.3942		2.58	0.1608	

*Significant terms

6.5 Results and discussion

The current section is divided into three sub sections. Firstly, the effect of AFF process input parameter (extrusion pressure, number of AFF cycles and wt. % of abrasive particles) on the output responses (*% ΔR_a* and *% ΔR_z*). Secondly, the mechanism of material removal during the finishing of microholes by AFF process is discussed. At last, the best surface roughness obtained on the microhole surface is presented.

6.5.1 Effect of abrasive flow finishing process input parameters

The regression equation of the experimental output responses in terms of actual values of the input parameters as found out by ANOVA can be given as:-

$$\%\Delta R_a = -243.58 + 68.75P + 8.54N + 5.65W - 0.39PN - 0.23PW - 3.85\times10^{-2}NW - 6.09P^2 - 0.27N^2 - 0.04W^2 \quad (6.1)$$

$$\%\Delta R_z = -213.75 + 82.33P + 7.00N + 3.37W - 0.76PN - 0.41PW - 3.25\times10^{-3}NW - 6.46P^2 - 0.18N^2 - 0.01W^2 \quad (6.2)$$

Table 6.4 *Experimental input conditions for validation of output responses regression model obtained for finishing of microholes by AFF process.*

Experiment number	**Input conditions**			**Output responses**			
	P	**N**	**W**	**Experimental % ΔR_a**	**Predicted % ΔR_a**	**Experimental % ΔR_z**	**Predicted % ΔR_z**
1	3.50	6	45	77.99	76.79	76.79	79.41
2	4.00	10	50	86.79	84.76	84.76	90.31
3	4.50	8	40	88.41	87.70	87.70	85.48
4	4.30	9	50	90.43	89.90	89.90	91.37

Confirmation tests are carried out to validate the regression eq. 6.1 and eq. 6.2. Table 6.4 shows the various combinations of AFF input parameters used to carry out confirmation test. It is found out that the minimum error between the experimental and the predicted value

of $\% \Delta R_a$ is 0.94 % while maximum error is 3.52 %. Similarly, the minimum and maximum error % in case of $\% \Delta R_z$ is 0.13 % and 5.01 % respectively. Both the output responses are plotted in Fig. 6.13

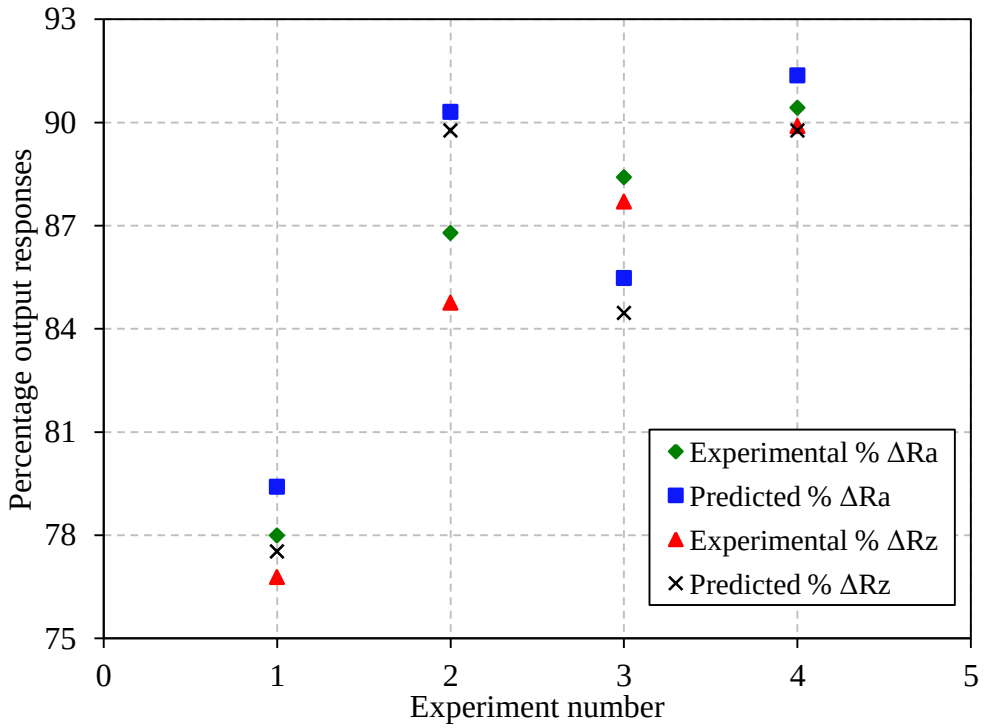

Fig. 6.13 *Comparison between the predicted and experimental obtained AFF output responses for various validation tests.*

➢ ***Extrusion pressure***

As the extrusion pressure increases, the shear rate of the medium increases. So, the amount of energy stored in the medium increases. This stored energy is then transferred by polymer chains to the abrasive particles in the form of finishing forces. Thus, at high extrusion pressure abrasive particles with increased magnitude of finishing forces shears workpiece surface roughness peaks. As a result, $\% \Delta R_a$ *and* $\% \Delta R_z$ increases with an increase in extrusion pressure (Fig. 6.14(a-b)).

However, increasing the extrusion pressure beyond a critical value (4.50 MPa), results in approximately constant value. This is because at high extrusion pressure, abrasive particles indent the workpiece surface with the high amount of F_R forces. As a result, these abrasive particles not only finish but also create deep shearing marks on the finished workpiece surface (Fig. 6.15).

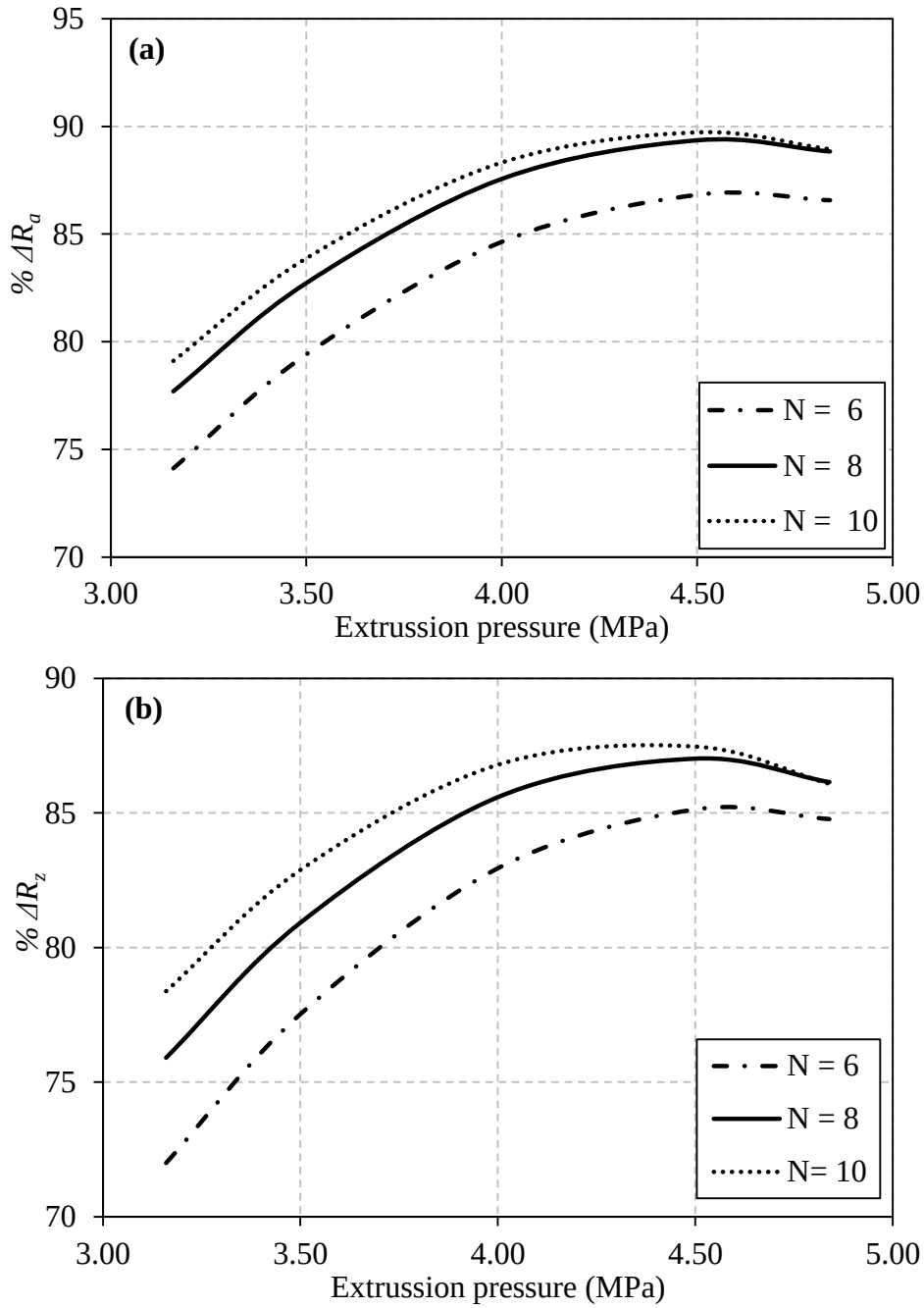

Fig. 6.14 *Effect of extrusion pressure at different number of AFF cycles on* ***(a)*** *% ΔR_a* ***(b)*** *% ΔR_z (wt. % of abrasives = 45 %, # 180).*

Sometimes, the sharp cutting edges of abrasive particle get blunted and abrasive particle losses its capacity to act as a good cutting tool [94]. As a result, the improvement in surface roughness is reduced by the deep shearing marks of the abrasive particles on workpiece surface. Thus, the value of *% ΔR_a* and *% ΔR_z* almost remains constant by increasing the extrusion pressure beyond the critical value (Fig. 6.14(a-b)).

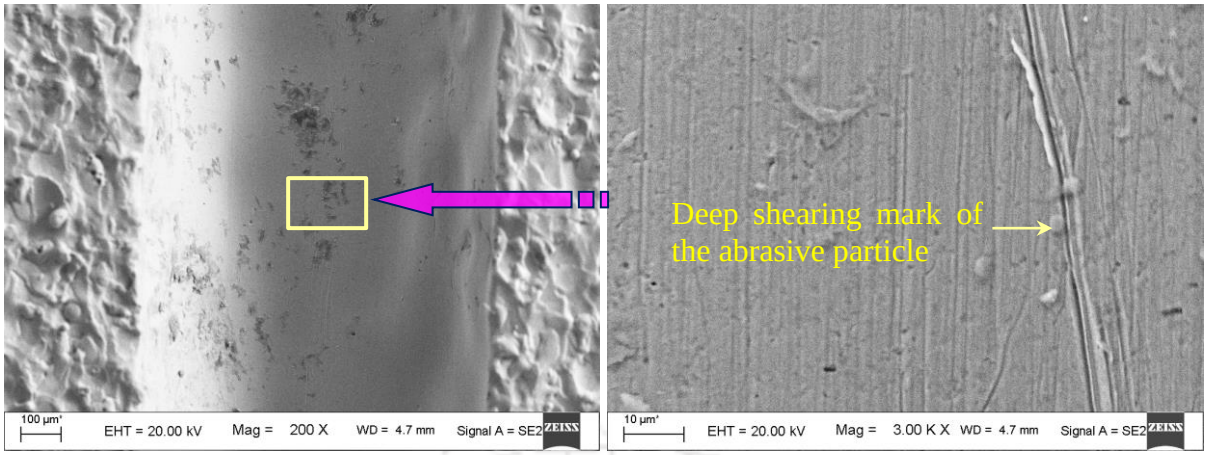

Fig. 6.15 *Workpiece surface topography at 4.90 MPa (8 AFF cycles, 45 % wt. % of the abrasive particles, # 180).*

➢ ***Number of abrasive flow finishing cycles***

It is found out from the parametric study that number of AFF cycles is one of the significant parameters that affect the magnitude of the $\% \Delta R_a$ and $\% \Delta R_z$. As shown in Fig. 6.16(a-b) with the increase in number of AFF cycles, the value of $\% \Delta R_a$ and $\% \Delta R_z$ increases because with the increase in number of AFF cycles, more number of times surface roughness peaks get sheared by the abrasive particle. Thus, the improvement is surface roughness occurs with an increase in AFF cycles.

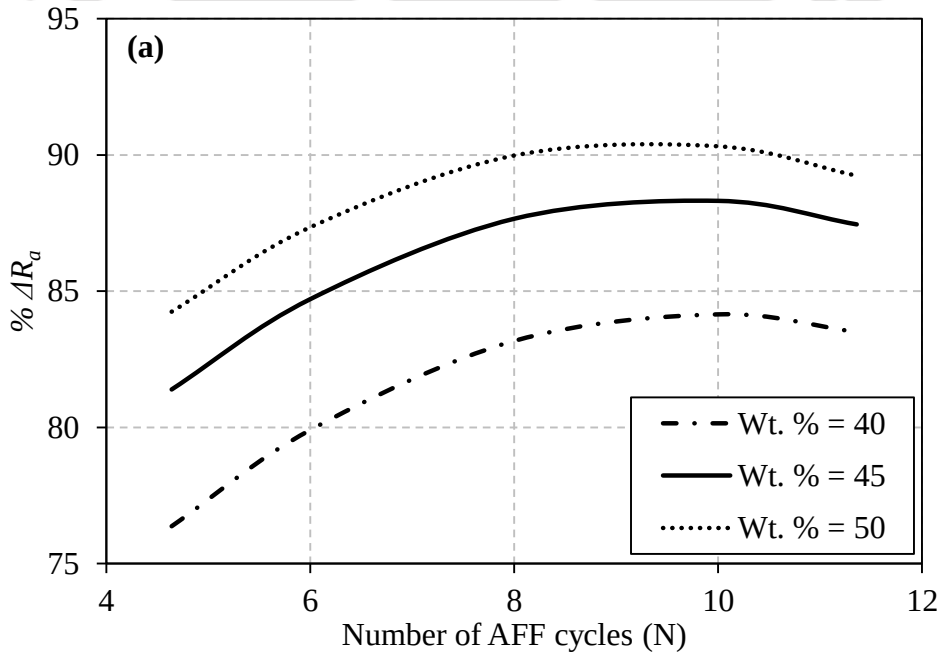

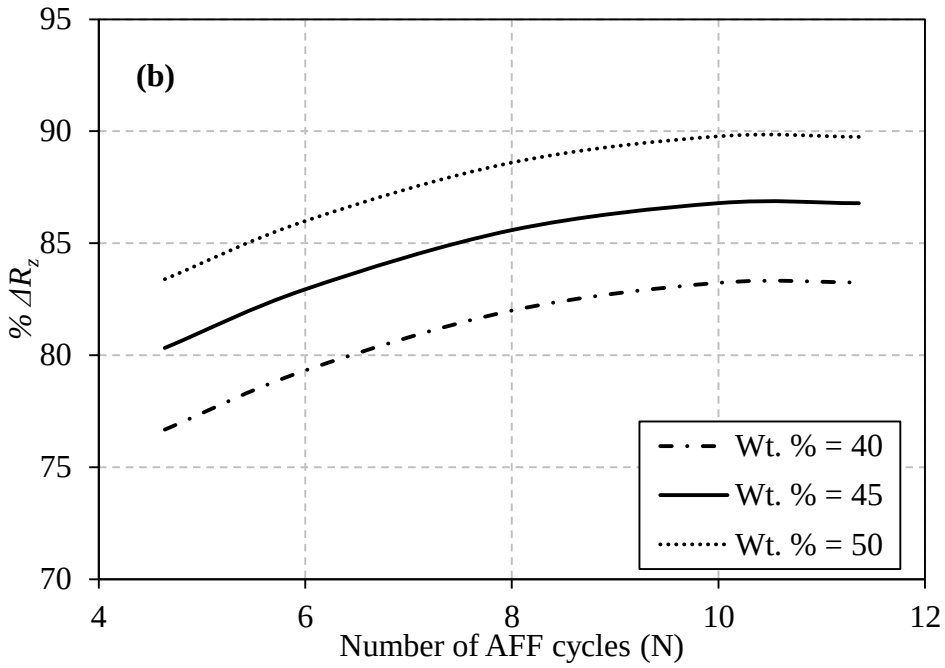

Fig. 6.16 *Effect of number of AFF cycles at different wt. % of abrasives particles on* ***(a)*** *% ΔR_a* ***(b)*** *% ΔR_z (extrusion pressure = 4 MPa, # 180).*

However, finishing the workpiece surface beyond 10 AFF cycles leads to a slight decrease in *% ΔR_a* but the value of *% ΔR_z* remains approximately constant. This may be due to the reason that at high AFF cycles, the abrasive particle doesn't find much roughness peaks to shear instead they start shearing the finished workpiece surface. Due to the repetitive indentation of abrasive particles, the width of these existing surface valleys increases during finishing the workpiece above 10 AFF cycles. As a result, the value of *% ΔR_a* decrease, but the value of *% ΔR_z* remains constant beyond 10 AFF cycles.

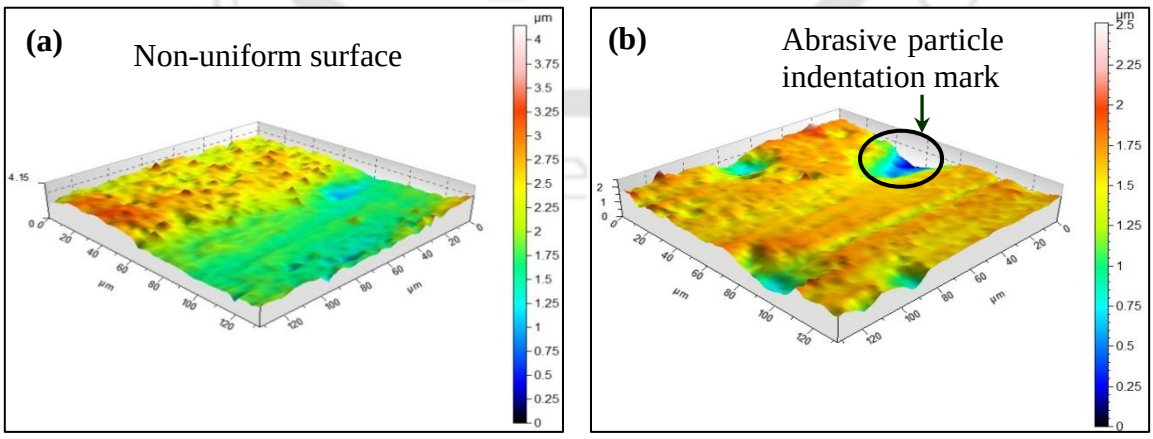

Fig. 6.17 *Workpiece surface topography after finishing at AFF cycles* ***(a)*** *5* ***(b)*** *11 (4 MPa, 45 % abrasive particles wt. %, # 180).*

As shown in Fig. 6.17(a) during the initial AFF the surface is not uniform because of the roughness peaks. However, as the number of AFF cycle increases, these roughness peaks are sheared and a more uniform surface is achieved. However, beyond a critical value, the surface improvement is slightly reduced by partial indentation of the abrasive particle on the finished surface (Fig. 6.17(b)).

➢ ***Weight percentage of abrasive particle***

Wt. % of the abrasive particle is the second most significant model term with a contribution of 40.74 % (W + W^2) while deciding % ΔR_a and 38.18 % in case of % ΔR_z. As shown in Fig. 6.18(a-b) the value of % ΔR_a and % ΔR_z increases with the increase in the wt. % of the abrasive particle in the medium. As the wt. % of the abrasive particle increases the surface becomes more uniform, free from the roughness peaks. This is mainly due to two reasons. Firstly, as wt. % of abrasive particle in the medium increases the number of active abrasive particle in the medium increases. As a result, surface roughness peaks are sheared more number at higher wt. % of the abrasive particle.

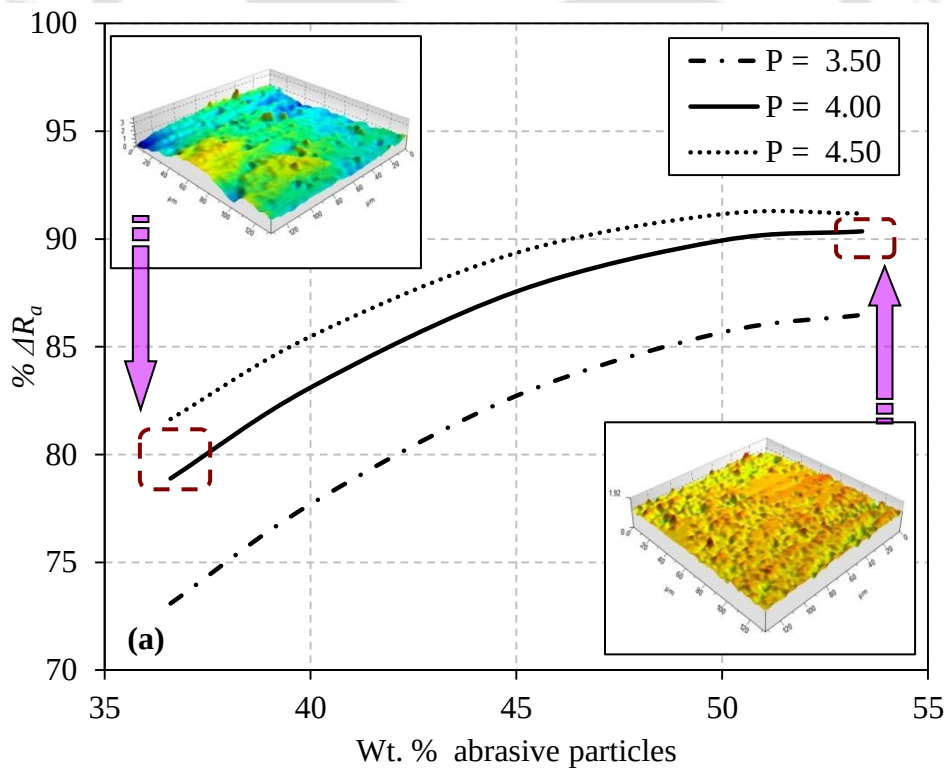

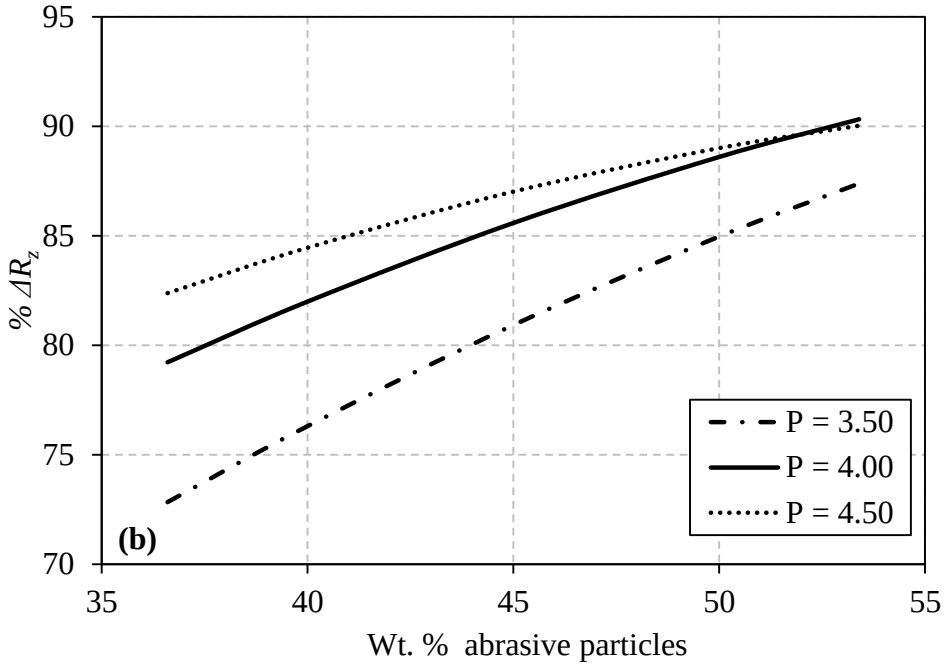

Fig. 6.18 *Effect of wt. % of abrasives particles at different extrusion pressure on* ***(a)*** *% ΔR_a* ***(b)*** *% ΔR_z (number of AFF cycles = 8, # 180).*

Secondly, the medium with higher wt. % of the abrasive particles possess high viscosity (Fig. 3.22(c)). During the finishing of microholes, the medium with high viscosity helps the abrasive particle to effectively and efficiently shear the surface roughness peak. Thus, the medium with higher wt. % of abrasive particle possesses, better finishing capabilities as compared to medium with lower wt. % of the abrasive particle content.

6.5.2 Material removal mechanism

The process of material removal mechanism (i.e., shearing surface roughness peaks) across the microhole surface involves several steps. Fig. 6.19(a) shows microhole initial surface after micromachining it into the workpiece with the help of EDµM process. The initial workpiece surface contains solidified recast layer of molten material with loosely bonded re-solidified metal spheroids. Recast layer is harder than the parent material. This is mainly due to the reason that molten material traps carbon atoms from the dielectric fluid leads to the formation of carbides with high hardness [33]. During AFF process, this loosely bonded metal debris are removed by the abrasive particles in first few cycles (Fig. 6.19(b)). Thereafter, the start of recast layer removal is carriedout by the abrasive particles with increase in magnitude of AFF input parameters. However, the hardness of the recast layers varies due to the non-uniform thickness of the recast layer that formed during EDµM process.

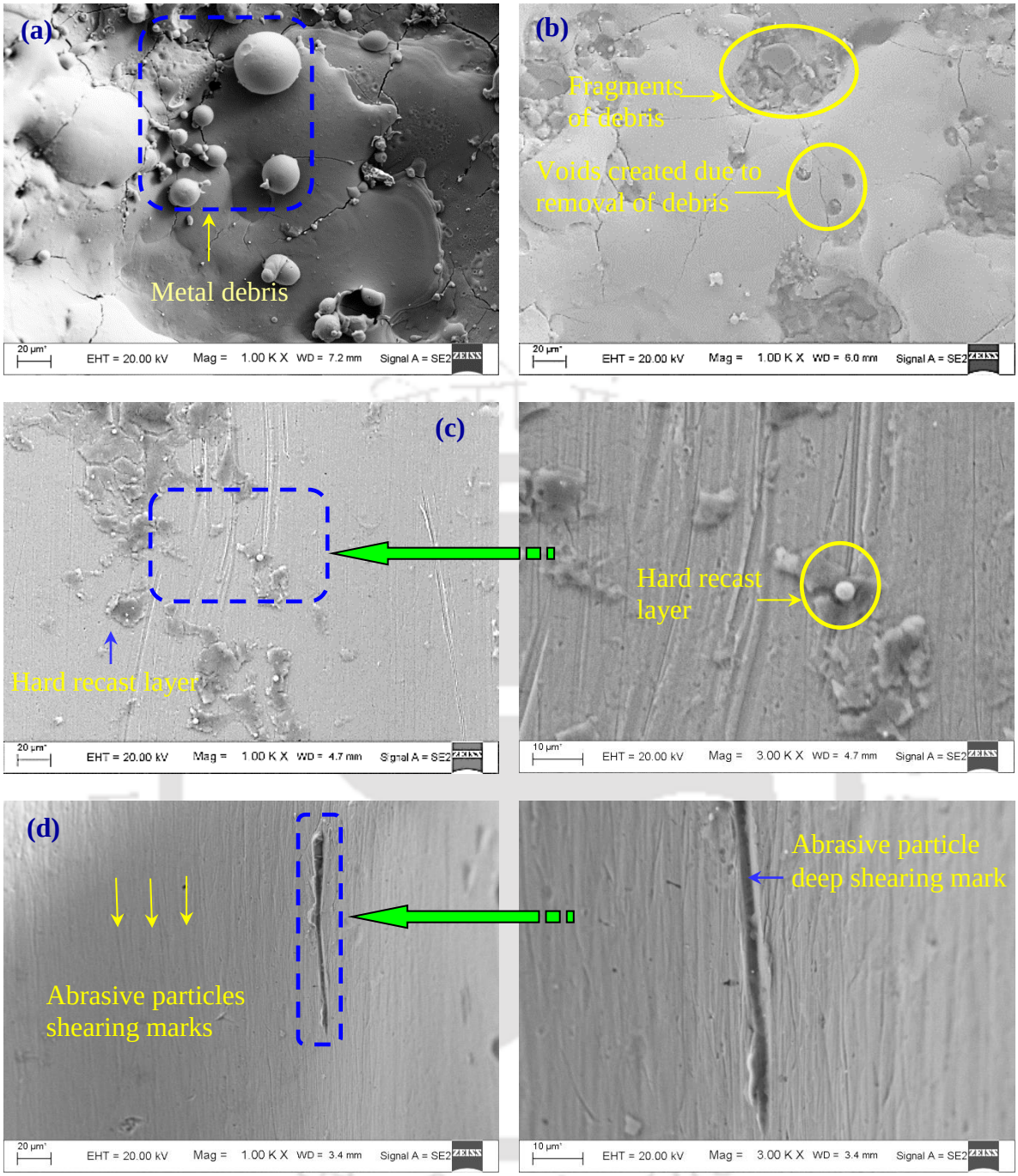

Fig. 6.19 *Surface morphology of the electric discharge micromachined surface at various stages during the abrasive flow finishing process* ***(a)*** *initial* ***(b)*** *surface with almost removed metal debris* ***(c)*** *surface with hard recast layer* ***(d)*** *finished surface with deep scratches.*

There are few locations of the recast layer that are comparably harder on the workpiece surface (Fig. 6.19(c)). These patches of the hard recast layer are removed in two ways. Firstly, by finishing the workpiece at high number of AFF cycles. Due to high number of AFF cycles the repetitive interaction of the abrasive particle with surface roughness peaks helps in the surface roughness improvement. Secondly, by increasing the extrusion pressure,

this increases the finishing forces on the workpiece surface. With help of increased finishing forces, the abrasive particle effectively removes the left over patches of hard recast layer. After finishing microholes with AFF process final workpiece surface obtained is fine finished, free from any recast layer. Sometimes, at high magnitude of the extrusion pressure abrasive particle agglomeration creates deep shearing marks on the finished surface which distorts the final surface roughness (Fig. 6.19(d)). Thus, there is always a critical value of the surface roughness achievable beyond it surface roughness start deteriorates. Also, surface morphology of the workpiece surface shows the sharp shearing marks of the abrasive particle (Fig. 6.19(d)). Thus, confirming that mode of material removal during the current set of AFF experiments is by microcutting process.

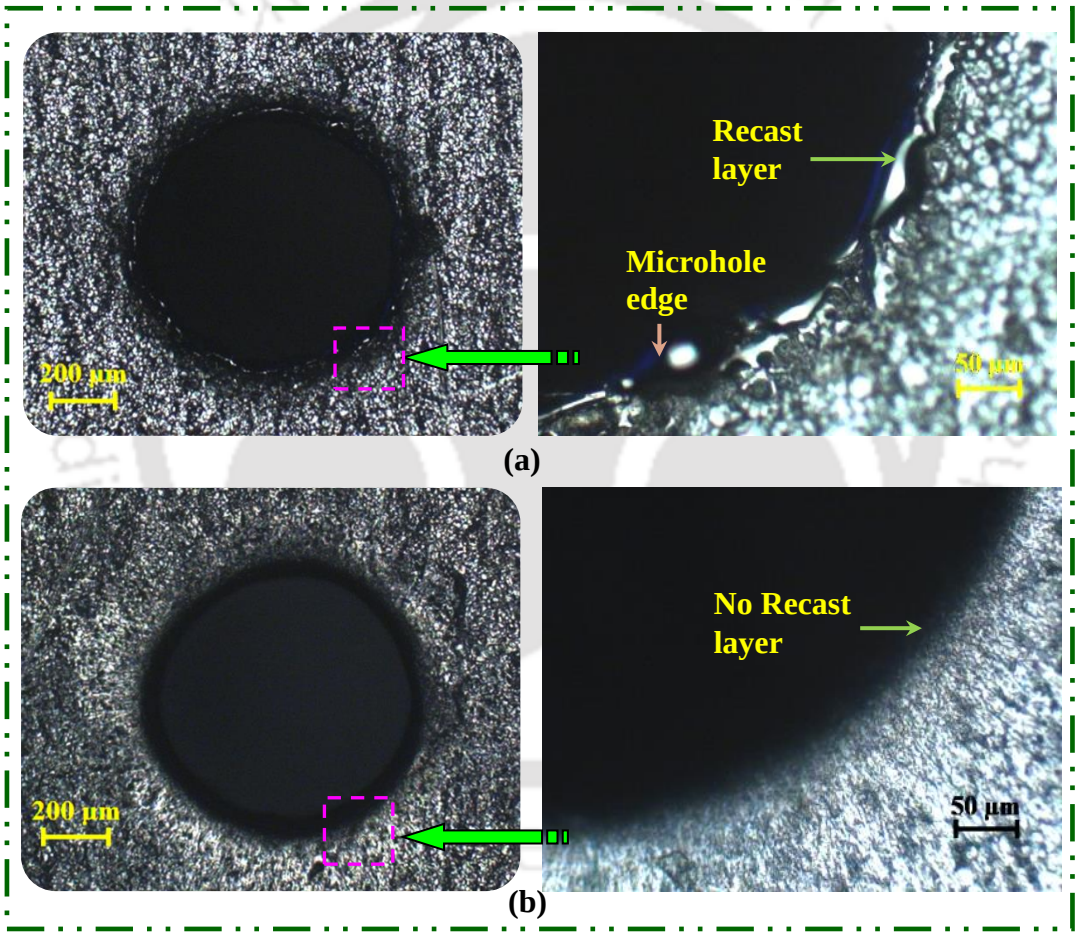

Fig. 6.20 *Microhole edge morphology* ***(a)*** *before finishing,* ***(b)*** *after finishing.*

Surface edge morphology of EDµM surface shows recast layer and heat affected zone which are elementally modified due to thermal micromachining process (Fig. 6.20(a)). These layers are clearly removed as well as finished to nano scale by AFF process (Fig. 6.20(b)). AFF process not only finished the microhole but also did radiusing of sharp microhole edges.

6.5.3 Best surface roughness

Best surface roughness is obtained by finishing the microholes with AFF process at 4 MPa extrusion pressure, 8 number of AFF cycles using medium containing 53.40 % of the abrasive particle content. Final surface roughness obtained is 130 nm with $\% \Delta R_a$ of 91.16 %. As shown in Fig. 6.21(a) the initial surface of microhole is rough, which is clearly shown by its 2-D surface profile. The height and depth of surface roughness peaks and valleys fall in the maximum range of ± 6.0 µm. After finishing these microholes with the AFF process, the surface roughness on these microhole walls reduces greatly and a smooth surface is obtained (Fig. 6.21(b)). 2-D surface profile shows that surface roughness peaks and valleys fall in between ±0.6 µm. Thus, there is a 10 times improvement in the surface roughness.

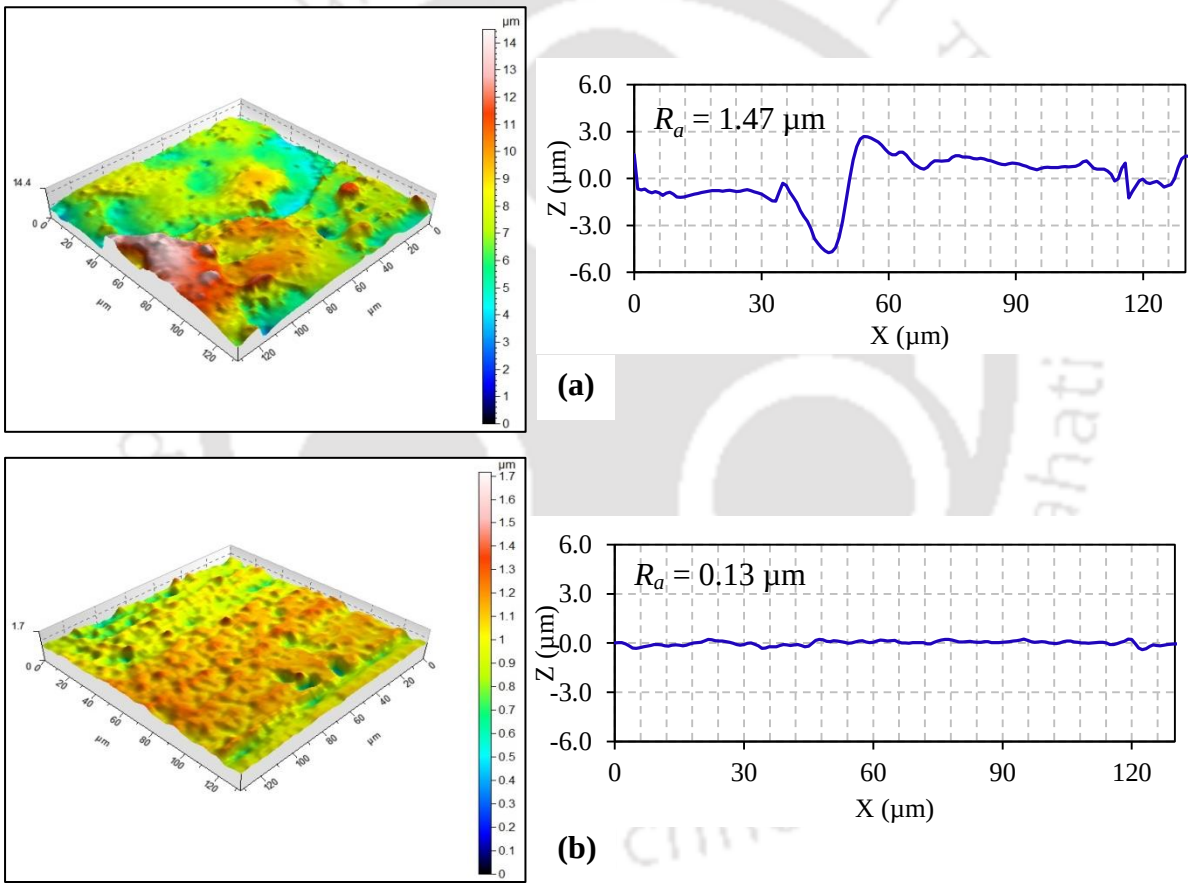

Fig. 6.21 *Workpiece surface topography and corresponding 2-D surface roughness profile* ***(a)*** *initial workpiece surface* ***(b)*** *finished workpiece surface (8 cycles, # 180, 4 MPa, 53.40 wt. % abrasives particles).*

Not only surface roughness and topography but surface metallurgy is also important. Therefore, in the current work elemental analysis of microhole before and after AFF process is carriedout (Fig. 6.22). EDµM process removes material by thermal energy, thus microhole

surface possess recast layer and heat affected zone. Fig 6.22(a) shows the surface metallurgy of recast layer that is formed due to thermal energy of EDµM along with the chemical reactions of dielectric fluid. Dielectric fluid is carbon based oils, so there is high amount of carbon presence on EDµM surface (Fig 6.22(a)). Since the EDµM surface is harder than the parent material, there are chances of metal carbides formation. However, AFF can remove the recast layer by gradual shearing with abrasive particles. Thus, AFF process can reduce metallurgically contaminated layers (Fig 6.22(b)).

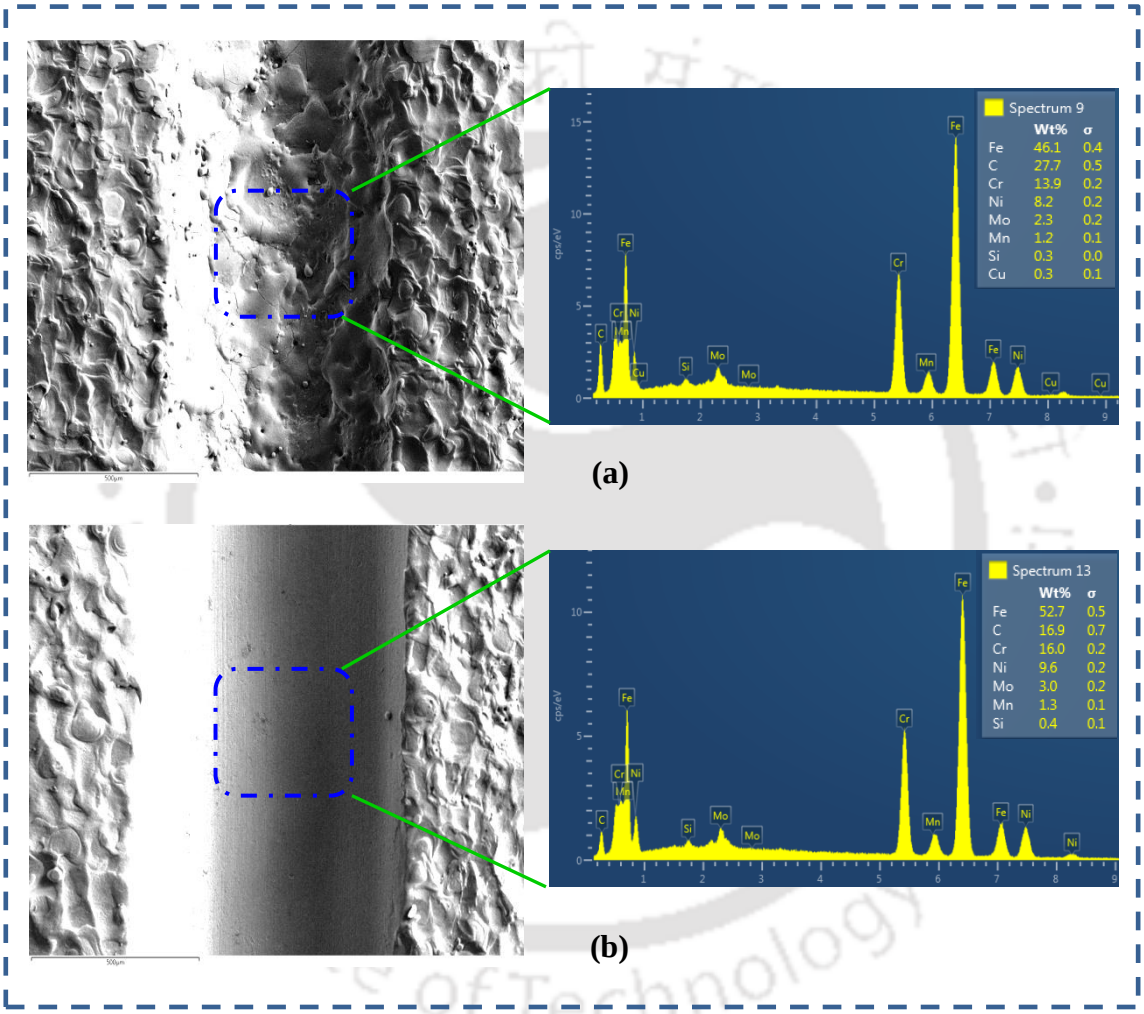

Fig. 6.22 *Topography of the microhole surface with corresponding energy-dispersive X-ray spectroscopy* ***(a)*** *before finishing* ***(b)*** *after finishing.*

As shown in Fig. 6.23(a), microhole surface along the length is too rough due to the presence of re-solidified molten material (recast layer) formed and heat affected zone during EDµM process. The recast layer elemental composition is different compared to parent material. DES delivers the drug to the point care at a specified rate. If the microhole is machined by EDµM process, the wall surface is too rough containing loosely bonded

spheroids and the elemental composition is different from parent SS 316L. There is a heavy chance of drug entrap in valleys of the rough surface for a prolonged time. This might cause chemical interaction and contaminate the drug. Along with it, the loosely bonded re-solidified spheroids on EDμM surface can also dislodge and came along with the drug, which is medically dangerous. But in the case of finished microholes by AFF process (Fig. 6.23(b)), due to finely finished surface as well as removal of recast layer, results in smooth drug delivery with no/minimal contamination.

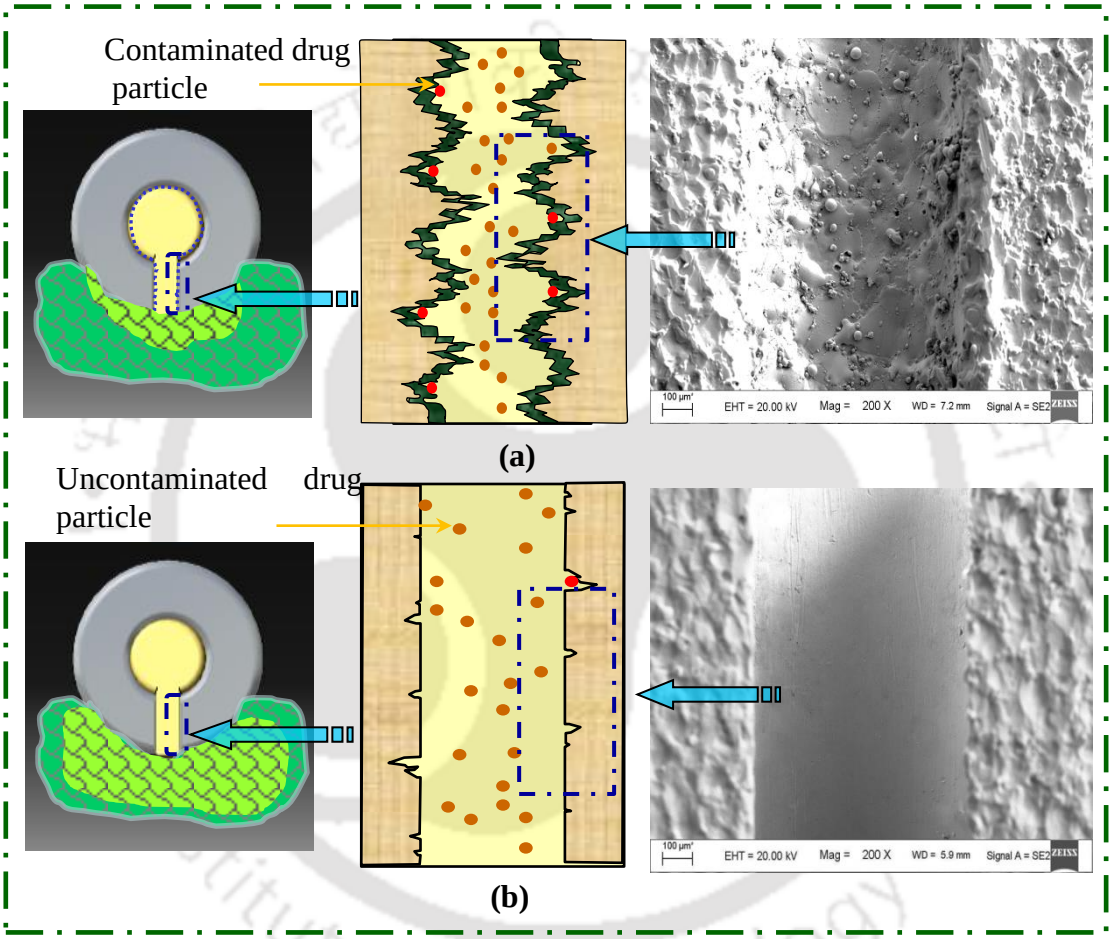

Fig. 6.23 *Schematic representation of drug eluting through microholes of stainless steel based drug eluting stents. Drug flow (a) rough microhole surface (b) nanofinished microhole.*

6.6 Conclusions

In the present chapter, the finishing of microholes with the help of AFF process is carried out. Initially, preliminary experiments are conducted to obtain the effective ranges of the AFF input parameters. Later, based on the preliminary study, AFF experiments are designed with the help of CCRD method. Based on the above study, following important conclusions are made:-

1. AFF process successfully finishes the microholes by EDµM machined on SS 316L workpiece.
2. In-house made AFF medium performs effectively while finishing of microholes.
3. From ANOVA it is found that in case of *% ΔR_a*, extrusion pressure (P and P^2) and wt. % of the abrasive particles (W + W^2) are the most significant term affecting AFF output responses. Contribution of extrusion pressure (P + P^2) (42.81 %) is the highest followed by the contribution of wt. % of the abrasive particles (W + W^2) (40.74 %), and number of AFF cycles (N + N^2) (14.72 %) in deciding *% ΔR_a*.
4. In case of *% ΔR_z*, it is observed that among the significant terms combined contribution of extrusion pressure (P + P^2) (41.81%), wt. % of the abrasive particles (W + W^2) (38.18 %) is highest followed by combination of number of AFF cycles (N + N^2) (14.73 %).
5. The best surface roughness of 130 nm with *% ΔR_a* of 91.16 % is obtained on the microhole wall by finishing them with AFF process. The corresponding input process parameters are 4 MPa extrusion pressure, 8 AFF cycles and medium with 53.40 % of abrasive particle content.
6. AFF process not only finishes but also can remove metallurgically contaminated layers.

Chapter 7

MODELING OF ABRASIVE FLOW FINISHING PROCESS AND SIMULATION OF SURFACE ROUGHNESS DURING FINISHING: MACRO AND MICRO FEATURES

7.1 Introduction and need of modeling/simulation

AFF is one of the advanced finishing processes which is very effective in finishing of macro to micro components having simple to complex geometries. AFF process uses a flexible finishing tool containing abrasive particles with random cutting edges. Also, AFF process involves a large number of input variables and its inherent random nature physics it is complex to understand. However, for controlling and to develop any process to its full

potential it is necessary to understand the process physics. As found out from the literature review (chapter 1), for understanding the mechanism of AFF process, many researchers made efforts in three field's i.e. experimental, theoretical modeling and numerical modeling. Modeling is one more effective way for understanding physics of any process.

As found from the literature, the theoretical models developed to predict AFF process mechanism suffers the disadvantage of too many variables to handle [78]. So, the emphasis is given more on numerical models. However, most of the developed numerical models consider medium to be Newtonian or non-Newtonian following power law. Developed models provide the output as finishing forces that are to be used as input during the simulation of final surface roughness. AFF process due to its random nature greatly hampered the proper predictions of AFF output responses by the previously developed theoretical and simulation models. In the current section, an effort is made to model AFF process as realistically as possible. The amount of finishing forces generated on the workpiece surface at various AFF input parameters is computed by the finite element (FE) model. A new way to model the viscoelastic behaviour of the medium is proposed. To accurately model AFF process, FE analysis of the viscoelastic medium is carried out using its experimentally measured rheological properties as input. Also, a new simulation model is proposed to predict the surface roughness during AFF process as a function of AFF input parameters (number of AFF cycles, extrusion pressure and wt. % of abrasive particles). The main highlights of the roughness simulation model are the incorporation of real initial surface roughness profile (that taken experimentally from surface roughness profilometer) and abrasive particles with multiple cutting edges during shearing of the roughness peaks. These two parameters play a major role in reducing the error between simulated and experimental results. Final surface roughness obtained from simulation is compared with its corresponding experimental value.

7.2 Finite element modeling of the viscoelastic medium

In the current section, FE analysis is carried out by modelling the flow of the viscoelastic medium during the AFF experiments. In order to reduce the computational expenses, two dimensional (2D) finite element (FE) modeling of the AFF process during finishing of cylindrical SS 316L tubes is done. However, three dimensional (3D) FE modeling of AFF process during finishing of microslots and microholes is carried out. The commercial FE software especially developed to model the viscoelastic flow (Polyflow (Ansys® 14.5)) is used. Modeling viscoelastic flow is comparatively difficult due to its unique static and

dynamic rheological properties which are non-linear in nature. Hence, following assumptions are made to analyze the medium flow during AFF process:-

1. The medium flow is steady, laminar and fully developed.
2. Viscoelastic medium is incompressible i.e. the medium density remains constant during the flow.
3. The medium is isotropic and homogeneous.
4. The temperature of the medium does not change during its flow from one cylinder to another and vice versa

FE analysis is done in Ansys® Polyflow and is divided into three steps:

7.2.1 Pre-processing

Pre-processing comprises of the following steps:-

1. Defining geometry: - All the components through which medium flows during the AFF experiments are designed and assembled in Ansys® design modeler for carrying out the FE analysis of viscoelastic medium.

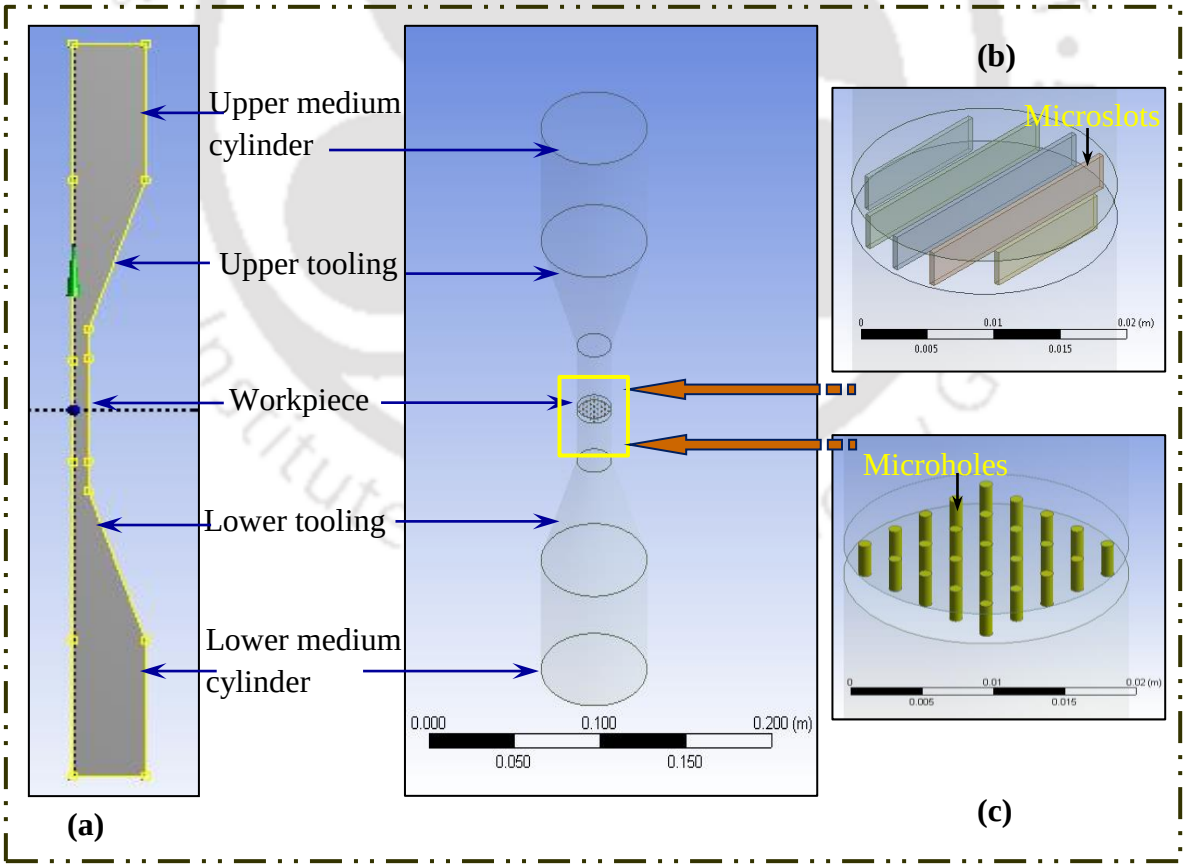

Fig. 7.1 *Modeled domain of the viscoelastic medium of abrasive flow finishing process during finishing of* ***(a)*** *tubes* ***(b)*** *microslots* ***(c)*** *microholes.*

After designing the components, the medium is filled inside them and the components are suppressed leaving the medium domain. Basically, it is the medium domain in which the computational analysis is done. Fig. 7.1(a) shows the 2-D axisymmetric model for AFF process during finishing the tubes, while Fig. 7.1(b) and Fig. 7.1(c) shows the 3-D model for the AFF process during finishing microslots and microholes respectively. The 3-D model during finishing the microslots and microholes is the similar except the workpiece region.

2. Meshing and boundary conditions:- The geometry of the viscoelastic domain representing AFF process during finishing of tubes (Fig. 7.2(a)), microslots (Fig. 7.2(b)) and microholes (Fig. 7.2(c)) is meshed in this step. A fine mesh is generated near the boundary to capture the accurate gradient change. Solving a problem by the FE method formulation requires prescribing information about the flow along the domain boundary. Model is divided into three sections viz. inlet, outlet and wall (Fig. 7.3).

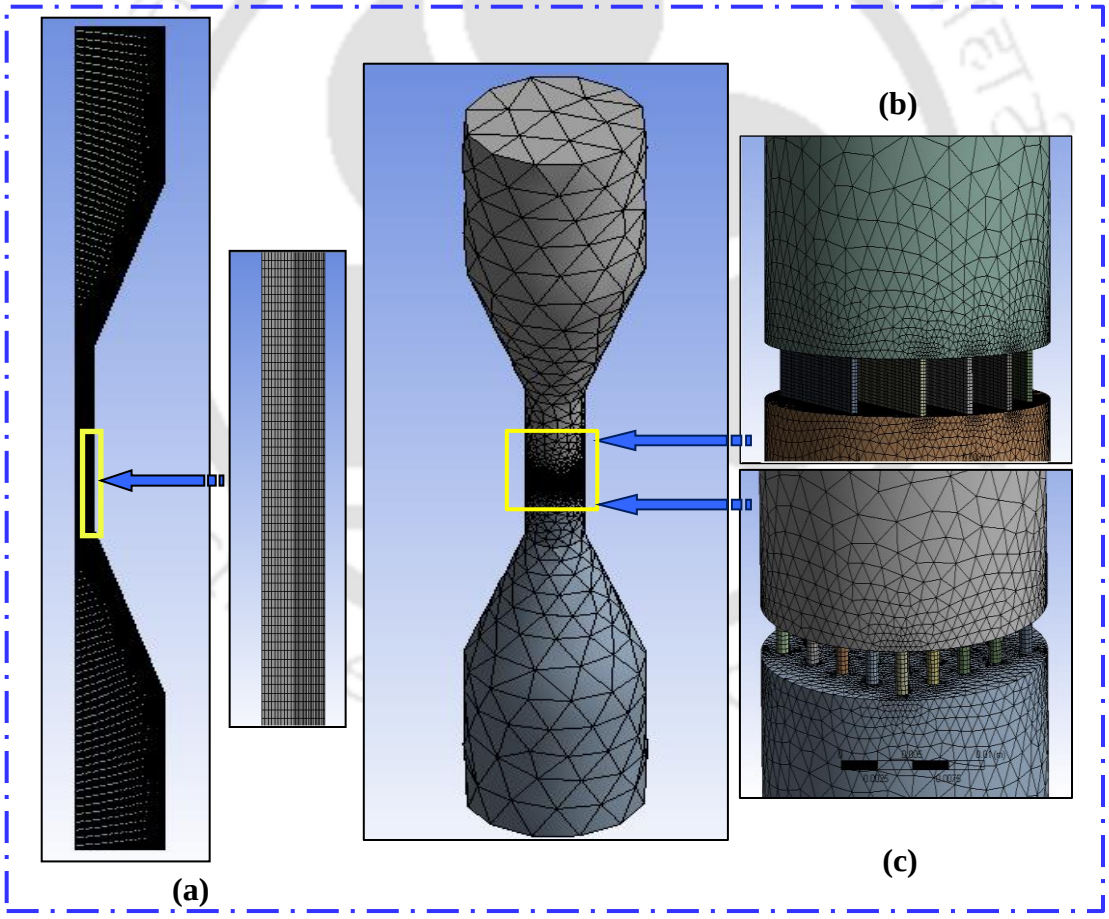

Fig. 7.2 *Meshed domain of the viscoelastic medium of abrasive flow finishing process during finishing of* ***(a)*** *tubes* ***(b)*** *microslots* ***(c)*** *microholes*.

3. The following boundary conditions considered during the FE simulation for flow of the medium:-

i. Inlet: - At the inlet the medium flows with the piston pressure force from the inlet to the outlet section. Thus, the conditions on the inlet is chosen to be:-

$$F_n = F_0 \text{ (piston pressure force) and } V_s = 0$$

ii. Outlet: - At the outlet as the medium doesn't flow tangentially and normal force is zero. Thus, the outlet boundary conditions are:-

$$F_n = 0 \text{ and } V_s = 0$$

iii. Wall: - In case of tube (macro feature) full slip boundary condition is assumed at the wall i.e.:-

$$F_s = V_n = 0$$

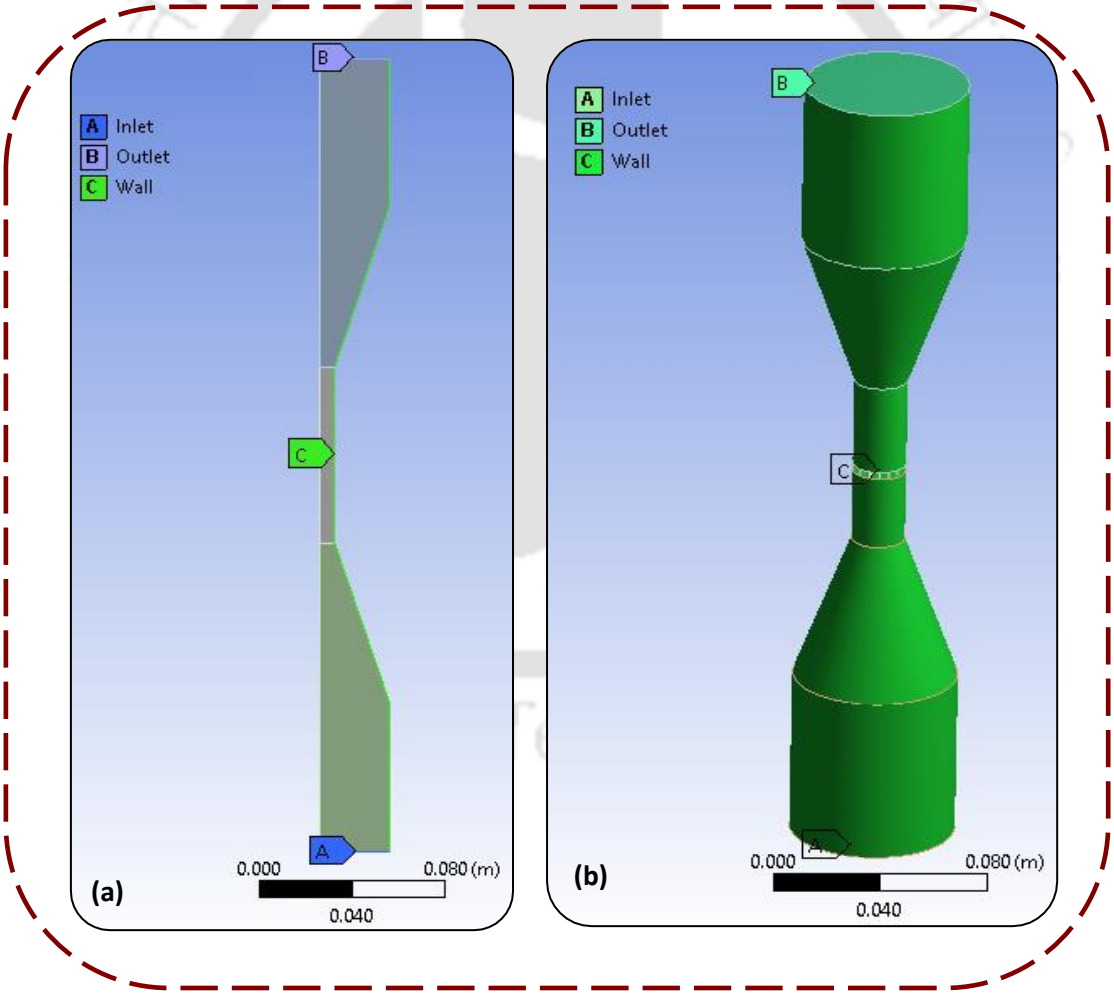

Fig. 7.3 *Various domain of the viscoelastic medium during finishing of* ***(a)*** *tubes* ***(b)*** *microslots, microholes.*

However, during finishing of the micro features (microslots and microholes) medium flows at a very low velocity. This is due to the high restriction provided by the narrow passage of the micro features to the medium. Also, the medium prepared for finishing micro features is having less viscosity as compared to the medium prepared for finishing tubes. Thus, the intermolecular force between the polymer molecules is very weak. While the adhesion forces at the workpiece and medium interface are considerably high. Therefore, no slip boundary condition is assumed at the wall i.e.:-

$$V_s = V_n = 0$$

where, F_n is normal force, V_s, V_n are tangential and normal velocities respectively.

Experimentally measured rheological properties (Chapter 3) are used as input during the FE analysis. Three input properties required to model the viscoelastic flows are namely shear rate vs. viscosity, storage modulus vs. frequency and loss modulus vs. frequency. The inclusion of experimentally measured predicting properties makes the FE model more realistic in nature. This helps in accurately modeling the amount of finishing forces generated in the medium.

7.2.2 Processing

After defining the whole setup with proper boundary conditions and material properties, Ansys® Polyflow solver is implemented for the solution. The viscoelastic model (Giesekus model [93]) is used to simulate the behavior of polymer solution through the contraction/expansion domain. The basic equations that govern the steady state flow of the incompressible viscoelastic medium by treating the medium as a continuum are laws of conservation of mass (continuity equation), conservation of momentum and the viscoelastic constitutive equation.

i. Conservation of mass (Continuity equation)

For the flow of steady state incompressible medium flow, density is constant i.e., independent of space and time, therefore the continuity equation reduces to:-

$$\nabla \bullet \hat{U} = 0 \qquad (7.1)$$

where, $\hat{U}$ is the velocity vector.

ii. Conservation of momentum equation

For steady, incompressible and isothermal flows conservation of momentum equation can be expressed as:-

$$\rho_m(\hat{U}\bullet\nabla\hat{U}) = \nabla\bullet T + f \tag{7.2}$$

where, $T = -pI + \tau$ is the total extra stress tensor for incompressible medium, p = hydrostatic pressure; τ = extra stress tensor (component of total extra stress tensor); I the identity tensor and f = internal forces expressed here as a force per unit volume (e.g. gravity); ρ_m = density of the medium.

iii. Viscoelastic constitutive equation (Rheology model for abrasive medium)

To model the viscoelastic nature of the medium one of the most realistic differential viscoelastic model the so-called Giesekus model is adopted. This model is commonly used for simulating the flows with shear thinning properties. Extra stress tensor is divided into two components namely viscoelastic component (σ_p), and purely viscous (Newtonian) component (σ_s) given as:-

$$\tau = \sigma_p + \sigma_s \tag{7.3}$$

Giesekus model computes σ_p from the following eq.:-

$$(\mathrm{I} + \frac{\alpha\lambda}{\eta_1}\sigma_p).\sigma_p + \lambda\overset{\nabla}{\sigma}_p = 2\eta_1 D \tag{7.4}$$

Where, $\overset{\nabla}{\sigma}_p$ is upper-convected derivative of viscoelastic extra stress which is defined as:-

$$\overset{\nabla}{\sigma}_p = \frac{D\sigma_p}{Dt} - \sigma_p\bullet\nabla\hat{U} - \left(\nabla\hat{U}\right)^T\bullet\sigma_p \tag{7.5}$$

The Newtonian solvent contribution is given by:-

$$\sigma_s = 2\eta_2 D \tag{7.6}$$

where, D is the rate of deformation tensor, I is the unit tensor (identity tensor), α is a material constant, λ is the relaxation time, η_1 is the viscosity factor for the viscoelastic component and η_2 is the viscosity factor for the purely viscous component of the extra stress tensor.

7.2.3 Post-processing

During the post processing step, radial finishing stresses generated on the workpiece surface (tubes, microslots and microholes) during the AFF process are evaluated from medium flow FE model (section 7.2.1 and section 7.2.2). These stresses are later used to predict surface roughness. For modeling the finishing stresses firstly, governing equations (conservation of mass, conservation of momentum and viscoelastic constitutive equation) are solved by the Ansys® Polyflow solver. In the post processing step, radial finishing stresses are extracted from the nodes located on the center of workpiece meshed geometry (Fig. 7.4). Then their average stress is taken to get the stresses at center of the workpiece surface.

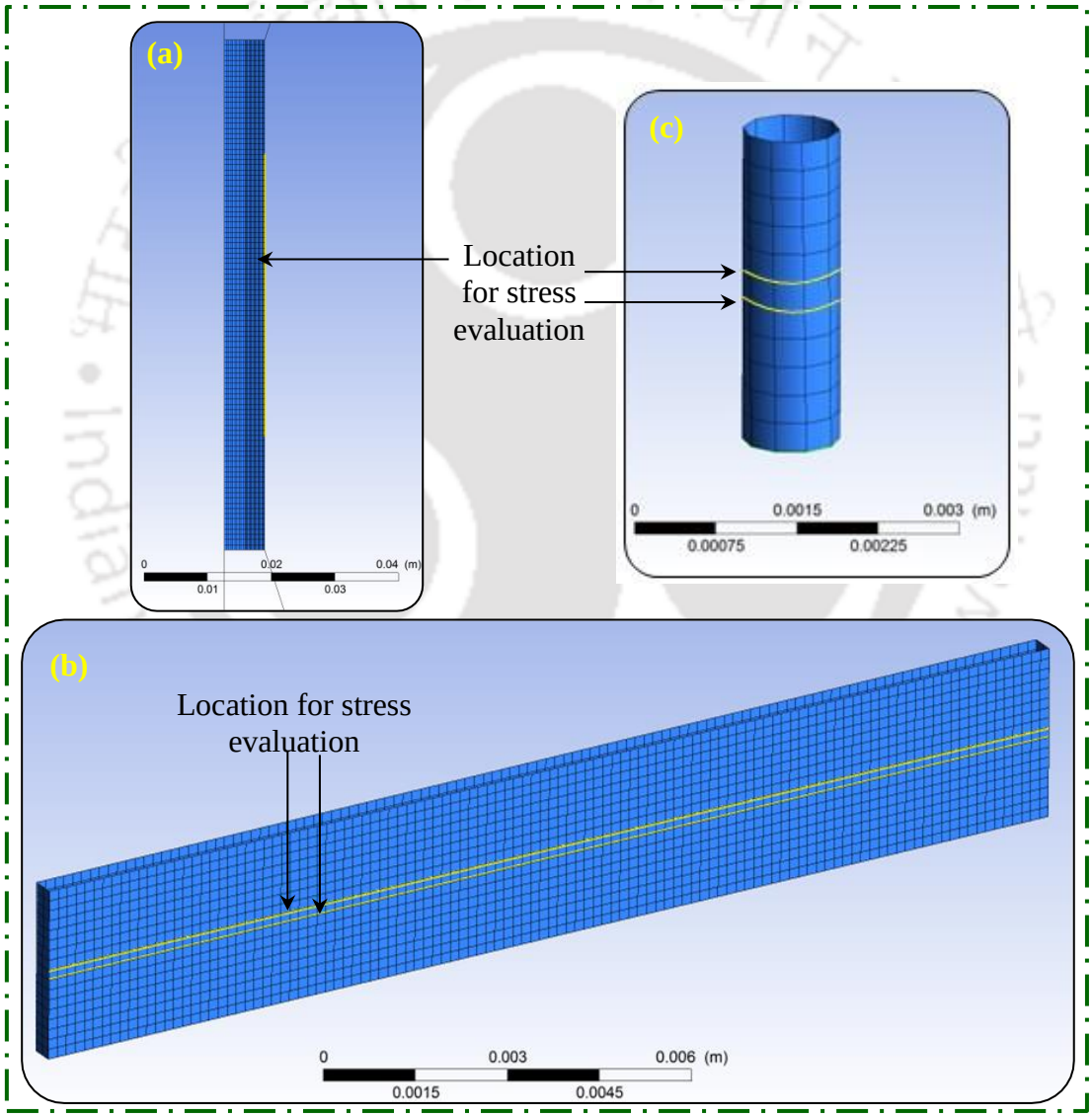

Fig. 7.4 *Workpieces finite element model showing the location of stress evaluation* ***(a)*** *2-D axisymmetric tube geometry, 3-D geometry of* ***(b)*** *microslot* ***(c)*** *microhole.*

7.3 Simulation of the surface roughness

The procedure of generating the simulated surface profile of the workpiece after having undergone AFF process can be divided into three parts:-

1. Getting of initial surface roughness profile data from the experimental measurement of workpiece surface roughness using surface profilometer.
2. Generation of abrasive particles by using various parameters such as density of abrasives, size of abrasives, etc.
3. Simulating the cutting/shearing action of the abrasive particles during AFF process.

In the simulation following assumptions are made:-

1. During AFF process, improvement in surface roughness can be a result of both microcutting as well as microploughing of the surface roughness peaks [78]. During simulation, only microcutting action is considered.
2. Abrasive particle center coordinates (*X*, *Y*, *Z*) which represent their axial (direction of medium flow), transverse and perpendicular position in the medium (Fig. 7.5(a)) with respect to the workpiece surface are produced randomly from the normal distribution.
3. Abrasive particles are considered to be spherical in shape.

7.3.1 Initial surface roughness profile data

The initial roughness profile of the workpiece surface is measured from 3-D surface profilometer (make: Taylor Hobson). This profile is incorporated during simulation of the cutting action of roughness peaks which makes the surface roughness simulation model more realistic. Surface roughness profile measurement location on workpiece surface is same as that of radial stresses extraction from FE model. In the case of tube and microslots, initial surface roughness profile data is taken for a length of 600 µm with coordinates at 0.833 µm resolution. While due to the curved surface of microhole, the focusing area on the microhole surface of the optical profilometer is decreased to 130 µm. Surface roughness is measured in a direction perpendicular to the initial machining marks on the workpiece surface. Tubes are internally bored on the lathe with boring marks in the direction perpendicular to the medium flow direction. As a result, surface roughness in the case of tube is measured in the direction of medium flow. This results in a 1-D interaction between the abrasive particle and the roughness peaks. Profile information is extracted in the form of *X*, *Z* coordinates of the surface in a datasheet, where *Z* is the height of a roughness peak and *X* is its corresponding position along the length of the workpiece (i.e., in axial direction). In the case of microslots and microholes the dominant machining marks are in the direction of medium flow. Thus, the

surface roughness profile is extracted in a direction perpendicular to the medium flow. Therefore, 2-D interaction occurs between the abrasive particle and the surface roughness peaks. Profile information is extracted in the form of *Y*, *Z* coordinates of the surface in a datasheet, where Z is the height of a roughness peak and *Y* is its corresponding position in the transverse direction. Fig. 7.5(b-d) shows the initial surface roughness profile data for tube, microslot, and microholes respectively.

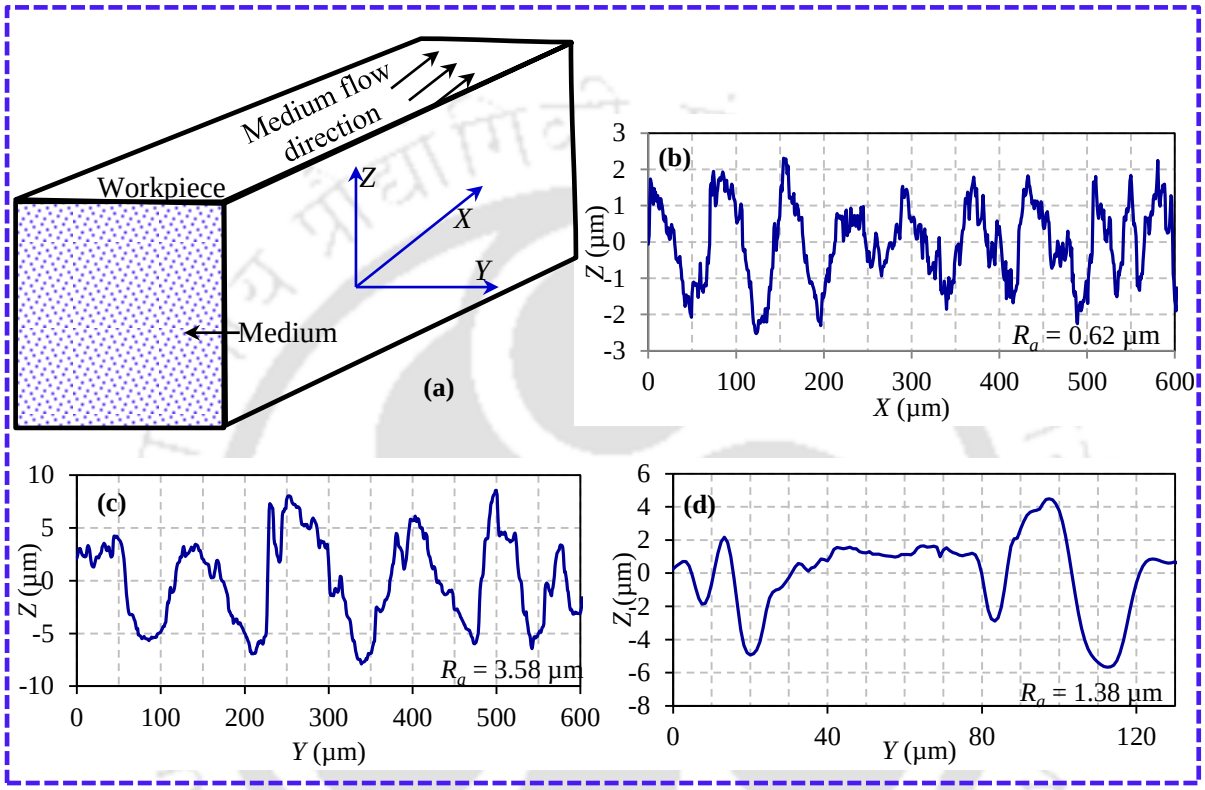

Fig. 7.5 (a) *Schematic representation of simulated medium; Initial roughness profile of the workpiece surface* ***(b)*** *tube* ***(c)*** *microslot* ***(d)*** *microhole*.

7.3.2 Generation of the abrasive particles

In order to optimize the simulation time of AFF process, instead of taking whole volume of the medium and generating abrasive particles (Fig. 7.6(a)), a small volume of the medium is considered (Fig. 7.6(b)). The volume of the medium is chosen in such a way that the particles lying in this volume possess the highest probability of taking part in micro-cutting action along the length of the workpiece surface under consideration for surface roughness simulation. The particles lying outside this region won't contribute in improving surface roughness along the simulation path. The volume of the medium region used for simulation is a fraction of the total medium volume. It results in minimizing the computational time.

Also, the simulation path is along the medium flow direction in the case of tube, while it is perpendicular in the case of microslot and microhole.

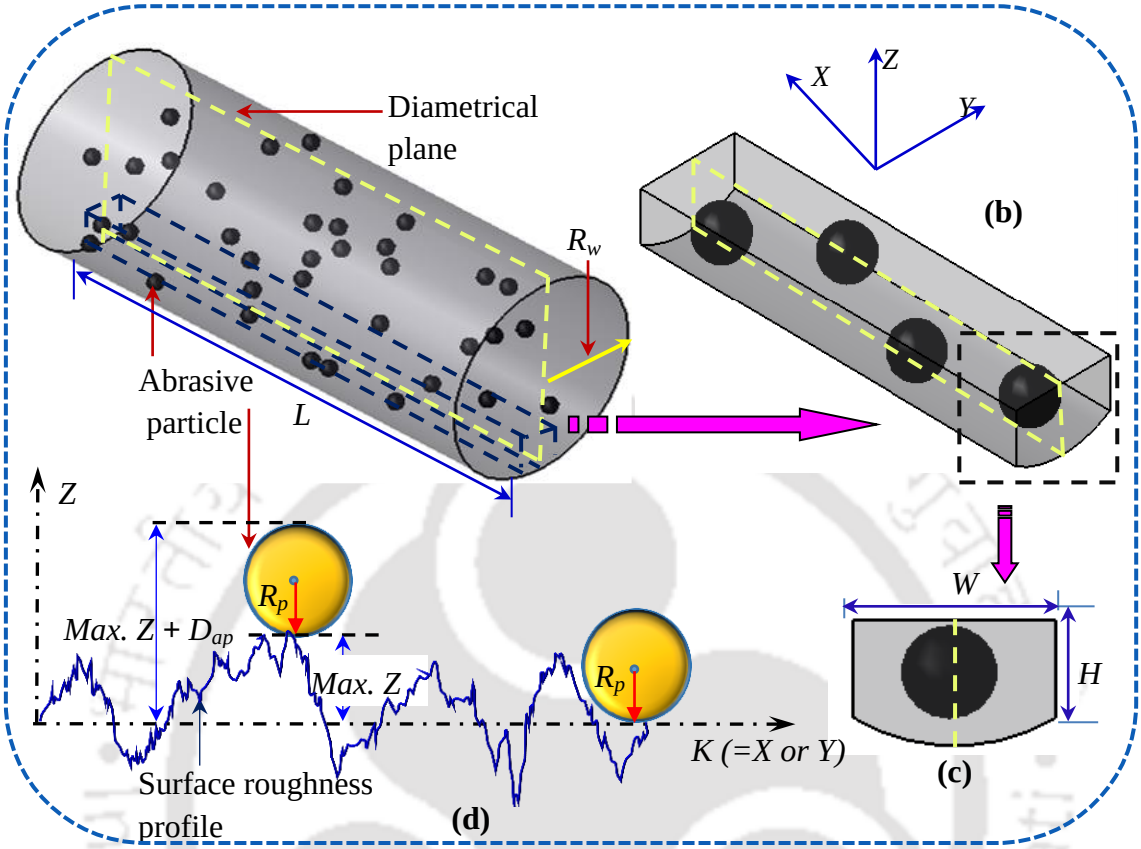

Fig. *7.6 (a)* *Schematic view of medium slug containing abrasive particles* ***(b)*** *a small volume of the medium used for simulation* ***(c)*** *cross-sectional view of the medium volume used for simulation* ***(d)*** *2-D view of the surface roughness profile and a few abrasive particles*.

The dimensions of the fractionated medium (Fig. 7.6(b)) used in simulation is determined in the following way:

1. Total length of medium (L) passed through workpiece in one stroke length (L_s) is given by,

$$L = \frac{V_m}{A_s} \tag{7.7}$$

where, V_m is volume of medium cylinder with radius R_m given as:-

$$V_m = \pi R_m^2 L_s \tag{7.8}$$

A_s is the cross sectional area of the workpiece which is given as:-

In case of tubes with radius R_t

$$A_s = \pi R_t^2 \tag{7.9}$$

For microslots m_{ms} in number having width W_{ms}, and length L_{ms} micromachined on one workpiece, A_s is given as:-

$$A_s = m_{ms} L_{ms} W_{ms} \tag{7.10}$$

In case of microholes m_{mh} in number having radius R_{mh} micromachined on one workpiece, A_s is given as:-

$$A_s = m_{mh} \pi R_{mh}^2 \tag{7.11}$$

2. Width (W) of the fractionated medium volume is given as:

   The 2-D schematic surface roughness profile is shown in Fig 7.6(d). 2-D surface roughness profile is described by the Z, K coordinates. Where, K represents the X direction (along the medium flow) in case of tube and Y direction (transverse to the medium flow) in case on the microslots and microholes. Thus, W in case of tube is:-

$$W = 2D_{ap} \tag{7.12}$$

   While, in case of microslots and microhole W is equal to the assessment length of the surface roughness profile which is measured from surface roughness profilometer i.e. 600 µm and 130 µm in case of microslot and microhole respectively.

3. Height (H = *Max.* Z+ D_{ap}) of the medium in all the cases (tubes, microslots and microholes) is taken as sum of maximum roughness peak "Z" in the assessment length of the surface roughness and diameter of abrasive particle because above this height abrasive particles doesn't contribute in AFF cutting action. The abrasive particles which are below this height are going to take part in the shearing of the surface roughness peaks during AFF process (Fig. 7.6(c-d)).

Abrasive particles in the effective medium volume are generated as follows:

1. Overall mass of the abrasives in the effective medium volume is:

   Volume of the medium, V_m used in simulation of AFF process during one stroke can be given as:-

$$V_m = A_s L \tag{7.13}$$

   Density of medium, ρ_m can be calculated by using density of abrasives, ρ_a and density of carrier medium, ρ_c by the following relation [80]:-

$$\rho_m = \frac{(100\rho_a\rho_c)}{\left[(C\rho_c)+\left((100-C)\rho_a\right)\right]} \tag{7.14}$$

where, C is the weight percentage of abrasive particles in the medium.

Total mass of the abrasive in the medium, M_a with abrasive percentage concentration C is given by:-

$$M_a = \frac{\rho_m V_m C}{100} \tag{7.15}$$

2. It is assumed that abrasive particle radius follows the normal distribution about the mean radius, R_{mean} given as:-

$$R_{mean} = \frac{R_A + R_B}{2} \tag{7.16}$$

With standard deviation, σ_d which is 1/6th the range of normally distributed variables i.e.:-

$$\sigma_d = \frac{(R_B - R_A)}{6} \tag{7.17}$$

where, R_B , R_A is the range for the radius of normally distributed abrasive particles having mean radius, R_{mean} and standard deviation, σ_d.

Also, the relation between the radius of the abrasive particle, R_p and mesh size, M_p is given as [80]:-

$$R_p\,(\text{mm}) = \frac{7.62}{M_p} \tag{7.18}$$

Total number of abrasives, N_a having radius, R_{pj} (j=1 to N_a) are generated until the sum of the mass of all abrasive particle is equal to the mass of abrasives in the medium i.e.,

$$\frac{4}{3}\pi\rho_a\sum_{j=1}^{N_a} R_{pj}^3 = M_a \tag{7.19}$$

where, R_{pj} is the radius of the j^{th} abrasive particle.

3. Condition for avoiding overlapping of the abrasive particles

The coordinates of the abrasive particles were generated at random from uniform distribution curve. After generating the abrasive particles, there is possibility of overlap of few abrasive particles. The two adjacent particles overlap if the distance between their centers is less than the sum of their radii. This condition can be stated as:-

$$\sqrt{((X_0(\mathrm{i})-X_0(j))^2+(Y_0(\mathrm{i})-Y_0(j))^2+(Z_0(\mathrm{i})-Z_0(j))^2)} \; < \; (R_{pi}+R_{pj}) \qquad (7.20)$$

where (X_0 *(i)*, Y_0 *(i)*, Z_0 *(i)*) denotes the center coordinates of the i^{th} abrasive particle and (X_0 *(j)*, Y_0 *(j)*, Z_0 *(j)*) are center coordinates of the j^{th} abrasive particle. After finding the overlapping abrasive particles, the smallest particle of the two is selected and its position is again randomly generated as done in the initial stage. This process is continued till no two particles overlap.

Average radial force (F_{Rj}) acting on the j^{th} abrasive particle of diameter (D_{apj}) causes it to indent into a surface is calculated by using the average radial stresses, σ_R by the following formula [78]:-

$$F_{Rj} = \sigma_R \frac{\pi D_{apj}^2}{4} \qquad (7.21)$$

Brinell hardness number (BHN) takes care of the effect of workpiece material property on surface roughness during simulation of the AFF process. BHN is given by the following formula:-

$$\mathrm{BHN} = \frac{F_{Rj}}{\pi/2\, D_{apj}(D_{apj} - \sqrt{D_{apj}^2 - D_{idj}^2})} \qquad (7.22)$$

BHN of the SS 316L workpiece is 209 BHN. Thus, for the j^{th} abrasive particle, putting the value of F_{Rj} acting on the abrasive particle, diameter of abrasive particle into eq. 7.22, its indentation diameter D_{idj}, can be calculated.

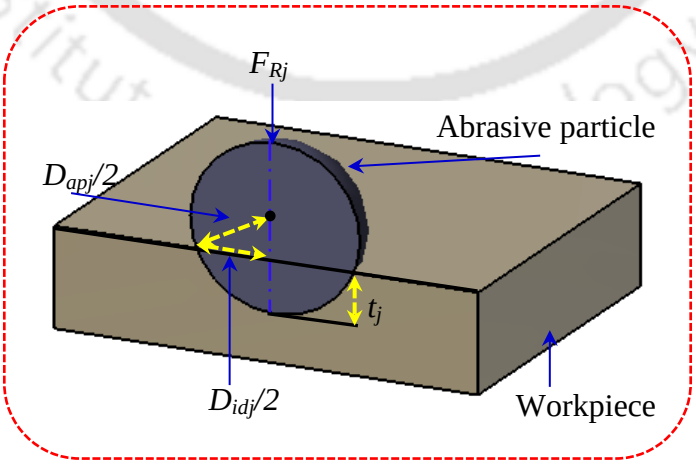

Fig. 7.7 *Schematic diagram of the indentation of an abrasive particle on the workpiece surface.*

Indentation depth (t_j) of the j^{th} abrasive particle into the workpiece surface (Fig. 7.7) is given as [78]:-

$$t_j = \frac{D_{apj}}{2} - \frac{1}{2}\sqrt{D_{apj}^2 - D_{idj}^2} \tag{7.23}$$

7.3.3 Shearing of the surface roughness peaks by abrasive particles

Type of interaction between the abrasive particles and surface roughness depends upon the direction of medium flow and the direction in which surface roughness profile is measured. Thus, in the case of tube there is 1-D interaction of abrasive particles with the surface roughness profile. Also, there is a 2-D interaction between the roughness profile and the abrasive particles in case of microslots and microholes. Accordingly shearing of surface roughness peaks by abrasive particles is done in respective cases.

7.3.3.1 Finishing of tubes

Shearing of the surface roughness peaks in case of tubes is done in two steps:

1. Transformation of abrasive particles

   Simulation of AFF cutting action is done in the diametrical plane but the abrasive particles generated are in volume, so there are many abrasive particles in the medium whose centers lays outside the diametrical plane. Therefore, the actual radii of particles do not contribute as the cutting edge instead the projected radius of abrasive particles on the diametrical plane (*Z-X* plane) acts as cutting edge (Fig. 7.8).

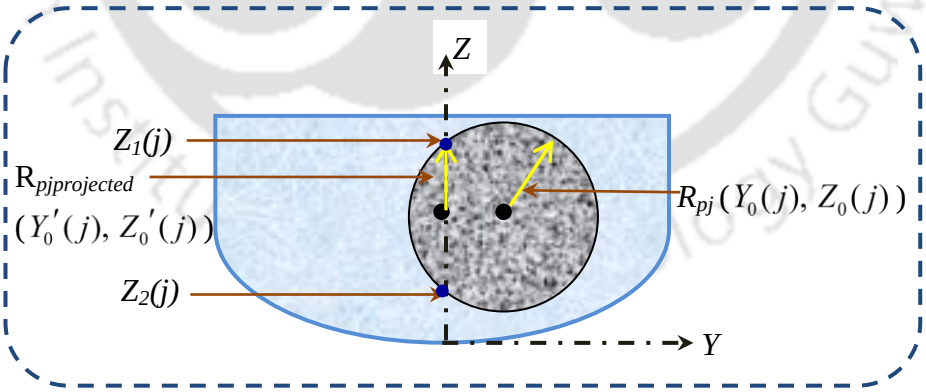

Fig. 7.8 *Cross-sectional area of the medium slug and an abrasive particle.*

Now, as shown in Fig. 7.8, the 2-D equation of the j^{th} abrasive particle having radius, R_{pj} and center coordinates ($Z_0(j)$, $Y_0(j)$) is given by:-

$$(Z(j) - Z_0(j))^2 + (Y(j) - Y_0(j))^2 = R_{pj}^{\ 2} \tag{7.24}$$

Solving eq. (7.24) for the interaction of the particle with the diametrical plane i.e. putting $Y(j) = 0$ in eq. 7.24, the projected radius, for j^{th} abrasive particle $R_{pjprojected}$ given as:-

$$R_{pjprojected} = \frac{Z_1(j) - Z_2(j)}{2} \tag{7.25}$$

where,

$$Z_1(j) = Z_0 + \sqrt{\left(R_{pj}{}^2 - Y_0(j)^2\right)} \tag{7.26}$$

$$Z_2(j) = Z_0 - \sqrt{\left(R_{pj}{}^2 - Y_0(j)^2\right)} \tag{7.27}$$

2. Shearing of the surface roughness peaks

After finding the medium volume by eq. 7.13 and generating the abrasive particles in that volume by eq. 7.19 followed by finding out the projected radii on the diametrical plane calculated by eq. 7.25, simulation of the AFF cutting action is done by passing abrasive particles over the surface roughness peaks. Active abrasive particles are the ones which are responsible for shearing of roughness peaks. Some of the active particles have their Z coordinates lying below the Z' coordinate of the surface roughness peaks i.e.

$$Z' \geq Z_0'(j) - R_{pjprojected} \tag{7.28}$$

When an active abrasive particle passes over the roughness peak, cutting action is simulated by updating the roughness peak profile according to the interaction of abrasive particle and that particular peak. After passing of all the abrasive particles in one stroke heights of each peak are updated and used as initial surface roughness for the next AFF stroke.

During cutting, following three cases arise:-

i. The abrasive particles are generated randomly in the medium slug, as shown in Fig. 7.9(a). The distance between the coordinate of the roughness peak, Z' and coordinate of the abrasive particle $Z_0'(j) - R_{pjprojected}$ is more than the maximum depth of indentation, t_j (eq. 7.23) i.e.:-

$$Z' - (Z_0'(j) - R_{pprojected}) \geq t_j \tag{7.29}$$

As the abrasive particle can't cut the roughness peak more than the maximum effective depth of indentation so the new update peak coordinate, Z'' after passing of active abrasive particle is given as:

$$Z'' = Z_0'(j) - t_j \tag{7.30}$$

ii. As shown in Fig. 7.9(b), when the distance between coordinate of the roughness peak, Z' and coordinate of the abrasive particle $Z_0'(j) - R_{pjprojected}$ is less than the maximum depth of indentation, t_j i.e.-

$$Z' - (Z_0'(j) - R_{pjprojected}) < t_j \tag{7.31}$$

The new update peak coordinate, Z'' after passing of active abrasive particle is given as:-

$$Z'' = Z_0'(j) - R_{pjprojected} \tag{7.32}$$

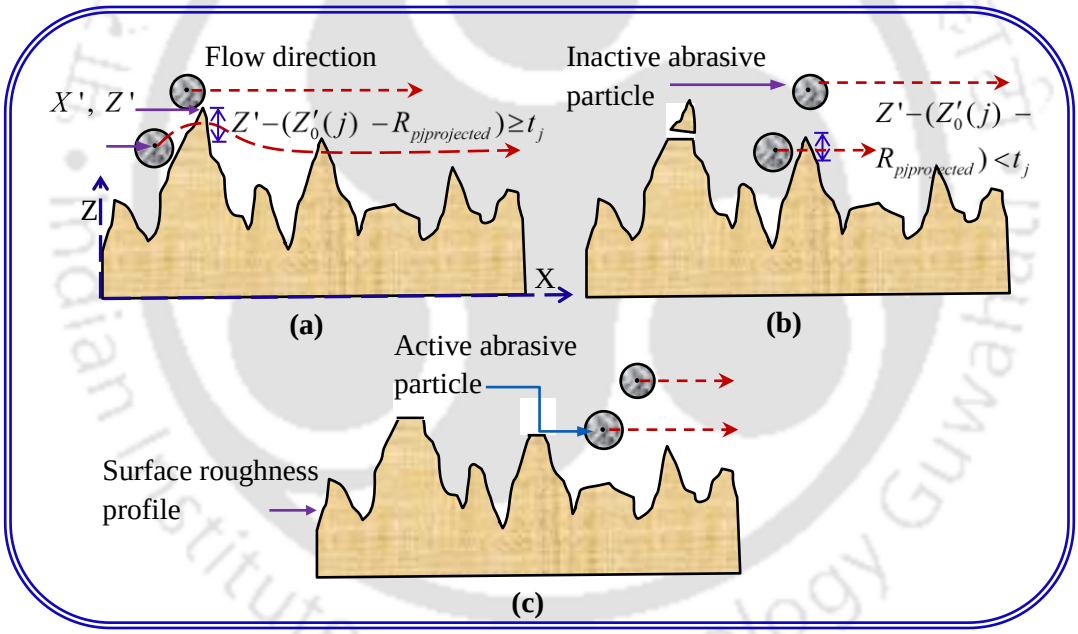

Fig. 7.9 *Abrasive flow finishing/micro-cutting action* ***(a)*** *depth of indentation of abrasive particle greater than maximum depth of indentation,* ***(b)*** *depth of indentation of abrasive particle less than maximum depth of indentation,* ***(c)*** *abrasive particle is not indenting into the roughness peak.*

iii. As shown in Fig. 7.9(c) when the coordinate of roughness peak, Z' lays below the coordinate of the abrasive particle, $Z_0'(j)$ i.e.:-

$$Z' < (Z_0'(j) - R_{pjprojected}) \tag{7.33}$$

In such cases, abrasive particle will roll over the roughness peak without shearing the peak.

7.3.3.2 Finishing of microslots and microholes

During finishing of microslots and microholes surface roughness profile is measured in a direction perpendicular to the medium flow Thus, there is a 2-D (*Y*, *Z*) interaction of the abrasive particle with the surface roughness peaks. To simulate the surface roughness, during microcutting by abrasive particle, the single large cutting edge is split into small segments. Each small segment acts as a miniature cutting edge of the abrasive particle (Fig. 7.10). Thus, the abrasive particle is considered to possess multiple numbers of cutting edges. The Y, Z coordinates of k^{th} cutting edge for j^{th} abrasive particle are given as y_{kaj}, z_{kaj}. Surface roughness profile is extracted from the workpiece surface by the 3-D profilometer in the *Y* and *Z* coordinates at an interval of 0.833 µm. Let y_{ir}, z_{ir} be the position coordinates defining the i^{th} roughness peak. Thus, by solving the equation of the circle (with center $Y_0(j)$, $Z_0(j)$) for discrete values of y_{kaj} (i.e., at an interval of 0.833 µm) the corresponding z_{kaj} can be calculated. Therefore, the coordinates of cutting edge of the abrasive particles are calculated. Later, simulation of the cutting action is carried out. Detailed explanation of this mentioned phenomenon is explained in the following sections.

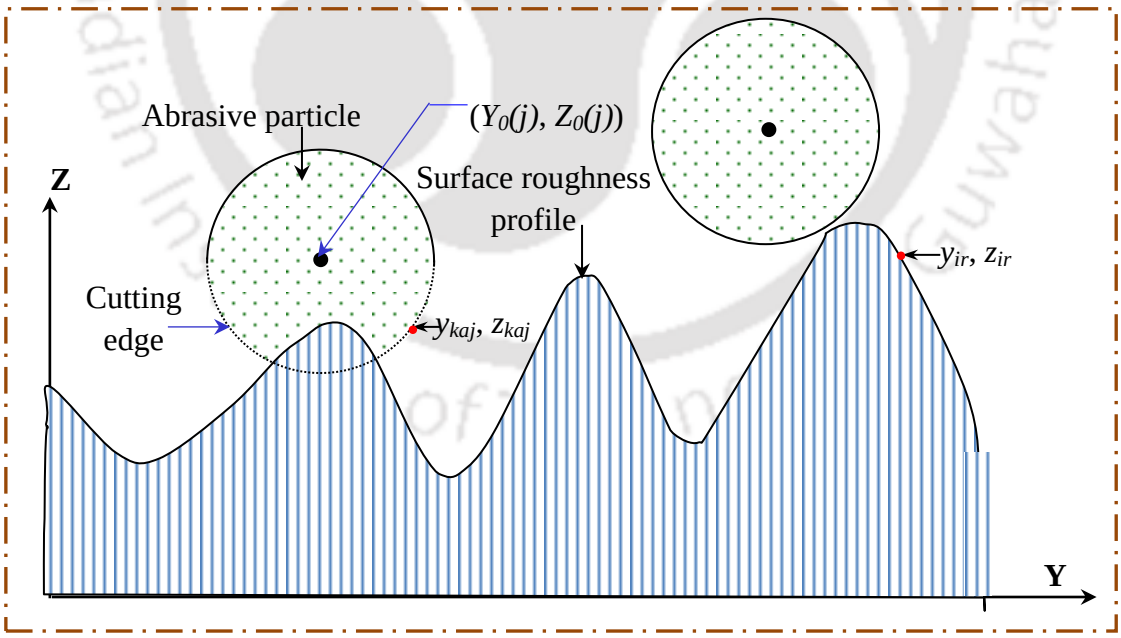

Fig. 7.10 *Schematic showing the interaction between abrasive particle and workpiece surface roughness (microslots and microholes).*

A total of 720 for microslots and 156 for microholes roughness points define the roughness profile in the assessment length. Let, y_{ir} is Y coordinate of the i^{th} roughness peak having z_{ir} as corresponding height in the Z coordinate. Also, in whole assessment length, let z_m is the maximum height of the roughness peak for a particular AFF stroke.

Cutting action is performed in the following steps:-

1. Finding the maximum number of cutting edges of an abrasive particle that can take part in cutting action during an AFF stroke.

   Maximum roughness height that can be overlapped by the abrasive particle during an AFF stroke is z_m. Thus, z_m is the maximum height of the cutting edge of the abrasive particle that can take part in the cutting action of the roughness peak. The Y coordinate of i^{th} cutting edge of the j^{th} abrasive particle, y_{iaj} corresponding to z_m can be calculated as:

$$(y_{iaj} - Y_0(j))^2 + (z_m - Z_0(j))^2 = R_{pj}^{\ 2} \tag{7.34}$$

   Therefore, number of cutting edges N_{maxj} (N_{maxj}, if comes in decimal, then next whole number) on the left side of the diameter of the j^{th} abrasive particle (circle) that can take part in the cutting action of the roughness peak are:-

$$N_{maxj} = \frac{y_{iaj}}{0.833} \tag{7.35}$$

   Thus, the maximum numbers of cutting edges of the j^{th} abrasive particle that can take part in the cutting action of roughness peak N_{tmaxj} are:-

$$N_{tmaxj} = 2N_{maxj}(both\ sides\ of\ the\ diameter) + 1(centre\ point) \tag{7.36}$$

2. Shifting of the abrasive particle

   Y coordinate of the abrasive particles center is shifted to their nearest Y coordinate at which surface roughness profile is defined. As shown in Fig. 7.11, center of the abrasive particle is updated as:

$$new Y_0(j) = y_{nr} \tag{7.37}$$

   Thus, now for the same Y coordinate, y_{lr} there is j^{th} abrasive particle's cutting edge having Z coordinate, z_{kaj} and a roughness peak having Z coordinate, z_{lr} respectively (Fig. 7.11).

3. Determination of the Z coordinate of the abrasive particle cutting edges

   N_{tmaxj} number of cutting edges of j^{th} abrasive particle are generated whose Z coordinates are given by the following eq.:-

$$(y_{nr} - newY_0(j))^2 + (z_{naj} - Z_0(j))^2 = R_{pj}^{\ 2} \tag{7.38}$$

i. Z coordinates of the j^{th} abrasive particle cutting edges in the left side of the abrasive particle (ABD) are given when y_{nr} is given as :-

$$y_{nr} = newY_0(j) - n \times 0.833 \quad for\ n = 1 to\ N_{max} \tag{7.39}$$

ii. Z coordinates of the j^{th} abrasive particle cutting edges in the right side of the abrasive particle (CBD) are given when y_{nr} is given as:-

$$y_{nr} = newY_0(j) + n \times 0.833 \quad for\ n = 1 to\ N_{max} \tag{7.40}$$

iii. Z coordinates of the central cutting edge (D) is given when y_{nr} is given as :-

$$y_{nr} = newY_0(j) \tag{7.41}$$

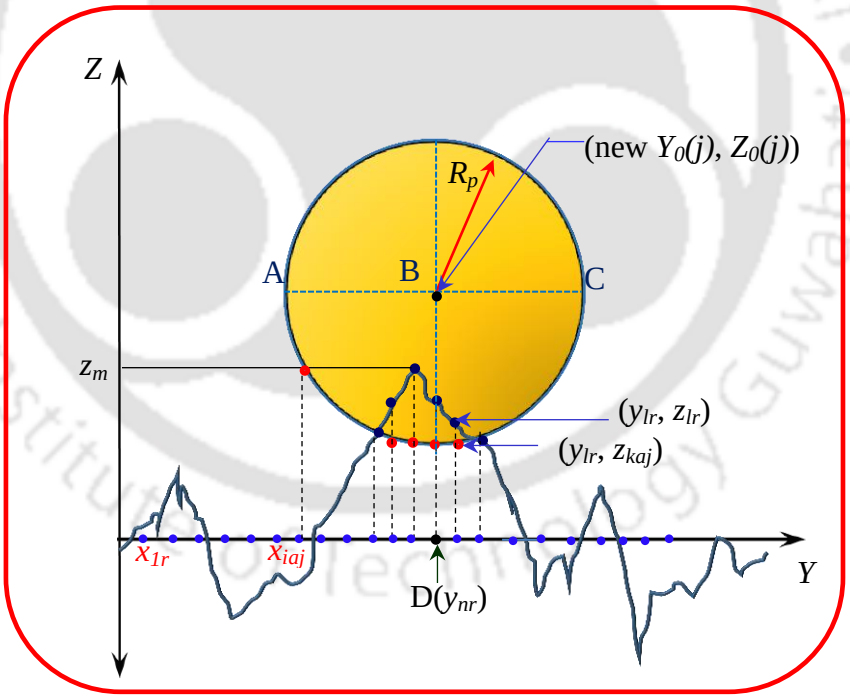

Fig. 7.11 *Schematic view of 2D interaction of an abrasive particle with the surface roughness profile during simulation of AFF process.*

4. Cutting of the surface roughness peaks:-

For the j^{th} abrasive particle, comparison is made between the Z coordinate of abrasive particle cutting edges (z_{1aj}, z_{2aj}……z_{kaj}) and corresponding Z coordinate of the roughness peak (z_{1r}, z_{2r}……z_{kr}) for the same Y coordinate. Depending on their relative positions cutting is done.

There are 3 cases for the cutting of the surface roughness peaks during the AFF process:-

1. When the difference between some of the Z coordinates of the roughness peak and corresponding Z coordinates of j^{th} abrasive particle cutting edges is more than maximum depth of the indentation, t_j (Fig. 7.12(a)) i.e.:-

$$\left(z_{1r}-z_{1aj}\right),\left(z_{2r}-z_{2aj}\right),\left(z_{3r}-z_{3aj}\right)\ldots\ldots\ldots\left(z_{kr}-z_{kaj}\right)>t_j;\ k=1to\,N_{tmaxj} \tag{7.42}$$

During the experimentation, abrasive particles can remove the roughness peaks from the workpiece surface in the form of micro/nano chips only if they indent into the workpiece surface upto a maximum depth indentation (t_j). However, if the abrasive particles indent beyond dj then the force needed for removing the material is more than the applied finishing force by the abrasive particles. As a result, abrasive particles only make indentation marks on the workpiece surface. Later, indented abrasive particle adjusts itself in upcoming AFF cycles until it reaches the depth, t_j thereafter it moves in the axial direction [44]. The same phenomenon is included during simulation. If abrasive particle cutting edges indent more than t_j then to reach t_j it adjusts in the following way:-

a. The maximum positive difference between the Z coordinates of j^{th} abrasive particle cutting edge and the corresponding Z coordinates of the roughness peak is found out i.e.

$$Max\left[\left(z_{1r}-z_{1aj}\right),\left(z_{2r}-z_{2aj}\right),\left(z_{3r}-z_{3aj}\right)\ldots\ldots\ldots,\left(z_{kr}-z_{kaj}\right)\right]=M_j;\ \ k=1to\,N_{tmaxj} \tag{7.43}$$

b. The abrasive particle is shifted upwards w.r.t to the workpiece surface. This is done by updating the Z coordinate of abrasive particle cutting edges in the following way:-

$$\left[\begin{array}{l} z_{u1aj}=z_{1aj}+(M_j-t_j) \\ z_{u2aj}=z_{2aj}+(M_j-t_j) \\ . \\ . \\ . \\ z_{ukaj}=z_{kaj}+(M_j-t_j) \end{array}\right] k=1to\,N_{tmaxj} \tag{7.44}$$

where, z_{u1aj}, z_{u2aj}…..z_{ukaj} are the updated Z coordinates of the j^{th} abrasive particle.

Now the abrasive particle is at the maximum depth of indentation. So, to simulate the cutting action the Z coordinates of the roughness peak that lie below the Z coordinates of the j^{th} abrasive particles are updated as:-

$$\begin{bmatrix} z_{1r} = z_{u1aj} \\ z_{2r} = z_{u2aj} \\ . \\ . \\ . \\ z_{kr} = z_{ukaj} \end{bmatrix}; k = 1 to\ N_{tmaxj} \tag{7.45}$$

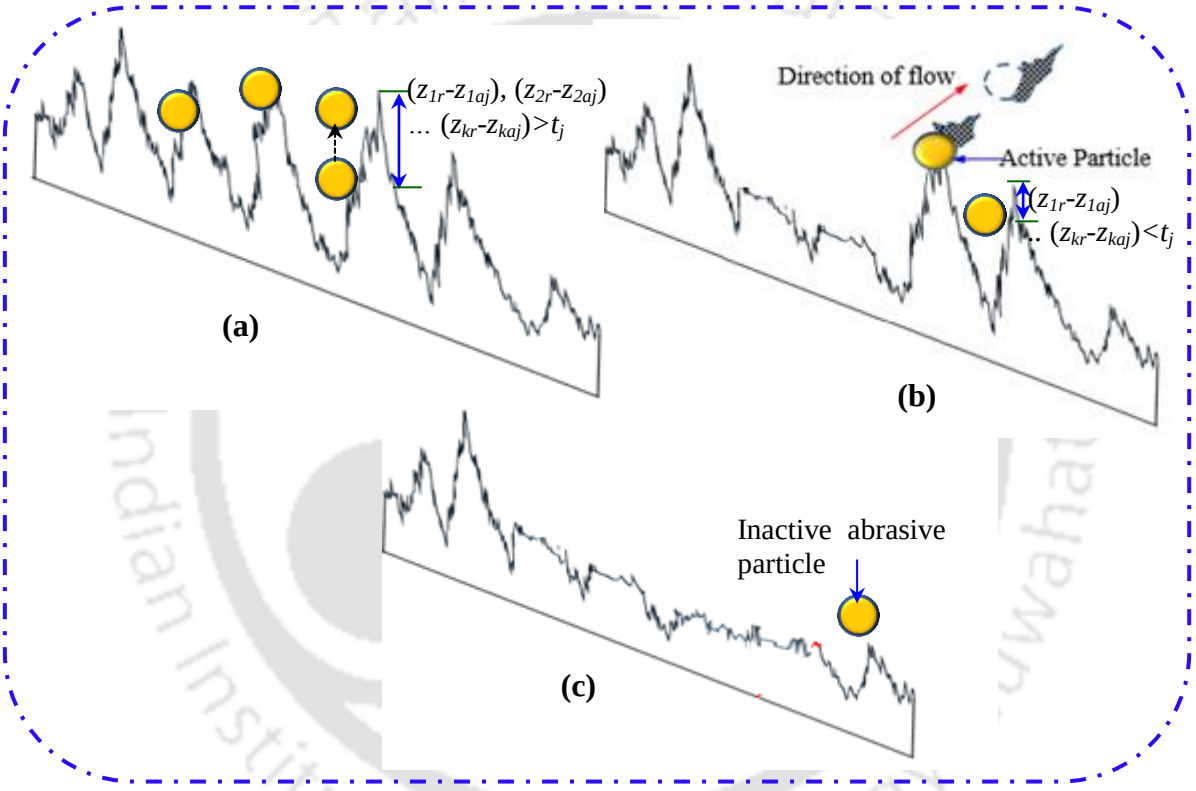

Fig. 7.12 *Schematic view of simulation of AFF cutting action* ***(a)*** *indentation depth of abrasive particle cutting edges is greater than maximum indentation depth* ***(b)*** *indentation depth of abrasive particle cutting edges is less than maximum indentation depth* ***(c)*** *abrasive particle not indenting into the workpiece surface.*

2. When the difference between some of the Z coordinates of the roughness peak and corresponding Z coordinates of the j^{th} abrasive particle cutting edges is less than the maximum depth of the indentation, t_j (Fig. 7.12(b)) i.e.:-

$$\left(z_{1r} - z_{1aj}\right), \left(z_{2r} - z_{2aj}\right), \left(z_{3r} - z_{3aj}\right) ..... \left(z_{kr} - z_{kaj}\right) < t_j;\ k = 1 to\ N_{tmaxj} \tag{7.46}$$

Then the cutting acting action of the roughness peak is performed by updating the Z coordinate of the roughness peaks as:-

$$\begin{bmatrix} z_{1r} = z_{1aj} \\ z_{2r} = z_{2aj} \\ . \\ . \\ . \\ z_{kr} = z_{kaj} \end{bmatrix}; k = 1 to\, N_{tmaxj} \tag{7.47}$$

3. When all the generated Z coordinate of the abrasive particle cutting edges lies above the corresponding Z coordinate of the roughness (Fig. 7.12(c)) i.e.,

$$\left(z_{1r} - z_{1aj}\right), \left(z_{2r} - z_{2aj}\right), \left(z_{3r} - z_{3aj}\right) ..... \left(z_{kr} - z_{kaj}\right) < 0;\ k = 1 to\, N_{tmaxj} \tag{7.48}$$

   In that circumstance, the abrasive particle becomes an inactive particle which doesn't take part in cutting action of surface roughness peak. In such cases Z coordinate of the roughness peaks remains the same.

When all the generated abrasive particles are passed over roughness peaks it completes one AFF stroke. After completion of one stroke, AFF process again starts from generating the abrasive particles and continues till the required number of AFF strokes is completed. Simulated surface roughness value (R_{as}) of the finished surface after each stroke is calculated. For the calculation of R_{as}, the mean line is shifted after each stroke such that the area occupied by the peaks above the mean line is equal to the area occupied by the valleys below the mean line. Flowchart for the simulation of the AFF cutting action is shown in Fig. 7.13. The R_{as} value from the mean line is calculated as follows:-

In case of tubes:

$$R_{as} = \frac{1}{L}\int_0^L \left|Z(\mathrm{x})\right| dx \tag{7.49}$$

In case of microslots and microholes:

$$R_{as} = \frac{1}{L}\int_0^L \left|Z(y)\right| dy \tag{7.50}$$

where $Z(x)$, $Z(y)$ is the height of the profile from the mean line and L is the sampling length taken for calculation of R_{as}.

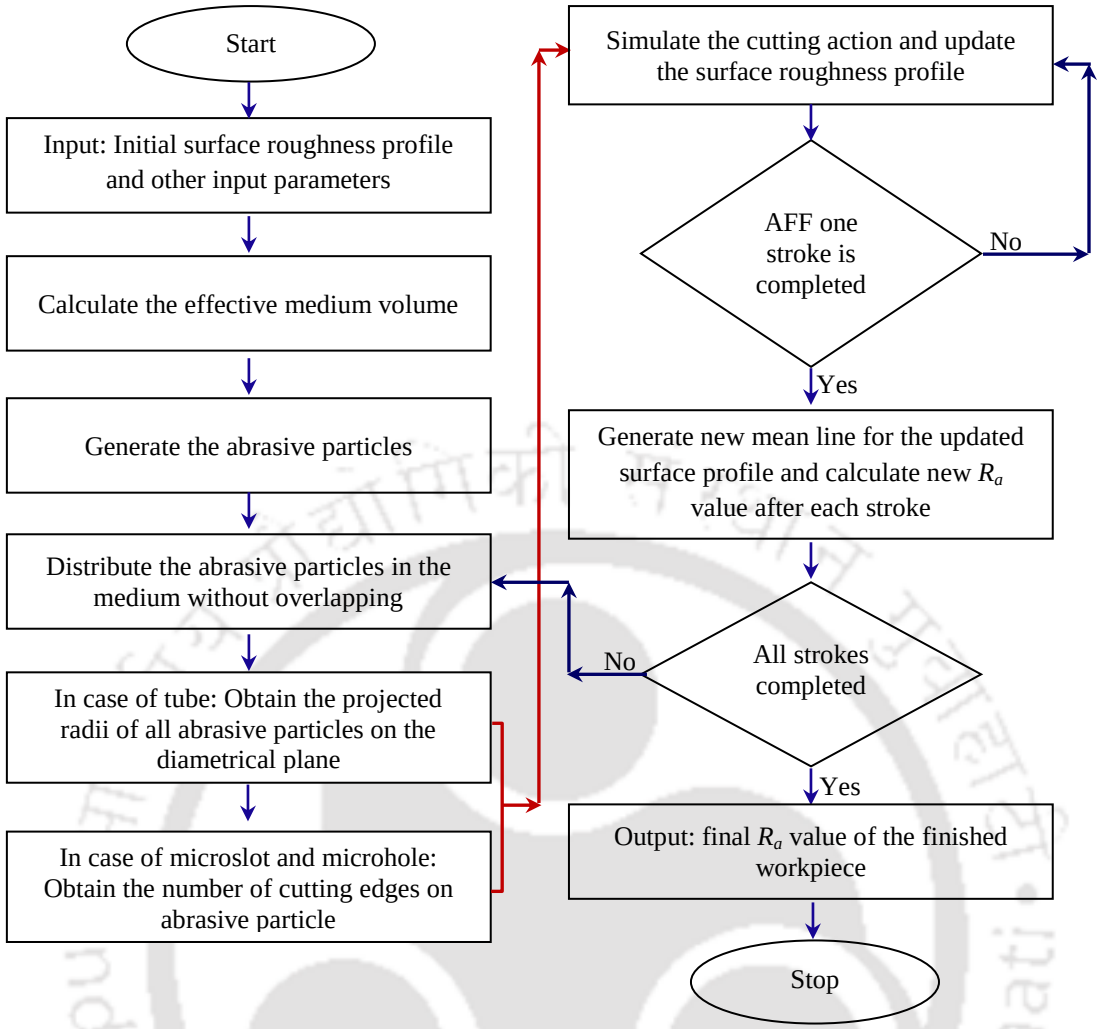

Fig. 7.13 *Flowchart for AFF simulation.*

During finishing processes, a critical surface roughness (R_{cj}) exists due to the indentation of the abrasive particles on the workpiece surface. Beyond R_{cj}, j^{th} abrasive particle is not able to remove the material from the workpiece surface. Therefore, there is no improvement in the surface roughness beyond R_c and is given as [78]:-

$$R_{cj} = \frac{D_{apj}}{2} - \frac{1}{2}\sqrt{D_{apj}^2 - D_{idj}^2} \tag{7.51}$$

7.4 Results and discussion

The present section is divided into two parts. Initially, the finishing stresses generated in the medium as found out from the FE analysis of viscoelastic medium during the finishing of the tubes, microslots and microholes are discussed. Later, using these modeled stresses simulation of the surface roughness generated on the workpiece wall after the AFF process is presented. Simulated results are compared with the experimental result and found both are in

good agreement. Values of the input parameters used during the simulation are given in Appendix A**.**

7.4.1 Variation of finishing stresses

During the AFF experiments, finishing stresses are generated in the medium by the application of external forces (in the present thesis it is hydraulic extrusion pressure) which are responsible for providing the fine roughness on workpiece surface. Finishing stresses generated in the medium are transferred to abrasive particles by medium polymer chains. Radial stresses that are generated due to radial force (F_R) acting in the medium helps in indentation of the abrasive particle on the workpiece surface.

7.4.1.1 Extrusion pressure

With the rise in extrusion pressure, the force exerted by the hydraulic piston on the medium gradually increases.

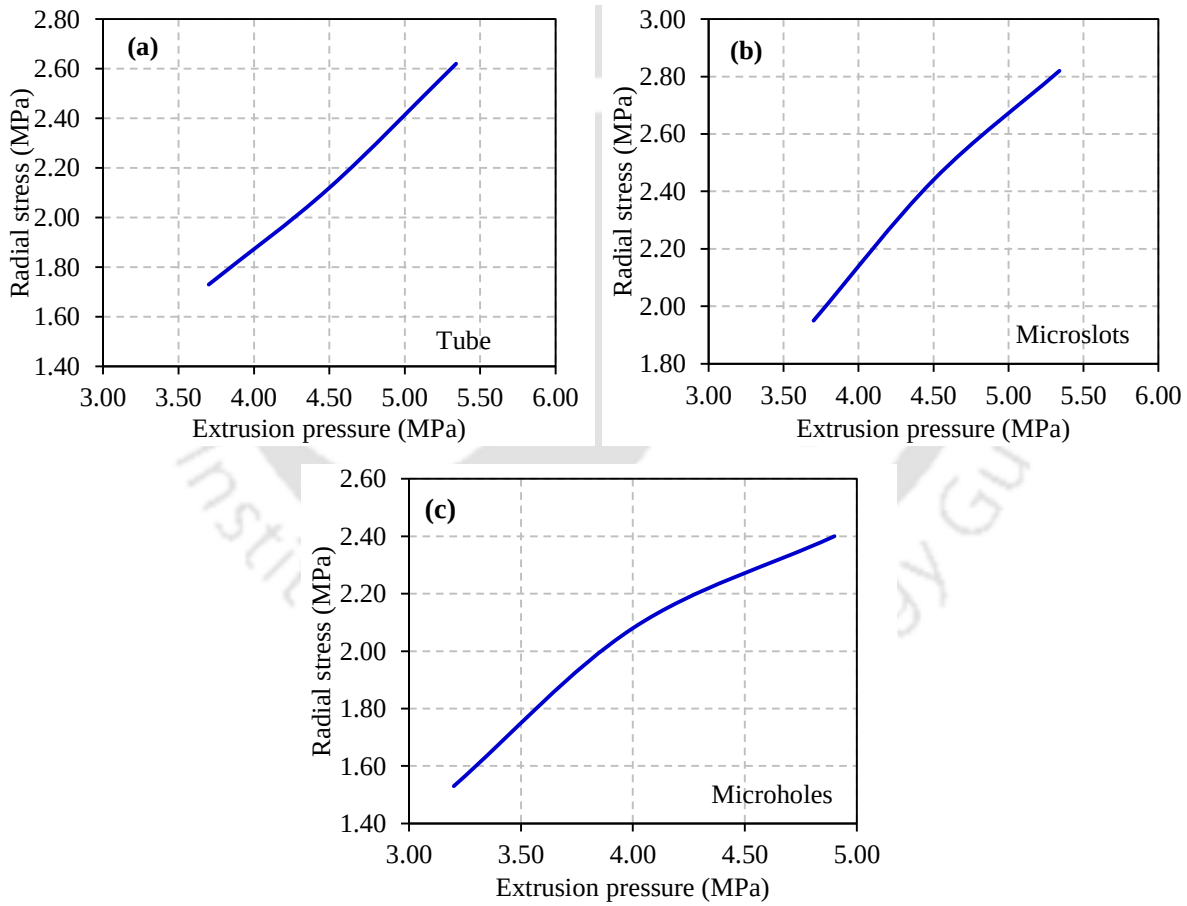

Fig. 7.14 *Variation of radial stresses generated in the medium with respect to extrusion pressure* ***(a)*** *tube (wt. % of abrasive particles = 50 %)* ***(b)*** *microslot (wt. % of abrasive particles = 45 %)* ***(c)*** *microhole (wt. % of abrasive particles = 45 %).*

More the magnitude of external forces acting on the viscoelastic medium larger the amount of energy is stored by the elastic nature of the medium. This large amount of energy is released by polymer chains in the form of stresses acting in the radial direction. Thus, the magnitude of radial stress acting on a single abrasive particle also increases. Fig. 7.14(a-c) shows the magnitude of radial stresses generated on various workpiece surface i.e. tube, microslot and microhole.

7.4.1.2 Weight percentage of abrasive particles

As the wt. % of the abrasive particles increases, the free moment of polymer chains is restricted by the presence of abrasive particles. This results in an increase of medium viscosity.

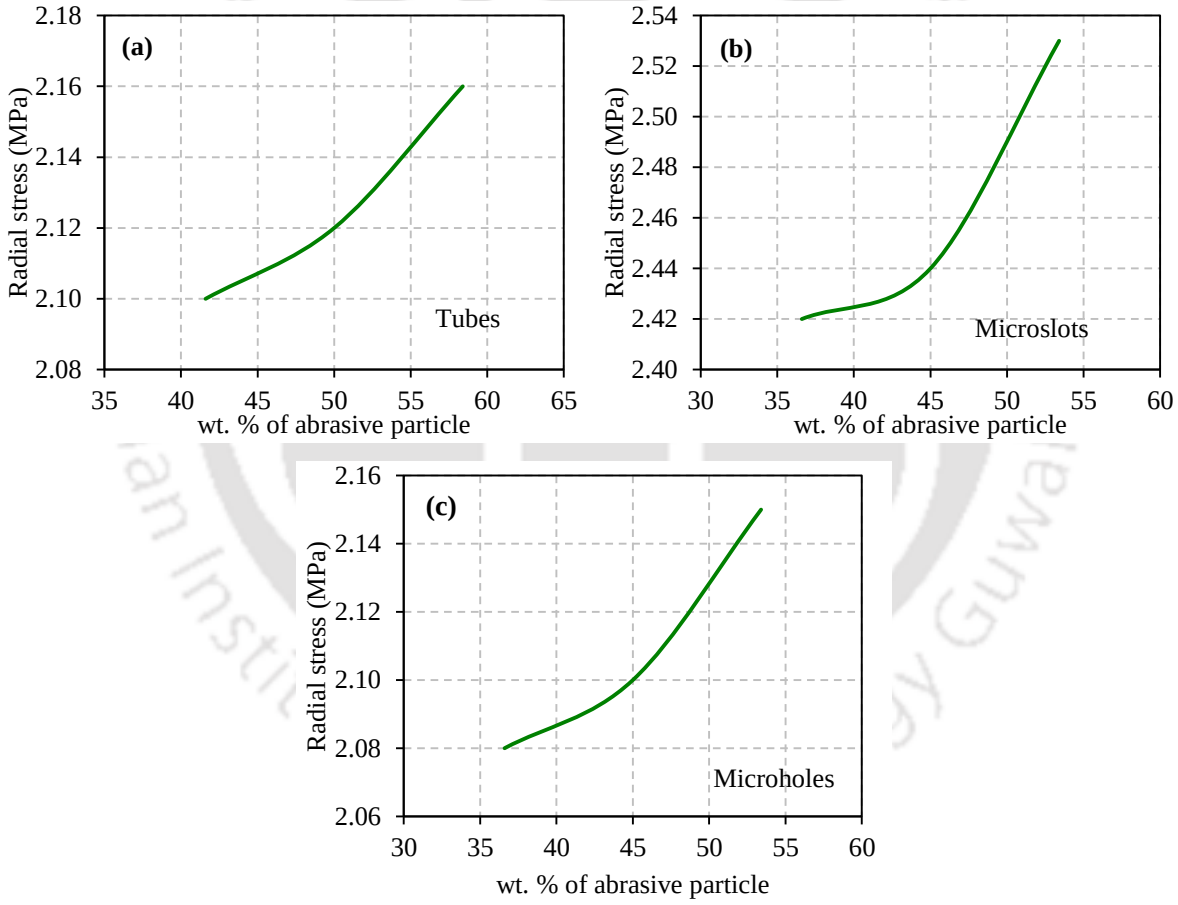

Fig. 7.15 *Variation of radial stresses generated in the medium with respect to* wt. % of abrasive particles in the medium ***(a)*** *tube (extrusion pressure = 4.50 MPa)* ***(b)*** *microslot (extrusion pressure = 4.50 MPa)* ***(c)*** *microhole (extrusion pressure = 4.00 MPa).*

Higher viscous medium, polymer chains strongly support the abrasive particles during the micro cutting of roughness peaks and effectively transfer the radial stresses generated in

the medium. Thus, radial stresses in the case of all the workpieces (tube, microslot and microhole) increase with an increase in wt. % of abrasive particles in the medium (Fig. 7.15(a-c)).

7.4.2 Effect of abrasive flow finishing input parameters

In the present section, experimentally obtained percentage change in surface roughness (% ΔR_a) and simulated value of percentage change in surface roughness (% ΔR_{as}) at various combination of AFF input parameters are compared. Effect of AFF input parameters (viz. extrusion pressure, number of cycles and weight percentage of abrasive particles in the medium) on AFF output responses is presented. ANOVA analysis of % ΔR_{as} in case of tube, microslot and microholes is carried out (Appendix B). The final simulation equations of the output responses in terms of input parameters are given as:

In case of tube:

$$\begin{aligned}\%\Delta R_{as} = &-657.10 + 145.84P + 0.75N + 6.58W - 0.03PN - 0.55PW \\ &- 2.60\times10^{-3}NW - 10.08P^2 - 4.20\times10^{-4}N^2 - 0.02W^2\end{aligned} \tag{7.52}$$

In case of microslot:

$$\begin{aligned}\%\Delta R_{as} = &-164.15 + 56.07P + 0.72N + 3.93W - 0.16PN - 0.331PW \\ &- 3.64\times10^{-2}NW - 3.45P^2 - 2.50\times10^{-2}N^2 - 3.11\times10^{-2}W^2\end{aligned} \tag{7.53}$$

In case of microhole:

$$\begin{aligned}\%\Delta R_{as} = &-72.10 + 41.90P - 1.52N + 2.55W - 0.61PN - 0.40PW \\ &- 5.50\times10^{-2}NW - 3.26P^2 - 0.16N^2 - 0.01W^2\end{aligned} \tag{7.54}$$

7.4.2.1 Extrusion pressure

Extrusion pressure is one of the important AFF input parameters that decides the amount of end surface roughness achieved on the workpiece surface after AFF process. As the extrusion pressure increases, more is the amount of radial stresses generated in the medium (Fig. 7.14(a-c)). These radial stresses help abrasive particles in efficient removal of surface roughness peaks from workpieces surfaces. Also, the velocity with which the abrasive particle hit surface roughness peak increases with an increase in extrusion pressure. This further enhances the cutting efficiency of abrasive particles. Fig. 7.16 shows the velocity streamlines of the viscoelastic medium during finishing of microslots. Maximum value of the velocity is mainly confined in workpiece finishing region. This is mainly due to the passageway converging of the medium from the medium cylinder inlet towards the

workpiece inlet. During the finishing of tubes, microslots and microholes the magnitude of $\% \Delta R_{as}$ is more as compared to $\% \Delta R_a$ (Fig. 7.17(a-c)). This is because of two reasons. First, during the simulation, it is assumed that the amount of finishing stresses generated in the medium are transferred to the abrasive particle in the same amount which is not the case of AFF experiments. Secondly, microslots and microholes are machined by the EDµM process. This leads to the formation of recast layer which is harder than the parent material on their surface. Therefore, the removal of surface roughness peaks is difficult during the finishing of workpieces with the AFF process. But during the simulation hardness of the parent material is considered. Therefore, the magnitude of $\% \Delta R_{as}$ is more compared to $\% \Delta R_a$.

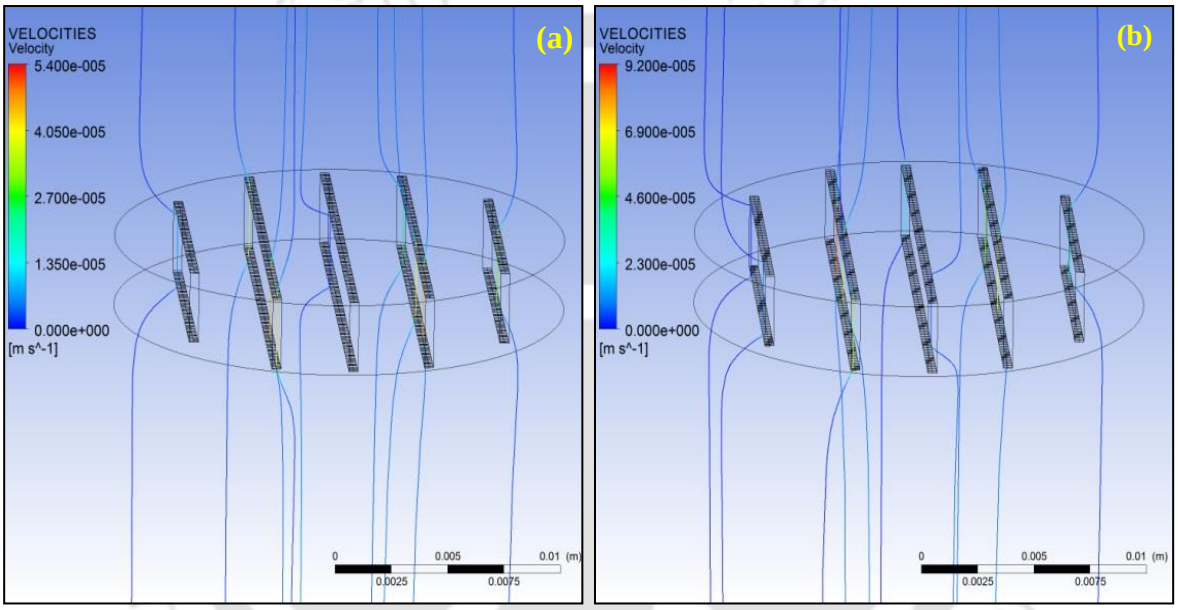

Fig. 7.16 *Velocity streamlines of the medium passing from the microslots during the abrasive flow finishing process at various extrusion pressure* ***(a)*** *3.70 MPa* ***(b)*** *5.30 MPa (wt. % of abrasive particles = 45 %).*

Increasing extrusion pressure beyond the critical value, result in the bluntness of the abrasive particles sharp cutting edges. This is due to the impact of the abrasive particle on the workpiece surface with the high radial force, F_R. Also, abrasive particles create indentation marks on the workpiece surface. This results in decrease of $\% \Delta R_a$ beyond the critical value of extrusion pressure. However, above phenomenon is not incorporated in the simulation on $\% \Delta R_{as.}$ Thus, in simulated results, $\% \Delta R_{as}$ increases with an increase in extrusion pressure beyond the critical value of extrusion pressure (Fig. 7.17(a-c)).

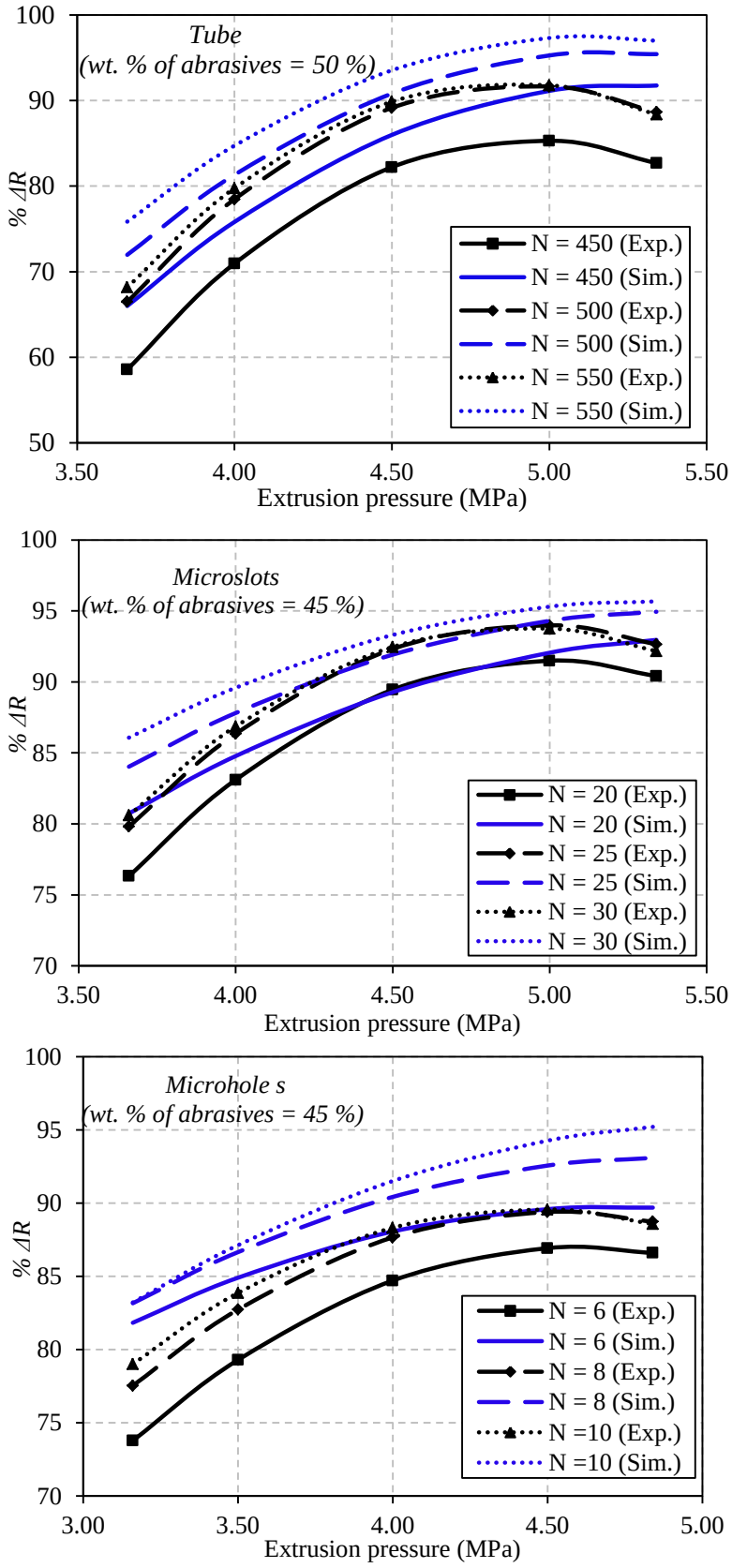

Fig. 7.17 *Effect of extrusion pressure for different number of AFF cycles on percentage change in surface roughness (% ΔR_a, % ΔR_{as}) for various workpieces (Exp. stands for experiments and Sim. stands for the simulation).*

7.4.2.2 Number of abrasive flow finishing cycles

Surface roughness improvement during the AFF process takes place due to the repeated interaction between abrasive particles and the surface roughness peaks. The probability of such interactions increases with an increase in number of AFF cycles. Thus, *% ΔR_a* and *% ΔR_{as}* in case of tubes, microslots and microholes increases with an increase in number of AFF cycles (Fig. 7.18(a-c)). However, while performing AFF experiments repeated interaction between the roughness peaks and abrasive particles leads to the bluntness edges of the abrasive particles cutting. Thus, abrasive particles losses their capacity to cut the surface roughness peaks effectively and efficiently at a high number of AFF cycles. Also, experimentally due to lack of proper bonding between polymer chains and abrasive particles, finishing forces are not transferred in the same amount. Thus, the value of *% ΔR_a* is more than the value of % ΔR_{as}.

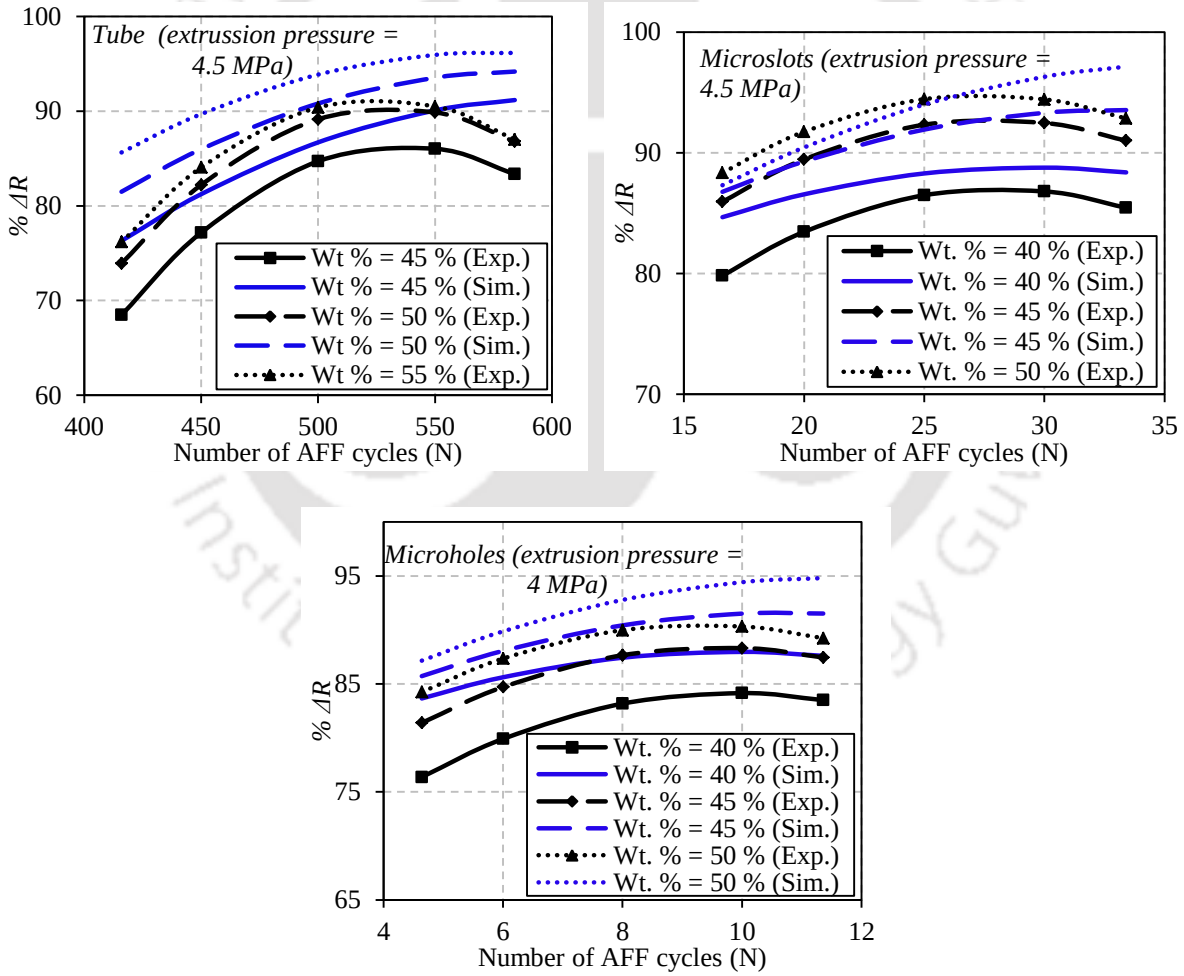

Fig. 7.18 *Effect of number of AFF cycles for different wt. % of abrasives particles on percentage change in surface roughness (% ΔR_a, % ΔR_{as}) for various workpieces (Exp. stands for experiments and Sim. stands for the simulation).*

Increasing the AFF cycles beyond a critical value leads to the creation of new indentation marks of the abrasive particle on the finished workpiece surface. Thus, $\% \Delta R_a$ decreases with the increasing AFF cycles above the critical value. However, in the simulation, indentation of the abrasive particles on the finished surface is not considered. As a result in all the three cases, ΔR_{as} increases beyond the critical value of AFF cycles (Fig. 7.18(a-c)).

7.4.2.3 Weight percentage of abrasive particles

Increase in wt. % of abrasive particles in the medium enhances the performance of AFF process in two ways. First, as wt. % of the abrasive particle increases, the amount of radial stresses acting on abrasive particle increases during finishing of tubes, microslots and microholes (Fig. 7.15(a-c)).

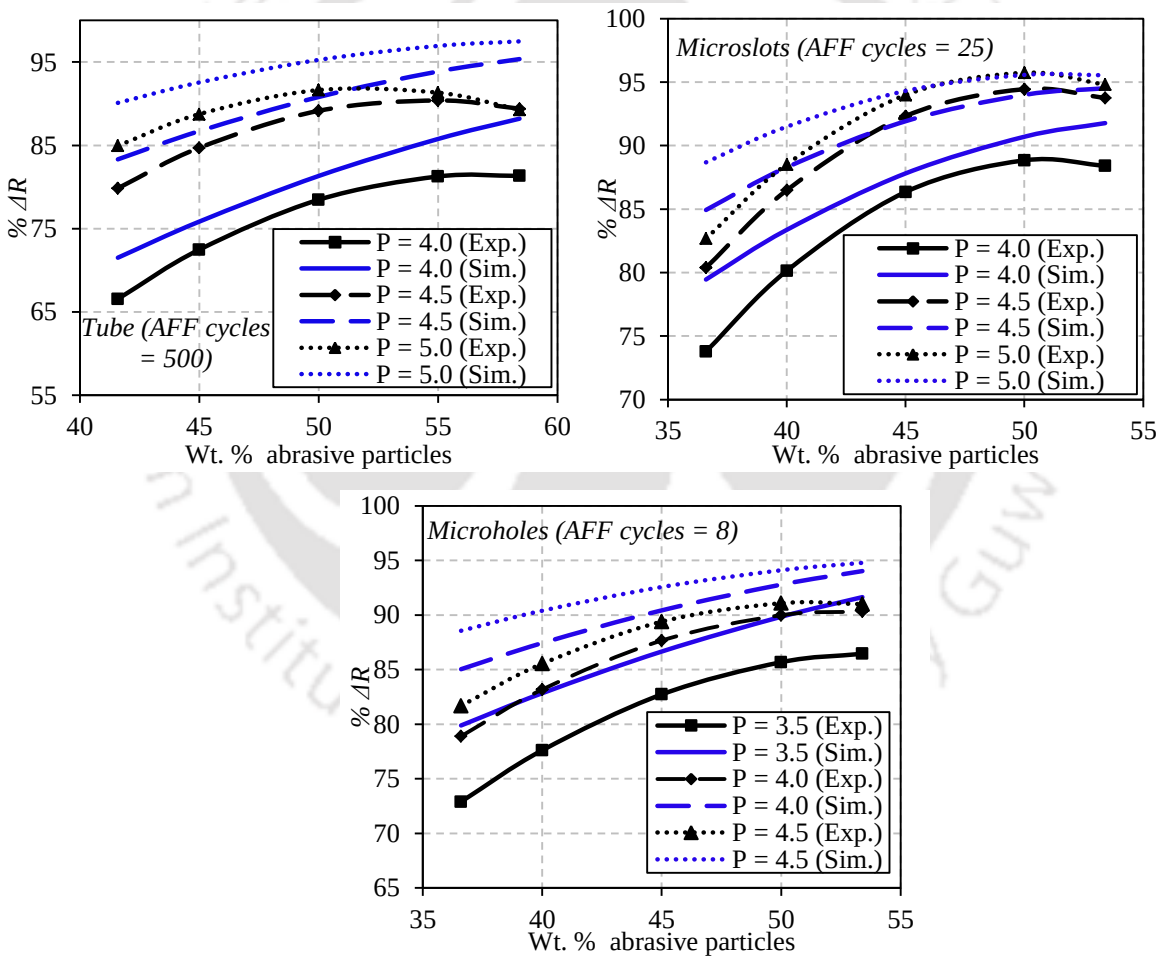

Fig. 7.19 *Effect of wt. % of abrasives particles for different extrusion pressure on percentage change in surface roughness ($\% \Delta R_a$, $\% \Delta R_{as}$) for various workpieces (Exp. stands for experiments and Sim. stands for the simulation).*

Secondly, the number of abrasive particles taking part in the cutting action of surface roughness peaks increases with an increase in wt. % of the abrasive particle in the medium. Thus, as shown in Fig. 7.19(a-c) improvements in the surface roughness both experimentally and simulation increases with an increase in wt. % of abrasive particles.

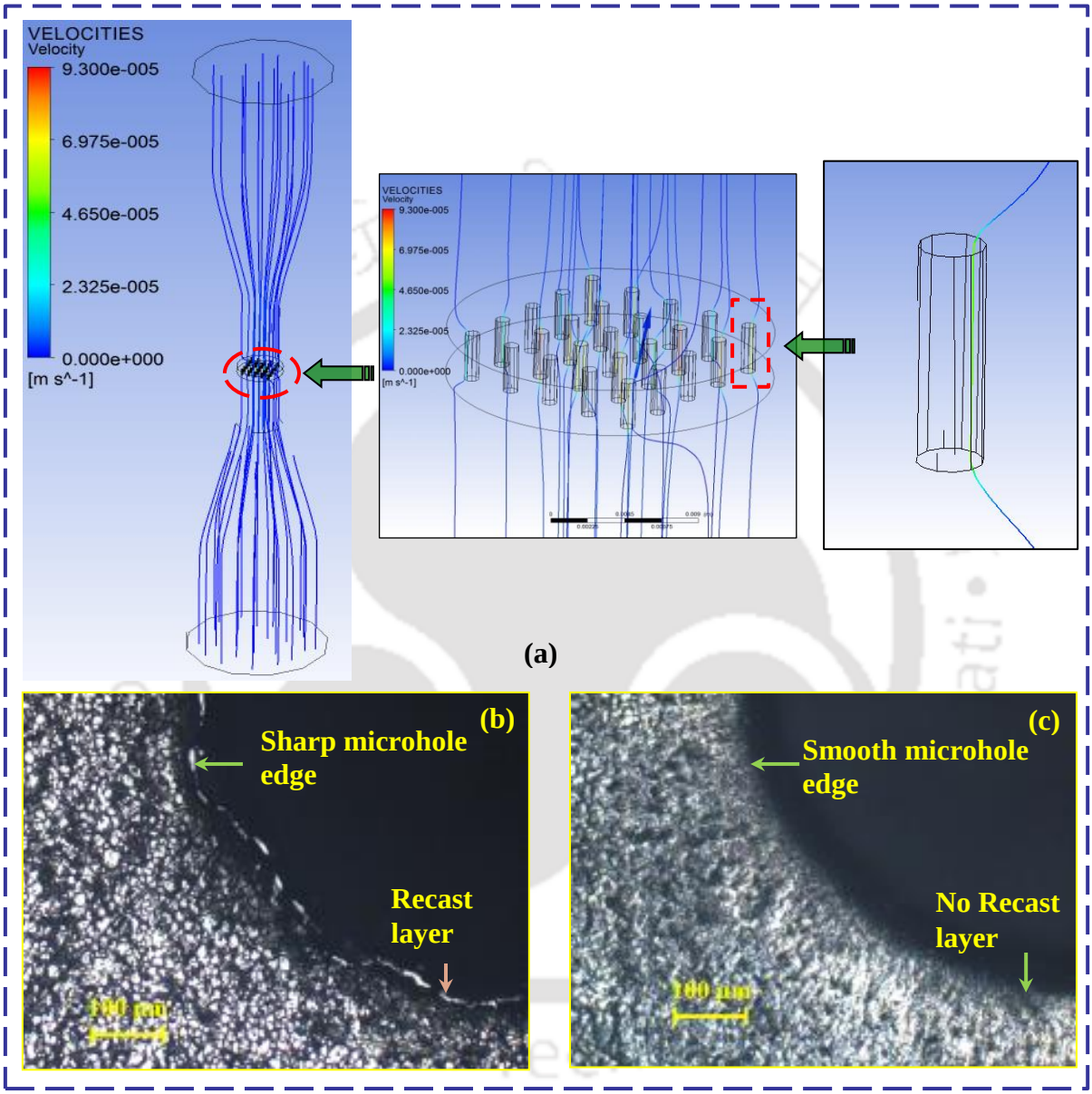

Fig. 7.20 (a) *Velocity streamline of the medium during the AFF process and microhole edge morphology* ***(b)*** *before finishing i.e., EDµM* ***(c)*** *after finishing (8 cycles, # 180, 4 MPa, 53.40 wt. % abrasives particles).*

Finishing of microholes with the help of viscoelastic medium during AFF process not only removes hard recast layer from the microhole walls but also provides radiusing on its outer edges. Viscous nature of the medium helps it to flow in the axial direction. While the elastic nature of the medium controls its radial movement. Due to the elastic nature of the

medium after flowing through restricted microhole passageway at the exit of the microhole medium tries to gain its original un-deformed shape. As a result, medium velocities streamline moves in radial as well as axial direction (Fig. 7.20(a)). Initial edge of the microhole is irregular with sharp burrs formed due to the EDµM process (Fig. 7.20(b)). The radial movement of the medium at microhole exit not only removes burrs and recast layer along its inner wall, but provides radiusing on the sharp microhole edges (Fig. 7.20(c)).

7.4.3 Simulated surface roughness profile

In the present section, simulated surface roughness profile corresponding to the best experimental surface roughness achieved during the finishing of tubes, microslots and microholes is presented. Simulated value of surface roughness, R_{as} is compared with the corresponding experimentally achieved surface roughness, R_a value.

- **Tube**

Initial surface roughness profile with R_{as} of 0.650 µm is taken from profilometer and used for simulating the final surface roughness at 5 MPa, 550 cycles, 55 wt. % of abrasive particles of AFF input parameters (Fig. 7.21(a)).

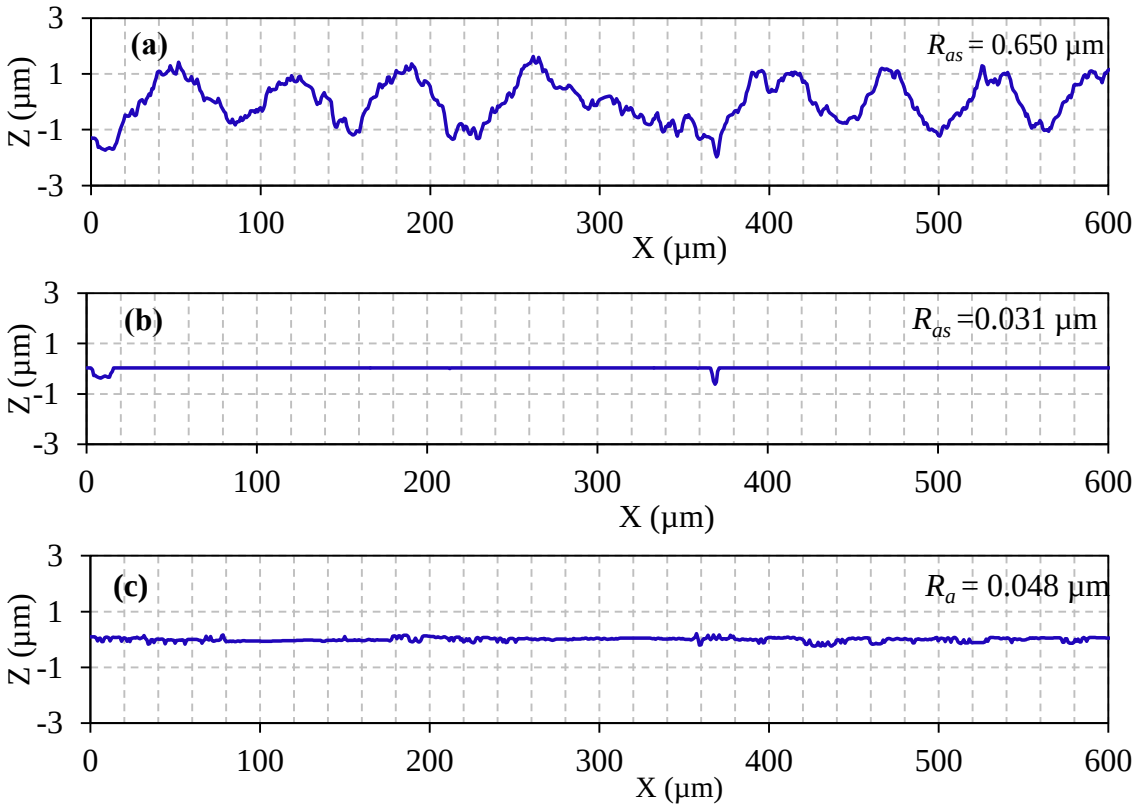

Fig. 7.21 *Surface roughness profile of the workpiece surface* ***(a)*** *initial,* R_{as} *= 0.650 µm* ***(b)*** *simulated* ***(c)*** *experimental (5 MPa, 550 cycles, 55 wt. % of abrasive particles).*

Simulated value of R_{as} is 31 nm with $\% \Delta R_{as}$ of 95.23 % (Fig. 7.21(b)). At the same value of AFF input parameters during the experiments R_a of 48 nm with $\% \Delta R_a$ of 92.24 % is achieved (Fig. 7.21(c)). Thus, there is a minimal error of 2.99 % between the values of $\% \Delta R_{as}$ and $\% \Delta R_a$.

➢ **Microslot**

Initial surface roughness profile having a R_{as} of 3.44 µm is used during predicting the final surface roughness value after finishing the microslot at 5 MPa extrusion pressure for 30 cycles, with medium containing 50 wt. % abrasives particles (Fig. 7.22(a)). With $\% \Delta R_{as}$ of 96.22 %, final R_{as} is 0.13 µm (Fig. 7.22(b)). Experimentally obtained 2-D surface roughness profile for the same input conditions is having R_a of 0.19 µm and $\% \Delta R_a$ of 94.56 (Fig. 7.22(c)). Thus, there is 1.66 % error between the simulated and experimentally obtained value of percentage improvement in surface roughness.

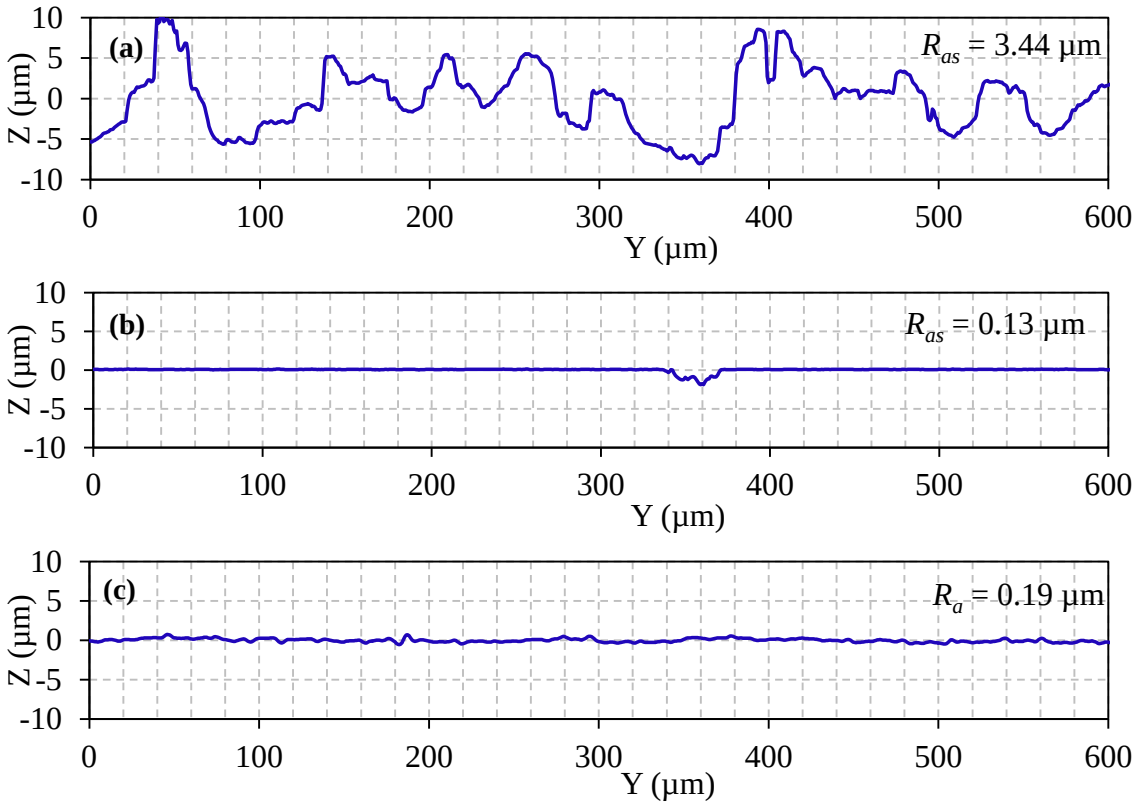

Fig. 7.22 *2-D surface roughness profile of the microslot surface* ***(a)*** *initial* ***(b)*** *simulated final* ***(c)*** *experimental final (5 MPa, 30 cycles, 50 wt. % abrasives particles).*

➢ **Microhole**

At 8 AFF cycles, 4 MPa of extrusion pressure and 53.40 wt. % of abrasives particles R_{as} of 0.09 µm with an improvement of 93.79 % in surface roughness is predicted during the

simulation (Fig. 7.23(a-b)). Corresponding to the same AFF input parameters during the experiments surface roughness of 0.13 µm with 91.16 % improvement in surface roughness is achieved (Fig. 7.23(c)). Thus, there is a reasonable error of 2.63 % between the experimental and simulated value of $\% \Delta R$.

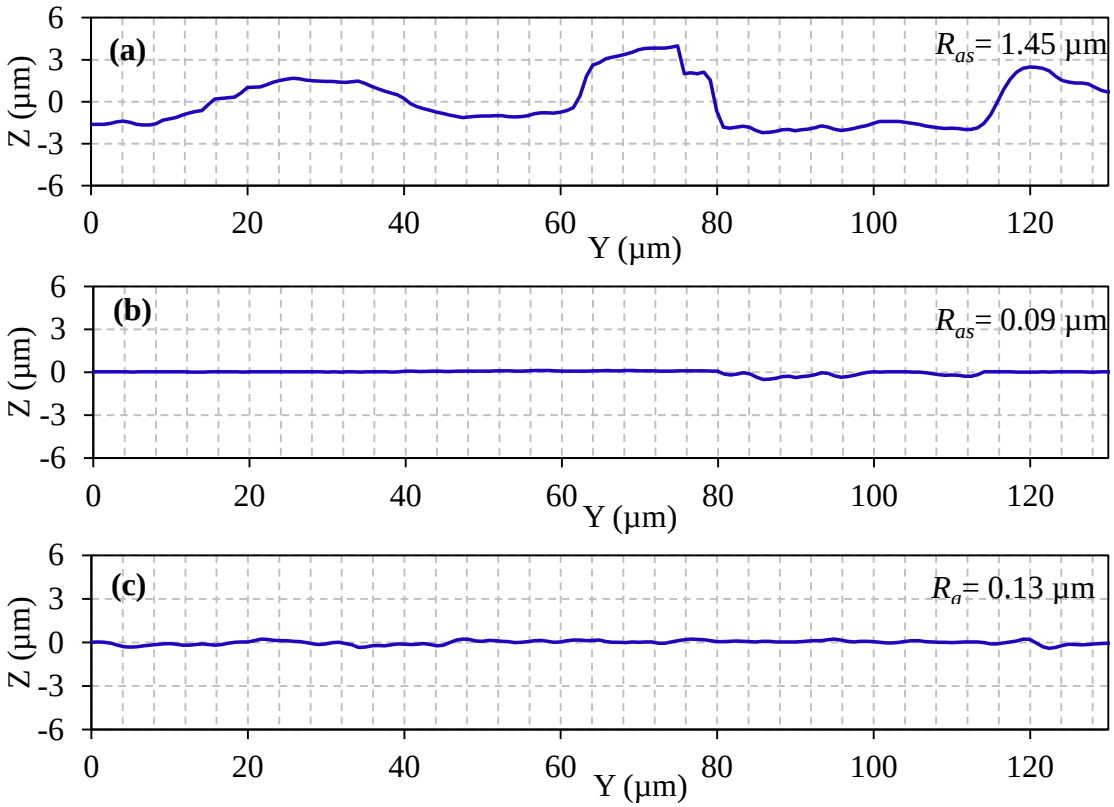

Fig. 7.23 *2-D surface roughness profile of the microhole surface* ***(a)*** *initial* ***(b)*** *after performing AFF experiments* ***(c)*** *simulated (4 MPa, 8 cycles, 53.40 wt. % abrasives particles).*

7.5 Conclusions

In the present chapter, FE analysis of AFF process during the finishing of SS 316L tubes, microslots and microholes is carried out. As per the process requirements, 2-D FE model of the viscoelastic medium domain during finishing tubes while 3-D FE model during finishing of microslots and microholes is developed using Ansys® Polyflow. The developed FE model simulates the flow of viscoelastic medium during AFF process. To accurately model the flow, experimentally measured rheological properties of the medium are used as input. Also, a new simulation model is developed for predicting the surface roughness generated by AFF process on the workpiece surface. Abrasive particles with multiple cutting edges and the incorporation of the actual initial surface roughness profile during the simulation are few of

the many new features of the developed simulation model over the previously developed surface roughness simulation models. Some of the important findings of current work are:

1. The developed FE model of the viscoelastic medium accurately predicts more accurately the amount of finishing stresses generated in the medium.
2. Amount of radial stresses generated in medium increases with the increase in extrusion pressure and wt. % of the abrasive particles.
3. Developed surface roughness simulation model is more accurate in predicting the surface roughness values at various combinations of AFF input parameters.
4. Maximum error of 13 %, during the finishing of tubes there is a good agreement between the simulated and experimentally obtained values of percentage improvement in surface roughness.
5. In case of microslots, simulated values of percentage improvement in surface roughness are in good agreement with the experimental results with a maximum error of 7 %.
6. Surface roughness simulation model predicts percentage change in surface roughness with a maximum of 8 % error when compared with the experimental results during the finishing of microholes.

Chapter 8

CONCLUSIONS AND SCOPE FOR FUTURE WORK

8.1 Novelty of the work

The novelty of the current work is as follows:-

1. The AFF process setup that can easily finish components with macro to micro features.
2. Indigenously develop multiple polymer blended medium whose viscosities can be varied to suit the openings of the workpiece.
3. Development of an accurate FE model of the AFF process by using experimentally measured rheological properties of the medium as input.
4. A more realistic surface roughness simulation with fewer assumptions as compared to the simulation models proposed in literature.

8.2 Conclusions

In the current work experimental study, modeling and simulation of AFF process during finishing of workpieces with macro as well as micro features is carried out. The main objective is to design and develop complete AFF process, AFF experimental setup, economic polymer rheological abrasive medium, tooling for macro and micro workpiece, modeling and simulation of surface generated during this process. The economic rheological medium by blending various polymers is developed in-house. Later, modeling of AFF process and simulation of the surface roughness generated during AFF process is carried out. On the basis of work reported in fields of designing and fabrication of setup, development of the medium,

experimental, modeling and simulation study of AFF process, following conclusions are drawn:-

8.2.1 Abrasive flow finishing setup and medium development

1. AFF setup is designed and fabricated for finishing of workpieces with macro and micro features.
2. To ensure the safety of the developed setup its static structural FE analysis is carried out. Maximum equivalent stress generated in the complete assembly is 229.02 MPa, while the maximum total deformation generated in AFF setup is 276.32 µm. Since the maximum stress and total deformation are too small, these can be neglected during operating conditions of AFF setup.
3. Various in-house economic AFF medium is developed to replace the expensive commercial medium. Base polymer of the medium is a blend of soft styrene butadiene polymer and silicon polymer. Rheological additives such as plasticizers and softeners are mixed to polymers blend along with silicon carbide abrasive particles. Detailed rheological study of the medium is carried out with the help of MCR-101 parallel plate rheometer.
4. Various medium developed for finishing of SS 316L tubes, microslots and microholes are viscoelastic in nature. Rheological study showed that medium follow shear thinning behaviour.
5. Elastic nature of the medium is highest in the medium developed for finishing SS 316L tubes followed by the microslots and least in microholes.
6. Microslots and microholes provide high resistance to the medium flow during its extrusion through them. Therefore, to aid in the medium easy flow its viscosity is reduced by the addition of plasticizers and softeners.
7. Viscosity of the medium decreases with increase in temperature. The viscosity varies from 1.58 x 10^6 Pa-s at 30 ºC to 8.24 x 10^4 at 60 ºC with 94.78 % decrease, 2.08 x 10^5 Pa-s at 30 ºC to 3.44 x 10^4 at 60 ºC with 83.46 % decrease, 3.35 x 10^5 Pa-s at 30 ºC to 3.58 x 10^4 at 60 ºC with 89.31 % decrease, for medium with 40 wt. % of abrasive particles prepared for finishing tubes, microslots and microholes respectively.
8. With the increase in frequency, storage modulus of the medium increases gradually. Therefore, more energy it can stores during the deformation process.

8.2.2 Experimental study

- ***Finishing of tubes***

1. Developed AFF setup successfully that can finishes the SS 316L cylindrical tubes to the nanometer ranges.
2. Preliminary experiments are conducted to find the best input parameters range for achieving minimum surface roughness value. The range of extrusion pressure, number of AFF cycles and wt. % of abrasive particle are 4 - 5 MPa, 450 - 550 cycles and 45 % - 55% respectively.
3. From the ANOVA, it was found that extrusion pressure is the most significant input parameter affecting the AFF output responses. During the experimental analysis, the percentage contribution of extrusion pressure is 61.88 %. Whereas, the contribution of number of AFF cycles and wt. % of abrasives particles in the medium is 25.12 % and 10.92 % respectively. During the simulation study, extrusion pressure possesses the highest contribution (62.32 %) followed by the contribution of number of AFF cycles (17.36 %) and wt. % of abrasives particles in the medium (14.77 %).
4. The best surface roughness of 48 nm with a percentage improvement in surface roughness of 92.24 % is achieved during finishing of SS 316L tubes with AFF process.

- ***Finishing of microslots***

1. Microslots with width 450 µm are micromachined on SS316 L workpieces with the help of electrical discharge micromachining (EDµM) process. Later, the same nano finished using AFF process.
2. Preliminary experiments shows that 4 - 5 MPa, 20 - 30 AFF cycles and 40 % - 50 % are the effective ranges of extrusion pressure, AFF cycles and abrasive particles wt. %.
3. From the ANOVA, it is found that extrusion pressure is the most significant input parameter affecting AFF output responses. During the experimental analysis, the contribution of extrusion pressure (44.49 %) is the highest followed by the wt. % of abrasive particle (44.47 %), and number of AFF cycles (9.65 %) in deciding $\% \Delta R_a$. While during the simulation study, the most significant is extrusion pressure (43.73 %) followed by the abrasive particles wt. % (33.87 %), and number of AFF cycles (17.26 %).
4. The best experimental surface roughness of 192 nm from an initial surface roughness of 3.49 µm with a surface improvement of 94.51 % is achieved on SS 316L microslots.

➢ ***Finishing of microholes***

1. Microholes are machined on the SS 316L workpieces with the help of EDµM. Initial surface roughness of the microholes about 1.40 ± 0.10 µm
2. Preliminary AFF experiments shows that 3.5 - 4.5 MPa extrusion pressure, 6 - 10 number of AFF cycles and 40 % - 50 % are the effective ranges of AFF input parameters during the finishing of the microholes.
3. Parametric study of AFF during the finishing of the microholes is carried out by designing the experiments (CCRD). After conducting the experiments a minimum improvement of 74 % in surface roughness is noticed
4. From the ANOVA of experimental and simulated $\% \Delta R_a$, it is found that extrusion pressure is the most significant input parameter. During the experimental analysis the contribution of extrusion pressure (42.81 %) is the highest followed by abrasive particles wt. % (40.74 %) and AFF cycles (14.72 %). During the simulation, extrusion pressure processes highest contribution (45.00 %) followed by the contribution of abrasive particles wt.% (34.66 %) and AFF cycles (16.26 %).
5. Best surface roughness of 130 nm is achieved from the initial surface roughness of 1.47 µm with the $\% \Delta R_a$ of 91.16 % during AFF of microholes.

8.2.3 Modeling of abrasive flow finishing process and simulation of surface roughness

1. Finishing forces generated on the workpiece surface during AFF experiments are computed by using Ansys Polyflow.
2. 2-D axisymmetric FE modeling of AFF process during finishing of SS 316L tubes (macro features) and 3-D FE modelling of AFF process during finishing of micro features (microslots and microholes) is carried out by using the rheological properties of the medium as input.
3. New surface simulation models are developed to predict the surface roughness generated after AFF process during finishing of SS 316L tubes, microslots and microholes. By using modeled finishing forces generated on the workpiece surface as one of the input, final surface roughness after AFF process is predicted.
4. Simulated surface roughness values are compared with the corresponding experimentally obtained surface roughness values. It is found out that simulated results are in good agreement with the experimental results.

5. Surface roughness simulation model predicts percentage change in surface roughness with a maximum of 13 %, 7 % and 8 % error when compared to experimental results during the finishing of SS 316L tubes, microslots and microholes respectively.

8.3 Publications from the current work

Book chapter

1. **Sachin Singh**, M. Ravi Sankar, V. K. Jain, J. Ramkumar, "**Abrasive Flow Finishing Process and Modeling**" Nanofinishing Science and Technology : Basic and Advanced Finishing and Polishing Processes, CRC Press, Taylor and Francis, 2017, Chapter 4, Pages 75–110, eBook ISBN: 978-1-315-40409-7.

International Journal : Published and Accepted

1. **Sachin Singh**, Deepu Kumar, M. Ravi Sankar, K. Rajurkar, "**Nanofinishing of Microslots on Surgical Stainless Steel using Abrasive Flow Finishing Process: Experimentation and Modeling**" ASME Journal of Micro and Nano-manufacturing (**Accepted**).
2. **Sachin Singh**, Deepu Kumar, M. Ravi Sankar, V. K. Jain "**Finite element modeling of viscoelastic medium and simulation of nano-surface roughness achieved on microholes finished by abrasive flow finishing process**" The International Journal of Advanced Manufacturing Technology (**Accepted**).
3. **Sachin Singh**, M. Ravi Sankar, V. K. Jain "**Experimental and Theoretical Investigations into Abrasive Flow Nanofinishing of Surgical Stainless Steel Tubes**", Machining Science and Technology, DOI: 10.1080/10910344.2017.1365897.
4. **Sachin Singh**, Deepu Kumar, M. Ravi Sankar, 2017 "**Experimental, Theoretical, and Simulation Comparative Study of Nano Surface Roughness Generated during Abrasive Flow Finishing (AFF) Process**", Journal of Manufacturing Science and Engineering. Volume 139(6), Pages 061014(1-12).
5. **Sachin Singh**, A.S Arjun Raj, M. Ravi Sankar, V. K. Jain, 2016 " **Finishing Force Analysis and Simulation of Nanosurface Roughness in Abrasive Flow Finishing process using medium rheological properties**" The International Journal of Advanced Manufacturing Technology, 2016, Volume 85-9, Pages 2163-2178.
6. **Sachin Singh**, M. Ravi Sankar, V. K. Jain, J. Ramkumar, 2016 "**Modeling of Nano Finishing Forces and Surface Roughness in Abrasive Flow Finishing (AFF) Process using Rheological Properties**", International Journal of Precision Technology Volume 6-2, Pages 123-141.
7. **Sachin Singh ,** M. Ravi Sankar, U. S. Dixit, 2014 **"State of art on Micro-Abrasive Flow Finishing (μ-AFF) Process" ,** Journal of Manufacturing Technology Research, Volume 5, Pages 167-177.

International Journal : (Under Review)

1. **Sachin Singh**, M. Ravi Sankar, **"Nanofinishing of Microholes on Surgical Stainless Steel using Abrasive Flow Finishing Process"** The International Journal of Advanced Manufacturing Technology (**1st revision completed**).
2. M. Ravi Sankar, V. K. Jain, J. Ramkumar, S. K. Sareen, **Sachin Singh**, **"Rheological characterization of soft silicone based polymer rheological based medium and its performance in nanofinishing of Al alloy/ SiC MMCs"** The International Journal of Advanced Manufacturing Technology (**1st revision completed**).
3. **Sachin Singh**, M. Ravi Sankar, "**Rheological Study of the Developed Medium and Its Performance Evaluation during Abrasive Flow Finishing of Microslots"** Materials and Manufacturing Processes (**Under review**).

Conference

1. **Sachin Singh,** M. Ravi Sankar,, P. Ranjan, R. Balasubramaniam "**Development and rheological study of the polymer blended viscoelastic medium for finishing of microholes**" 2017 2nd International Conference on Advanced Materials Research and Manufacturing Technologies (AMRMT 2017), Thailand **(Best Paper Award).**
2. M. Ravi Sankar, **Sachin Singh**, T. N. Deepu Kumar, Debasish Sekar, Bikramjit Basu "**Finishing of Complex Sculptured Orthopedic Bio-Implants using Polymer Rheological Abrasive Semisolid Medium**" IITG-KIT Joint Symposium on Soft and Biobased Materials at Kyto Institute of Technology, Japan, August 03, 2016.
3. M. Ravi Sankar, **Sachin Singh**, Debasish Sekar, Bikramjit Basu "**Nano Finishing of Complex Featured Bio Implants using Polymer Rheological Abrasive Semisolid Medium**" Gifu-U/IITG and Gifu-U/UKM Joint Symposium-2016, at Gifu University, Japan, August 01, 2016.
4. T. N. Deepu Kumar, **Sachin Singh,** M. Ravi Sankar, "**Effect of abrasive particle bluntness on nano finishing using abrasive flow finishing process**" International Conference on Nanotechnology for Better Living-2016 (NBL-2016), NIT Srinagar, India May 25-29, 2016.
5. **Sachin Singh**, M. Ravi Sankar "**Design and Performance Evaluation of Abrasive Flow Finishing Process during Finishing of Stainless Steel Tubes**" 4th International Conference on Materials Processing and Characterization, Hyderabad, March 14-15, 2015.
6. **Sachin Singh**, M. Ravi Sankar, V. K. Jain, J. Ramkumar **"Modeling of Finishing Forces and Surface Roughness in Abrasive Flow Finishing (AFF) Process using Rheological Properties",** All India Manufacturing Technology, Design and Research (AIMTDR) Conference, Indian Institute of Technology, Guwahati, Dec. 12-14, 2014.
7. M. Ravi Sankar, **Sachin Singh**, **"Polymer Rheological Nano fluids for Nano finishing of Flat and Free form Surfaces"**, 3rd International Conference on Nanomaterials and Nanotechnology (ICANN-2013), IIT Guwahati, Dec. 01-03, 2013.
8. **Sachin Singh**, M. Ravi Sankar, "**State of the Art on Micro-Abrasive Flow Finishing (AFF) Process**", National Conference on Manufacturing: Vision for Future (MVF-2013), Indian Institute of Technology, Guwahati, Oct. 12-13, 2013.

Publications outside thesis work

Book chapter

1. **Sachin Singh**, Deepu Kumar M. Ravi Sankar, V. K. Jain, "**Magnetic Abrasive Finishing Process and Modelling**" Nanofinishing Science and Technology : Basic and Advanced Finishing and Polishing Processes, CRC Press, Taylor and Francis, Chapter 8, Pages 179–214, eBook ISBN: 978-1-315-40409-7.

8.4 Scope for future work

AFF process with proper modification in tooling and medium can be used for finishing of any workpieces. Workpieces made of advanced materials with complex geometry that is almost impossible to be finished by any other advanced finishing process can be easily finished by the AFF process. There is a lot of scope for further research work as briefly stated in the following section.

8.4.1 Medium development

1. More polymer chemistry orientated study can be possible to strengthen the bonding between the polymer chains and the abrasive particles.
2. Development of medium for uniformly finishing workpieces with high aspect ratio and non-uniform cross-section.

8.4.2 Experiments

1. Actual drug eluting stents, knee and hip implants finishing by AFF process can be explored.
2. Effect of different mesh size abrasive particles mixture on the finishing need to be studied.
3. Tubes with high length/diameter ratio are yet to be finished by the AFF process.
4. Uniform finishing of the workpieces of irregular cross-section with the help of AFF process by developing converse shaped tooling.
5. Experimental study on finding the least possible size of workpiece internal feature that can be finished by the AFF process still needs to be done.

8.4.3 Simulation

1. Surface roughness by using the exact amount of finishing force transferred from the polymer chains to the abrasive particle can be studied.
2. Incorporation of indentation of the abrasive particle on the finished workpiece surface in the roughness simulation mode can be explored.